

VOLUME 30

DECEMBER 1952

NUMBER 12

Canadian Journal of Chemistry

Editor: LÉO MARION

Published by THE NATIONAL RESEARCH COUNCIL
OTTAWA CANADA

CANADIAN JOURNAL OF CHEMISTRY

(Formerly Section B, Canadian Journal of Research)

The CANADIAN JOURNAL OF CHEMISTRY is published monthly by the National Research Council of Canada under the authority of the Chairman of the Committee of the Privy Council on Scientific and Industrial Research. Matters of general policy are the responsibility of a joint Editorial Board consisting of members of the National Research Council of Canada and the Royal Society of Canada.

The National Research Council of Canada publishes also: *Canadian Journal of Botany*, *Canadian Journal of Medical Sciences*, *Canadian Journal of Physics*, *Canadian Journal of Technology*, *Canadian Journal of Zoology*.

The CANADIAN JOURNAL OF CHEMISTRY and the CANADIAN JOURNAL OF TECHNOLOGY have been chosen by the Chemical Institute of Canada as its medium of publication for scientific papers.

EDITORIAL BOARD

Representing

NATIONAL RESEARCH COUNCIL

DR. J. H. L. JOHNSTONE (*Chairman*),
Professor of Physics,
Dalhousie University,
Halifax, N.S.

DR. OTTO MAASS,
Macdonald Professor of
Physical Chemistry,
McGill University,
Montreal, P.Q.

DR. CHARLES W. ARGUE,
Dean of Science,
University of New Brunswick,
Fredericton, N.B.

DR. A. G. MCCALLA,
Dean, Faculty of Agriculture,
University of Alberta,
Edmonton, Alta.

Ex officio

DR. LÉO MARION (*Editor-in-Chief*),
Director, Division of Pure Chemistry,
National Research Laboratories,
Ottawa.

DR. H. H. SAUNDERSON,
Director, Division of Information Services,
National Research Council,
Ottawa.

Representing

ROYAL SOCIETY OF CANADA

DR. G. M. VOLKOFF,
Professor of Physics,
University of British Columbia,
Vancouver, B.C.

DR. T. THORVALDSON,
Dean Emeritus of Graduate
Studies,
University of Saskatchewan,
Saskatoon, Sask.

DR. D. L. BAILEY,
Department of Botany,
University of Toronto,
Toronto, Ont.

DR. E. HORNE CRAIGIE,
Department of Zoology,
University of Toronto,
Toronto, Ont.

Section
III

Section
V

Representing

THE CHEMICAL INSTITUTE OF CANADA

DR. H. G. THODE,
Department of Chemistry,
McMaster University,
Hamilton, Ont.

THE CANADIAN ASSOCIATION OF PHYSICISTS

DR. G. M. VOLKOFF,
Professor of Physics,
University of British Columbia,
Vancouver, B.C.

Manuscripts should be addressed to:

DR. LÉO MARION,
Editor-in-Chief,
Canadian Journal of Chemistry,
National Research Council,
Ottawa, Canada.

Each manuscript should be typewritten, double-spaced, and the original and one extra copy submitted (see **Notice to Contributors** inside of back cover).

Subscriptions, renewals, and orders for back numbers should be addressed to:

Administrative Services,
National Research Council,
Ottawa, Canada.

Subscription rate: \$4.00 a year; single numbers: 50 cents. Special rates can be obtained for subscriptions to more than one of the Journals published by the National Research Council.

Canadian Journal of Chemistry

Issued by THE NATIONAL RESEARCH COUNCIL OF CANADA

VOL. 30

DECEMBER, 1952

NUMBER 12

THE REACTION OF ACTIVE NITROGEN WITH PROPYLENE¹

By G. S. TRICK AND C. A. WINKLER

ABSTRACT

The reaction of nitrogen atoms with propylene has been found to produce hydrogen cyanide and ethylene as the main products, together with smaller amounts of ethane and propane and traces of acetylene and of a C_4 fraction. With excess propylene, the nitrogen atoms were completely consumed and for the reaction at 242°C ., 0.77 mole of ethylene was produced for each mole of excess propylene added. For reactions at lower temperatures, less ethylene was produced. The proposed mechanism involves formation of a complex between the nitrogen atom and the double bond of propylene, followed by decomposition to ethylene, hydrogen cyanide, and atomic hydrogen. The ethylene would then react with atomic nitrogen in a similar manner.

INTRODUCTION

The reactions of active nitrogen with ethylene (7, 8) and with methane and ethane (4) have been discussed in previous papers from this laboratory. The reaction with propylene has now been studied, with the results recorded in the present paper. As before, the interpretation assumes the reactive species to be atomic nitrogen.

EXPERIMENTAL

The investigation was made using an apparatus which was essentially identical with that described previously (4, 7). The reaction products were analyzed by distilling the hydrocarbon fraction from the hydrogen cyanide at -85°C ., after which the hydrocarbon fraction, containing small quantities of hydrogen cyanide, was separated into C_2 , C_3 , C_4 , and HCN fractions by distillation in a column of the type described by LeRoy (10). The still was modified so that it was possible to distill directly from the still-pot to a condenser cooled by liquid nitrogen. A Toepler pump was used only to remove the last traces of one fraction before the next fraction was distilled off. By this procedure it was possible to obtain a sufficiently large sample to determine the unsaturates by the Bone and Wheeler method. The unsaturates were removed by absorption in a sulphuric acid solution of mercuric sulphate. Acetylene was absorbed in alkaline potassium iodomercurate.

Hydrogen cyanide from the first fraction was determined by weight and also by titration in alkaline solution with silver nitrate. To the value so obtained was added the amount of hydrogen cyanide analyzed by the LeRoy still.

¹ Manuscript received March 20, 1952.

Contribution from the Physical Chemistry Laboratory, McGill University, Montreal, Que., with financial assistance from the Defence Research Board, Ottawa. Permission of the Defence Research Board to publish this paper is gratefully acknowledged.

RESULTS

With increase in propylene flow rate at constant nitrogen atom input, the yield of hydrogen cyanide increased almost linearly until it attained a constant value (within $\pm 5\%$) at a propylene flow rate beyond which consumption of nitrogen atoms was presumably complete. Complete consumption of nitrogen atoms was observed at a different flow rate of propylene when the reaction vessel was cleaned and re-poisoned with metaphosphoric acid. Presumably this was due to differences in nitrogen atom concentrations as a result of different wall conditions in the reaction vessel. For this reason, a complete series of experiments was made without altering the conditions of the walls. The curves for two different series of experiments are shown in Fig. 1.

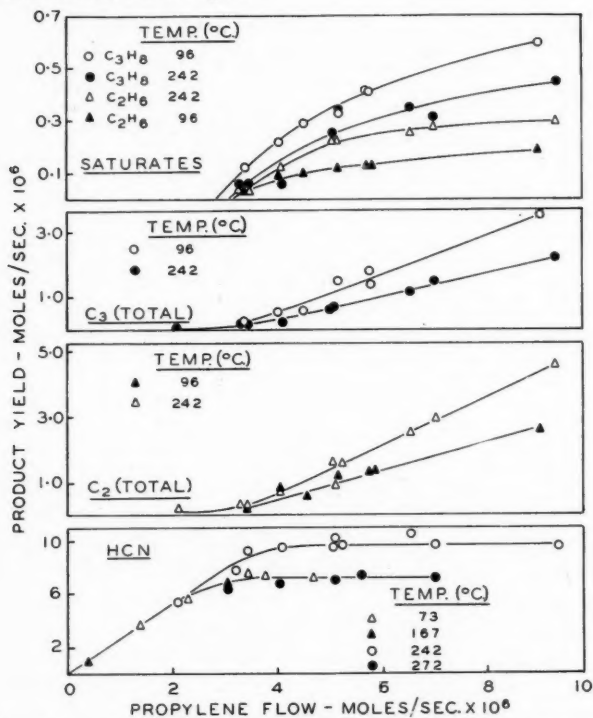


FIG. 1. Rate of formation of various products in the nitrogen atom - propylene reaction, as a function of the propylene flow rate.

Measurements of atom concentrations were made using a Wrede gauge at the entrance and exit of the reaction bulb. A small decrease in concentration of nitrogen atoms across the bulb was noted but the average value of the nitrogen atom concentration as measured by the Wrede gauge was always 15 to 25% greater than that inferred from the amount of hydrogen cyanide produced at propylene flow rates where consumption of nitrogen atoms was complete. Owing to possible errors in the Wrede gauge measurements (11) and its lack of sensitivity the

hydrogen cyanide yield with complete nitrogen atom consumption probably gives the more accurate estimate of the nitrogen atom concentration.

The main product of the reaction, apart from hydrogen cyanide, was found to be ethylene. Smaller quantities of propane and ethane and traces of acetylene (about 1% of the propylene input) were also found. A C_4 fraction, to the extent of about 2% of the propylene input, was found to consist mainly of unsaturated material. The average carbon balance accounted for about 96% of the propylene input.

In Table I are summarized the results of a series of experiments made at $242 \pm 3^\circ\text{C}$. The yield of hydrogen cyanide is plotted in Fig. 1 and is seen to correspond to an average nitrogen atom flow of 9.7×10^{-6} moles per sec.

TABLE I
PRODUCTION OF HYDROGEN CYANIDE AND OTHER PRODUCTS AT
VARIOUS PROPYLENE FLOWS (TEMP = $242 \pm 3^\circ\text{C}$.)

Propylene flow	Yield of products—moles/sec. $\times 10^6$						
	HCN	C_2	C_2H_4	C_2H_6	C_3	C_3H_6	C_3H_8
2.12	5.40	0.25	—	—	0.08	—	—
3.29	7.80	0.32	0.29	0.03	0.25	0.19	0.06
3.46	9.30	0.33	0.29	0.04	0.27	0.21	0.06
4.12	9.50	0.69	0.57	0.12	0.26	0.20	0.06
5.08	9.50	1.62	1.40	0.22	0.68	0.43	0.25
5.12	10.2	0.90	0.68	0.22	0.75	0.41	0.34
5.24	9.7	1.58	—	—	—	—	—
6.55	10.5	2.50	2.25	0.25	1.18	0.83	0.35
7.01	9.66	2.95	2.68	0.27	1.52	1.21	0.31
9.32	9.60	4.60	4.31	0.29	2.20	1.75	0.45

In Table II are shown the results of another series of experiments made at $96 \pm 2^\circ\text{C}$. All these experiments were made with a propylene flow greater than that corresponding to complete nitrogen atom consumption, with an average yield of hydrogen cyanide of 8.0×10^{-6} moles per sec.

In Fig. 1 is shown the total yield of C_2 hydrocarbons (ethane and ethylene) as a function of the rate of addition of propylene for experiments at the two

TABLE II
PRODUCTION OF HYDROGEN CYANIDE AND OTHER PRODUCTS AT
VARIOUS PROPYLENE FLOWS (TEMP. = $96 \pm 2^\circ\text{C}$.)

Propylene flow	Yield of products—moles/sec. $\times 10^6$						
	HCN	C_2	C_2H_4	C_2H_6	C_3	C_3H_6	C_3H_8
3.43	8.1	0.30	0.27	0.03	0.28	0.16	0.12
4.05	8.0	0.86	0.77	0.09	0.58	0.36	0.22
4.52	8.7	0.61	0.51	0.10	0.60	0.31	0.29
5.17	7.6	1.24	1.12	0.12	1.35	1.02	0.33
5.78	8.0	1.31	1.18	0.13	1.80	1.38	0.42
5.82	8.0	1.35	1.22	0.13	1.40	0.98	0.42
9.02	8.2	2.60	2.41	0.19	3.50	2.90	0.60

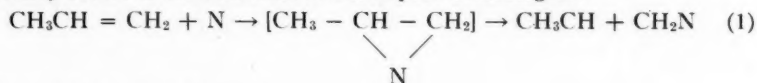
temperatures. It can be seen that the rate of production of C_2 products is essentially linear with the rate of introduction of propylene, once conditions are reached corresponding to complete removal of nitrogen atoms. The C_2 yield at the higher temperature is about 65% greater, on the average, than at the lower temperature.

In Fig. 1 are also shown the yields of saturated products and recovered C_3 hydrocarbons (propane and propylene).

DISCUSSION

The absence of any product containing nitrogen, other than hydrogen cyanide, would seem to eliminate the possibility that any nitrogen-containing complex of appreciable stability is formed, or that hydrogen is abstracted from the propylene molecule by the nitrogen atom to form the NH radical.

The appearance of C_2 hydrocarbons as the principal product of the reaction leaves little doubt that the main reaction is removal of one carbon atom by an attacking nitrogen atom. The fact that ethylene is considerably more reactive than ethane towards nitrogen atoms suggests that the initial attack is at the carbon-carbon double bond, rather than at the single bond, to form a complex which may revert to the reactants or decompose according to:



which would then be followed by:

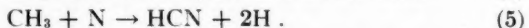
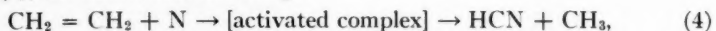


It is interesting, perhaps, that compounds such as CH_2N have been suggested by Geib and Harteck (6) as intermediates in the production of CH_3N in the reaction between hydrogen atoms and hydrogen cyanide at liquid nitrogen temperatures.

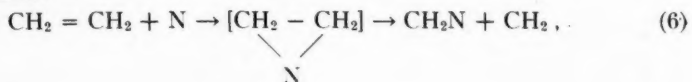
The ethylidene radical has been postulated by various workers as an intermediate in free radical reactions. For example, Bawn and Dunning (1) and Bawn and Milsted (2) found ethylene as a product of the reaction of ethylidene dibromide with excess sodium atoms. Since the addition of molecular hydrogen did not produce any ethane, they considered the ethylidene radical to rearrange very rapidly to ethylene, thus:



The reaction of ethylene with nitrogen atoms could then proceed as previously outlined (8), the main reactions being:



However, the attack on ethylene by a nitrogen atom to form the methylene radical would correspond more closely to the formation of the ethylidene radical from propylene, thus:





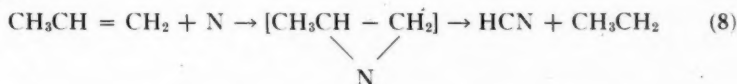
and these reactions might be followed by:



The methylene radical is electronically similar to, but more stable than, the ethylidene radical (2).

Owing to the conflicting values of bond dissociation energies found in the literature and the absence of a well established dissociation energy for the nitrogen molecule (5) it is difficult to make an estimate of the heat of reaction for the mechanism proposed. It might be suggested that the rearrangement of the ethylidene radical to ethylene takes place in the activated complex and this extra energy of stabilization would be available for decomposition of the complex. However, no such energy of rearrangement is available in reaction (6) between nitrogen atoms and ethylene. Since nitrogen atoms attack both propylene and ethylene with velocities of the same order of magnitude, it may be concluded that the ethylidene radical is formed in the free state and that its energy of rearrangement is not available to aid the decomposition of the complex in reaction (1).

It is also possible that the initial reaction of nitrogen atoms with propylene could be:

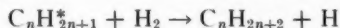
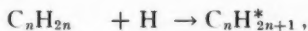


which is energetically more favorable than reaction (1). The ethyl radical then could undergo further reaction with nitrogen atoms. However, to obtain considerable ethylene as a product, it would be necessary for the ethyl radicals to be comparatively inactive towards nitrogen atoms and to disproportionate



This would lead to equal quantities of ethane and ethylene formed in the reaction chamber and since the nitrogen atoms remaining would react more rapidly with the unsaturate, more ethane than ethylene should be trapped out. This is contrary to the observed behavior, and it may be concluded, therefore, that reaction (8) is of little significance.

The saturated products obtained when nitrogen atoms attack propylene are probably formed by hydrogenation of the corresponding olefin, in reactions of the type (12)



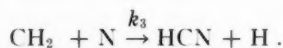
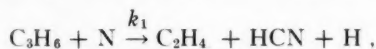
where $\text{C}_n\text{H}_{2n+1}^*$ represents a radical containing the heat of hydrogenation.

In addition to their reaction with nitrogen atoms to form hydrogen cyanide, methylene radicals may react with propylene to form the butene detected in the products, or may suffer hydrogenation to methane (3) sufficiently to account for the small deficiency in the carbon balance. The possible reactions of the methyl-

ene radical are difficult to establish since its reactivity depends upon whether it occurs in the singlet or triplet state (9).

The traces of acetylene found in the reaction products may be readily explained by slight dehydrogenation of ethylene (cf. 13, p. 262).

From the preceding remarks, it seems reasonable to represent the main reactions involving consumption of nitrogen atoms by the sequence



From rate expressions of the usual form for the rates of reaction of propylene and ethylene, it is readily shown that

$$\frac{d[\text{C}_2\text{H}_4]}{d[\text{C}_3\text{H}_6]} = \frac{k_2[\text{C}_2\text{H}_4]}{k_1[\text{C}_3\text{H}_6]} - 1.$$

On integration and evaluation of the integration constant for the condition that $[\text{C}_2\text{H}_4] = 0$ when $[\text{C}_3\text{H}_6] = [\text{C}_3\text{H}_6]_0$,

$$[\text{C}_2\text{H}_4]_1 = \frac{[\text{C}_3\text{H}_6]_0 \left(\frac{[\text{C}_3\text{H}_6]_1}{[\text{C}_3\text{H}_6]_0} \right)}{1 - \frac{k_2}{k_1}} \left\{ \left(\frac{[\text{C}_3\text{H}_6]_1}{[\text{C}_3\text{H}_6]_0} \right)^{(k_2/k_1) - 1} - 1 \right\}$$

where $[\text{C}_3\text{H}_6]_0$ is the concentration of propylene at the inlet to the reaction vessel (propylene flow rate) and $[\text{C}_2\text{H}_4]_1$ and $[\text{C}_3\text{H}_6]_1$ are the concentrations of ethylene and propylene respectively at the outlet of the reaction vessel when nitrogen atom consumption is complete. These latter concentration terms may be expressed as the amounts of ethylene and propylene trapped out in unit reaction time.

Values of $[\text{C}_2\text{H}_4]_1$ may now be calculated for different assumed values of k_2/k_1 and different values of $[\text{C}_3\text{H}_6]_0$, the input flow rate of propylene. In Table III are shown values of $[\text{C}_2\text{H}_4]_1$ for k_2/k_1 ratios of 0.75 and 1.75 calculated from the data at 96° and 242°C. respectively. The total C_3 yields have been used for $[\text{C}_3\text{H}_6]_0$ in making the calculations, since the propane included in this figure essentially represents, in all probability, propylene that remained unreacted with nitrogen atoms and was subsequently hydrogenated. In the table are also included, for comparison, the experimentally determined yields of C_2 products, i.e. ethylene plus its probable hydrogenation product, ethane.

It is apparent that for both temperatures the calculated and experimental ethylene contents of the mixture issuing from the reaction vessel show the same general trends with propylene flow rates. The difference in the values of k_2/k_1 at the two temperatures corresponds to an activation energy for the attack of nitrogen atoms on propylene about 2 kcal. higher than the activation energy for

TABLE III
 COMPARISON OF CALCULATED AND EXPERIMENTAL YIELDS OF ETHYLENE

Temp. = 242°C., $k_2/k_1 = 0.75$			Temp. = 96°C., $k_2/k_1 = 1.75$		
[C ₃ H ₆] ₀	[C ₂ H ₄] _{calc.}	[C ₂ H ₄] _{exp.} (as total C ₂)	[C ₃ H ₆] ₀	[C ₂ H ₄] _{calc.}	[C ₂ H ₄] _{exp.} (as total C ₂)
2.12	Incomplete removal of		3.43	0.31	0.30
3.29	nitrogen atoms		4.05	0.59	0.86
3.46	0.95	0.33	4.52	0.63	0.61
4.12	0.62	0.69	5.17	1.15	1.24
5.08	1.78	1.62	5.78	1.38	1.31
5.12	1.84	0.90	5.82	1.22	1.35
6.55	2.54	2.50	9.02	2.36	2.60
7.01	2.78	2.95			
9.32	3.87	4.60			

the corresponding reaction with ethylene. No reliable values for the individual activation energies are possible from the available data, owing to the complete consumption of the reactant that is present in smaller amount. However, the upper limit of the activation energy for the ethylene reaction is almost certainly less than 4 kcal. (14), and probably less than about 2 kcal. (8). Hence, the activation energy for the nitrogen atom - propylene reaction may be taken as less than 6 kcal., and probably less than 4 kcal.

Note added in proof (prompted by discussions at the meeting of the Faraday Society, Toronto, September 8 - 9, 1952). The results of this investigation, and of previous similar studies in this laboratory, have been interpreted by assuming atomic nitrogen to be the reactive species in active nitrogen. This view is based mainly on the approximate correspondence between the amount of nitrogen-containing products of reaction and the nitrogen atom content of the active nitrogen determined by Wrede gauge measurements, although the questionable reliability of atom concentrations inferred from such measurements is recognized. Should it be subsequently proven that other reactive species are involved, e. g. the N₃ molecule, it seems likely that the fundamental kinetic features could be represented with relatively little modification of the tentative schemes based on atomic nitrogen.

REFERENCES

1. BAWN, C. E. H. and DUNNING, W. J. Trans. Faraday Soc. 35:185. 1939.
2. BAWN, C. E. H. and MILSTED, J. Trans. Faraday Soc. 35:889. 1939.
3. BAWN, C. E. H. and TIPPER, C. F. H. Discussions Faraday Soc. 2:104. 1947.
4. BLADES, H. and WINKLER, C. A. Can. J. Chem. 29:1022. 1951.
5. DOUGLAS, A. E. and HERZBERG, G. Can. J. Phys. 29:294. 1951.
6. GEIB, K. H. and HARTECK, P. Ber. 66(B):1815. 1933.
7. GREENBLATT, J. H. and WINKLER, C. A. Can. J. Research, B,27:721. 1949.
8. GREENBLATT, J. H. and WINKLER, C. A. Can. J. Research, B,27:732. 1949.
9. LAIDLER, K. J. and CASEY, E. J. J. Chem. Phys. 17:1087. 1949.
10. LE ROY, D. J. Can. J. Research, B,28:492. 1950.
11. POOLE, H. G. Proc. Roy. Soc. (London), A,163:404. 1937.
12. RABINOVITCH, B. S. DAVIES, S. G., and WINKLER, C. A. Can. J. Research, B,21: 251. 1943.
13. STEACIE, E. W. R. Atomic and free radical reactions. Reinhold Publishing Corporation, New York. 1946.
14. VERSTEEG, J. and WINKLER, C. A. Unpublished results.

MOLTEN SALTS

ELECTRICAL CONDUCTIVITY IN THE SYSTEM SILVER NITRATE-SODIUM NITRATE¹

BY JUNE BYRNE, HELEN FLEMING, AND F. E. W. WETMORE

ABSTRACT

Conductivity and density data have been obtained for the system silver nitrate-sodium nitrate. The Arrhenius energy of activation for electrical migration in sodium nitrate and in the binary melts decreases with rising temperature above the melting point, as was shown previously for silver nitrate. The equivalent conductivity isotherms for the binary melts are almost linear in the mole fraction.

MATERIALS AND PROCEDURE

Silver nitrate and sodium nitrate of reagent grade were recrystallized from water three times. The apparatus and method used for determining conductivity and density were essentially the same as those described by Spooner and Wetmore (5).

RESULTS AND DISCUSSION

In Table I are shown interpolated values of the specific conductivity of the unary and binary melts. In Table II are given coefficients for calculating the densities of the melts in the units gm. cm.⁻³

Data for sodium nitrate have been reported earlier (3, 4). The density data of Table II are in fair agreement with those cited; except for the two lowest entries of Table I, the conductivity values lie between those of the two sets cited.

From the data of Tables I and II the values of the equivalent conductivities of the melts have been computed. Although the relation between equivalent conductivity and temperature is linear or approximately so for the melts over the range of temperature studied, there is no theoretical basis for such behavior

TABLE I
SPECIFIC CONDUCTIVITY OF SILVER NITRATE-SODIUM NITRATE MELTS

Temp., °C.	Weight, %						
	0	10	20	30	40	60	100
	Mole %						
	0	5.27	11.12	17.66	25.01	42.88	100
Proportion of silver nitrate							
370	1.251	1.267	1.264	1.277	1.272	1.289	
360	1.209	1.224	1.223	1.235	1.230	1.247	
350	1.165	1.180	1.182	1.194	1.189	1.204	
340	1.120	1.134	1.139	1.150	1.147	1.161	1.180
330	1.076	1.088	1.094	1.104	1.103	1.118	1.141
320	1.032	1.041	1.046	1.057	1.059	1.075	1.100
310	0.987	0.995	1.001	1.009	1.013	1.032	1.059
300		0.948	0.954	0.960	0.967	0.987	1.017
290		0.900	0.907	0.910	0.920	0.941	0.973
							1.010

¹ Manuscript received July 8, 1952.

Contribution from the Electrochemical Laboratory, University of Toronto, Toronto, Canada.

TABLE II
DENSITY OF SILVER NITRATE - SODIUM NITRATE MELTS
Density, gm. cm.⁻³ = $a - b(t - 300)$. $t = ^\circ\text{C}$.

Wt. % silver nitrate	0	10	20	30	40	60	80	100
a	1.914	2.013	2.126	2.249	2.379	2.764	3.169	3.867
10^6b	70	71	77	79	79	70	90	100

and the simple Arrhenius equation used in previous work (5) has been applied. Smoothed values of the activation energy thus calculated are given in Table III. There appears to be a maximum in the activation energy - composition curve between 0 and 20 mole % silver nitrate, which decreases with rising temperature. However, the apparent maximum is little more than can be accounted for in terms of the calculated experimental error (about 70 cal. mole⁻¹). Furthermore, a plot of the equivalent conductivity against mole % shows but little deviation from linearity, which is taken to indicate that there is no marked complexity of the binary melts.

TABLE III
ENERGY OF ACTIVATION FOR CONDUCTIVITY, CAL. MOLE⁻¹

Temp., °C.	Weight % silver nitrate							
	0	10	20	30	40	60	80	100
365	3120	3150	2930	2960	2930	2920		
345	3200	3260	3100	3140	3010	2940		
325	3290	3380	3270	3350	3170	2960	2770	2690
305	(3380)	3490	3440	3550	3340	3120	2860	2710

It should be noted that there is no simple theory to correlate energy of activation and composition for this system. Frenkel's theory (1, 2) applies only with the assumption of a single conducting ion species; here there are two cations. The analogue of Frenkel's derivation takes the form

$$\Lambda = A. \exp(-\Delta U_1/RT) + B. \exp(-\Delta U_2/RT) = C. \exp(-\Delta U/RT),$$

in which A and ΔU_1 refer to one cation, B and ΔU_2 to the other, and C and ΔU to the binary melt. It is evident that there can be no simple relation between ΔU and the composition of the melt so long as ΔU_1 and ΔU_2 are of the same order of magnitude.

ACKNOWLEDGMENT

Grateful acknowledgment is made to the Advisory Committee on Scientific Research of this University for financial support of this project.

REFERENCES

1. FRENKEL, J. Bull. acad. sci. U.R.S.S. Sér. phys. 3: 287. 1937.
2. FRENKEL, J. Kinetic theory of liquids. The Clarendon Press, Oxford. 1946. p. 439.
3. GOODWIN, H. M. and MAILEY, R. D. Phys. Rev. 25: 469. 1907; 26: 28. 1908.
4. JAEGER, F. M. and KAPMA, B. Z. anorg. Chem. 113: 27. 1920.
5. SPOONER, R. C. and WETMORE, F. E. W. Can. J. Chem. 29: 777. 1951.

SYNTHESIS OF ORGANIC DEUTERIUM COMPOUNDS

III. 1,2-DIBROMOETHANE- d_4 AND ITS DERIVATIVES¹

BY L. C. LEITCH² AND A. T. MORSE²

ABSTRACT

Acetylene and hydrogen bromide react thermally without catalysts as well as photochemically to give high yields of 1,2-dibromoethane. The preparation of the following compounds containing 99+ % deuterium is described: acetylene- d_2 , 1,2-dibromoethane- d_4 , 1,2-dibromoethane-1,2- d_2 , ethylene- d_4 , 1,2-dichloroethane- d_4 , and ethylene- d_4 oxide. The vapor pressure of ethylene- d_4 oxide was determined in the temperature range -42 to 0°C .

INTRODUCTION

Several deuterated organic compounds containing at least 99 atom % deuterium were required for investigations now in progress by Steacie and co-workers (8). It was felt this need might best be met by preparing a few basic compounds which would serve as starting materials in the synthesis of others as needed. After careful consideration 1,2-dibromoethane- d_4 was selected as one which would meet this requirement since it is easily converted into ethylene- d_4 from which a large number of other useful deuterated compounds are readily accessible.

Wilson and Wylie (11) reported the preparation of deuterated 1,2-dibromoethane of high isotopic purity from acetylene- d_2 and deuterium bromide in the presence of activated carbon at 180°C . The main drawback of this synthesis is that a large volume of deuterium bromide is required to remove adsorbed hydrogen on the catalyst and to activate it. Furthermore, the best yield of 1,2-dibromoethane- d_4 was only 70%. Photochemical addition of deuterium bromide to acetylene- d_2 was used by Jungers and Verhulst (5) to prepare considerable amounts of 1,2-dibromoethane- d_4 in quantitative yield. To account for the influence of ultraviolet illumination on the reaction, although neither reactant absorbs light of the frequency employed, they assumed that traces of impurities in the acetylene had photosensitized the reaction. In the absence of sunlight no reaction between acetylene and fuming hydrobromic acid was observed at 100°C . over a period of several months. Several years previously Wibaut (10) had likewise observed no reaction between acetylene and hydrogen bromide at 100°C . in the absence of catalysts such as silica gel impregnated with mercuric bromide. However, Bauer (1) patented the preparation of 1,2-dibromoethane in excellent yields from acetylene and hydrogen bromide either under the influence of sunlight or in the presence of oxygen or ozone. These conflicting observations indicate that the reaction in question requires further investigation.

In the present work experiments were made in the apparatus shown in Fig. 4

¹ Manuscript received August 12, 1952.

Contribution from the Division of Chemistry (Applied), National Research Laboratories. Issued as N.R.C. No. 2850.

² Present address—Division of Pure Chemistry, National Research Council, Ottawa, Ontario.

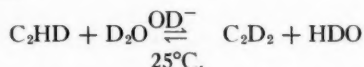
to determine whether a thermal reaction occurs between acetylene and hydrogen bromide, and if so, under what conditions. Hydrogen bromide and acetylene were introduced into the reactor in the ratio 2:1 by volume respectively until the pressure was nearly atmospheric. Reaction took place rapidly not only when the flask was irradiated with ultraviolet light but also in diffused sunlight and even in total darkness. Several liters of acetylene and hydrogen bromide reacted in this manner to give nearly quantitative yields of 1,2-dibromoethane.

Before repeating this work with deuterated reactants it was thought advisable to react hydrogen bromide under the same conditions with acetylene which had been prepared in the laboratory from calcium carbide and water. To obtain a rapid reaction in this case it was essential to purify the crude acetylene by bubbling it through concentrated sulphuric acid. When this treatment was omitted reaction was very sluggish and eventually stopped. Several other reagents besides sulphuric acid were tried, such as dilute aqueous sodium hydroxide, soda lime, and finally 5% aqueous chloramine-T as reported by Kennedy and Holm (6). None of these effectively removed the inhibitor. Activated granular carbon was very efficient with acetylene but the deuterium content of deuterioacetylene was seriously reduced by exchange with hydrogen adsorbed on the carbon. For example, the deuterium content of the acetylene- d_2 fell from 96 to 52 mole % C_2D_2 after passage through activated carbon which had been degassed under vacuum overnight. Fortunately, acetylene- d_2 underwent no detectable loss of deuterium during passage through sulphuric acid. This reagent is believed to remove traces of hydrogen sulphide or phosphine present in the crude acetylene. It was easily established that hydrogen sulphide acts as a powerful inhibitor by introducing a trace of the gas while rapid reaction was in progress between acetylene and hydrogen bromide. The reaction stopped at once. The apparatus had to be washed with concentrated nitric acid to remove the inhibitor. It appears therefore that, with suitably purified acetylene, addition of hydrogen bromide takes place rapidly in the absence of ultraviolet light and in fact even in total darkness.

In order to obtain 1,2-dibromoethane- d_4 containing at least 99 atom % deuterium it was, of course, necessary to make sure that the isotopic purity of the reactants was of the same order. The deuterium bromide used was prepared by the action of deuterium oxide (99.8 mole % D_2O) on redistilled phosphorus tribromide. As the mass spectrum of the product could not be interpreted accurately in the spectrometer available, the apparatus was always flushed out once with deuterium bromide before use. This procedure was evidently satisfactory since the deuterium content of the dibromoethane never fell below that of the acetylene- d_2 employed for the reaction.

The preparation of acetylene- d_2 with a deuterium content in excess of 99 atom % proved to be more difficult. Previous workers had assumed the isotopic purity of the acetylene- d_2 to be as high as that of the deuterium oxide used in its preparation. Our experience has shown this assumption to be incorrect. When deuterium oxide (99.8 mole % D_2O) was added to calcium carbide the acetylene- d_2 evolved analyzed on the average 97 mole % C_2D_2 . Its deuterium

content was obviously too low for our purpose. Since the equilibrium constant at 25°C. for the reaction



is reported to be 1.37 (7), the acetylene- d_2 would probably be rapidly enriched by repeated exchange with alkaline deuterium oxide provided that intimate contact was obtained between the gaseous and liquid phases. After four exchanges in the apparatus shown in Fig. 3 the deuterium content attained a constant value of 98.7 mole % C_2D_2 or 99.4 atom % D. The progressive enrichment with each exchange is shown in Table I. Table II shows the deuterium content of acetylene- d_2 before and after exchange in a series of experiments. For the preparation of acetylene- d_2 for synthetic purposes this procedure is simpler and more economical than collecting the acetylene- d_2 in fractions and burning those of low deuterium content to recover the deuterium.

TABLE I

No. of exchanges	Deuterium content* (mole % C_2D_2)
0	94.0
1	96.2
2	97.8
3	98.5
4	98.7
5	98.8

*Corrected for C^{13} .

TABLE II

No. of experiment	Deuterium content* (mole % C_2D_2)		Remarks
	Before exchange	After exchange	
1	94.0	97.8	Same carbide as 2 Same carbide as 2 New charge of carbide
2	96.4	98.7	
3	—	98.8	
4	—	98.4	
5	97.0	98.9	
6	99.1	98.7	

*Corrected for C^{13} .

Acetylene- d_2 and deuterium bromide reacted at a somewhat slower rate than the ordinary compounds to give quantitative yields of 1,2-dibromoethane- d_4 . Incidental to this work was the preparation of 1,2-dibromoethane-1,2- d_2 from ordinary acetylene and deuterium bromide. The yields were similar.

Ethylene- d_4 was prepared in excellent yield by the action of zinc dust suspended in dioxane on 1,2-dibromoethane- d_4 . Ethylene-1,2- d_2 was prepared similarly

from 1,2-dibromoethane-1,2- d_2 . The addition of chlorine to ethylene- d_4 gave 1,2-dichloroethane- d_4 which has not been previously reported.

Finally, ethylene- d_4 oxide was prepared from ethylene- d_4 in two steps. An aqueous solution of ethylene- d_4 chlorohydrin was obtained by adding hypochlorous acid to ethylene- d_4 as described by Gomberg (4). The chlorohydrin was not isolated from the solution but converted directly into ethylene- d_4 oxide by distillation from dilute alkali.

Since ethylene- d_4 oxide is now reported for the first time it was thought of interest to compare its vapor pressure with that of the ordinary compound. The measurements were made in an apparatus similar to that of Booth and Swinehart (2). The values obtained for the vapor pressure of ethylene- d_4 oxide in the range -42 to 0°C . are shown in Table III and plotted logarithmically in Fig. 1. In contrast with the deuterated organic compounds containing C-D bonds reported up to now, the vapor pressure of ethylene- d_4 oxide is slightly

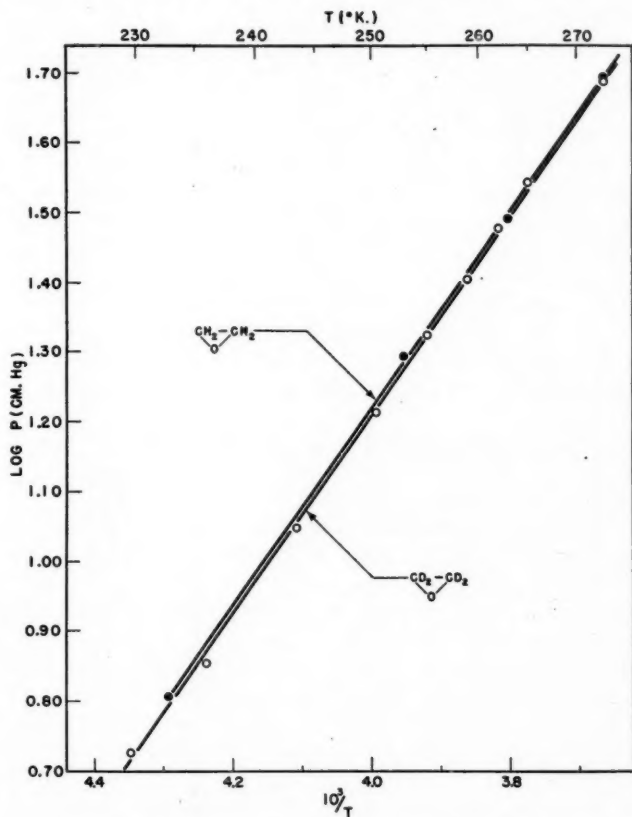


FIG. 1. Vapor pressures of ethylene oxide and ethylene- d_4 oxide.

TABLE III
 VAPOR PRESSURE OF ETHYLENE- d_4 OXIDE

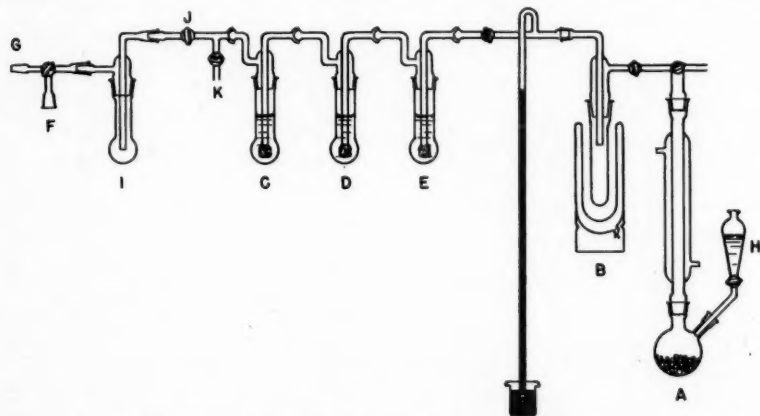
Temp. (°C.)	Vapor pressure (mm.)
0	48.47
- 7.9	34.86
- 10.95	29.96
- 13.9	25.31
- 17.9	21.04
- 22.6	16.30
- 29.5	11.14
- 37.0	7.13
- 42.7	5.32

decreased rather than increased as a result of deuterium substitution. No satisfactory explanation for this fact can be offered at present.

EXPERIMENTAL

Acetylene- d_2

This compound was prepared in the apparatus shown in Fig. 2. A large piece of fresh calcium carbide was broken up in an iron mortar into small chips which were then sorted out, selecting only those with a bright surface and discarding the remainder. Seventy-five grams of this material were placed in the generator *A*. The trap *B* was cooled to -40°C . with dry ice and acetone. The three gas wash bottles *C*, *D*, *E* with sintered glass tips were each filled with 50 ml. of concentrated sulphuric acid. A gas holder of 8 liters' capacity (not shown in the figure) containing mercury was connected to the apparatus at *F*. After evacuating the system to 1 mm. or less at *G*, a solution of deuterium oxide (22.0 gm.; 99.8 mole %) in dry dioxane (20 ml.) which had been distilled over sodium was added dropwise through funnel *H*. By carefully cooling trap *I* with liquid nitrogen, the deuteroacetylene generated was slowly sucked through the gas


 FIG. 2. Apparatus for preparation of acetylene- d_2 .

wash bottles and frozen in the trap. The gas was then distilled into the holder by closing stopcock *J* and removing the liquid nitrogen from trap *I*. Towards the end of the experiment it was necessary to apply heat to the generator. The deuterium content of the product averaged 97 mole % C_2D_2 . The yield of deuterioacetylene was 70–75% based on the deuterium oxide consumed.

Since the isotopic purity of the deuterioacetylene was not high enough for the present purpose, it was enriched in deuterium by repeated exchange with alkaline deuterium oxide in the apparatus shown in Fig. 3. It consists of two wash bottles *A* and *B* each containing 25 ml. of heavy water to which a small pellet of metallic sodium had been added, a manometer, a drying tube filled with indicating Drierite, a trap *C* to condense the acetylene- d_2 , and a bypass *E*.

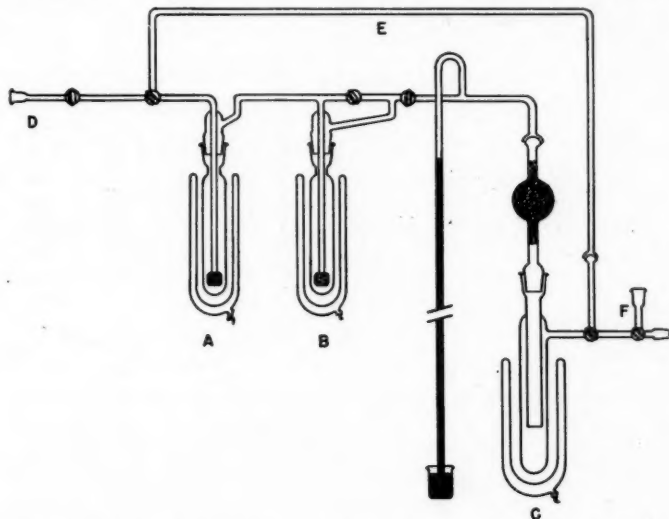


FIG. 3. Apparatus for enrichment of acetylene- d_2 by exchange with D_2O .

After the apparatus was evacuated, deuterioacetylene from the gas holder was introduced at *D*. The exchanged acetylene was frozen with a Dewar flask of liquid nitrogen which was placed at such a height under *C* that the acetylene was bubbled through the wash bottles at the rate of about 4 liters per hour. When the exchange was complete, the acetylene was distilled back to the holder through the bypass *E*. A sample of gas was collected at *F* after each exchange and analyzed. The process was repeated until the deuterium content remained constant. This was generally the case after three or four exchanges. The final product contained 98.7 mole% C_2D_2 . There was practically no loss of acetylene- d_2 during these operations.

1,2-Dibromoethane- d_4

The reaction between acetylene- d_2 and deuterium bromide was carried out in the apparatus illustrated in Fig. 4. The U-tubes *A* and *B* were half-filled with

freshly distilled phosphorus tribromide. Trap *C* was cooled to $-40^{\circ}\text{C}.$ to remove any phosphorus tribromide vapor in the deuterium bromide. The latter was condensed in a receiver *D* cooled to $-78^{\circ}\text{C}.$ with dry ice and acetone. The manometer at *E* was used to indicate the pressure in the generator; that at *F* to meter deuterium bromide and acetylene into the reactor and to observe the rate of reaction. The reactor *G* (2.0 l.) is similar to that reported by Taylor and Morey (9). The gas holder *H* contained the deuterioacetylene over mercury.

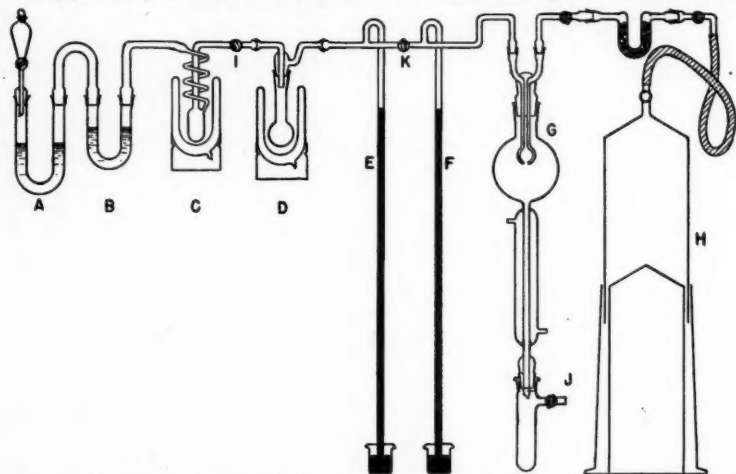
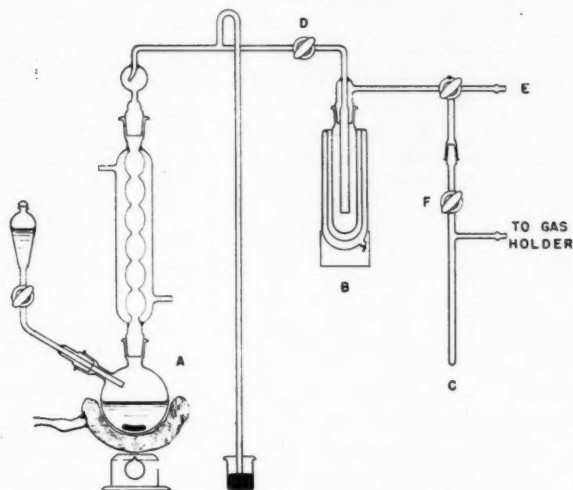


FIG. 4. Apparatus for preparation of deuterium bromide and 1,2-dibromoethane- d_4 .

At the start of an experiment the apparatus was evacuated to 1 mm. or less at *J* and the stopcock was closed. Deuterium oxide (99.8 mole%) was added dropwise through the funnel to the phosphorus tribromide. The deuterium bromide initially generated was used to flush the entire apparatus and removed through *J*. The rest of the deuterium bromide was condensed in *D*. When 10 to 20 ml. of clear colorless liquid had collected, the generator was closed off at *I* and deuterium bromide was distilled into the reactor until the pressure was 500 mm. Acetylene- d_2 (98.8 mole% C_2D_2) was then added until the pressure was nearly atmospheric and finally a few millimeters of dry air. After a variable induction period, or irradiation for a few minutes with ultraviolet light, the manometer began to rise and the surface of the reactor became covered with condensed dibromoethane. The proportion of deuterium bromide to acetylene- d_2 was kept at 2:1 during the entire run. The yield of crude dibromoethane which collected in the receiver was nearly quantitative. It was washed out with methylene chloride and shaken with dilute potassium carbonate solution until free of acid, dried over solid potassium carbonate, and distilled. The yield of 1,2-dibromoethane- d_4 , b.p. $129.5^{\circ}\text{C}.$, was nearly quantitative. The product analyzed 98.0 mole % $\text{C}_2\text{D}_4\text{Br}_2$ and 2.0% $\text{C}_2\text{D}_3\text{HBr}_2$ by mass spectrometry; d_4^{20} , 2.2266, n_D^{20} , 1.5360.

Ethylene- d_4

This compound was prepared by treating 1,2-dibromoethane- d_4 with zinc

FIG. 5. Apparatus for preparation of ethylene- d_4 .

dust suspended in dioxane in the apparatus shown in Fig. 5. Zinc dust (40.0 gm.) and a crystal of sodium iodide were placed in the two-necked flask *A* and the apparatus was evacuated at *E*. Trap *B* was kept at -78°C . with dry ice and acetone. With stopcock *D* closed, a few milliliters of solution of 1,2-dibromoethane- d_4 (38.4 gm.; 98.0 mole% $\text{C}_2\text{D}_4\text{Br}_2$) in dioxane (50 ml.) was added slowly to the zinc. The mixture was heated gently with stirring. When the ethylene- d_4 evolved was at a pressure of nearly 1 atm., stopcock *D* was opened and the ethylene- d_4 was collected in the gas holder over mercury. The contents of the funnel were then added dropwise while the suspension was slowly heated to boiling. The ethylene- d_4 in the apparatus at the end of the experiment was frozen in trap *C* with liquid nitrogen, stopcock *F* was closed, and the contents distilled into the gas holder. The yield of ethylene- d_4 was 4.0–4.3 liters (80–86% of the theoretical amount). It analyzed 97.8 mole% C_2D_4 (99.45 atom % D).

1,2-Dichloroethane- d_4

Methylene chloride (10.0 ml.) was placed in each of two spiral traps which were then tared and cooled to -78°C . in dry ice and acetone. Slightly more than the theoretical amount of chlorine to react with the ethylene- d_4 (8.0 liters) was condensed into the traps. The ethylene- d_4 was then bubbled through the dissolved chlorine at such a rate that practically no gas escaped from the second trap into a gas bottle containing bromine water (25 ml.). The reaction mixture was washed with cold dilute sodium hydroxide and then with ice water. After it was dried over potassium carbonate, the solution was fractionated in a small column filled with glass helices. The 1,2-dichloroethane- d_4 distilled at 82°C . The yield was 28.6 gm. (90% of the theoretical amount); d_4^{20} , 1.3034, n_D^{20} , 1.4420.

Ethylene- d_4 Oxide

Ethylene- d_4 chlorohydrin was prepared by Gomberg's method (4) from ethylene- d_4 (0.2 mole) and chlorine water. The reaction mixture which contained

5-6% ethylene chlorohydrin was slowly added to a suspension of calcium hydroxide (50.0 gm.) in water (200 ml.) heated under reflux. The ethylene- d_4 oxide evolved was condensed in a trap at -40°C . connected at the top of the condenser. When the solution of chlorohydrin had all been added, the ethylene oxide was swept out of the reactor into the trap by a stream of nitrogen. The ethylene- d_4 oxide was purified by distillation into a graduated trap cooled to -40°C . The yield of product, b.p. 12°C ., was 70% based on the ethylene- d_4 . Its mass spectrum indicated it contained 97.8 mole% $\text{C}_2\text{D}_4\text{O}$; in other words, the isotopic purity of the product was the same as that of the ethylene- d_4 . Analysis by the method of Eastham and Latremouille (3) gave 97.5% ethylene- d_4 oxide.

The vapor pressure measurements were made on a fraction of ethylene- d_4 oxide of constant vapor pressure at 0°C .

ACKNOWLEDGMENTS

The authors are grateful to Dr. F. P. Lossing and Miss F. Gauthier for measuring the mass spectra of several compounds, to Mr. R. Renaud for the drawings, to Mr. G. Latremouille for several density determinations, and to Mr. G. Benson of Shawinigan Chemicals Ltd. for the gift of a sample of calcium carbide.

REFERENCES

1. BAUER, W. German patent 368,467; 394,194. 1925.
2. BOOTH, H. S. and SWINEHART, C. F. J. Am. Chem. Soc. 57: 1333. 1935.
3. EASTHAM, A. and LATREMOUILLE, G. Can. J. Research, B, 28: 264. 1950.
4. GOMBERG, M. J. Am. Chem. Soc. 41: 1414. 1919.
5. JUNGERS, J. C. and VERHULST, J. Acad. roy. Belg., classe sci., Mém. 23 (2): 1. 1949.
6. KENNEDY, D. J. and HOLM, A. C. Can. Chem. Process Inds. 23: 490. 1939.
7. RYERSON, L. H. and GILLESPIE, B. J. Am. Chem. Soc. 59: 900. 1937.
8. STEACIE, E. W. R. and co-workers. To be published.
9. TAYLOR, R. F. and MOREY, G. H. Ind. Eng. Chem. 40: 432. 1948.
10. WIBAUT, J. Rec. trav. chim. 50: 313. 1931.
11. WILSON, C. L. and WYLIE, A. W. J. Chem. Soc. 596. 1941.

STERIODS. I. A CASE OF WALDEN INVERSION WITH NUCLEOPHILIC SUBSTITUTION AT POSITION 3 OF Δ^5 -STERIODS¹

By G. R. VAVASOUR, H. I. BOLKER, AND A. F. MCKAY²

ABSTRACT

When 3(β)-chlorocholest-5-ene is heated with benzylamine, inversion with partial racemization occurs to give a mixture of N-benzyl-3(α)-aminocholest-5-ene and N-benzyl-3(β)-aminocholest-5-ene. The configurations of the N-benzyl- and N-acetyl-3-aminocholest-5-enes have been determined.

The preparation of N,N-bis-(2-chloroethyl)-3(ξ)-aminocholest-5-ene hydrochloride is described.

The original aim of this work was to prepare N,N-bis-(2-chloroethyl)-3(ξ)-aminocholest-5-ene hydrochloride for testing as a possible chemotherapeutic agent for cancer. A low yield in the conversion of 3(β)-chlorocholest-5-ene to N,N-bis-(2-chloroethyl)-3(ξ)-aminocholest-5-ene hydrochloride led to an investigation of the reaction of benzylamine with 3(β)-chlorocholest-5-ene. Benzylamine was chosen because the properties of 3(ξ)-benzylaminocholest-5-ene and 6(ξ)-benzylamino-3:5-cyclocholestane are known (7).

The preparation of N,N-bis-(2-chloroethyl)-3(ξ)-aminocholest-5-ene hydrochloride from 3(β)-chlorocholest-5-ene was straightforward, although the yields at each stage were low. When 3(β)-chlorocholest-5-ene was heated with diethanolamine at 180°C., a 44% yield of N,N-bis-(2-hydroxyethyl)-3(ξ)-aminocholest-5-ene hydrochloride was obtained. If, however, the reaction temperature was raised from 180°C. to 265°C., the product consisted of a mixture of cholestadienes. No attempt was made to resolve this mixture. To complete the preparation of N,N-bis-(2-chloroethyl)-3(ξ)-aminocholest-5-ene hydrochloride (m.p. 227–229°C.), N,N-bis-(2-hydroxyethyl)-3(ξ)-aminocholest-5-ene hydrochloride was chlorinated with thionyl chloride in benzene.

Benzylamine and 3(β)-chlorocholest-5-ene heated together at 180°C. gave as the major identifiable product a hitherto undescribed benzylaminocholest-5-ene. This new benzylcholesterylamine melted at 90–91°C. ($[\alpha]_D^{25} - 9^\circ$). The position of the benzylamino group was established by degradation to cholesterylamine which was converted into an N-acetyl-3(ξ)-aminocholest-5-ene (m.p. 189°) (12). Since this N-acetyl-3(ξ)-aminocholest-5-ene had been prepared previously by reduction of the oxime of cholestene-one-3 with sodium and alcohol, the benzylamino group must be at position 3. However, it might be argued that the benzylamino group was originally at position 6 and then rearranged to position 3 during the course of the degradation. This possibility was eliminated by the failure of the hydrochloride of this benzylcholesterylamine to give cholesterylamine on refluxing with aniline. Benzyl-*i*-cholesterylamine under similar conditions gives a good yield of cholesterylamine (7). Also Julian

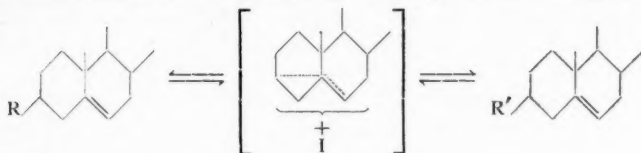
¹Manuscript received July 7, 1952.

Contribution from Defence Research Chemical Laboratories, Ottawa, Ont. and Department of Chemistry, Queen's University, Kingston, Ont. Issued as DRCL Report No. 97.

²Enquiries concerning this paper should be addressed to Defence Research Chemical Laboratories, Corner John and Sussex Streets, Ottawa, Ont.

et al. (7) have degraded benzyl-*i*-cholesterylamine to *i*-cholesterylamine without rearrangement. The position of the benzylamino group in the N-benzylcholesterylamine melting at 115.5–117°C. was shown previously by Julian *et al.* to be at C₃. The latter compound on degradation gave a 3-cholesterylamine which was converted into a 3-cholesterylacetamide melting at 243°C. Thus the N-benzylcholesterylamines melting at 90–91°C. ($[\alpha]_D - 9^\circ$) and 115.5–117°C. ($[\alpha]_D - 23^\circ$) are C₃ epimers. In accordance with the rule that the C₃α-form of any steroid will have a higher positive rotatory power than the C₃β-form (1), the low melting epimer is assigned the α-configuration, while the high melting form must possess the β-configuration. Moreover, since in the degradation of the benzylcholesterylamines the bond broken is between the N and benzyl group instead of the N–C₃ bond, no rearrangement is to be expected and the configurations of the cholesterylacetamides are established. The 3-cholesterylacetamide which melts at 245°C. (12) has the β-configuration and the 3-cholesterylacetamide melting at 189°C. possesses the α-configuration.

In the reaction of cholesteryl chloride with benzylamine some N-benzyl-3(β)-aminocholest-5-ene was obtained along with the main product N-benzyl-3(α)-aminocholest-5-ene. Since cholesteryl chloride (m.p. 96°C.) has been shown to possess the β-configuration (4,9) this reaction occurs with inversion and partial racemization. Generally substitution at position 3 of Δ⁵-steroids proceeds without inversion (4,6,9). This retention of configuration is explained by the participation of the double bond in the formation of a hybrid ion intermediate (1), which contributes to the stabilization of the pyramidal transition state (9).



Thus the chlorination of cholesterol with thionyl chloride proceeds with retention of configuration to give 3(β)-chlorocholest-5-ene and the acetolysis of cholest-5-ene-3(β)-ol *p*-toluenesulphonate gives cholest-5-ene-3(β)-ol acetate. The present work shows that the reaction of benzylamine with cholest-5-ene-3(β)-ol *p*-toluenesulphonate also occurs in the usual manner with retention of configuration. Thus the inversion obtained in the reaction of benzylamine with 3(β)-chlorocholest-5-ene was unexpected. It raises the question of the possible existence of inversions in other nucleophilic substitution reactions at position 3 of Δ⁵-steroids.

An attempted degradation of cholesterylamine in the usual manner to establish its configuration gave N-*p*-chlorophenyl-3(ξ)-aminocholest-5-ene.

EXPERIMENTAL³

3(β)-Chlorocholest-5-ene

Cholesteryl chloride was prepared by a modification of the method of Diels

³All melting points taken on a Kofler block. Analyses by Mr. C. W. Beazley, Skokie, Illinois.

and Blumberg (3). Fifty grams (0.129 mole) of cholesterol were added slowly to 50 gm. (0.42 mole) of thionyl chloride. The solution was stirred during the addition and the product crystallized within 10 min. After being allowed to stand for 24 hr., the solid was triturated with 500 cc. of 1% potassium hydroxide solution and extracted twice with ether. The combined ether extracts were washed with 1% aqueous potassium hydroxide solution followed by water until the water washings were neutral. Ether was removed from the dried ethereal solution and the residue was crystallized from acetone, yield 40 gm. (76.4%). This material melted at 95–96°C.; $[\alpha]_D^{25} - 26.4^\circ$ (CHCl_3). The physical constants for cholesteryl chloride recorded in the literature (2) are m.p. 95°C. and $[\alpha]_D^{20} - 27.4^\circ$ (CHCl_3).

Reaction of 3(β)-Chlorocholest-5-ene with Diethanolamine

A. At 265°C.

A mixture of 10 gm. (0.025 mole) of cholesteryl chloride and 2.6 gm. (0.025 mole) of diethanolamine was heated slowly to a temperature of 265°C. At this temperature signs of decomposition were in evidence so the reaction mixture was cooled. It was extracted with petroleum ether (b.p. 30–60°C.) and the ether extract taken to dryness. The residue was dissolved in refluxing ethanol (ca. 1000 cc.) and on cooling long needlelike crystals appeared. These crystals were removed by filtration and washed with ethanol, yield 3.5 gm. (38%, calculated as a mixture of cholestadienes). Five crystallizations from acetone raised the melting point from 68–70°C. to 77–78°C.; $[\alpha]_D^{25} - 116^\circ$ (CHCl_3). Calc. for $\text{C}_{27}\text{H}_{44}$: C, 87.97; H, 12.03%. Found: C, 87.92; H, 12.10%. Pure cholest-3:5-diene has a melting point of 80–81°C. and $[\alpha]_D^{20} - 129.6^\circ$ (CHCl_3) (10) while the physical constants for cholest-4:6-diene are m.p. 91–92°C.; $[\alpha]_D + 4.27$ (CCl_4) (5).

B. At 180°C.

3(β)-Chlorocholest-5-ene (25 gm., 0.062 mole) in 75 cc. of diethanolamine was heated with stirring at 180°C. for two hours. The reaction mixture was poured into 750 cc. of water and the aqueous suspension extracted thrice with ether. The ethereal solution was washed with water until no longer alkaline and then dried over anhydrous sodium sulphate. After concentration of the ether solution to ca. 600 cc., it was treated with dry hydrogen chloride. A gelatinous precipitate formed which was separated by centrifugation. The yield of red waxy solid was 14.0 gm. (44.3% based on the formation of *N,N*-bis-(2-hydroxyethyl)-3(ξ)-aminocholest-5-ene hydrochloride). Attempts to obtain a sharp melting product were unsuccessful so this reddish colored wax was used directly for chlorination to *N,N*-bis-(2-chloroethyl)-3(ξ)-aminocholest-5-ene hydrochloride.

N,N-Bis-(2-chloroethyl)-3(ξ)-aminocholest-5-ene Hydrochloride

Impure *N,N*-bis-(2-hydroxyethyl)-3(ξ)-aminocholest-5-ene hydrochloride (13.5 gm., 0.0265 mole) was dissolved in 100 cc. of benzene and treated with 14.7 gm. (0.12 mole) of thionyl chloride. This solution was refluxed for two hours and then allowed to stand overnight. The precipitate was washed white with acetone, yield 3.51 gm. (24.2%). Two crystallizations from absolute alcohol raised the melting point from 225–227°C. to 227–229°C.; $[\alpha]_D^{26} - 23.7^\circ$ (CHCl_3). Calc. for

$C_{31}H_{54}Cl_3N$: C, 68.03; H, 9.94; Cl, 19.46; N, 2.56%. Found: C, 68.61; H, 9.93; Cl, 19.03; N, 2.48%.

Reaction of Cholesteryl Chloride with Benzylamine

Cholesteryl chloride (23.9 gm., 0.059 mole) in 50 cc. of benzylamine (must be freshly distilled) was refluxed for two hours. After being cooled, it was added to 500 cc. of absolute ether and the precipitate of benzylamine hydrochloride was removed by filtration, yield 6.2 gm. (73.2%). A sample of this hydrochloride was converted to the picrate (m.p. 198–199°C.) in the usual manner. A mixed melting point determination with an authentic sample of benzylamine picrate established its identity. The ethereal filtrate was evaporated to dryness and the excess benzylamine removed by steam distillation. The residual mixture of oil and water was extracted with ether. After the ether solution was dried over Drierite it was treated with dry gaseous hydrogen chloride. A white precipitate was obtained which was filtered off and washed with ether, yield 7.5 gm. (24.9%). This mixture of benzylcholesterylamine hydrochlorides was shaken with a mixture of ether and 5% ammonium hydroxide solution until all the solid had dissolved. The ether layer was washed alkali-free with water, dried, and evaporated to dryness. The residual oil slowly crystallized after which it melted at 81–91°C., yield 6.32 gm. An aliquot (1.22 gm.) of this solid was dissolved in 50 cc. of petroleum ether and separated into its components by the liquid chromatogram method using 40 gm. of activated alumina (Alcoa, F-20, neutralized and reactivated) in a column of 24 mm. diameter. This column was washed with 50 cc. portions of solvent (*vide infra*).

LIQUID CHROMATOGRAM

Fraction No.	Solvent	Residue (mgm.)	m.p. (°C.)
1–5	Pet. ether (60–70°)	—	Oil
6–12	Pet. ether (60–70°) – benzene (9:1)	626	87.5–91
13–22	Pet. ether – benzene (from 9:1 to pure benzene) and benzene – ether (1:1)	269	Semicrystalline oil
23–25	Ether	149	105–111
26–27	Ether	60	Gum
28–29	Acetone	132	Gum

Fractions 6–12 were combined and crystallized from acetone giving 0.535 gm. of crystals melting at 90–91°C., $[\alpha]_D^{25} - 9^\circ$ ($CHCl_3$). Calc. for $C_{34}H_{52}N$: C, 85.83; H, 11.23; N, 2.95%. Found: C, 86.07; H, 11.07; N, 3.20%. This compound has been identified as N-benzyl-3(α)-aminocholest-5-ene. Fractions 13–22 inclusive on crystallizing from acetone gave another crop (0.065 gm.) of the same compound (m.p. 88.5–89.5°C.).

Fractions 23–29 were combined and crystallized from acetone to a constant melting point of 116.5–117.5°C., yield 0.225 gm. A mixed melting point determination with an authentic sample of N-benzyl-3(β)-aminocholest-5-ene (m.p. 116–117°C.) prepared from cholest-5-ene-3(β)-ol *p*-toluenesulphonate and benzylamine (7) gave no depression.

The ether filtrate from the hydrogen chloride treatment of the reaction mixture was washed with water until acid-free and evaporated to dryness. A viscous oil (13.3 gm.) was obtained. This oil yielded 1.52 gm. (5%) of crude N-benzyl-6(ξ)-amino-3:5-cyclocholestane hydrochloride (m.p. 185°C.). After purification from acetone-chloroform, it melted at 224–226°C. Its identity was established by a mixed melting point determination with an authentic sample of N-benzyl-6(ξ)-amino-3:5-cyclocholestane hydrochloride (m.p. 222–224°C.)⁴ prepared as described by Julian *et al.* (7).

In one reaction in which the heating of the cholesteryl chloride in benzylamine was continued for 18 hr., the ether solution, after precipitation of the benzyl-cholesterylamine with hydrogen chloride, gave a 31.5% yield of a mixture of cholestadienes, m.p. 77.5–78.2°C., $[\alpha]_D^{25} - 114.3^\circ$ (CHCl₃). Calc. for C₂₇H₄₄: C, 87.97; H, 12.03%. Found: C, 87.90; H, 12.14%.

Degradation of N-Benzyl-3(α)-amincholest-5-ene

N-Benzyl-3(α)-amincholest-5-ene (1.5 gm., 0.0032 mole) was dissolved in 50 cc. of absolute ether and treated at 0°C. with 7 cc. of an ether solution of hypochlorous acid (0.57 gm., 0.011 mole) (7). A white flocculent precipitate formed. This mixture was allowed to warm to room temperature after which it was washed successively with 10 cc. of cold 8% sulphonic acid, 10 cc. of cold 5% sodium hydroxide, and finally with cold water until alkali-free. The white precipitate remained throughout these operations and did not dissolve on the addition of 50 cc. of absolute ether. The solid, probably the N-chloramine (m.p. 222–235°C.), was separated by centrifuging and weighed (0.070 gm.). The dried ether solution and solid were combined and treated with 0.75 gm. of sodium in 75 cc. of absolute ethanol. A precipitate of sodium chloride slowly formed. The ether was distilled off and the remainder refluxed for 30 min. After cooling, 50 cc. of 1:5 hydrochloric acid was added and the mixture steam-distilled. The benzaldehyde in the distillate was precipitated as the 2,4-dinitrophenylhydrazone (m.p. 233–238°C.), yield 0.425 gm. (46.5%). A recrystallized sample (m.p. 236–238°C.) did not depress the melting point of an authentic sample of the 2,4-dinitrophenylhydrazone of benzaldehyde (m.p. 237–238°C.).

After addition of 25 cc. of 10% ammonium hydroxide to the residual aqueous suspension from the steam distillation, it was extracted with ether. This ethereal solution was washed to neutrality with water and then shaken with 5% hydrochloric acid. A white precipitate of cholesterylamine hydrochloride formed which was recovered by filtration and washed with ether, yield 0.55 gm. (41%). The melting point of the product was raised from 213–223°C. to 220–230°C. by crystallization from ethanol containing hydrochloric acid.

The cholesterylamine hydrochloride (0.35 gm., 0.00083 mole) was shaken with ether and 10% sodium hydroxide solution (20 cc.) until all the solid had dissolved. The ether solution was dried over potassium hydroxide pellets and then treated with 1 cc. of acetic anhydride. After this was refluxed for 10 min., the ether was distilled off and the remaining acetic anhydride decomposed with water. A white solid separated which was extracted with ether. The ether solution was

⁴Melting point determined with bath preheated to 190°C.

washed with 10% sodium carbonate solution followed by water until the water washings were neutral. On evaporation of the ether, an oily white solid (m.p. 130–178°C.) was obtained, yield 0.293 gm. (82.6%). Two crystallizations from methanol and one from acetone gave pure cholesterylacetamide melting at 188–189°C., yield 0.115 gm. (32.4%). Calc. for $C_{29}H_{49}NO$: C, 81.42; H, 11.56; N, 3.28%. Found: C, 81.37; H, 11.41; N, 3.15%. One of the cholesterylacetamides reported by Windaus and Adamla (12) melted at 190°C.

Treatment of N-Benzyl-3(α)-aminocholest-5-ene Hydrochloride with Aniline

Aniline (3 cc.) and N-benzyl-3(α)-aminocholest-5-ene hydrochloride (0.21 gm., 0.00041 mole) were refluxed for four hours. The cooled reaction mixture was dissolved in ether and shaken with 10% hydrochloric acid solution. A white precipitate formed which was filtered off and washed with ether, yield 0.175 gm. (83.4%). This hydrochloride was converted to the free base in the usual manner and crystallized from acetone, yield 0.11 gm. (56.4%). This material melted at 89.5–91°C. alone and on admixture with a known sample of N-benzyl-3(α)-aminocholest-5-ene. The mother liquor from this crystallization was taken to dryness and an infrared absorption spectrum of the residue taken. A comparison of this spectrum with that of pure cholesterylaniline showed the absence of cholesterylaniline in the reaction products.

Cholesterylaniline

Cholesterylaniline (m.p. 191.5–192.5°C.) was prepared in 74% yield by the method of Lieb *et al.* (8).

Attempted Degradation of Cholesterylaniline

Cholesterylaniline (2.0 gm., 0.0043 mole) was suspended in 75 cc. of absolute ether and cooled to 0°C. and 6 cc. of an ether solution of hypochlorous acid (0.28 gm., 0.0053 mole) added. This mixture was cooled to –20°C. and after 15 min. a clear solution was obtained. The ether solution was washed immediately with 10 cc. of cold 8% sulphuric acid, 10 cc. of cold 5% sodium hydroxide, and finally with water until the water washings were neutral. After the ether solution was dried over anhydrous sodium sulphate, 0.5 gm. of sodium dissolved in 50 cc. of absolute alcohol was added. Then the ether was evaporated off and the remaining alcoholic solution refluxed for 45 min. The precipitate (m.p. 140–173°C.) was removed by filtration, yield 1.72 gm. (80.6%). Several crystallizations from petroleum ether (b.p. 90–110°C.) raised the melting point to 192–193°C. Calc. for $C_{33}H_{50}NCl$: C, 79.95; H, 10.15; N, 2.83; Cl, 7.15%. Found: C, 80.31; H, 10.28; N, 3.17; Cl, 6.80%. A sample did not depress the melting point of a known sample of N-*p*-chlorophenyl-3(ξ)-aminocholest-5-ene (m.p. 192.5°C.).

N-p-Chlorophenyl-3(ξ)-aminocholest-5-ene

This compound was prepared by the method of Lieb *et al.* (8) by heating cholesteryl chloride (2.0 gm., 0.0049 mole) and *p*-chloroaniline (2.0 gm., 0.016 mole) together at 170–200°C. for 15 min. After the black mixture was cooled, it was triturated with alcohol and filtered, yield 2.06 gm. (83.5%). One crystallization from petroleum ether raised the melting point from 152–172°C. to 191.0–192.5°C.

Cholest-5-ene-3(β)-ol p-Toluenesulphonate

Fifty grams (0.129 mole) of cholesterol were converted to cholesteryl *p*-toluenesulphonate (m.p. 133–134.5°C.) in 82.4% yield by the method of Wallis *et al.* (11).

N-Benzyl-3(β)-aminocholest-5-ene

N-Benzyl-3(β)-cholesterylamine (m.p. 115.5–116°C.) and N-benzyl-*i*-cholesterylamine hydrochloride [m.p. 227–229°C. dec., $[\alpha]_D^{25} - 28^\circ$ (CHCl₃)] were prepared by the method of Julian *et al.* (7) in 15.8% and 27.1% purified yields respectively. Julian *et al.* (7) report a melting point of 115.5–117°C. for N-benzyl-3(β)-cholesterylamine and 217–218°C. ($[\alpha]_D^{25} - 27^\circ$) for N-benzyl-*i*-cholesterylamine hydrochloride.

ACKNOWLEDGMENT

The authors are grateful to the National Cancer Institute of Canada for financial support of part of this work and a grant-in-aid to one of them (H.I.B.). The infrared absorption spectra were determined by Dr. C. E. Hubley of Defence Research Chemical Laboratories, Ottawa.

REFERENCES

1. BERNSTEIN, S., HICKS, E. M., CLARK, D. M., and WALLIS, E. S. *J. Org. Chem.* 11: 646. 1946.
2. BEYNON, J. H., HEILBRON, I. M., and SPRING, F. S. *J. Chem. Soc.* 907. 1936.
3. DIELS, O. and BLUMBERG, P. *Ber.* 44: 2847. 1911.
4. DOBSON, R. M. and RIEGEL, B. *J. Org. Chem.* 13: 424. 1948.
5. ECK, J. C., VAN PEURSEM, R. L., and HOLLINGSWORTH, E. W. *J. Am. Chem. Soc.* 61: 171. 1939.
6. FIESER, L. F. and FIESER, M. *Natural products related to phenanthrene*. 3rd ed. Reinhold Publishing Corporation, New York. 1949. p. 642.
7. JULIAN, P. L., MAGNANI, A., MEYER, E. W., and COLE, W. *J. Am. Chem. Soc.* 70: 1834. 1948.
8. LIEB, H., WINKLEMAN, K., and KOEPL, F. *Ann.* 509: 214. 1934.
9. SHOPPEE, C. W. *J. Chem. Soc.* 1147. 1946.
10. SPRING, F. S. and SWAIN, G. *J. Chem. Soc.* 83. 1941.
11. WALLIS, E. S., FERNHOLZ, E., and GEPHART, F. T. *J. Am. Chem. Soc.* 59: 137. 1937.
12. WINDAUS, A. and ADAMLA, J. *Ber.* 44: 3051. 1911.

DIELECTRIC PROPERTIES OF POLYVINYL ACETALS¹

By B. L. FUNT AND T. H. SUTHERLAND

ABSTRACT

Measurements of dielectric dispersion in vinyl acetal and formal polymers were performed over the frequency range 0.050 to 100 kc. at temperatures between 25 and 135°C. The results reflect the effects of internal plasticization on the electrical properties of the polymers. With increasing size of the substituent groups from formal to butyral the dispersion range is shifted to lower temperatures at a given frequency. Electrical relaxation times and transition temperatures were obtained and values of enthalpies, free energies, and entropies of activation were calculated. A tentative physical picture of the mechanism of dielectric relaxation in these polymers was also formulated.

INTRODUCTION

The study of the electrical properties of linear polar polymers furnishes a promising avenue of approach to the elucidation of the structure and properties of these substances. The results of previous investigations, particularly those of Fuoss and his co-workers (7, 9), have shown that at least semiempirical agreement between measurements of dielectric dispersion and the physical and mechanical properties of polymers can be obtained.

When one seeks more quantitative correlation between electrical and physical properties the results are often disappointing. Although Boyer and Spencer (1), Tuckett (10), and others have attempted to relate dielectric dispersion with properties such as brittle points and second order transition temperatures, recent work by Dyson (2) showed that agreement for polyvinyl chloride was poor.

Since much of the previously reported work on dielectric dispersion has been confined to studies of plasticizer action, one finds that the number of polymers investigated is relatively small. It is apparent that further experimental work is necessary before adequate comparisons can be made.

It appeared to us that an investigation of a closely related family of linear polymers would yield results of interest. The polyvinyl acetals were chosen for this purpose. The results of our work on polyvinyl butyral have already been reported (6) and our investigation of polyvinyl formal and acetal is herewith presented.

EXPERIMENTAL

Apparatus

The experimental apparatus has already been described (6). Briefly it consisted of a General Radio, type 716 C, Capacitance Bridge with associated equipment and a parallel plate condenser which acted as a sample holder. The test condenser was placed in an insulated thermostated box whose temperature was automatically controlled to $\pm 0.1^\circ\text{C}$. The procedure for preparing disks of polymer and for coating samples has been described (6).

Several minor refinements in technique have now been adopted. In order to

¹Manuscript received June 23, 1952.

Contribution from Department of Chemistry, University of Manitoba, Winnipeg, Man. This work was carried out with the financial assistance of the National Research Council.

obtain samples of uniform thickness it was found that a final grinding and polishing of our pressed disks of polymer yielded samples uniform to ± 0.0003 in. It was also found advisable to insert thermocouple leads into our test condenser. This provided a more reliable measurement of the sample temperature than was obtainable from the average air temperature.

Materials

Samples of polyvinyl acetal (PVA), Alvar 7/70, and of polyvinyl formal (PVF), Formvar 15/95, were supplied to us by courtesy of Canadian Resins and Chemicals, Shawinigan Falls, Que. These resins had been prepared from Gelva (polyvinyl acetate) of molecular weight 33,000 and 60,000 respectively. A preliminary fractionation showed that these samples were of quite uniform molecular weight. The samples were dried *in vacuo* before use, and were then pressed into disks of approximately 0.050 in. thickness. It was found that PVF had to be conditioned at 100°C. for 24 hr. before reproducible results could be obtained.

Results

Measurements of the dielectric constant and loss factor were performed at

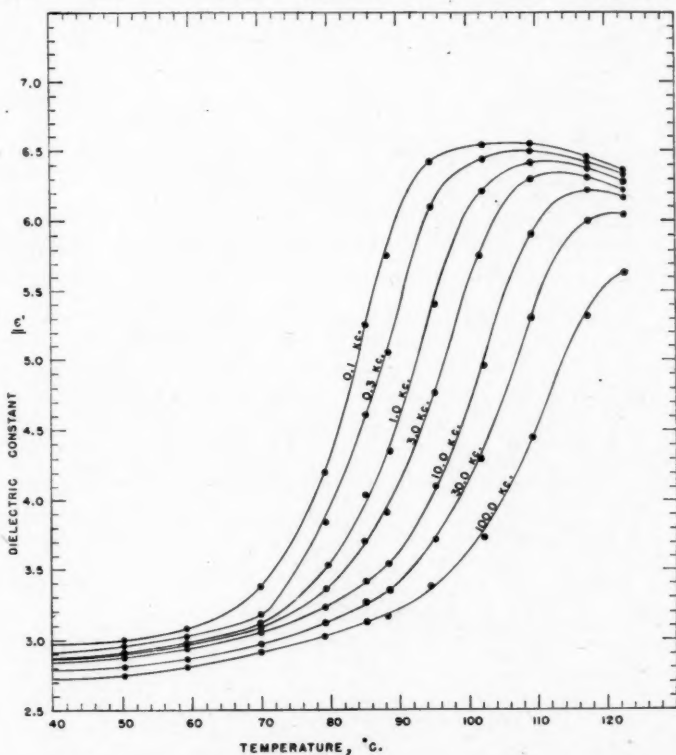


FIG. 1. Dielectric constants of polyvinyl acetal (PVA) at 0.1, 0.3, 1, 3, 10, 30, and 100 kc.

frequencies of 0.050, 0.1, 0.3, 1.3, 10, 30, and 100 kc. at temperatures ranging from 25 to 135°C. Fig. 1 shows the values of dielectric constants for PVA in the dispersion region. The loss factors for this substance are shown in Fig. 2. It is evident that dielectric dispersion occurred at all frequencies in the temperature range investigated. Similar data for PVF are shown in Figs. 3 and 4 where the results of dielectric constant and loss factor measurements respectively are presented. It can be noted that the dispersion range has been shifted to consider-

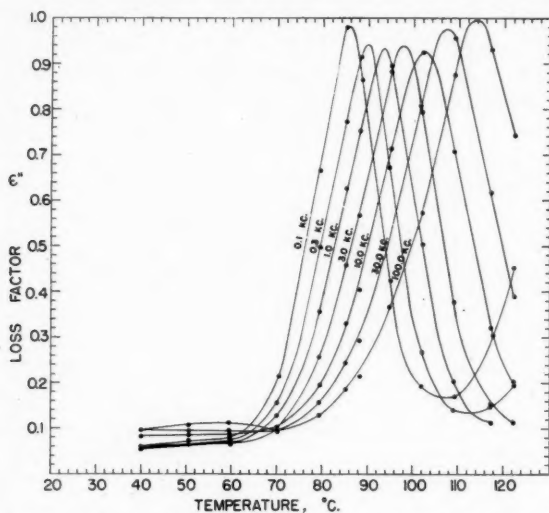


FIG. 2. Loss factors of polyvinyl acetal at frequencies of 0.1, 0.3, 10, 30, and 100 kc.

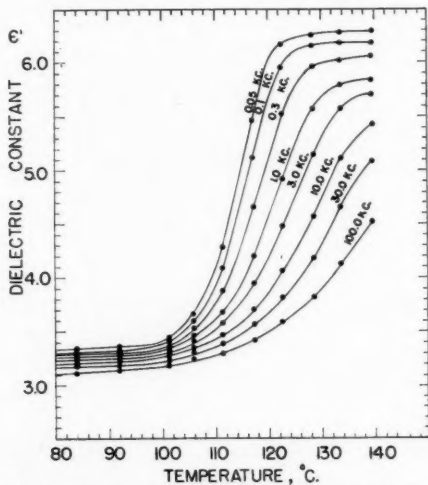


FIG. 3. Dielectric constants of polyvinyl formal (PVF).

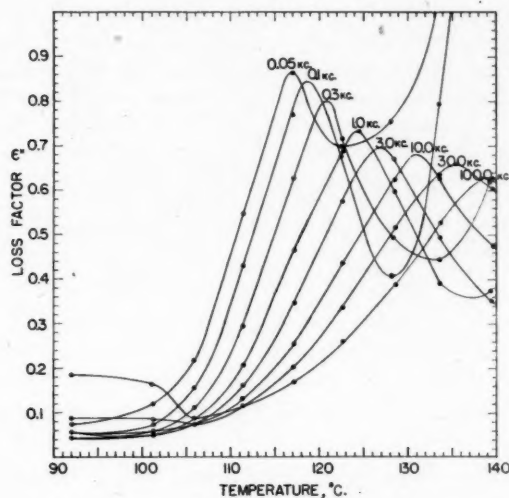


FIG. 4. Loss factors of polyvinyl formal.

TABLE I

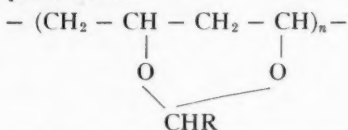
DIELECTRIC CONSTANTS AND LOSS FACTORS FOR POLYVINYL ACETAL AND POLYVINYL FORMAL IN THE DISPERSION REGION

Temp., °C.	Frequency—kc.													
	0.1		0.3		1.0		3.0		10.0		30.0		100.0	
	ϵ'	ϵ''	ϵ'	ϵ''	ϵ'	ϵ''	ϵ'	ϵ''	ϵ'	ϵ''	ϵ'	ϵ''	ϵ'	ϵ''
<i>Polyvinyl acetal</i>														
40	2.95	0.061	2.91	0.053	2.90	0.055	2.88	0.060	2.84	0.083	2.79	0.097	2.72	0.095
50	3.00	0.069	2.96	0.064	2.94	0.063	2.90	0.064	2.87	0.085	2.82	0.095	2.75	0.108
60	3.08	0.079	3.03	0.074	3.00	0.070	2.96	0.067	2.94	0.087	2.89	0.095	2.81	0.111
70	3.36	0.200	3.17	0.158	3.13	0.129	3.08	0.099	3.04	0.101	2.99	0.097	2.93	0.098
80	4.33	0.707	3.94	0.523	3.56	0.383	3.39	0.274	3.26	0.273	3.14	0.163	3.04	0.132
90	6.02	0.774	5.36	0.944	4.58	0.828	4.13	0.653	3.66	0.502	3.40	0.354	3.21	0.261
100	6.53	0.218	6.40	0.344	6.08	0.616	5.55	0.895	4.62	0.895	4.18	0.733	3.66	0.505
110	6.54	0.174	6.50	0.137	6.43	0.187	6.32	0.324	6.00	0.667	5.46	0.938	4.56	0.912
120	6.38	0.371	6.37	0.168	6.34	0.116	6.27	0.128	6.21	0.246	6.04	0.494	5.56	0.829
<i>Polyvinyl formal</i>														
90	3.32	0.052	3.30	0.041	3.28	0.043	3.25	0.050	3.22	0.060	3.18	0.089	3.14	0.190
100	3.38	0.065	3.34	0.052	3.32	0.048	3.29	0.048	3.27	0.057	3.22	0.085	3.18	0.170
110	3.92	0.348	3.76	0.237	3.62	0.169	3.53	0.132	3.43	0.111	3.35	0.098	3.28	0.105
120	5.68	0.813	5.10	0.782	4.57	0.581	4.18	0.470	3.87	0.348	3.68	0.269	3.49	0.213
130	6.17	0.433	5.99	0.363	5.68	0.532	5.30	0.617	4.75	0.666	4.31	0.556	3.91	0.423
140	6.19	6.07	0.663	5.84	0.388	5.73	0.342	5.44	0.469	5.12	0.595	4.57	0.624

ably higher temperatures in this substance. Only at the lower frequencies is the dispersion region completely covered in the experimental temperature range. It was considered inadvisable to work at more elevated temperatures because of the dangers of decomposing the samples. The data are summarized in Table I.

DISCUSSION

A consideration of the structure of the polyvinyl acetals shows that the results are in qualitative agreement with the accepted picture of these polymers. The polymer can be represented as



where R = C₃H₇ for butyral (PVB), CH₃ for acetal (PVA), and H for formal (PVF).

It is evident that the polar groups are bonded to the main chain fairly rigidly. This would be expected to yield the stiff physical structure associated with these materials and one would expect the dielectric dispersion to occur at relatively high temperatures and at low frequencies.

The steric effect of the substituent R is also evident from both the electrical measurements and the physical properties. In passing from PVB to PVA the dispersion region at a given frequency is moved by 7.5°C.; a further shift of 31°C. is observed in passing from acetal to formal. This is evident in Fig. 5

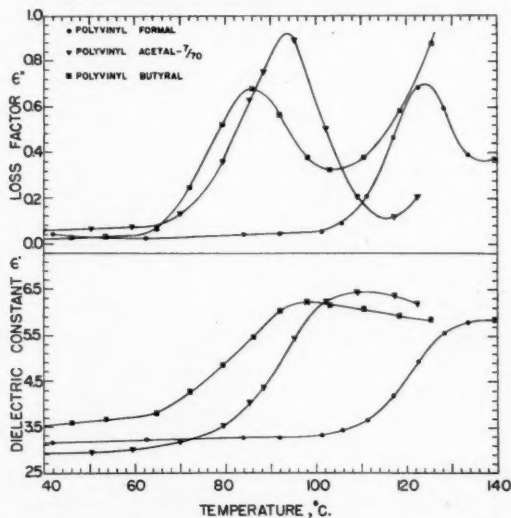


FIG. 5. Loss factors (top) and dielectric constants (bottom) of polyvinyl butyral, acetal, and formal at 1 kc.

where the loss factors and dielectric constants for the three polymers are shown for a frequency of 1 kc.

It is interesting to consider the change in electrical and physical properties as due to "internal plasticization". An analogous shift in properties from polyvinyl formal to acetal could probably be achieved by the addition of foreign plasticizer molecules. In the present instance it can be seen that the function of the plasticizer molecules is achieved by the chain radical substituent. As the size of this group increases the chains are forced further apart. This looser physical structure results in greater freedom of rotation for the polar groups and consequently in a lower dispersion temperature. By analogy it can be seen that a more flexible polymer should be obtained.

An analysis of the data presented in Figs. 1-4 was made on the basis of the theory of absolute reaction rates. At a temperature obtained from the maximum of the loss factor curve at a given frequency, the relaxation time, τ , was defined by the relationship

$$\tau = \frac{1}{\omega_{\max.}}$$

where $\omega_{\max.}$ is the angular frequency of maximum absorption.

The logarithmic plot of the relaxation time against the reciprocal absolute temperature proved to be linear for the acetals as shown in Fig. 6. It should be

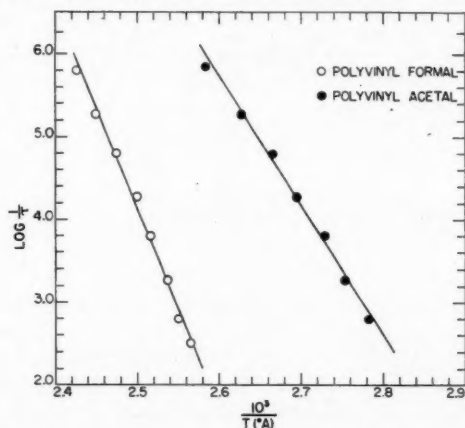


FIG. 6. Variation of relaxation time with reciprocal temperature of polyvinyl formal (left) and polyvinyl acetal (right).

noted that the data for PVF are subject to a relatively greater experimental error because the absorption data were not complete at all frequencies investigated in the experimental temperature range. This is evident from the experimental data in Fig. 4. The data of Fig. 6 can be extrapolated to yield two interesting results for comparison. At a temperature of 25°C. the values of the relaxation times become 10^6 sec. for PVA and 10^{16} sec. for PVF as compared with 10^4 sec.

for PVB (6). Fuoss has shown that the electrical relaxation time is linearly dependent on the weight average molecular weight (7). Although the molecular weights of the samples used in this work were not identical, the values of the relaxation times given would not be affected significantly by the variations in molecular weight of the materials utilized. Extrapolation of the data to a relaxation time for one second yields a temperature of 63°C. for PVA and 101°C. for PVF as compared to 56°C. (corrected value from (6)) for PVB. These temperatures should form a basis for comparison with the second order transition and brittle point temperatures for these polymers (10). A detailed study of the mechanical properties of some polyvinyl acetals has appeared recently (3). Further work which may furnish a comparison with the present electrical data is in progress (4).

The slopes of the linear plots in Fig. 6 can be used to calculate the experimental values of the enthalpy ΔH^* . The entropy ΔS^* and free energy ΔF^* of activation can also be calculated (6). The results are presented in Table II.

TABLE II
ENTHALPIES (ΔH^*), ENTROPIES (ΔS^*), AND FREE ENERGIES (ΔF^*)
FOR DIELECTRIC RELAXATION OF POLYVINYL FORMAL AND ACETAL

f_0 , kc.	Polyvinyl formal				Polyvinyl acetal			
	$T_{\max.}$, °A.	ΔF^* , kcal.	ΔH^* , cal. per mole per deg.	ΔS^* , cal. per mole per deg.	$T_{\max.}$, °A.	ΔF^* , kcal.	ΔH^* , kcal.	ΔS^* , cal. per mole per deg.
0.05	389	18.7	111.2	237				
0.1	392.1	18.3		237	359.2	16.7	71.2	152
0.3	394.2	17.5		238	363.2	16.1		152
1	397.5	16.7		238	366.6	15.2		152
3	400.2	15.9		238	371.2	14.7		152
10	404.2	15.1		238	375.2	14.0		153
30	408.4	14.4		237	380.7	13.4		152
100	412.2	13.6		237	387.2	12.7		151

The values of the enthalpies and entropies of activation shown are very high. This is not surprising when the rigid bonding of the dipoles to the chain is considered. The calculated values for PVB and PVA are very similar. The entropy and enthalpy values shown for PVF are very large. This would be expected from the greater possibility for interchain attraction that exists in the latter polymer.

An interesting interpretation of the entropy and enthalpy values has recently been given by Dyson (2). If it is assumed that n monomer units each have r alternative configurations available in the activated state, then the entropy of activation is

$$\Delta S^* = R \ln(r^n)$$

where R is the gas constant.

The forces of attraction between polymer chains may be estimated from the specific molar cohesion. This is defined as the attractive energy per 5 Å length.

The values for the acetals are apparently not available but an estimate can be made from the published values for polyvinyl chloride, acetate, and alcohol. These are 2600, 3200, and 4200 cal. per mole per 5Å length (8). The repeat distance for polyvinyl alcohol is $2.52 \pm .02$ Å (5). Using the value for polyvinyl alcohol the molar cohesion per monomer unit is approximately 2100 cal. per mole. If the relaxation mechanism involves n monomer units in cooperative motion, the heat of activation will be of the order of 2100 n cal. per mole.

The ratio of heat to entropy of activation is seen to be

$$\theta = \frac{\Delta H}{\Delta S} = \frac{n \cdot 2100}{R n \cdot \ln r} = \frac{2100}{R \cdot \ln r}$$

For the polymers investigated the values of θ were PVF 469°A., PVA 468°A., and PVB 468°A.

A value of θ of 468°A. gives a value of r between 9 and 10. At this temperature the free energy of activation is zero and there should be only a single relaxation time independent of the value of n .

Another calculation of interest is to determine an approximate value of n . For the above example $n = 30$ to 35 monomer units. This would, in principle, imply that large portions of the polymer molecule must be involved in the process of dielectric relaxation. It must be emphasized that these calculations involve serious approximations. They do, however, provide a physical picture of the processes involved.

REFERENCES

1. BOYER, R. F. and SPENCER, R. S. J. Polymer Sci. 2: 157. 1947.
2. DYSON, A. J. Polymer Sci. 7: 133. 1951.
3. FITZHUGH, A. F. and CROZIER, R. N. J. Polymer Sci. 8: 225. 1951.
4. FITZHUGH, A. F. Private Communication.
5. FULLER, C. S. Chem. Revs. 26: 143. 1940.
6. FUNT, B. L. Can. J. Chem. 30: 84. 1952.
7. FUOSS, R. M. J. Am. Chem. Soc. 63: 2401, 2410. 1941.
8. MARK, H. and TOBOLSKY, A. V. High polymers. Vol. 2. Interscience Publishers, Inc., New York. 1950.
9. MEAD, D. J. and FUOSS, R. M. J. Am. Chem. Soc. 63: 2832. 1941.
10. TUCKETT, R. F. Trans. Faraday Soc. 40: 448. 1941.

INFRARED SPECTRUM, MOLECULAR STRUCTURE, AND THERMODYNAMIC FUNCTIONS OF HYDROXYLAMINE¹

BY PAUL A. GIGUÈRE AND I. D. LIU

ABSTRACT

The absorption spectrum of pure hydroxylamine in the vapor and solid states was measured with a prism instrument in the range 1.5–25 μ . Except in one case the fundamental vibrations were clearly outlined and in some instances, particularly the 1115 cm^{-1} band, the fine structure was resolved well enough for a significant calculation of the rotational constants. From the latter it was possible to confirm, within fairly close limits, the probable structure of the hydroxylamine molecule, a nearly symmetric top of point group C_s . At least two of the bands appeared to be doubled owing, presumably, to existence of a mixture of *cis*- and *trans*-forms of the molecule. The O–H and N–H distances have nearly the same value as in water and ammonia respectively and the N–O distance is 1.46 Å.

The thermodynamic functions of gaseous hydroxylamine were calculated using the observed fundamental frequencies; some uncertainty accrues from the torsional oscillation. The infrared spectrum of crystalline hydroxylamine hydrochloride was also studied.

INTRODUCTION

The close resemblance between hydrogen peroxide, hydrazine, and hydroxylamine with respect to their physical and chemical properties has been pointed out by several authors (1, 2, 30, 31, 35). If hydrazine is looked upon as the nitrogen analogue of hydrogen peroxide, then hydroxylamine is the intermediate aquo ammonio compound. Following the theoretical treatment of Penney and Sutherland (24) the molecular structure of hydrogen peroxide and hydrazine have been studied extensively. Because of the growing importance of these two compounds in recent years their infrared spectra were re-examined in this laboratory and new data were reported for both (11, 12). On the other hand very little work has been done on the structure of hydroxylamine because of its great instability. Thus an attempt with the electron diffraction method resulted in complete failure (13). A number of Raman investigations of aqueous solutions of the compound and of its hydrochloride have been made in the past (3, 7, 9, 22, 27). Assignment of the observed frequencies (Table I) remained uncertain, however, since the molecule was not in the free state. A rather sketchy infrared study of hydroxylamine hydrochloride made by Heinitz (16) yielded four bands at 2860, 1620, 1480, and 1280 cm^{-1} in poor agreement with the Raman shifts. Therefore we presumed that a spectroscopic study of free hydroxylamine, if successful, would provide valuable information on that molecule.

EXPERIMENTAL

Methods of preparation of pure hydroxylamine based on dissociation of a salt, such as the tertiary phosphate (34), or of an addition compound, such as $\text{ZnCl}_2 \cdot 2\text{NH}_2\text{OH}$ (5), are extremely ineffective owing to the instability of free hydroxylamine at the temperatures required to bring about dissociation. After a

¹Manuscript received August 1, 1952.

Contribution from the Department of Chemistry, Laval University, Quebec, Que., with financial assistance from the National Research Council.

TABLE I
RAMAN SPECTRUM OF HYDROXYLAMINE AND ITS HYDROCHLORIDE IN AQUEOUS SOLUTIONS
(FREQUENCIES IN CM.⁻¹)

NH ₂ OH				
Médard (22)		Bernstein and Martin (3)		
897-921	(s.)	906	(10)	
1045	(v.w.)	1042		
1108	(w.)	1120	(6)	
1311	(v.w.)	1290	(1)	
1605	(m.)	1365	(1)	
3259	(m.)	3257	(1)	
3306	(m.)			

NH ₂ OH·HCl				
Bernstein and Martin (3)	Edsall (7)	Redlich and Friedman (27)		
			†	Assignment
1007 (10)	1006 (10)	1005 (10)	987 (8)	N-O str.
1195 (2)	1205	1197 (2)	880 (2)	NH bend.
1290 (1)				
	1533	1519 (3)	1138 (3)	NH bend.
	1625	1618 (3)	1195 (2)	OH bend. (?)
	2741	2700 (0)	2035 (2)	N-H str.
	2953	2960 (5)	2150 (4)	N-H str.
			2230 (4)	
	3200	3240 (4)	2360 (5)	
		3470 (7)	2520 (7)	O-H str. (?)
		3630 (3)	2620 (3)	
			2980 (1)	

†For ND₂OH·HCl.

few trials we found that the method of Lecher and Hofmann (21) gives the best results. One hundred milliliters of a freshly prepared solution of sodium ethoxide in absolute alcohol were added slowly to 17.5 gm. of finely powdered hydroxylamine hydrochloride suspended in absolute alcohol. A trace of phenolphthalein served to indicate the end point of the reaction. In order to reduce oxidation of the ethoxide while it was being added to the mixture a stream of dry nitrogen was blown into the reaction flask.

After the reaction was completed the sodium chloride was filtered off and the filtrate was kept in an ice-box until needed. Immediately before taking a spectrum the alcoholic solution was cooled to - 15° in an ice-salt mixture and the long white needles of crystalline hydroxylamine that separated were quickly filtered and transferred to a desiccator thoroughly flushed with dry nitrogen. After 20 to 30 min. this sample was introduced in the absorption cell and the spectrum recorded. The yield was of the order of 10 gm. of free hydroxylamine, somewhat higher than originally reported (21). The compound thus prepared melted at 32-33°C. (accepted value, 32.05°). It was quite stable when kept in the ice-box

in an atmosphere of dry nitrogen but it decomposed rapidly in air at room temperature.

For recording the spectrum of the vapor a 1-meter absorption cell (37), with the sample contained in a side tube, was continuously evacuated through a throttling valve in order to remove the decomposition products. It was not possible to ascertain, even roughly, the partial pressure of hydroxylamine in the cell and, therefore, the absorption coefficient of the various bands could not be estimated. The sample was usually kept at 45–50°C. and the absorption cell, at about 10° higher to prevent condensation. A fresh sample of hydroxylamine was needed for each recording of the spectrum.

Because of the extreme instability of liquid hydroxylamine its spectrum could not be measured. As for the solid, the only practical method was by mulling the crystals in Nujol; one drop of this mull was pressed between salt windows in a low-temperature absorption cell (36). In the case of the hydrochloride an alcoholic solution was evaporated on a rock-salt plate.

DISCUSSION OF RESULTS

As may be judged from Fig. 1 hydroxylamine exhibits a fairly strong infrared spectrum in keeping with its low symmetry. The molecule may be thought of as made up of one half of a hydrazine and one half of a hydrogen peroxide molecule. Therefore it can have, at most, one symmetry plane (point group C_s) provided the O–H bond lies in the plane bisecting the HNH angle (Fig. 2). This

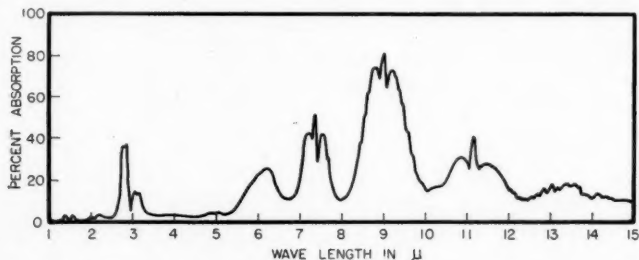


FIG. 1. Infrared absorption spectrum of gaseous hydroxylamine.

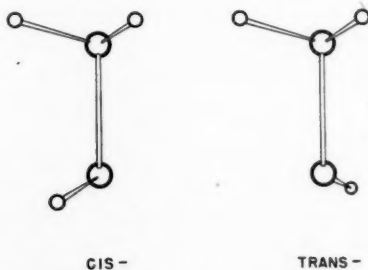


FIG. 2. Probable configurations of the hydroxylamine molecule.

assumption, which appears most likely a priori, is in fact confirmed by the normal intensity distribution in some of the absorption bands.

Of the nine fundamental modes six must be symmetric (a') and three anti-symmetric (a'') with respect to the C_s plane. They may be classified as follows: four stretching vibrations, namely two N-H, one O-H, and the skeletal N-O; four bending vibrations, that is, three NH_2 and one OH; and the torsional oscillation about the N-O bond. On that basis interpretation of the spectrum offered no particular difficulty; indeed, except in one instance (the N-H stretching vibrations) there was no overlapping and the regular contour of most of the bands made their assignment quite straightforward. This favorable situation is largely due to absence of identical nuclei exchangeable by rotation, in contrast with the case of hydrogen peroxide and hydrazine.

Stretching Vibrations

The fundamental having the highest frequency, 3656 cm^{-1} , is obviously identified with the O-H stretching mode ν_1 (Table II); it is remarkable that it has almost exactly the same value as in water. Because the NOH angle is not much greater than 90° this band should be predominantly perpendicular. Even

TABLE II
INFRARED SPECTRUM OF HYDROXYLAMINE

Vapor		Solid ν (cm^{-1})	Assignment
ν (cm^{-1})	Slit (cm^{-1})		
430 (?) (v.w.)	4.0	490 (?) (v.w.)	ν_9 (a'') torsion
765 (w.)	2.0	580 (v.w.)	
895 (m.)	2.0	845 (m.)	ν_8 (a'') NH_2 rock.
1115 } (v.s.)	3.6	913 (w.)	
1125 }		926 (s.)	ν_6 (a') N-O str.
1297 (w.)	4.8	1187 (v.s.)	ν_5 (a') NH_2 wag.
1357 (s.)	5.6	1287 (v.w.)	$\nu_8 + \nu_9$ (A')
1605 (m.)	8.6	1502 (m.)	$\nu_6 + \nu_9$ (A'')
		1657 (m.)	ν_4 (a') OH bend.
		2046 (v.w.)	ν_3 (a') NH_2 bend.
		2438 (v.w.)	$\nu_5 + \nu_6$ (A')
		2687 (v.w.)	$\nu_3 + \nu_8$ (A'')
2740 (v.w.)	6.0	3088 (m.)	$\nu_3 + \nu_4$ (A') (?)
3297 (m.)	6.5	3207 (s.)	ν_2 (a') N-H str.
3350 (?) (w.)	6.5	3268 (s.)	ν_7 (a'') N-H str.
3656 (s.)	9.0	3331 (s.)	ν_1 (a') O-H str.
		3597 (v.w.)	$\nu_2 + \nu_9$ (A'') (?)
		4184 (v.w.)	$\nu_1 + \nu_6$ (A')
		4508 (v.w.)	$\nu_3 + 2\nu_4$ (A') (?)
		4615 (v.w.)	$\nu_2 + \nu_4$ (A')
4655 (v.w.)	20.		$\nu_4 + \nu_7$ (A'')
		4840 (v.w.)	$\nu_3 + \nu_7$ (A'')
4946 (v.w.)	22.	4902 (v.w.)	$\nu_1 + \nu_3$ (A')
			$\nu_1 + \nu_4$ (A')
6545 (v.w.)	64.	6410 (v.w.)	$\nu_1 + \nu_7$ (A'')
7200 (v.w.)	70.		$2\nu_2$ (A')
			$2\nu_1$ (A')

with a lithium fluoride prism and the narrowest possible slit the resolution was not sufficient to reveal any structure besides three about equally intense maxima at 3675, 3656, and 3620 cm^{-1} (Fig. 3). The first of these may overlap the combination $3300 + 430 \text{ cm}^{-1}$; another possibility is that the O-H band is doubled, as explained below. In the solid (Fig. 4) this fundamental is shifted to an appreciably lower frequency, 3330 cm^{-1} , by formation of strong hydrogen bonds of the O-H \cdots N type.

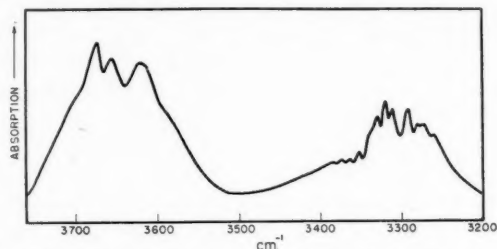


FIG. 3. The O-H and N-H stretching bands of hydroxylamine vapor.

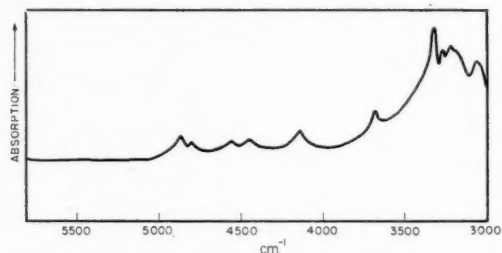


FIG. 4. Absorption spectrum of crystalline hydroxylamine in the region 2-3 μ .

Identification of the two N-H stretching vibrations presented the only ambiguity. In the region of irregular absorption near 3 μ the stronger peak at 3297 cm^{-1} resembles unmistakably the *Q* branch of a hybrid band, and as such, is assigned to the symmetric vibration ν_2 . As for the asymmetric vibration ν_7 , it should have a slightly higher frequency and greater intensity than ν_2 . The only indication of such a band on the tracing is a weak absorption region centering around 3350 cm^{-1} and partly overlapped by the *R* branch of ν_2 . The same paradoxical situation exists in methylamine (4, 23) where the unsymmetrical N-H vibration has not been located definitely. The picture is equally confused in the case of the solid; our assignments are only tentative, especially for the 3088 cm^{-1} band which seems rather strong for a combination. It may be noted that the frequency shift on going to the solid state is much smaller for the N-H than for the O-H vibrations in agreement with the lesser electronegativity of nitrogen and the weaker N-H hydrogen bonds.

The N-O stretching vibration ν_6 involves a change of electric moment mainly along the least axis of inertia of the molecule; it should give rise to a rather

strong hybrid band in the 10–12 μ region. Such is the 895 cm^{-1} band with its sharp Q branch and fairly regular shape (Fig. 5). This is in marked contrast with hydrogen peroxide and hydrazine where the skeletal valence vibration is

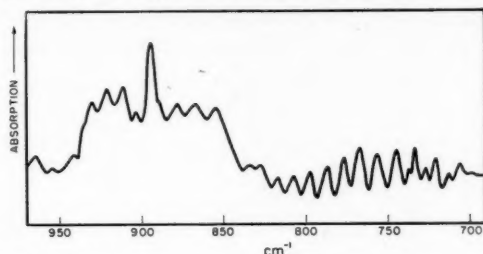


FIG. 5. The N–O stretching (895 cm^{-1}) and NH_2 rocking (765 cm^{-1}) bands in gaseous hydroxylamine.

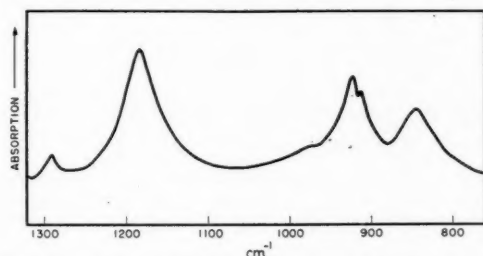


FIG. 6. Infrared absorption by solid hydroxylamine from 7 to 12 μ .

almost inactive in infrared because of nuclear symmetry. It is interesting to compare the present frequency with that in a few other molecules studied recently (Table III). That this vibration should be shifted by as much as 30 cm^{-1} towards higher frequencies in the solid (Fig. 6) seems surprising as it does not involve directly the hydrogen atoms; an even greater shift (40 cm^{-1}) has been reported for nitric acid (8).

TABLE III
N–O STRETCHING FREQUENCY IN VARIOUS MOLECULES

Compound	Vapor (cm^{-1})	Liquid (cm^{-1})	Reference
$(\text{CH}_3)_2\text{C:NOH}$		935	(14)
$(\text{CH}_3)_2\text{NO}$		947	(15)
CH_3ONO <i>cis</i> -	844		(32)*
<i>trans</i> -	814		
HONO <i>cis</i> -	856		(19)
<i>trans</i> -	794		
DONO <i>cis</i> -	816		(19)
<i>trans</i> -	739		
HONO_2	880	920	(8)

*Besides methyl nitrite Tarte has studied a whole series of primary nitrites, for which he found N–O frequencies ranging from 790 to 844 cm^{-1} .

Bending Vibrations

By analogy with hydrazine (12) and methylamine (4, 23) the medium-strength band at 1605 cm^{-1} (Fig. 7) is unequivocally assigned to ν_3 , the NH_2 bending mode; in this vibration the two hydrogen atoms in the amino group move

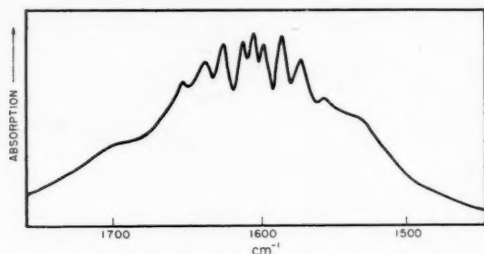


FIG. 7. NH_2 bending vibration in hydroxylamine vapor.

towards, or away from each other, causing a change of dipole moment nearly perpendicular to the N-O axis. The fact that the ONH angle is greater than 90° (probably near 107°) accounts for the weak but unmistakable Q branch; in methylamine the parallel component of the band at 1625 cm^{-1} is much more pronounced, contrary to normal expectation. It is possible that overlapping by combination tones (here $\nu_2 + \nu_3$) contributes to the total intensity in that region. The rotational subbands were clearly visible up to $K = 3$; beyond that level absorption by atmospheric water vapor interfered seriously.

Next in decreasing frequency is the OH bending vibration at 1357 cm^{-1} (Fig. 8) with its sharp Q branch, as expected of a predominantly parallel band. That the rotational structure was not better resolved may be due to overlapping by a satellite band as explained below. Here again hydrogen bonding causes a considerable shift of the frequency in the solid.

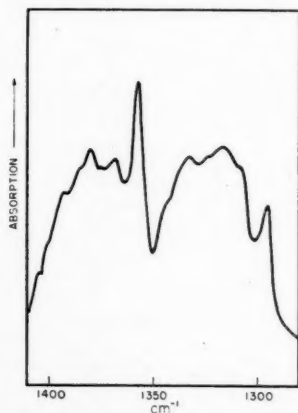


FIG. 8. Absorption at $7\text{--}8\text{ }\mu$ due to the OH bending mode in gaseous hydroxylamine.

The remaining two bands in the 9–13 μ region must correspond to the NH_2 bending vibrations ν_5 and ν_8 , usually described as "wagging" and "rocking". They involve respectively symmetric and antisymmetric deformation of the HNO angles. Because the former has a strong parallel component we identify it with the beautifully developed band at 1115 cm^{-1} (Fig. 9); then the rather

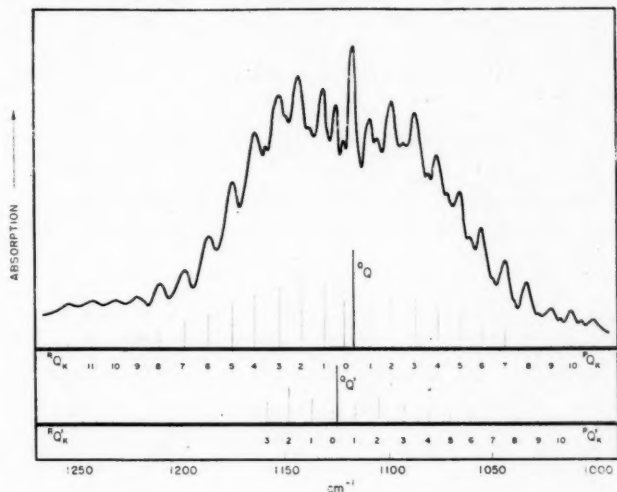
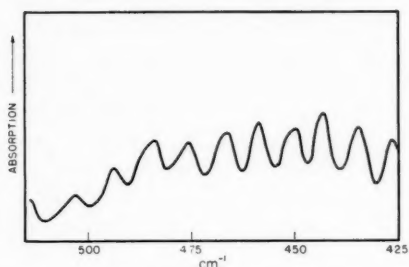


FIG. 9. Rotational structure of the double band at 1115–1120 cm^{-1} in hydroxylamine.

weak perpendicular band at 765 cm^{-1} is ascribed to the NH_2 rocking. Our choice is based on the shape of the bands much more than on their relative intensities which seem opposite to what one would normally expect of such vibrations. As noted before, the two N-H stretching vibrations show the same apparently reversed intensity relationship.

The above assignments are at variance with those for methylamine proposed by Cleaves and Plyler (4) who attributed the strong band at 783 cm^{-1} to the symmetric NH_2 bending (or wagging) on the ground that it showed a strong Q branch. However, this feature must have been spurious because a subsequent tracing of the same band by Barker and Owens (23) failed to reveal any sign of it. From present results it is clear that the 783 cm^{-1} band in methylamine belongs to the NH_2 rocking mode, and the equally strong, and as yet unassigned, hybrid band at 1127 cm^{-1} , to the wagging mode.

Finally the torsional oscillation ν_9 gives rise to a region of very weak absorption near the transmission limit of potassium bromide (Fig. 10). Because the whole band could not be explored and also because it is purely perpendicular, its center could not be located exactly; a value of 430–440 cm^{-1} agrees fairly well with the contour and with a few possible combination frequencies. The spacing of the coarse structure seemed less regular than in the other bands but this may be traced to poor accuracy of measurements in that region owing to very low

FIG. 10. Absorption by hydroxylamine vapor near $23\ \mu$.

absorption and a weak signal. The frequency $490\ \text{cm}^{-1}$ in the solid is equally uncertain; in hydrogen peroxide this vibration is believed to occur at $660\ \text{cm}^{-1}$ (11) whereas in hydrazine it is probably much lower, somewhere around $350\ \text{cm}^{-1}$ (12).

TABLE IV
FREQUENCY OF ABSORPTION BANDS IN THE INFRARED SPECTRUM OF SOLID $\text{NH}_2\text{OH} \cdot \text{HCl}$

$\nu(\text{cm}^{-1})$		Assignment	$\nu(\text{cm}^{-1})$		Assignment
1000	(s.)	N-O str.	2760		
1176			2795	(w.)	N-H str.
1200	(s.)	NH bend.	2940	(w.)	
1482	(s.) *	NH bend.	3025	(m.)	N-H str.
1563	(s.)	OH bend.	3080	(s.)	O-H str. (?)
1800	(v.w.)		4115	(v.w.)	(1176 + 3025)
1876	(s.)	(?)	4180	(v.w.)	(1200 + 3025)
1965	(v.w.)	(2×1000)	4560	(v.w.)	(1563 + 3025)
2140	(v.w.)	(1000×1176)	4595	(v.w.)	(1563 + 3080)
2170	(v.w.)	($1000 + 1200$)			
2440	(v.w.)	($1000 + 1482$)			
2680	(w.)	($1180 + 1563$)			

The spectrum of the hydroxyl ammonium ion (Table IV) is easily understood when compared with that of hydroxylamine in the solid state; the only unusual feature is the strong peak at $1876\ \text{cm}^{-1}$ for which there is no obvious explanation. One of the NH_2 bending modes appears as a doublet with a splitting of $25\ \text{cm}^{-1}$. In general the stretching frequencies are decreased and the bending frequencies increased with respect to those in crystalline hydroxylamine, with one notable exception: the N-O stretching vibration. (Cf. both infrared and Raman spectra.) In this last instance the effect must be due mostly to the formal charge on the hydroxyl ammonium ion (6, 20), not to addition of one hydrogen atom on the nitrogen, as claimed by Goubeau and Fromme (15).

Rotational Analysis

Besides the $1115\ \text{cm}^{-1}$ band, the strongest in the whole spectrum, four other bands showed more or less developed structure; the rotational constants $X_{01}^0 = A] - 1/2 (B + C)$ derived from these are fairly self-consistent (Tables V, VI, and VII). In order to compare them with constants calculated from moments

TABLE V
 FREQUENCY OF SUBBANDS (IN CM.⁻¹) IN THE DOUBLET BAND OF HYDROXYLAMINE AT 9 μ

K	PQ_K	RQ_K	$\frac{^RQ_K - ^PQ_K}{4K}$	$\frac{^RQ_{(K-1)} - ^PQ_{(K+1)}}{4K}$
0		1120.5		
1	1109.0	1131.6	5.65	5.50
2	1098.5	1143.1	5.58	5.54
3	1087.3	1153.2	5.49	5.50
4	1077.1	1164.5	5.46	5.46
5	1065.8	1175.5	5.49	5.48
6	1055.0	1187.1	5.50	5.48
7	1043.9	1198.1	5.51	5.50
8	1033.1	1210.2	5.53	5.52
9	1021.6	1220.8	5.53	5.50
10	1011.0	1231.0	5.48	5.50
11	1001.0	1243.0	5.50	
12		1255.0		
Average			5.52	5.50

K	$^PQ'_K$	$^RQ'_K$	$\frac{^RQ'_K - ^PQ'_K}{4K}$	$\frac{^RQ'_{(K-1)} - ^PQ'_{(K+1)}}{4K}$
0		(1125)		
1	(1115)	1137		
2	1104	1148	5.5	5.6
3	1092	1158	5.5	5.6
4	1081			
5	1071			
6	1061			
7	1050			
8	1039			
9	1027			
10	1017			
11	1007			

Note: The primed symbols refer to the satellite band.

 TABLE VI
 ROTATIONAL SUBBANDS OF THE 6.2 AND 11 μ BANDS OF HYDROXYLAMINE (FREQUENCIES IN CM.⁻¹)

K	PQ_K	RQ_K	$\frac{^RQ_K - ^PQ_K}{4K}$	$\frac{^RQ_{(K-1)} - ^PQ_{(K+1)}}{4K}$
0		1611		
1	1600	1623	5.7	5.5
2	1589	1633	5.5	5.6
3	1578	1644	5.5	

K	PQ_K	RQ_K	$\frac{^RQ_K - ^PQ_K}{4K}$	$\frac{^RQ_{(K-1)} - ^PQ_{(K+1)}}{4K}$
0		900.4		
1	889.5	911.0	5.38	5.50
2	878.4	921.0	5.35	5.51
3	866.8	931.0	5.37	5.53
4	854.5	941.2	5.42	
5		954.0		
6		966.0		

TABLE VII
ROTATIONAL STRUCTURE OF THE PERPENDICULAR
BANDS OF HYDROXYLAMINE AT 13 AND 23 μ (FREQUENCIES IN CM.⁻¹)

The 13 μ band		The 23 μ band
827.3	(734.7)	534
817.3	726.5	503
807.4	(721.7)	494
797.4	713.0	484
787.0	(707.8)	476
777.0	705	467
767.0	(699)	459
756.1	694	450
745.0	(687)	443
736.8	682	435
		427

Note: The frequencies in brackets belong to the satellite band.

of inertia the following assumptions had to be made regarding the structural parameters of the hydroxylamine molecule: first the O-H and N-H distances, upon which the main rotational constant depends mostly, were taken as 0.96 and 1.01 Å respectively by comparison with the accepted values (17) in water (0.958 Å) and ammonia (1.014 Å). Justification of this choice is seen in the marked closeness of corresponding frequencies. The value 1.46 Å for the N-O distance was obtained from Badger's rule and the calculated force constant k_{N-O} as explained below; however, this parameter is of little consequence here as it affects only the two large moments of inertia. The HON angle was set at 103°, by comparison with hydrogen peroxide (11), and the HNH angle, the same as in ammonia (107°), which seems plausible enough; the latter value was decreased by 2° for the HNO angles on account of substitution of a hydrogen atom by an OH group.

The results of calculations made for both the *cis*- and *trans*- models after the method of Hirschfelder (18) are summarized under A in Table VIII. As may be seen, hydroxylamine is a very nearly symmetric rotator; $I_A/I_B = 0.999$ (*cis*-) or 0.996 (*trans*-). Furthermore, the calculated rotational constant for the *cis*- configuration agrees well with the spectroscopic value, 5.5 cm.⁻¹ Other sets of constants were also calculated in order to find out what changes of parameters were needed to make $X_{01}^0 = 5.5$ cm.⁻¹ for the *trans*- model. Typical of these are the data listed under B in Table VIII. We believe that the latter parameters are less probable than the first ones; the O-H distance in hydrogen peroxide, 0.97 Å, corresponds to a frequency difference of 40 cm.⁻¹ with that of water (11) whereas the difference is only 4 cm.⁻¹ in the case of hydroxylamine. As for the longer N-H distance, the only previous example is the value 1.04 Å suggested by the electron diffraction curves of hydrazine (13); the uncertainty on this datum is obviously large (± 0.06 Å). Although the foregoing arguments are not decisive they indicate a trend for the *cis*- configuration.

In the simplified hypothesis of a diatomic model the measured N-O stretching frequency leads to a force constant 3.5×10^5 dynes per cm. and, by Badger's

TABLE VIII
CALCULATED MOMENTS OF INERTIA AND ROTATIONAL
CONSTANTS OF THE HYDROXYLAMINE MOLECULE

	A	B
<i>Molecular parameters</i>		
r_{N-O}	1.46 Å	1.46 Å
r_{O-H}	0.96	0.97
r_{N-H}	1.01	1.03
$\angle HON$	103°	102°
$\angle HNO$	105°	107°
$\angle HNH$	107°	107°
<i>Moments of inertia (gm. cm.² × 10⁴⁰)</i>		
	<i>cis-</i>	<i>trans-</i>
I_A	33.53	33.76
I_B	33.56	33.89
I_C	4.44	4.28
	<i>cis-</i>	<i>trans-</i>
	33.86	34.24
	33.87	34.08
	4.60	4.43
<i>Rotational constants (cm.⁻¹)</i>		
A	0.834	0.829
B	0.834	0.826
C	6.303	6.538
X_{01}^0	5.47	5.71
	5.26	5.50

rule, to a bond length (1.48 Å) exactly equal to the sum of the single-bond atomic radii of nitrogen and oxygen. A more accurate calculation of the force constants was carried out using a potential energy function of the form

$$\begin{aligned}
 2V = & k_{N-O}(\Delta R)^2 + k_{O-H}(\Delta r_1)^2 + k_{N-H}[(\Delta r_2)^2 + (\Delta r'_2)^2] \\
 & - 2k'_{N-H}(\Delta r_2 \cdot \Delta r'_2) + \delta_{HNH} r_2^2(\Delta \alpha)^2 + \delta_{HON} r_1^2(\Delta \alpha_1)^2 \\
 & + \delta_{HNO} r_2^2[(\Delta \alpha_2)^2 + (\Delta \alpha'_2)^2] - 2\delta'_{HNO} r_2^2(\Delta \alpha_2 \cdot \Delta \alpha'_2) + \gamma r_1^2(\Delta \phi)^2
 \end{aligned}$$

where ΔR , Δr_1 , Δr_2 , and $\Delta r'_2$ are the change in the N-O, O-H, and the two N-H distances, and r_1 and r_2 , the equilibrium O-H and N-H distances. The change in the HNH, HON, and the two HNO angles are $\Delta \alpha$, $\Delta \alpha_1$, $\Delta \alpha_2$, and $\Delta \alpha'_2$ respectively, and $\Delta \phi$ is that of the azimuthal angle. The solution of the secular equations after the general method of Torkington (33) yielded the following force constants (Table IX).

TABLE IX
FORCE CONSTANTS OF HYDROXYLAMINE (IN DYNES PER CM.)

k_{N-O}	3.89×10^5	δ_{HNH}	1.14×10^5
k_{O-H}	7.46	δ_{NOH}	0.95
k_{N-H}	6.11	δ_{HNO}	0.52
k'_{N-H}	0.015	δ'_{HNO}	0.21
		γ	0.035

The k_{N-O} force constant thus obtained makes the bond length 1.46 Å, the same as found recently in nitrous acid (19). Because of its partial ionic character

the N-O bond in hydroxylamine must be shorter than a purely covalent bond; on that basis Schomaker and Stevenson (29) calculated it to be 1.43 Å but this seems too short to be reconciled with the present spectroscopic data. Goubeau and Fromme (15) arrived at a force constant 4.4×10^6 dynes per cm., and hence, at an N-O distance 1.43 Å from the observed frequencies in hydroxylamine hydrochloride, acetoxime, and trimethylamine oxide (Table III); however, these molecules do not possess a normal covalent N-O single bond due either to formal charge or to the possibility of resonance.

Satellite Bands

While analyzing the rotational structure of the 1115 cm^{-1} band a strong peak was noticed at 1125 cm^{-1} which did not fit into the normal intensity pattern. On closer examination of the tracings other weaker maxima could be seen about halfway between the main ones, particularly in the *P* wing (Fig. 9). Taken together these seemed to be part of a secondary band with the same general contour but somewhat lower intensity than the main band, and separated from it by $5\text{--}6\text{ cm}^{-1}$ except for the central *Q* branch which, oddly enough, was shifted by nearly twice as much to the high frequency side. Only one other fundamental, the asymmetric NH_2 bending at 765 cm^{-1} , showed definite indications of similar doubling (Fig. 5) although the resolution may not have been sufficient to reveal it in other bands.

A number of explanations have been considered for these satellites but none appears entirely satisfactory. Combinations and overtones are ruled out on the basis of either anharmonicity or intensity; for the same reason the possibility is excluded of so-called "upper stage" bands (17) in which a low frequency fundamental (here ν_9) is excited in both the upper and lower states. On the other hand a double minimum vibration due to inversion doubling, as in hydrazine, would result in equal intensity for the two components of the doublet. Rather it is likely that hydroxylamine, like nitrous acid* (19) and the alkyl nitrites (32), exists as a mixture of *cis*- and *trans*- tautomers. True, the frequency difference between the main and subsidiary bands seems too small on that account; also the spacing of the rotational levels should be slightly different in both bands, as shown by the data of Table VIII. However, the present frequency measurements are not accurate enough to check this last point. Obviously an adequate explanation of these features will have to await further experimental work either on the deuterated compound or on the over-tone region.

Thermodynamic Functions

The above moments of inertia for the *cis*- model (*A* in Table VIII) were combined with the fundamental frequencies to calculate the thermodynamic properties of hydroxylamine for the ideal gaseous state from 300° to 1200° K . (Table X). The reduced moment, $I_{\text{red.}} = 0.953 \times 10^{-40}\text{ gm. cm}^2$, was evaluated by the definition of Pitzer (25) for molecules with a single asymmetric top

* NOTE ADDED IN PROOF. The same conclusion has been reached by L. d'Or and P. Tarte in an investigation of the infrared spectrum of nitrous acid that has just come to our attention (Bull. soc. roy. sci. Liège, 20: 478, 1951).

TABLE X
 THERMODYNAMIC FUNCTIONS OF GASEOUS HYDROXYLAMINE AT 1 ATM.

T , °K.	$\frac{F^\circ - H^\circ}{T}$, cal./deg./mole	$\frac{H^\circ - H^\circ_0}{T}$, cal./deg./mole	S° , cal./deg./mole	C°_p , cal./deg./mole	$H^\circ - H^\circ_0$, cal/mole
298.16	47.36 (47.08)	8.98 (8.32)	56.33 (55.40)	11.17 (9.60)	2677 (2482)
300	47.42 (47.13)	9.00 (8.33)	56.39 (55.46)	11.20 (9.63)	2700 (2500)
350	48.83 (48.43)	9.36 (8.57)	58.19 (57.00)	12.14 (10.37)	3276 (3000)
400	50.10 (49.59)	9.76 (8.84)	59.88 (58.44)	13.02 (11.11)	3904 (3537)
500	52.38 (51.63)	10.57 (9.43)	62.95 (61.06)	14.53 (12.46)	5285 (4717)
600	54.36 (53.40)	11.34 (10.04)	65.70 (63.44)	15.74 (13.61)	6804 (6022)
700	56.17 (55.00)	12.04 (10.62)	68.21 (65.61)	16.69 (14.59)	8428 (7433)
800	57.82 (56.45)	12.67 (11.17)	70.49 (67.62)	17.39 (15.45)	10136 (8936)
900	59.37 (57.79)	13.24 (11.69)	72.62 (69.48)	17.92 (15.97)	11916 (10521)
1000	60.81 (59.05)	13.77 (12.18)	74.59 (71.23)	18.80 (16.92)	13770 (12179)
1100	62.17 (60.23)	14.25 (12.64)	76.43 (72.87)	19.34 (17.55)	15675 (13903)
1200	63.45 (61.35)	14.69 (13.07)	78.17 (74.42)	19.82 (18.11)	17628 (15686)

Note: The numbers in parentheses do not include the contribution of internal rotation.

attached to a rigid frame. As usual, a rigid rotator, harmonic oscillator was assumed and the nuclear spin of hydrogen atoms was disregarded. Throughout the calculations the latest recommended values of the fundamental constants (28) were used. The contribution of restricted internal rotation is the least accurately known of all terms; it was estimated by means of the usual potential function,

$$V = \frac{V_0}{2}(1 - \cos n\theta)$$

where V_0 is the barrier height, n , the number of minima, and θ , the angle of hindered rotation. By means of the "Tables Relating to Mathieu Functions" prepared by the Computation Laboratory of the National Applied Mathematics Laboratories (Columbia University Press, N.Y. 1951), and with a Mathieu equation of the form

$$\frac{\partial^2 M(x)}{\partial x^2} + (b + s \cos^2 x) M(x) = 0$$

where

$$b = \frac{32\pi^2 I_{\text{red.}}}{n^2 h^2} (E - V_0),$$

$$s = \frac{32\pi^2 I_{\text{red.}} V_0}{n^2 h^2},$$

$$E - E_0 = hc\omega_t,$$

ω_t being the torsional frequency, 430 cm^{-1} for hydroxylamine, a potential barrier $V_0 = 5120$ cal. per mole was found. Linear interpolation was then made from the tables of Pitzer and Gwinn (26). A first approximation by the perturbed oscillator treatment had given a barrier height of 5140 cal. per mole which seems reasonable when compared with that in hydrogen peroxide (10).

ACKNOWLEDGMENT

The Bureau of Scientific Research of the Province of Quebec has granted a

fellowship to one of us (I.D.L.) for which we are very grateful. We are also greatly indebted to Mr. Osias Bain for many helpful discussions and for setting up the *A* matrix of Torkington used in calculating the force constants.

RÉSUMÉ

Le spectre d'absorption de l'hydroxylamine à l'état gazeux et solide a été étudié dans l'infrarouge de 1.5 à 25 microns. Sauf pour les vibrations de valence N-H, les fréquences fondamentales ont pu être identifiées sans ambiguïté. Quelques bandes avaient une structure de rotation assez développée pour permettre de calculer les constantes de rotation de la molécule. À la lumière de ces résultats la structure probable de la molécule d'hydroxylamine a pu être fixée entre des limites assez rapprochées. Cependant il n'est pas possible de décider laquelle des configurations *cis*- ou *trans*- est la plus stable, bien que les deux semblent coexister. Les liaisons O-H et N-H ont presque exactement la même longueur que dans les molécules d'eau et d'ammoniac; la distance N-O est de 1.46 Å. Une barrière de potentiel, dont la hauteur est évaluée à 5 kcal. par mole, empêche la rotation libre autour de la liaison N-O à l'intérieur de la molécule. Enfin les fonctions thermodynamiques de l'hydroxylamine à l'état de gaz parfait à 1 atmosphère ont été calculées à plusieurs températures à partir des présentes données.

REFERENCES

1. ANGELI, A. Atti. reale accad. Lincei, (5) 19: 94. 1910.
2. AUDRIETH, L. F. and OGG, B. A. The chemistry of hydrazine. John Wiley & Sons, Inc., New York. 1951.
3. BERNSTEIN, H. L. and MARTIN, W. H. Trans. Roy. Soc. Can. III, 95: 105. 1937.
4. CLEAVES, E. K. and PLYLER, J. J. Chem. Phys. 7: 563. 1939.
5. CRISMER, L. Bull. soc. chim. France (3) 3: 115. 1890.
6. DONOHUE, J. and LIPSCOMB, W. N. J. Chem. Phys. 15: 115. 1947.
7. EDSALL, J. T. J. Chem. Phys. 5: 225. 1937.
8. FRÉJAQUES, C. Compt. rend. 234: 1769. 1952.
9. FREYMAN, M. and RUMPF, P. Compt. rend. 201: 608. 1935.
10. GIGUÈRE, P. A. J. Chem. Phys. 18: 88. 1952.
11. GIGUÈRE, P. A. and BAIN, O. J. Phys. Chem. 56: 340. 1952.
12. GIGUÈRE, P. A. and LIU, I. D. J. Chem. Phys. 20: 136. 1952.
13. GIGUÈRE, P. A. and SCHOMAKER, V. J. Am. Chem. Soc. 65: 2025. 1943.
14. GOUBEAU, J. Z. physik. Chem. B, 36: 45. 1937.
15. GOUBEAU, J. and FROMME, I. Z. anorg. Chem. 258: 18. 1949.
16. HEINITZ, I. Arch. phys. biol. 14: 131. 1937.
17. HERZBERG, G. Infrared and Raman spectra of polyatomic molecules. D. Van Nostrand Company Inc., New York. 1945.
18. HIRSCHFELDER, J. O. J. Chem. Phys. 8: 431. 1940.
19. JONES, L. H., BADGER, R. M., and MOORE, G. E. J. Chem. Phys. 19: 1599. 1951.
20. KRONBERG, M. L. and HARKER, D. J. Chem. Phys. 10: 309. 1942.
21. LECHER, H. and HOFMANN, J. Ber. B, 55: 912. 1922.
22. MÉDARD, L. Compt. rend. 199: 421. 1934.
23. OWENS, R. G. and BARKER, E. F. J. Chem. Phys. 8: 229. 1940.
24. PENNEY, W. G. and SUTHERLAND, G. B. B. M. J. Chem. Phys. 2: 492. 1934.
25. PITZER, K. S. J. Chem. Phys. 14: 240. 1946.
26. PITZER, K. S. and GWINN, W. D. J. Chem. Phys. 10: 428. 1942.
27. REDLICH, O. and FRIEDMAN, I. I. J. Am. Chem. Soc. 67: 893. 1945.
28. ROSSINI, F. D., GUCKER, F. T., JOHNSTON, H. L., PAULING, L., and VINAL, G. M. J. Am. Chem. Soc. 74: 2699. 1952.
29. SCHOMAKER, V. and STEVENSON, D. P. J. Am. Chem. Soc. 63: 37. 1941.
30. SISLER, S. S. and AUDRIETH, L. F. Trans. Illinois State Acad. Sci. 31: 144. 1938.
31. STIEGLITZ, J. and SENIOR, J. K. J. Am. Chem. Soc. 38: 2727. 1916.
32. TARTE, P. Bull. soc. chim. Belges, 60: 227, 240. 1951.
33. TORKINGTON, P. J. Chem. Phys. 17: 1026. 1949.
34. UHLENHUTH, R. Ann. 311: 117. 1900.
35. WAGNER, E. Chem. Zentr. 1: 244. 1899.
36. WAGNER, E. L. and HORNIG, D. F. J. Chem. Phys. 18: 296. 1950.
37. WHITE, J. U. J. Optical Soc. Am. 32: 285. 1942.

VIBRATION SPECTRA OF CIS AND TRANS DICHLOROETHYLENE- d_1 ¹

BY H. J. BERNSTEIN AND A. D. E. PULLIN²

ABSTRACT

The infrared spectra of the vapor and the liquid, and the Raman spectra of liquid *cis* and *trans* C_2HDCl_2 have been obtained in the region 400–3300 cm^{-1} . The observed spectra are in accordance with the assignment of Bernstein and Ramsay for *cis* and *trans* $C_2H_2Cl_2$ and $C_2D_2Cl_2$.

INTRODUCTION

In the assignment of frequencies made previously (4) for *cis* and *trans* $C_2H_2Cl_2$ and $C_2D_2Cl_2$ all fundamentals were observed directly* except the A_u torsion vibration and a B_u in-plane bending vibration** of the *trans* compounds. The frequencies of these vibrations, which are infrared active, but which lie beyond the range of the potassium bromide prism, were obtained from infrared combination tones. In *cis* and *trans* C_2HDCl_2 all vibrations are allowed both in the Raman and infrared spectra, and it was hoped that it would be possible to observe the two low-lying frequencies in *trans* C_2HDCl_2 . These frequencies were not observed directly even on heavily overexposed plates. Further combination tones were observed, however, supporting the previously made assignment (4).

The data for the six compounds, *cis* and *trans* $C_2H_2Cl_2$, C_2HDCl_2 , and $C_2D_2Cl_2$; are consistent with the Teller–Redlich product rule, the sum rule (5, 7, 3), and the product rule for rotational isomers (2).

EXPERIMENTAL

The samples were prepared for us through the courtesy of Leitch and Morse, who have described the method of preparation in a previous publication (6).

The infrared spectra were obtained with a Perkin Elmer 12C infrared spectrometer (used in conjunction with a Brown pen recorder) employing lithium fluoride, sodium chloride, and potassium bromide optics where necessary. Vapor spectra were obtained at various pressures with a 10 cm. cell, and the spectra of the pure liquid and of dilute solutions in carbon disulphide and carbon tetrachloride with a 0.1 mm. cell. The results are given in Figs. 1 and 2, and Tables I and V.

The liquid Raman spectra were recorded photographically using a two prism instrument and a camera lens of aperture $F/7$, giving a linear dispersion of 50 cm^{-1} per mm. at 4358 Å. The results are given in Tables I and V.

The Raman and infrared spectra of *trans* C_2HDCl_2 were checked also against

¹ Manuscript received August 12, 1952.

Contribution from the Division of Chemistry, National Research Council, Ottawa. Issued as N.R.C. No. 2853.

² National Research Laboratories Postdoctorate Fellow 1950–52.

*The A_2 frequency ν_8 in *cis* $C_2D_2Cl_2$ was calculated in Reference (4) by means of the isotopic product rule. This is discussed below.

**Notation for symmetry types after G. Herzberg. *Infrared and Raman spectra*, D. Van Nostrand Co. Inc., New York, 1945.

spectra obtained on a sample prepared on an earlier occasion. Only minor differences were found.

In the attempt to observe the two low-lying fundamentals at 192 and 265 cm^{-1} heavily overexposed plates were obtained of *trans* C_2HDCl_2 , and of *trans* $\text{C}_2\text{H}_2\text{Cl}_2$ for comparison, since in *trans* $\text{C}_2\text{H}_2\text{Cl}_2$ these two fundamentals are forbidden in

TABLE I
INFRARED AND RAMAN FREQUENCIES FOR *cis* C_2HDCl_2

Infrared, cm^{-1}		Raman, cm^{-1} (Liquid)		Assignment
Vapor ^a	Liquid or dilute solution	Frequency	Optical density ^b	
		175	0.9	Fundamental A'
		387	0.6	Fundamental A''
$\begin{matrix} P & 552 \\ R & 564 \end{matrix}$	559^d (s)	561	0.5	Fundamental A'
$\begin{matrix} Q & 584 \\ R & 594 \end{matrix}$	583^d (vs)	590	0.2	Fundamental A''
	705 716	703	1.4	Fundamental A'
	~ 732 (w)			$560 + 175 = 735$ A'
$\begin{matrix} P & 781 \\ Q & 788 \\ R & 794 \end{matrix}$	783^d (vs)	781	0.15 ^c	Fundamental A'
$\begin{matrix} Q & 817 \\ R & 827 \end{matrix}$	813^d (vs)	817	0.2	Fundamental A''
$\begin{matrix} P & \sim 849 \\ Q & 856 \\ R & 862 \end{matrix}$	847^d (w)			<i>cis</i> $\text{C}_2\text{H}_2\text{Cl}_2$ impurity A_1
	~ 876 (w)			$175 + 703 = 878$ A'
	947^d (vs)	950	0.4	Fundamental A'
$\begin{matrix} 952 \\ 962 \end{matrix}$	970^d (w)	968	0.1	$387 + 590 = 977$ A'
	1036 (vw)			?
	~ 1072 (vw)			$1245 - 170 = 1070$ A'
	1117 (w)			$\begin{cases} 175 + 950 = 1125 & A' \\ 2 \times 560 = 1120 & A' \end{cases}$
$\begin{matrix} P & 1162 \\ Q & 1169 \\ R & 1176 \end{matrix}$	1168^d (m)			$387 + 783 = 1170$ A''
$\begin{matrix} P & 1247 \\ R & 1259 \end{matrix}$	1253^d (vs)	1245	0.4	Fundamental A'

^aFrequencies of bands in the vapor spectrum given only where additional structure is shown.

^bOptical densities not corrected for polarization effect on measured intensities. See D. H. Rank, *J. Optical Soc. Am.* 37: 798, 1947.

^cThis line is broad.

^dFrequency determined from the spectrum of the pure liquid. Other frequencies in this column determined from dilute solution spectra.

TABLE I (concluded)

Infrared, cm. ⁻¹		Raman, cm. ⁻¹ (Liquid)		Assignment	
Vapor ^a	Liquid or dilute solution	Frequency	Optical density ^b		
	1264 ^d (s)	1263	(0.05-0.1)	560 + 703 = 1263	A'
	1293 (w)			590 + 703 = 1293 or <i>cis</i> C ₂ H ₂ Cl ₂ impurity	A''
	1337 (w)			560 + 781 = 1341	A''
				387 + 950 = 1337	A''
P 1397 } R 1407 }	1401 ^d (s)			2 × 703 = 1406	A'
				1575 - 175 = 1400	A'
				590 + 817 = 1407	A'
~ 1478	1482 (m)			703 + 781 = 1484	A'
1553 } ^f 1571 } 1591 } ^f 1605 }	1552 ^d (s)	1553	(0.7)	Fundamental	A'' ^e
	1591 ^d (vs)	1591	(1.4)	2 × 781 = 1562	A'
	1628 ^d (m)			387 + 1245 = 1632	A''
	2193 (w)			950 + 1243 = 2193	A'
	~ 2255 (w)			?	
P 2299 } Q 2306 } R 2113 }	2299 (s)	2299	(0.9)	Fundamental	A'
2333 } 2341 }	~ 2335 (w) ^g			3 × 781 = 2343	A'
	2360 (w) ^g			1404 + 950 = 2354	A'
	~ 2500 (vw)			1264 + 1245 = 2509	A'
	2535 (vw)			1575 + 950 = 2525	A'
	2795 (w)			1245 + 1575 = 2818	A'
	2830 (w)			1264 + 1575 = 2839	A'
	2859 (w)			2299 + 561 = 2860	A'
	2979 (w)			{ 1404 + 1575 = 2979 A' 2299 + 703 = 3002 A'	
3090 unresolved	3076 (s)	3078	(~ 0.9)	Fundamental	A'
	3139 (m)			2 × 1575 = 3150	A'
	3181 (w)			?	
	3243 (w)			175 + 3076 = 3251	A'

^e Fermi resonance. Undisplaced fundamental at ~ 1575 cm.⁻¹^f Maxima displaced by overlapping of bands.^g Uncertainty in this frequency due to strong carbon dioxide absorption.

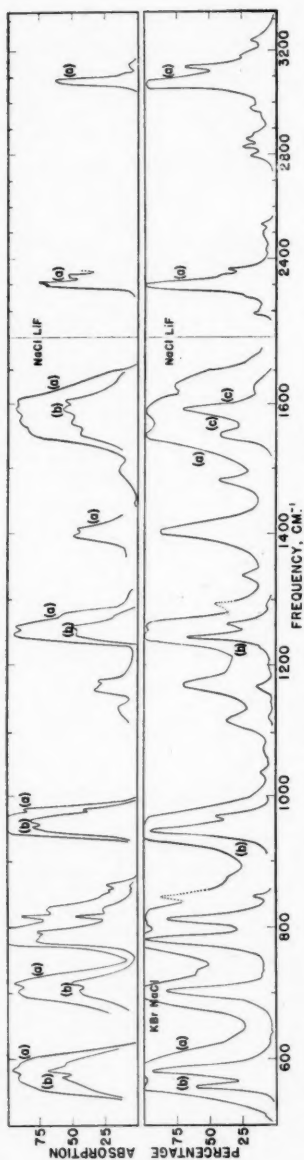


FIG. 1. *cis* C_2HDCl_2 . Upper panel: gas in 10 cm. cell (a) 120 mm. of Hg, (b) 30 mm. of Hg, (c) 10% in carbon disulphide, (c) 10% in carbon tetrachloride. Lower panel: liquid + solution in 0.1 mm. cell. (a) pure liquid, (b) 10% in carbon disulphide, (c) 10% in carbon tetrachloride.

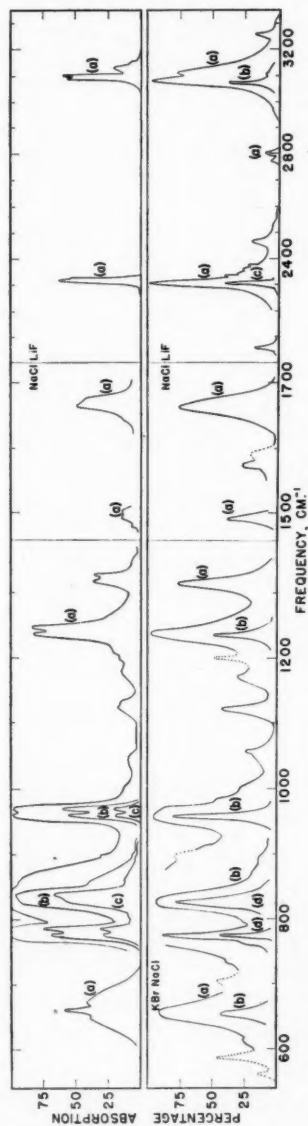


FIG. 2. *trans* C_2HDCl_2 . Upper panel: gas in 10 cm. cell (a) 120 mm. of Hg, (b) 20 mm. of Hg, (c) 5 mm. of Hg. Lower panel: liquid + solution in 0.1 mm. cell (a) pure liquid, (b) 10% in carbon disulphide, (c) 10% in carbon tetrachloride, (d) 2% in carbon disulphide. Dotted line denotes *cis* C_2HDCl_2 or *trans* $C_2H_2Cl_2$ as impurity.

the Raman spectrum. Although on these plates most of the fundamentals excited by $\lambda 4348$ and $\lambda 4338$ were visible no Raman lines at 192 or 265 cm^{-1} were observed. For these exposures a double-walled cooling jacket was used for the Raman cell and the inner annular compartment filled with a solution of praseodymium nitrate to cut down the continuous background from the arcs on the immediate long wave length side of the mercury line at $\lambda 4358$. One thickness of Wratten 34A gelatin filter was used to cut down the continuous background at longer wave lengths, and three thicknesses of Wratten 2B gelatin filter to remove mercury $\lambda 4047$ and $\lambda 4077$ radiation. No Raman lines excited by these mercury lines were detected.

To verify the Raman lines at $823, 834, 845,$ and 855 cm^{-1} (957 cm^{-1} excited by the $\lambda 4338$ mercury line falls in this region) microphotometer records were made at high linear magnification over the spectral region from 800 – 900 cm^{-1} . The plate was also examined visually with a low power microscope for anomalous irregularities in the plate grain and for dust particles. Raman exposures of various intensities (2–40 hr.) were made with and without filters for mercury $\lambda 4047$ radiation. Eastman Kodak 103a J plates were used throughout and were developed with D.K.76 developer. All plates were microphotometered on a Leeds and Northrup microphotometer.

CIS C_2HDCl_2

Assignment of Frequencies

There are two symmetry types A' and A'' for *cis* C_2HDCl_2 corresponding to in- and out-of-plane vibrations respectively. For convenience the frequencies (except for the choice between C–H and C–D stretching frequencies) have been arranged in the four symmetry types appropriate to *cis* $\text{C}_2\text{H}_2\text{Cl}_2$ and $\text{C}_2\text{D}_2\text{Cl}_2$ and are shown in Table II. The assignment for the *cis* compound was made immediately by comparison with the assignment for the d_0 and d_2 compounds (4). All fundamentals were observed in both the infrared and Raman spectra, except those at 175 and 387 cm^{-1} which were observed only in the Raman spectrum. The assignment is supported by the band contours of the infrared vapor bands as predicted qualitatively by the curves of Badger and Zumwalt (1) and the agreement with the product and sum rules (see below). No interpretation has been given for a number of weak frequencies in the region of the CH and CD stretching vibrations, owing to the large number of possible ternary combinations.

Product Rule Ratios for *cis* $\text{C}_2\text{H}_2\text{Cl}_2$, C_2HDCl_2 , and $\text{C}_2\text{D}_2\text{Cl}_2$

The moments of inertia of *cis* $\text{C}_2\text{H}_2\text{Cl}_2$, C_2HDCl_2 , and $\text{C}_2\text{D}_2\text{Cl}_2$ have been calculated using the bond lengths and angles quoted previously (4). The values are given below in units of 10^{-40} gm. cm^2 .

	<i>cis</i> $\text{C}_2\text{H}_2\text{Cl}_2$	<i>cis</i> C_2HDCl_2	<i>cis</i> $\text{C}_2\text{D}_2\text{Cl}_2$
I_A	70.4	76.5	82.5
I_B	329.8	332.3	334.8
I_C	400.2	408.8	417.2

One might expect the anharmonicity corrections to be approximately equal for the product ratios $\frac{\pi \text{cis } \text{C}_2\text{H}_2\text{Cl}_2}{\pi \text{cis } \text{C}_2\text{HDCl}_2}$ and $\frac{\pi \text{cis } \text{C}_2\text{HDCl}_2}{\pi \text{cis } \text{C}_2\text{D}_2\text{Cl}_2}$. For this approximate equal-

TABLE II
 FREQUENCY ASSIGNMENTS^a FOR *cis* C₂H₂Cl₂,^b C₂HDCl₂, AND C₂D₂Cl₂^b

Type	<i>cis</i> C ₂ H ₂ Cl ₂	<i>cis</i> C ₂ HDCl ₂	<i>cis</i> C ₂ D ₂ Cl ₂	
<i>A</i> ₁	<i>ν</i> ₁	3077 R. ^c	3078 or 2299 R. ^c , I. R. ^c	2325 R. ^c
	<i>ν</i> ₂	1587 R.	1575 R., I. R.	1570 R.
	<i>ν</i> ₃	1179 R.	950 R., I. R.	850 R.
	<i>ν</i> ₄	711 R.	703 R., I. R.	689 R.
	<i>ν</i> ₅	173 R.	175 R.	171 R.
<i>B</i> ₁	<i>ν</i> ₆	3072 I. R.	2299 or 3078 R., I. R.	2280 I. R.
	<i>ν</i> ₉	1294 I. R.	1245 R., I. R.	1040 I. R.
	<i>ν</i> ₁₀	848 I. R.	781 R., I. R.	761 I. R.
	<i>ν</i> ₁₁	571 I. R.	561 R., I. R.	540 I. R.
<i>A</i> ₂	<i>ν</i> ₆	876 R.	817 R., I. R.	695 ^d
	<i>ν</i> ₇	406 R.	387 R.	368 R.
<i>B</i> ₂	<i>ν</i> ₁₂	697 I. R.	590 R., I. R.	558 I. R.

^aLiquid frequencies are used throughout this table. All frequencies for *cis* C₂HDCl₂ are liquid Raman values.

^bFrequency assignment for *cis* C₂H₂Cl₂ and C₂D₂Cl₂ from Bernstein and Ramsay (Ref. 4). The Raman data for these molecules were taken from G. Herzberg, *Infrared and Raman spectra of polyatomic molecules*, D. Van Nostrand Co., Inc., New York, N.Y. 1945, p. 330, and B. Trumpy, *Z. Physik*, 98: 672, 1935.

^cR. and I. R. denote that the line has been observed as a Raman displacement and infrared band respectively.

^dRecalculated from product rule relations. See below.

ity to hold for the out-of-plane vibrations, the *A*₂ frequency of *cis* C₂D₂Cl₂ calculated previously (4) to be at 710 cm.⁻¹ should be lowered to 695 cm.⁻¹ The frequency at 695 cm.⁻¹ corresponds then to a value of the product ratio $\frac{\pi A_2 \text{ cis } C_2H_2Cl_2}{\pi A_2 \text{ cis } C_2D_2Cl_2}$ of 1.39 as compared with the theoretical (harmonic) value of 1.40.

The theoretical product rule ratios are compared in Table III with those obtained from the frequencies listed in Table II with the exception that *ν*₅ for *cis* C₂HDCl₂ is taken as 172 cm.⁻¹ instead of 171 cm.⁻¹ (4).

Application of the Sum Rules for Vibration Frequencies

A further check on the assignment can be made on the basis of the sum rules

 TABLE III
 PRODUCT RULE RATIOS FOR *cis* C₂H₂Cl₂, C₂HDCl₂, AND C₂D₂Cl₂

	In-plane vibrations		Out-of-plane vibrations	
	Theor. ratio	Obs. ratio	Theor. ratio	Obs. ratio
$\frac{\text{cis } C_2H_2Cl_2}{\text{cis } C_2HDCl_2}$	1.96	1.95	1.35	1.33
$\frac{\text{cis } C_2HDCl_2}{\text{cis } C_2D_2Cl_2}$	1.95	1.96	1.31	(1.31)*

*This ratio has been calculated with *ν*₆ = 695 cm.⁻¹ as in Table II.

(5, 7). Table IV gives the observed values of $\Sigma\nu^2$ for the in-plane and out-of-plane classes of *cis* C₂HDCl₂, and those found by interpolation between the $\Sigma\nu^2$ of the corresponding classes of *cis* C₂H₂Cl₂ and C₂D₂Cl₂. The comparison is also made using $\Sigma\nu$ instead of $\Sigma\nu^2$ since it can be shown empirically (3) that $\Sigma\nu$ may be used instead of $\Sigma\nu^2$ with a similar degree of accuracy in all cases covered by the sum rule for $\Sigma\nu^2$.

TABLE IV
SUM RULES FOR *cis* C₂H₂Cl₂, C₂HDCl₂, AND C₂D₂Cl₂

	<i>cis</i> C ₂ H ₂ Cl ₂	<i>cis</i> C ₂ HDCl ₂		<i>cis</i> C ₂ D ₂ Cl ₂
	Obs.	Obs.	Calc.	Obs.
In-plane vibrations (cm. ⁻¹)				
$\Sigma\nu$	12512	11367	11369	10226
$\Sigma\nu^2 \cdot 10^{-6}$	26.338	21.418	21.425	16.511
Out-of-plane vibrations (cm. ⁻¹)				
$\Sigma\nu$	1979	1794	1799	1618
$\Sigma\nu^2 \cdot 10^{-6}$	1.418	1.165	1.174	0.930

TRANS C₂HDCl₂

As with *cis* C₂HDCl₂, for the purpose of comparison, the frequencies have been arranged in the four symmetry classes appropriate to *trans* C₂H₂Cl₂ and C₂D₂Cl₂ and are shown in Table VI. Except for ν_4 and ν_6 , the assignment follows immediately from the assignments for *trans* C₂H₂Cl₂ and C₂D₂Cl₂. The assignment of frequencies of 824 and 834 cm.⁻¹ to ν_4 and ν_6 respectively seems, however, reasonably certain. The Raman frequencies at 823 and 834 cm.⁻¹ are partially overlapped, and the spectrum in this region is also complicated by the presence of the weak Raman line at 845 cm.⁻¹ due to *trans* C₂H₂Cl₂ impurity, and a weak Raman line at approximately 856 cm.⁻¹ arising from excitation of the strong 957 cm.⁻¹ Raman line by the mercury line at $\lambda 4339$. An attempt was made to measure the polarization of the Raman lines at 823 and 834 cm.⁻¹ but without success. (An added difficulty is the slow polymerization of the *trans* C₂HDCl₂, though this is much reduced if a strong filter for mercury radiation at $\lambda 4047$ is used.) Both the infrared vapor and liquid spectra indicate also the existence of more than one line in the region 820–849 cm.⁻¹ The stronger Raman line at 823 cm.⁻¹ has been assigned to ν_4 , which in the centrosymmetric molecules belongs to the symmetrical C–Cl stretching vibration, and the weaker to ν_6 , an out-of-plane vibration. Assigning the pair of frequencies in this way is consistent with interpreting the shoulder at ~ 857 cm.⁻¹ in the infrared vapor spectrum, as the *R* branch of ν_6 .

The 775 cm.⁻¹ frequency must be assigned to a C–Cl stretching vibration rather than to an out-of-plane vibration because the latter assignment would not give agreement with either the product or the sum rules.

Product Rule Ratios for *trans* C₂H₂Cl₂, C₂HDCl₂, and C₂D₂Cl₂

The moments of inertia of *trans* C₂H₂Cl₂, C₂HDCl₂, and C₂D₂Cl₂ have been calculated using the bond lengths and angles quoted by Bernstein and Ramsay

TABLE V
 INFRARED AND RAMAN FREQUENCIES OF *trans* C₂HDCl₂

Infrared, cm. ⁻¹		Raman, cm. ⁻¹ (Liquid)		Assignment
Vapor ^a	Liquid or dilute solution	Frequency	Optical density ^b	
	560	348	(1.2)	Fundamental A'
	585			<i>cis</i> C ₂ HDCl ₂ impurity
	613 (vw)			<i>cis</i> C ₂ HDCl ₂ impurity
				348 + 265 = 613 A'
P 648 } Q 660 } R 672 }	654 ^d (s)	659	(0.25)	Fundamental A''
	704 (w)	704	(0.01-0.02) ^c	<i>cis</i> C ₂ HDCl ₂ impurity
	736 (vw)			823 + 265 - 348 = 740 A'
	765 ^d (vw)			957 - 192 = 765 A''
P 766 } R 785 } P 824 } R 836 } R? 857 }	775 ^d (vs)	775	(0.25-0.3)	Fundamental A'
	825 ^d (vs)	823	(0.2)	Fundamental A'
		834	(0.1) ^c	Fundamental A''
	897 (w)	845	(0.05) ^c	<i>trans</i> C ₂ H ₂ Cl ₂ impurity
P 959 } R 968 }	958 ^d (vs)	957	(0.6)	<i>trans</i> C ₂ H ₂ Cl ₂ impurity
				Fundamental A'
	~ 980 (w)			1238 - 265 = 973 A'
	~ 995 (w)			347 + 658 = 1005 A''
	1056 (w)			1238 - 192 = 1046? A''
	1123 (m)			348 + 775 = 1123 A'
	1172 (w)			348 + 823 = 1171 A'
	1200 ^d (m)			<i>trans</i> C ₂ H ₂ Cl ₂ impurity
P 1236 } R 1246 } P 1316 } 1326 }	1236 (s)	1238	(0.7)	Fundamental A'
		1274	(0.02) ^c	<i>trans</i> C ₂ H ₂ Cl ₂ impurity
	1314 (ms)			2 × 659 = 1318 A'
	1493 (m)			{ 265 + 1238 = 1503 A' 659 + 834 = 1493 A'
		1541	(0.2)	2 × 775 = 1550 A''
	1574 (w)	1574	(0.75)	Fundamental A'
	1592 ^d (w)			{ 823 + 775 = 1598 A' or <i>cis</i> C ₂ HDCl ₂ impurity
	1662 (ms)	1647	(0.05-0.1)	2 × 822 A'
				823 + 834 = 1657 A''
		1736	(0.02) ^c	957 + 775 = 1732 A'
		1918	(0.02) ^c	2 × 957 = 1914 A'
	2058 (w)			823 + 1238 = 2061 A'
2310	2302 (s)	2304	(0.4)	Fundamental A'
	2333 (vw)			1574 + 775 = 2349 A'
	2357 (vw)			1123 + 1238 = 2361 A'
	2373 (vw)			1574 + 834 = 2408 A''
	2465 (w)			2 × 1238 = 2476 A'
	2771 (vw)			1314 + 1493 = 2807? A'
	2801 (w)			{ 1238 + 1574 = 2812 3075 - 265 = 2810
3082 } 3092 } 3124 }	3075 (s)	3074	(~ 0.4)	Fundamental A'
	3105 ^d (m)			2304 + 823 = 3127 A'
	3255 ^d (w)			2304 + 957 = 3261 A'

^aFrequencies of bands in the vapor given only when additional structure is shown.

^bOptical densities not corrected for polarization effect on measured intensities. See D. H. Rank. *J. Optical Soc. Am.* 37: 798. 1947.

^cThese lines observed more strongly on a more heavily exposed plate.

^dThese frequencies determined in dilute solution, all others are for the liquid.

^ePractically no Fermi resonance since the undisplaced fundamental cannot be very different from 1575 cm.⁻¹, the arithmetic mean of the corresponding d₀ and d₂ frequencies.

TABLE VI
 FREQUENCY ASSIGNMENT^a FOR *trans* C₂H₂Cl₂,^b C₂HDCl₂, AND C₂D₂Cl₂^b

Type	<i>trans</i> C ₂ H ₂ Cl ₂	<i>trans</i> C ₂ HDCl ₂	<i>trans</i> C ₂ D ₂ Cl ₂
<i>A_g</i>			
ν_1	3071 R. ^c	3074 or 2304 R. ^c , I. R. ^c	2325 R. ^c
ν_2	1576 R.	1574 R., I. R.	1570 R.
ν_3	1270 R.	1238 R., I. R.	922 R.
ν_4	844 R.	823 R., I. R.	765 R.
ν_5	349 R.	348 R.	346 R.
<i>B_u</i>			
ν_9	3080 I. R.	2304 or 3074 R., I. R.	2285 I. R.
ν_{10}	1200 I. R.	957 R., I. R.	912 I. R.
ν_{11}	817 I. R.	775 R., I. R.	784 I. R.
ν_{12}	265 I. R. ^d	265 I. R. ^d	265 I. R. ^d
<i>A_u</i>			
ν_6	895 I. R.	834 R.	658 I. R.
ν_7	192 I. R. ^d	192 I. R. ^d	192 I. R. ^d
<i>B_g</i>			
ν_8	758 R.	659 R., I. R.	657 R.

^aLiquid frequencies are used throughout this table. All frequencies for *trans* C₂HDCl₂ are liquid Raman values.

^bFrequency assignments for *trans* C₂H₂Cl₂ and C₂D₂Cl₂ from Bernstein and Ramsay (Ref. 4). The Raman data for these molecules were taken from G. Herzberg, *Infrared and Raman spectra of polyatomic molecules*, D. Van Nostrand Co., Inc., New York, N. Y. 1945, p. 330 and Trumpy, B. Z. Physik, 98: 672, 1935.

^cR., I. R., denote the line has been observed as a Raman displacement and infrared band respectively.

^dFrom combination tones.

(4). The values are given below in units of 10⁻⁴⁰ gm. cm.²

	C ₂ H ₂ Cl ₂	C ₂ HDCl ₂	C ₂ D ₂ Cl ₂
I_A	15.78	19.47	23.30
I_B	550.9	551.1	551.2
I_C	566.6	570.5	574.5

The theoretical product rule ratios are compared with those calculated from the frequencies listed in Table VI and are shown in Table VII.

In Table VIII the sum rule (5, 7) calculations are used as a further check on the assignment, just as for the corresponding calculations made for the *cis* compounds (see Table IV).

In Table IX the approximate product rule for rotational isomers (2) is used as a further check on the assignment. Since the agreement between theoretical

 TABLE VII
 PRODUCT RULE RATIOS FOR *trans* C₂H₂Cl₂, C₂HDCl₂, AND C₂D₂Cl₂

	In-plane vibrations		Out-of-plane vibrations	
	Theor. ratio	Obs. ratio	Theor. ratio	Obs. ratio
<i>trans</i> C ₂ H ₂ Cl ₂	1.96	1.86	1.27	1.23
<i>trans</i> C ₂ HDCl ₂				
<i>trans</i> C ₂ HDCl ₂	1.96	1.87	1.29	1.27
<i>trans</i> C ₂ D ₂ Cl ₂				

TABLE VIII
APPLICATION OF THE SUM RULES TO *trans* C₂H₂Cl₂, C₂HDCl₂, AND C₂D₂Cl₂

	<i>trans</i> C ₂ H ₂ Cl ₂	<i>trans</i> C ₂ HDCl ₂		<i>trans</i> C ₂ D ₂ Cl ₂
	Obs.	Obs.	Calc.	Obs.
In-plane vibrations				
$\sum \nu$	12472	11358	11358	10244
$\sum \nu^2 \cdot 10^{-6}$	26.026	21.153	21.162	16.297
Out-of-plane vibrations				
$\sum \nu$	1845	1685	1676	1507
$\sum \nu^2 \cdot 10^{-6}$	1.413	1.167	1.157	0.902

TABLE IX
THE APPROXIMATE PRODUCT RULE FOR ROTATIONAL ISOMERS

Molecule	Product of the in-plane frequencies in <i>trans</i>	
	Product of the in-plane frequencies in <i>cis</i>	
	Calculated	Observed
C ₂ H ₂ Cl ₂	1.19	1.06
C ₂ HDCl ₂	1.18	1.11
C ₂ D ₂ Cl ₂	1.17	1.16

and observed products for this rule is not better than within $\pm 10\%$, it may be regarded as satisfactory (see Table IX).

REFERENCES

1. BADGER, R. M. and ZUMWALT, L. R. J. Chem. Phys. 6: 711. 1938.
2. BERNSTEIN, H. J. J. Chem. Phys. 17: 256. 1949.
3. BERNSTEIN, H. J. and PULLIN, A. D. E. (In press.)
4. BERNSTEIN, H. J. and RAMSAY, D. A. J. Chem. Phys. 17: 556. 1949.
5. DECIUS, J. C. and BRIGHT WILSON, E. Jr. J. Chem. Phys. 19: 1410. 1951.
6. LEITCH, L. C. and MORSE, A. T. Can. J. Chem. 29: 1034. 1951.
7. SVERDLOV, L. M. Doklady Akad. Nauk S.S.S.R. 78: 1115. 1951.

BINDING OF ANIONS BY DENATURED PROTEINS¹

By J. ROSS COLVIN

ABSTRACT

The adsorption by soluble and insoluble heat-denatured lysozyme of eight anionic dyes, including methyl orange, has been determined at several temperatures and pH values. In addition, the adsorption of methyl orange by both the soluble and insoluble forms of seven other heat-denatured proteins has been determined as a function of temperature and pH. The isotherms, which are normal, reproducible, reversible, and independent of protein concentration confirm the notion of a sheath of strongly orientated water molecules about small positive proteins. They also demonstrate directly the importance of $-\Delta F$ of hydration in protein interaction studies. pH dependence of adsorption of methyl orange and other anions to denatured proteins is normal but $-\Delta H$ of adsorption per mole of anion bound is greater than for the corresponding native form.

These results discredit the current concept of unique specific binding sites on a protein for weak interactions of the type studied.

INTRODUCTION

During the last decade, investigators of protein-small molecule interaction have constructed a single theory of the mechanism of binding of some azobenzenesulphonates to plasma albumins (7, 8, 9, 12). The theory is based primarily on Coulomb attraction between the sulphonate ion and cationic groups on the protein but this may be reinforced by hydrogen bonding between the anion amino nitrogen and the hydroxyls of the protein.

Although such mechanisms explain the binding of anions to plasma albumins, recent work (3) demonstrates that they do not account for the interaction of the same anions with other proteins. The anion of methyl orange, for example, is bound strongly to negative plasma albumin but is not bound at all by lysozyme although this positive protein has approximately 20 cationic groups suitable for interaction with the sulphonate radical and 20 free hydroxyls available for forming hydrogen bonds with the dimethyl amino nitrogen (5). Several other organic anions which are adsorbed avidly on negative proteins also were not bound to lysozyme. Furthermore, the adsorption of larger azobenzenesulphonates on lysozyme, calf thymus histone sulphate, and protamine sulphate was characterized by an unusual sigmoid isotherm (3).

This behavior can be explained by assuming a solvent sheath maintained about the small positively charged protein by overlapping of the local fields of the cationic groups. Such a sheath would prevent the adsorption of small anions. Larger anions, with a greater van der Waals attraction, may penetrate the sheath and thereby decrease the net field strength. The resultant increased ease of binding of additional anions would be reflected in a sigmoid isotherm.

Such an hypothesis is susceptible to experimental test. The denaturation of lysozyme with resulting disorientation of the molecule and dispersion of the positive field over a larger volume should promote binding of small anions. This treatment should also convert the anomalous isotherms for the larger anions into

¹ Manuscript received August 14, 1952.

Contribution from the Division of Applied Biology, National Research Laboratories, Ottawa, Canada. Issued as N.R.C. No. 2856.

normal hyperbolas. Conversely, denaturation of large negative proteins should have little effect on their anion binding capacity. Since denaturation does promote the binding of methyl orange by lysozyme (3), the effects of thermal denaturation on the adsorption isotherms of several proteins and anions have been studied.

MATERIALS AND METHODS

The adsorption isotherms of all native and denatured proteins that remained soluble were determined by the method of dialysis equilibrium previously described (3). This technique involves determination of the distribution of small molecules between a protein solution on one side of a semipermeable membrane and a buffer solution on the other.

This method was not suitable for denatured proteins that coagulate on heating and, for these, a new technique was developed. Known amounts of protein and dye dissolved in a given volume of buffer were heated under reflux for 30 min. in boiling water, cooled, and the precipitate removed by centrifugation at room temperature. The difference between the total amount of dye used and the amount remaining in the supernatant was assumed to be bound to coagulated protein. Control experiments showed that no dye was destroyed during heating, and that the change in volume of solvent was negligible. In addition, it was shown that for methyl orange and denatured plasma albumin at pH 5.5, results obtained by this method were comparable to those by a modified dialysis equilibrium experiment (Fig. 6). Although precipitation of denatured plasma albumin was complete, a maximum of 10% of the total nitrogen of the lysozyme remained in solution after heat treatment. This means that figures given for number of dye anions bound per molecule of protein after denaturation are minimum values. Fortunately, all conclusions drawn from the results of this study are in such a direction that they would be strengthened if precipitation of any denatured protein were incomplete.

Denaturation of the protein, in conditions where it remained soluble, was carried out by heating under reflux in boiling water for 30 min. Adjustment of the pH of such solutions closer to the isoelectric point invariably caused precipitation of protein and was taken as proof of alteration of structure. It was assumed that denaturation was complete and that the change in volume of solution was negligible.

Lysozyme, plasma albumin, β -lactoglobulin, pepsin, and ovalbumin used in this study were crystallized products obtained from Armour and Company, Chicago. Lysozyme, plasma albumin, and β -lactoglobulin were homogeneous electrophoretically at pH 6.8 in 0.05 *M* phosphate buffer while pepsin was heterogeneous.

Ovalbumin, which appeared to be crystalline, was contaminated by a small amount of some substance, perhaps surface denatured material, which did not dissolve in buffer. This material remained suspended during an experiment.

All buffers were made according to Clark (2) from reagent grade materials and were checked against commercial standards.

Most of the adsorption isotherms were determined at room temperature (25° -

27°C.) with no attempt at rigid temperature control. However, experiments on the temperature dependence of binding were carried out in rooms maintained at a given temperature $\pm 0.5^\circ\text{C}$.

RESULTS

Test of Methods

Preliminary experiments were concerned with reproducibility of the adsorption isotherm for methyl orange on denatured coagulated lysozyme and plasma albumin. Concurrently, reversibility of the adsorption process and its dependence on such factors as protein concentration and degree of dispersion of precipitated protein were also tested. Results are given for lysozyme in Fig. 1. For each group, dotted lines indicate minimum and maximum limits of deviation for combined results of all experiments in this series. Clearly, methyl orange is bound strongly

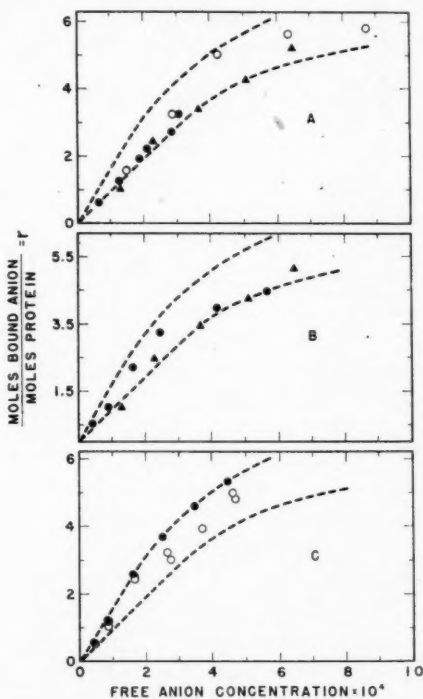


FIG. 1. A. Reproducibility of binding of methyl orange to heat-denatured precipitated lysozyme in 0.05 *M* phosphate buffer, pH 6.8. Similar symbols identify points belonging to the same independent experiment.

B. Independence of protein concentration of the binding of methyl orange by heat-denatured, precipitated lysozyme in 0.05 *M* phosphate buffer, pH 6.8

0.5% lysozyme ● 0.2% lysozyme ▲

C. Reversibility of binding of methyl orange to heat-denatured, precipitated lysozyme in 0.05 *M* phosphate buffer, pH 6.8

● equilibrium approached from above,

○ equilibrium approached from below.

and in normal fashion by denatured precipitated lysozyme at pH 6.8, in sharp contrast to its lack of adsorption by the native protein (3, 10, 11). Furthermore, the isotherm is reproducible (Fig. 1A), reversible (Fig. 1C), and independent of protein concentration (Fig. 1B) within experimental error. In a similar way, binding of methyl orange to denatured plasma albumin was found to be reversible, reproducible, and independent of protein concentration. Taken together, these results demonstrated that the adsorption characteristics of denatured proteins were well-defined equilibrium properties that were not sensitive to conditions of transition between the native and denatured forms.

Effect of Denaturation on Adsorption

Adsorption isotherms of denatured, precipitated lysozyme at pH 6.8 for anions of the dyes *p*-nitrophenol, sodium picrate, fluorescein, and *p*-hydroxyerioglucine are shown in Fig. 2. All of the anions were adsorbed, in contrast to previous work with native lysozyme that showed negligible adsorption. As expected, intensity of binding increased with the size and charge of the anion.

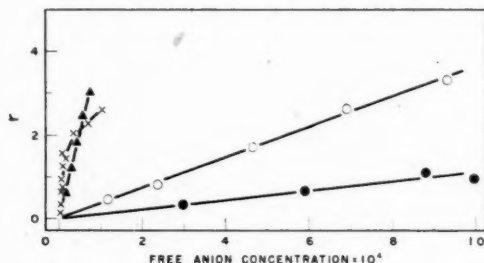


FIG. 2. Binding of *p*-nitrophenol, ●; picrate, ○; fluorescein, ▲; and *p*-hydroxyerioglucine, X, to heat-denatured precipitated lysozyme in 0.05 *M* phosphate buffer, pH 6.8.

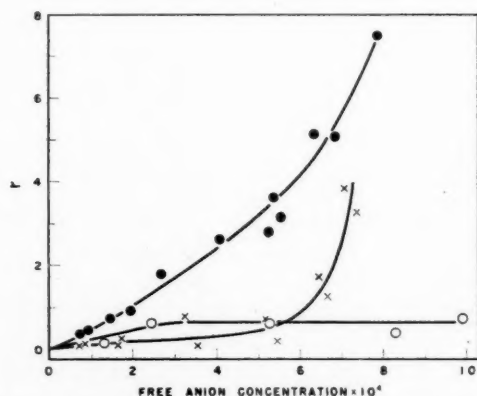


FIG. 3. Binding of sodium picrate, ○, and methyl orange, ●, to heat-denatured, soluble lysozyme in 0.05 *M* acetate buffer, pH 5.5. Also shown (X) is the adsorption isotherm for methyl orange on native lysozyme at pH 5.5.

Binding of sodium picrate and methyl orange to soluble denatured lysozyme, and to native lysozyme, at pH 5.5 is shown in Fig. 3. Contrary to expectations based on electrostatic effects, binding capacity of the denatured form for each anion is considerably less at pH 5.5 than at pH 6.8 (Figs. 1 and 2). The binding of *p*-nitrophenol and *p*-hydroxyerioglucine to soluble denatured lysozyme was also found to be negligible at pH 5.5. Adsorption isotherms for methyl orange at pH 5.5 were invariably exponential over the whole available concentration range although, because of the autocatalytic nature of the reaction, they were not readily reproducible in successive experiments.

Effect of denaturation of lysozyme at pH 6.8 on the shape of adsorption isotherms of anions which were bound with a sigmoid curve was investigated. Results are shown in Fig. 4 for Orange I, Orange II, and 2,4-dinitro-1-naphthol-

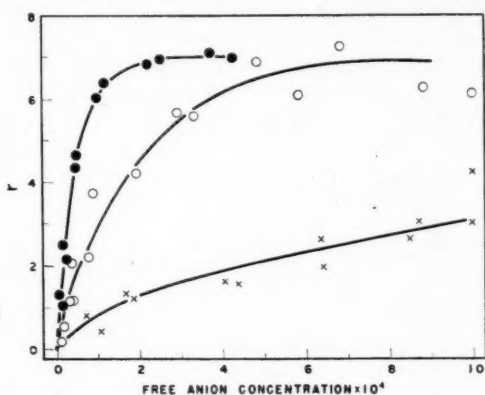


FIG. 4. Binding of Orange I, \circ ; Orange II, \bullet ; 2,4-dinitro-1-naphthol-7-sulphonic acid, \times , to heat-denatured precipitated lysozyme in 0.05 *M* phosphate buffer, pH 6.8.

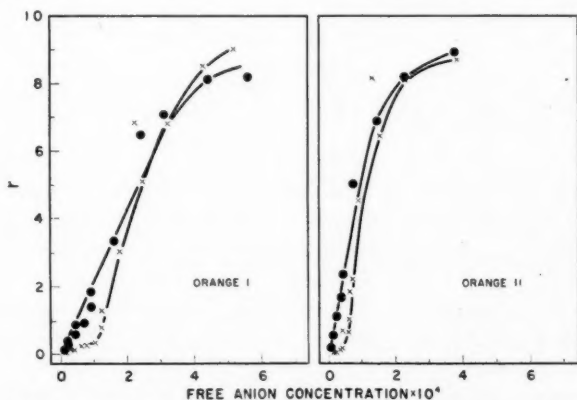


FIG. 5. Binding of Orange I and Orange II on native and heat-denatured soluble lysozyme in 0.05 *M* acetate buffer at pH 5.5.

\times native

\bullet denatured

7-sulphonic acid, which were shown previously to be bound with this type of isotherm (3). Clearly, the sigmoid isotherms have been eliminated completely by heat-denaturation although the total binding capacity of denatured insoluble lysozyme for a given anion has not been altered appreciably from that of the native form (3).

These results were confirmed by isotherms for Orange I and Orange II on denatured lysozyme at pH 5.5 where the protein is still soluble (Fig. 5). Isotherms for the native form under the same conditions are given for comparison. Because the accuracy and precision of experiments of this type are greatest at low anion concentrations (3) these isotherms show that denaturation has markedly altered the characteristics of adsorption at low, but not at high, dye concentrations.

Binding capacity of native and denatured plasma albumin for methyl orange at two pH levels is given in Fig. 6. At pH 6.8, the denatured protein was soluble, but its adsorption capacity was strikingly reduced compared with the native form. In contrast, at pH 5.5, where the denatured protein is insoluble, intensity of adsorption and total binding capacity were greater than in the native state.

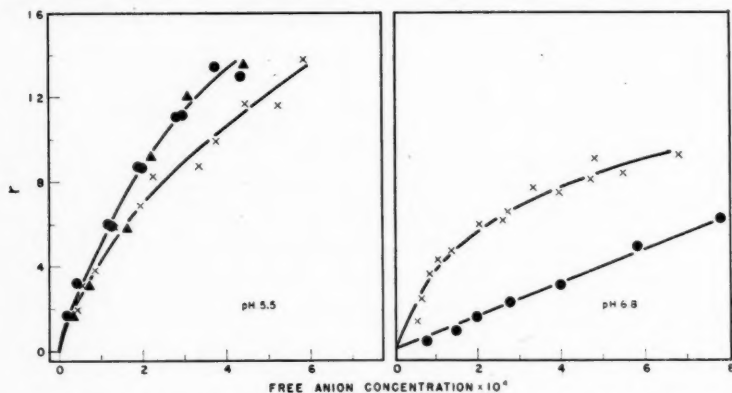


FIG. 6. Binding of methyl orange to native and heat-denatured plasma albumin in 0.05 *M* phosphate buffer, pH 6.8, and in 0.05 *M* acetate buffer, pH 5.5. At pH 5.5, those points which are indicated by a triangle, Δ , were estimated for heat-denatured plasma albumin using a modified dialysis equilibrium technique.

x native

● denatured

A similar situation exists for adsorption of methyl orange on β -lactoglobulin (Fig. 7). Denatured soluble β -lactoglobulin at pH 6.8 had a markedly lower affinity for methyl orange than the native form under the same conditions, whereas the insoluble form at pH 5.5 or 4.8 had a much higher adsorption capacity.

Since it was shown previously (3) that the binding of some anions on lysozyme was analogous to their binding on histone sulphate and protamine sulphate, the effect of heat treatment on adsorption properties of these two positive materials for methyl orange was investigated at pH 6.8. However, it was found that binding of this anion to both proteins was not perceptibly changed within the rather wide limits of experimental error.

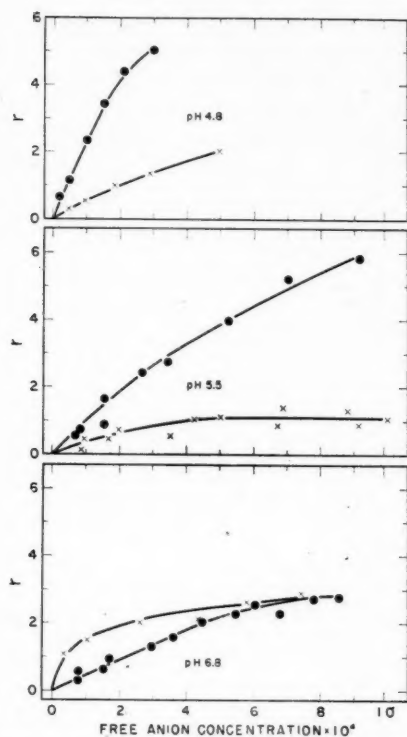


FIG. 7. Binding of methyl orange on native and heat-denatured β -lactoglobulin in 0.05 *M* phosphate buffer, pH 6.8; 0.05 *M* acetate buffer, pH 5.5; 0.05 *M* acetate buffer, pH 4.8. At pH 6.8 denatured β -lactoglobulin is soluble while at pH 5.5 and 4.8 it is not.

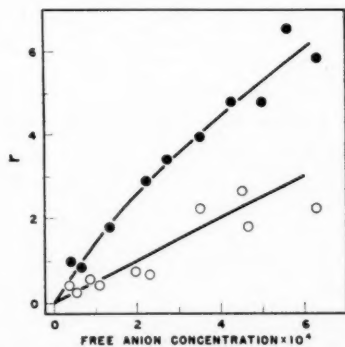


FIG. 8. Binding of methyl orange to heat-denatured precipitated ovalbumin in 0.05 *M* acetate buffer, pH 5.5, ●, and to soluble heat-denatured ovalbumin, 0.05 *M* phosphate buffer, pH 6.8, ○.

The negligible binding of methyl orange to native pepsin at pH 4.8 and 6.8 (10) was confirmed. In addition, it was shown that denaturation and precipitation of pepsin at pH 4.8 did not increase binding of methyl orange perceptibly.

Earlier observations by Klotz and Urquhart (10) on the negligible adsorption of methyl orange by native ovalbumin were confirmed at pH 5.5 and 6.8. In addition, like lysozyme, soluble denatured ovalbumin adsorbed methyl orange although its capacity was much less than that of the denatured precipitated protein (Fig. 8).

Temperature Coefficient of Adsorption by Denatured Proteins

Temperature dependence of binding of methyl orange and of Orange II to denatured lysozyme at pH 6.8 are shown in Fig. 9A and 9B respectively. The same function for methyl orange on denatured plasma albumin at pH 5.5 and

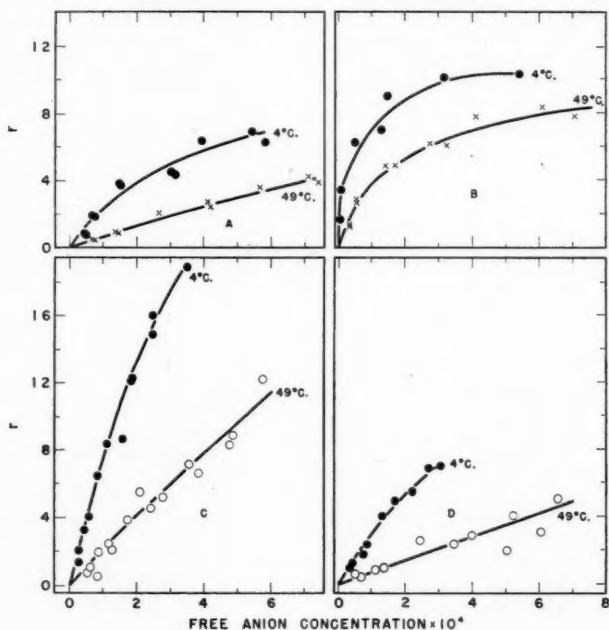


FIG. 9. Temperature dependence of binding of methyl orange and Orange II to heat-denatured lysozyme and serum albumin.

A. Methyl orange and insoluble denatured lysozyme in 0.05 *M* phosphate, pH 6.8.

B. Orange II and insoluble denatured lysozyme in 0.05 *M* phosphate, pH 6.8.

C. Methyl orange and insoluble denatured plasma albumin in 0.05 *M* acetate, pH 5.5.

D. Methyl orange and soluble denatured plasma albumin in 0.05 *M* phosphate, pH 6.8.

6.8 is shown by Fig. 9C and 9D. All of these figures show that the temperature coefficient for binding of anions to denatured protein is appreciable.

pH Dependence of Adsorption by Denatured Proteins

The effect of change in pH on adsorption of methyl orange and of Orange II

to denatured precipitated lysozyme is shown in Fig. 10. In both instances, the effect was appreciable and was in the direction to be expected from electrostatic causes.

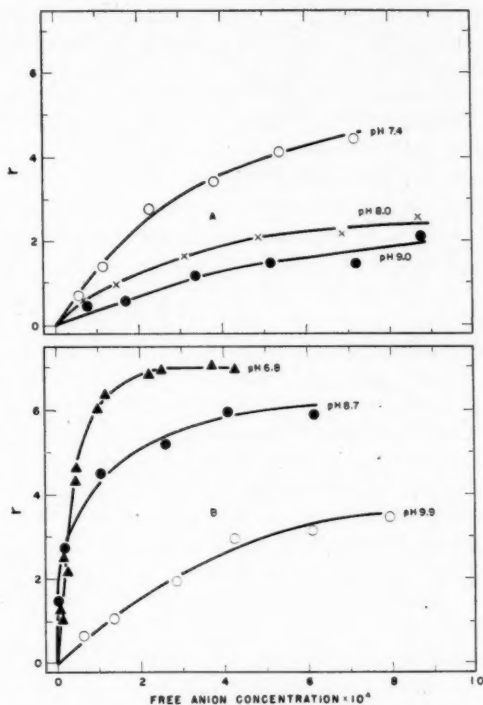


FIG. 10. Effect of pH change on the binding of:
 A. Methyl orange by heat-denatured precipitated lysozyme. pH 7.4 and 8.0, 0.05 *M* phosphate. pH 9.0, approximately 0.05 *M* glycinate.
 B. Orange II by heat-denatured, precipitated lysozyme. pH 6.8, 0.05 *M* phosphate; pH 8.7 and 9.9, approximately 0.05 *M* glycinate.

DISCUSSION

The foregoing results show that denaturation of lysozyme increases its binding capacity for small anions, and converts sigmoid isotherms for larger anions to normal hyperbolas without greatly altering total binding capacity. Since soluble denatured lysozyme adsorbs methyl orange appreciably while the native form does not, the increase is not due primarily to a phase change associated with denaturation. This interpretation is confirmed by nonadsorption of methyl orange on denatured precipitated pepsin. Furthermore, Verwey-Overbeek attraction between the double layers cannot explain these effects since it should be equally effective for native lysozyme (14). In addition, although some degradation of the protein does take place, it is not so extensive that the change in adsorption can be credited to changes in gross chemical composition. Moreover, since the very

high positive charge of lysozyme in solution, and the data of Fraenkel-Conrat (4), indicate that guanidinium and hydroxyl groups are free in lysozyme, these results are probably not due to an increase in available groups for bonding, as seems to be the situation for ovalbumin with sulphhydryl reagents (1). Finally, Klotz's concept (7) of competition between protein hydroxyls and free anions for available cationic groups on the protein might explain the low binding capacity of lysozyme for small anions but it offers no explanation of the sigmoid isotherms for larger radicals. In short, all these results are consistent only with the concept of partial disruption of a solvation sheath about the large molecule and, to that extent, they confirm the hypothesis advanced.

The lack of effect of thermal treatment on the binding of methyl orange to calf thymus histone sulphate and protamine sulphate is not inconsistent with the hypothesis. Although information on the periodicity of internal structure of these substances is meager, they seem to be random, extended polypeptides without much long range order. If so, heat treatment which did not cause degradation would not alter their adsorption properties.

The decrease in binding capacity of soluble denatured protein compared to the native form (except lysozyme and ovalbumin) and the increase in capacity of the insoluble modification is striking. Apparently, the solvation sheath that, under certain conditions, maintains the denatured protein in solution simultaneously decreases its binding capacity for anions. This total binding capacity of soluble denatured protein is less than that of the native protein because of lower van der Waals attraction due to disorientation of the original structure. When the extent of the solvent sheath is reduced or it is removed by a change in charge, the denatured protein precipitates. Its binding capacity for anions, however, is simultaneously increased.

Denatured soluble lysozyme has a higher binding capacity than the native form but the increase is less than for the insoluble denatured modification. The difference between the two increments is highly significant because denatured soluble lysozyme at pH 5.5 is more highly positively charged than the insoluble form at pH 6.8. Therefore one would expect binding of anions by soluble denatured lysozyme to be greater. Nonetheless, as shown by the isotherms, the total free energy decrease per mole of anion bound to denatured lysozyme is distinctly lower for all anions at pH 5.5 than at pH 6.8. This decrease can be attributed only to increased strength of attachment of solvent molecules around cationic groups on the soluble denatured protein as compared to the insoluble.

For negative proteins, such as ovalbumin, interpretation of a similar change in affinity is complicated by a simultaneous increase in charge on the negative denatured molecules. The direct evidence from lysozyme suggests strongly, however, that Coulomb forces cannot be the only, or even the most important, factor involved in such a change of affinity. Clearly, it is not permissible to neglect the ΔF of hydration in any attempt to estimate quantitatively relative binding capacities of proteins for anions (6, 13).

The increase in binding of soluble denatured lysozyme compared to the native form indicates that decrease in the over-all hydration sheath about the lysozyme

molecule on disorientation is more than sufficient to offset the decrease in the sum of the Coulomb plus van der Waals forces. This permits appreciable binding of anions even though the local fields about each cationic group are sufficient to maintain the protein in solution.

The exponential form of the isotherm for methyl orange on lysozyme at pH 5.5 (Fig. 3) shows that for this positive protein, heat treatment has not entirely removed interaction of such local fields with one another. For the larger negative proteins, however, these regions about the cationic groups do not overlap, the effect cannot occur, and only the local hydration sheaths about each group are of significance. Consequently, the adsorption isotherm for negative proteins has the normal Langmuir form, reflecting a steadily decreasing $-\Delta F$ of adsorption per mole of anion bound as the total number bound increases.

The appreciable temperature coefficient for binding of anions to denatured proteins (Fig. 9) is in marked contrast to the temperature insensitivity of binding to most native proteins. This increase in $-\Delta H$ of adsorption upon denaturation of the protein is consistent with the concept of a hydration sheath about charged groups on a protein (7) which was used above. Because the more disordered structure does not permit such close approach of the anion as in the native form, the adsorption of an anion to a denatured protein would be expected to be accompanied by a smaller release of water. Accordingly the electrostatic decrease in energy between oppositely charged groups will not be as closely balanced by an increase in energy owing to additional free water molecules and therefore $-\Delta H$ is increased.

Finally, the sharply exponential binding of methyl orange by native lysozyme at pH 5.5, in contrast to its behavior at pH 6.8, indicates that the orientation of solvent molecules about the protein approaches a saturation value as the total charge increases. Since Coulomb attractive forces are linear functions of the charge on one of the particles, there must be a shallow minimum in the total potential curve for an anion about such a protein analogous to those which exist for metastable lyophobic colloid systems (14).

These results provide additional evidence against the concept of a small number of different series of unique binding sites to which anions become attached. In recent interpretations of adsorption data for native proteins (6, 7, 8, 9, 12), these points of attachment have been assumed to differ discontinuously in intrinsic constants or to deviate from independent probabilities of reaction due to electrostatic interaction. Now, it is clear that one might interpret formally the present isotherms for denatured proteins in a similar fashion, since they are equally well-defined properties of the material. However, for denatured proteins the concept of a series of equal distinct "sites" for binding of a large anion can have no precise meaning because the random structure requires considerable variation in the immediate neighborhood of any given type of group. For these systems the isotherm must represent an average of anions bound to a quasi-continuous series of positions, the members of which differ from neighbors by very small free energy decreases per molecule of anion taken up. Hence, empirical curve fitting procedures cannot yield constants which may be used for

the description of precise reaction mechanisms or of characteristic groups on the denatured protein. This suggests strongly that a similar interpretation should be placed on adsorption data for native proteins in any system where direct evidence for unique discrete sites is lacking.

ACKNOWLEDGMENTS

The author wishes to thank Mr. L. Sowden for help with the tedious but exacting analytical work.

REFERENCES

1. ANSON, M. L. *Advances in Protein Chem.* 2: 361. 1945.
2. CLARK, W. M. *The determination of hydrogen ions.* 3rd ed. The Williams & Wilkins Company, Baltimore. 1928.
3. COLVIN, J. R. *Can. J. Chem.* 30: 320. 1952.
4. FRAENKEL-CONRAT, H. *Arch. Biochem.* 27: 109. 1950.
5. FROMAGEOT, C. and DE GARILHE, M. P. *Biochim. et Biophys. Acta*, 4: 509. 1950.
6. KARUSH, F. *J. Am. Chem. Soc.* 73: 1246. 1951.
7. KLOTZ, I. M. *Cold Spring Harbour Symposia Quant. Biol.* 14: 97. 1949.
8. KLOTZ, I. M., BURKHARD, R. K., and URQUHART, J. M. *J. Am. Chem. Soc.* 74: 202. 1952.
9. KLOTZ, I. M., BURKHARD, R. K., and URQUHART, J. M. *J. Phys. Chem.* 56: 77. 1952.
10. KLOTZ, I. M. and URQUHART, J. M. *J. Am. Chem. Soc.* 71: 1597. 1949.
11. KLOTZ, I. M. and WALKER, F. M. *Arch. Biochem.* 18: 319. 1948.
12. KLOTZ, I. M., WALKER, F. M., and PIVAN, R. B. *J. Am. Chem. Soc.* 68: 1486. 1946.
13. SCATCHARD, G. and BLACK, E. S. *J. Phys. & Colloid Chem.* 53: 88. 1949.
14. VERWEY, E. J. W. and OVERBEEK, J. TH.G. *Theory of the stability of lyophobic colloids; the interaction of sol particles having an electric double layer.* Elsevier Publishing Co. Inc., Amsterdam and New York. 1948.

KINETICS OF THE REACTIONS BETWEEN ISOPROPYL CUMENE AND TERTIARY BUTYL CUMENE HYDROPEROXIDES AND IRON(II) IN DILUTE AQUEOUS SOLUTIONS IN THE ABSENCE OF OXYGEN¹

By R. J. ORR AND H. LEVERNE WILLIAMS

ABSTRACT

From studies of the rate of reaction at 11°, 15°, 20°, and 26°C. it was deduced that the bimolecular reaction between iron(II) and isopropyl cumene hydroperoxide is represented by

$$k = 4.0 \times 10^9 e^{-10,800/RT}$$

At 0°C. the radical induced oxidation of iron(II) due to inability of the monomer to remove the free radicals became appreciable. Addition of up to 7.5% methanol did not change the rate appreciably. The effect of traces of oxygen was negligible.

Rate constants were measured at 15°, 9°, and 0°C. for the reaction between iron(II) and the tertiary butyl cumene hydroperoxide. The average probable error in the determinations was 5.4%. From the data, the Arrhenius equation was determined as

$$k = 1.8 \times 10^9 e^{-9,900/RT}$$

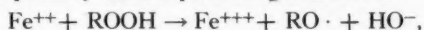
Comparison of the equations measured for cumene hydroperoxide, isopropyl cumene hydroperoxide, and tertiary butyl cumene hydroperoxide and iron(II) has been made. Changes in the constants have been explained qualitatively. The iodometric method of analysis when applied to tertiary butyl cumene hydroperoxide must be modified for accurate results. It is believed that the heating necessary in the presence of water decomposes the hydroperoxide.

INTRODUCTION

The induced decomposition of hydroperoxides has become the most widely used method of initiation of polymerization reactions in the production of general purpose rubbers in emulsion at temperatures just above 0° C. In a related paper (2) it was shown that various hydroperoxides differed in their ability to affect the rate of conversion of monomers to polymer and the final yield obtained by a given amount of hydroperoxide. Other studies have yielded data (3, 4) which are believed to represent a fundamental approach to the catalyst activator system used. In those studies the rate of the reaction between cumene hydroperoxide and iron(II) was studied. It was of importance to continue such studies with related hydroperoxides to ascertain whether the greater efficiency could be ascribed to the changes in the rate of the initial bimolecular reaction whereby free radicals are formed which then can initiate polymerization.

THEORETICAL

Suppose that the primary radical producing reaction is



then the rate of disappearance of iron (II) is given by

$$\begin{aligned} \frac{-d[\text{Fe}^{++}]}{dt} &= k_1 [\text{Fe}^{++}] [\text{RO}_2\text{H}] \\ &= k_1 [\text{Fe}^{++}] (a - b + [\text{Fe}^{++}]) \end{aligned}$$

¹ Manuscript received in original form April 23, 1952, and, as revised, August 29, 1952.

Contribution from Polymer Corporation Limited, Research and Development Division, Sarnia, Ontario, Canada. Part of a presentation before the High Polymer Forum, Chemical Institute of Canada, Montreal, Canada, June, 1952.

where $a = [\text{RO}_2\text{H}]_0$ = initial hydroperoxide concentration
 and $b = [\text{Fe}^{++}]_0$ = initial iron(II) concentration
 when all side reactions between Fe^{++} and $\text{RO}\cdot$ have been suppressed by the addition of acrylonitrile.

Integrating this equation we obtain

$$\ln \left[1 + \frac{(a-b)}{[\text{Fe}^{++}]} \right] = (a-b)kt + \ln a/b.$$

Hence a plot of $\log \left[1 + \frac{(a-b)}{[\text{Fe}^{++}]} \right]$ vs. t should be linear with a slope of $\frac{(a-b)}{2.3}k$.

EXPERIMENTAL

Analyses were made by a colorimetric procedure involving the complexing of iron(II) with α, α' -bipyridyl in an acidic solution (6). The water used was distilled over alkaline potassium permanganate. Methanol contained a maximum of 0.003% aldehydes and 0.005% water. The reaction was conducted in a cell which has been previously described (4) and in the presence of 0.3 *M* acrylonitrile. Polyacrylonitrile was removed by centrifuging all samples before analyzing them. All reactions were buffered at a pH of 4.2 with an acetic acid - sodium acetate buffer and started by the addition of iron(II) solution as sulphate.

The sodium salt of isopropyl cumene hydroperoxide was prepared by adding a 50% solution of the hydroperoxide to a saturated sodium hydroxide solution at 0° C. with vigorous agitation. The mixture was filtered on a sintered glass filter and the sodium salt washed two or three times with aliquots of pentane. The residue was dried under high vacuum. An analysis of this salt indicated that it was contaminated with sodium hydroxide since the average batch contained only 25% by weight of the hydroperoxide salt. When the salt was regenerated by acidifying an aqueous solution in contact with the salt to pH 8, it was observed that the liquid collected decomposed rapidly into a yellowish viscous oil. Dilution of the hydroperoxide with pentane slowed the rate of the decomposition. Aqueous solutions of the hydroperoxide could be prepared by adding the solution in pentane to water, evaporating the pentane, and shaking well. It was found that there was some oil which did not evaporate or dissolve. This layer could be separated from the aqueous layer.

As a test, a solution was made and analyzed, advantage being taken of the fact that in the presence of an excess of monomer and iron(II), the stoichiometric ratio of iron(II) reacted to hydroperoxide decomposed was one. Rate constants were measured over the period of a week using this solution. The results are in Table I.

TABLE I
STABILITY OF ISOPROPYL CUMENE
MONOHYDROPEROXIDE SOLUTIONS

Age of solution, hr.	k (0°C.), l./mole/sec.
0	17
48	11
120	8
168	3

It appeared that the rate constant decreased. Analysis of the isopropyl cumene hydroperoxide solution 168 hr. after the original analysis indicated that the concentration had decreased to $1.90 \times 10^{-5} M$ from $5.9 \times 10^{-5} M$. The isopropyl cumene hydroperoxide could not be stored in aqueous solution even as dilute as $5.9 \times 10^{-5} M$ without decomposition. This might have been caused by acidic constituents present after regeneration of the hydroperoxide. This difficulty has not been encountered elsewhere (5). To avoid this, preparation of a fresh isopropyl cumene hydroperoxide solution was done daily by weighing a sample of the sodium salt into a volumetric flask and adding a small measured amount of methanol. Acetic acid - sodium acetate buffer was added to regenerate the hydroperoxide. On dilution to the required volume a stable colloidal suspension of the hydroperoxide was formed which could be pipetted. It was possible to calculate the isopropyl cumene hydroperoxide concentration from the analytical data on the salt. It was shown that errors arising from lack of homogeneity in the sample were negligible.

Tertiary butyl cumene hydroperoxide consists of two phases at ordinary temperatures, a white solid and a supernatant liquid. It was cooled and filtered, the white precipitate being collected. This precipitate was reprecipitated twice from methanol and dried. Attempts at iodometric analyses by gentle boiling in an isopropanol-water solution of potassium iodide and glacial acetic acid failed. Results could not be closely reproduced and barely half enough iodine was liberated if the product were anywhere near 100% purity. However, on reaction with iron(II) with a large excess of acrylonitrile, there is every reason to believe that the ratio of iron(II) reacted to hydroperoxide consumed is unity. Assuming 100% purity and using always fresh solutions, we found this to be the case (Table II). For this reason it was assumed that the product was near enough to 100% purity to justify using it. The failure of the iodometric analysis has been found to be due to the presence of water in the medium. It is possible to obtain quantitative results if no water is added to the peroxide-iodide solution until heating is complete and the thiosulphate titration is ready to begin (5). Although small amounts of residual oxygen remaining in the system caused the stoichiometric ratio of iron(II)/tertiary butyl cumene hydroperoxide to be very slightly greater than unity (assuming 100% purity for the peroxide sample), it was found that on letting the stock solution of tertiary butyl cumene hydroperoxide stand, this stoichiometric ratio fell to much less than unity. This behavior is shown in Table II. This behavior is similar to that noted with isopropyl cumene hydroperoxide. For this reason fresh hydroperoxide solutions in 24% methanol were made up every

TABLE II
STOICHIOMETRIC RATIOS OF TERTIARY BUTYL CUMENE
HYDROPEROXIDE - Fe^{++} REACTION AT 15°C.

Age of hydroperoxide solution (days)	$[ROOH]_0$	$[Fe^{++}]_0/[Fe^{++}]$	$([Fe^{++}]_0 - [Fe^{++}])/[ROOH]_0$
0	6.39	6.65	1.04
0.5	6.39	6.30	0.98
1.0	6.39	4.74	0.74
1.5	6.39	4.60	0.72

day for rate constant determination. Occasionally, even fresh peroxide solutions gave erroneous stoichiometric ratios. It was found necessary to accept only those results calculated from experiments giving a normal stoichiometric ratio in the neighborhood of unity.

RESULTS

If any oxygen remains in the reagents at the beginning of the reaction, iron(II) will disappear by reaction with oxygen as well as hydroperoxide. Since no estimate could be made of the concentration of the oxygen, it was impossible to differentiate the two reactions. The best that can be done in this situation is to assume that the iron(II) reacts much more rapidly with the oxygen than with the hydroperoxide. In this event the only effect that oxygen has on the final rate equation is to alter the $(a - b)$ value. If $a < b$, and if every mole of iron(II) that disappears decomposes only one mole of hydroperoxide, then $b - a = [\text{Fe}^{++}]_{\infty}$, where $[\text{Fe}^{++}]_{\infty}$ is the iron(II) concentration when no further change can be detected experimentally. It was found that the iron(II) concentration after 75 to 100 min. of reaction could be used as the $[\text{Fe}^{++}]_{\infty}$ value.

If the assumption as to relative rates of reaction of iron(II) with hydroperoxide and oxygen is valid, then the plot of $\log(1 - [\text{Fe}^{++}]/[\text{Fe}^{++}]_{\infty})$ vs. t should be linear with the exception of the point at zero time. This was the case. Some typical results are shown on Fig. 1. Inspection of the data indicates that in some cases it takes more than five minutes before the results lie on a straight line. This indicates that the reaction between iron(II) and oxygen is not instantaneous. The rate constants, calculated under the various conditions, are in Table III.

The data indicate that on increasing the methanol content from 0.19 to 7.5%, the rate constant shows a slight increase which is not outside the experimental error.

Since isopropyl cumene hydroperoxide can exist in more than one isomeric

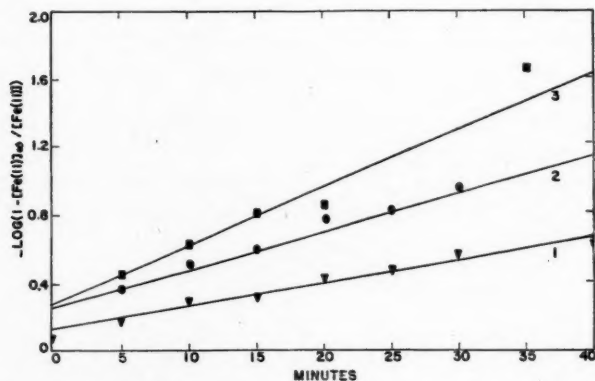


FIG. 1. Reaction of isopropyl cumene hydroperoxide with iron(II) at 20°C. with a methanol concentration of 0.19%. Curve 1, final iron(II) $1.55 \times 10^{-5} M$; Curve 2, $2.75 \times 10^{-5} M$; and Curve 3, $3.77 \times 10^{-5} M$.

TABLE III
 RATE CONSTANTS FOR ISOPROPYL CUMENE HYDROPEROXIDE - IRON(II) REACTION

Temp., °C.	$(b - a),$ $M \times 10^5$	$[\text{AcN}]_0,$ $M \times 10$	% MeOH	$k, \text{l.mole}^{-1}$ sec.^{-1}	$k_{\text{ab}}, \text{l.mole}^{-1}$ sec.^{-1}
11	4.70	1.0	0.19	19.1	19.9 ± 0.7
11	3.95	1.0	0.19	—	
11	4.00	1.0	0.19	20.0	
11	4.45	1.50	7.5	—	
11	2.25	1.50	7.5	22.1	
11	4.30	2.25	7.5	18.5	
11	2.15	2.25	7.5	23.9	
15	2.25	3.0	0.19	23.0	24.3 ± 1.2
15	5.05	3.0	0.19	24.2	
15	2.16	3.0	0.19	25.5	
15	3.10	3.0	7.5	24.2	
15	5.30	3.0	7.5	24.9	
20	3.77	2.25	0.19	33.5	32.7 ± 2.0
20	2.75	3.0	0.19	31.0	
20	1.55	3.0	0.19	31.2	
20	4.90	3.0	7.5	31.8	
20	1.82	3.0	7.5	35.5	
20	2.49	3.0	7.5	33.5	
25.5	2.30	3.0	0.19	51.0	50.2 ± 0.4
25.5	2.98	3.0	0.19	49.5	
25.5	3.25	3.0	0.19	50.0	

configuration, the question of proportions and types of isomers must be considered. Attempts to build the ortho isomer with Fischer-Herschfelder models indicated that this isomer could not exist owing to steric factors. Analyses of the hydroperoxide used in this investigation indicated that it was predominantly para with some meta (5). Late in the course of the investigation, a sample containing only the para form became available and rate constants were determined on this sample in order to determine whether the meta present in the initial sample was present in sufficient quantity to affect the validity of the results. Rate constants at 20° C. were determined as 33.8 and 31.1 at $[\text{Fe}^{++}]_{\infty}$ values of 6.46 and $2.00 \times 10^{-5} M$ respectively. The rate constant determined on the initial sample was 32.7 ± 2.0 ; thus results from the two samples agree within the experimental precision of the determination.

Attempts to study the reaction at 0° C. failed owing to the difficulty experienced in suppressing the radical induced oxidation reactions. The data obtained showed a rather large amount of scatter when plotted in the integrated rate equation. When the best straight line was drawn, very large values for the rate constant were obtained which decreased with increasing acrylonitrile concentration. Thus at a $(b - a)$ value of 3.4×10^{-5} , the apparent rate constant decreased from 50 $\text{l.mole}^{-1} \text{sec.}^{-1}$ to 34 $\text{l.mole}^{-1} \text{sec.}^{-1}$ when $[\text{AcN}]_0$ was increased from 0.10 to 0.15 M . Under conditions where $b > a$, $[\text{Fe}^{++}]_{\infty}$ decreased to values which were unreasonably low when compared with the value of $[\text{Fe}^{++}]_{\infty}$ calculated from analytical results. For example, at $[\text{AcN}]_0 = 2.0 \times 10^{-1} M$, the maximum value of $[\text{Fe}^{++}]_{\infty}$ was observed to be 2.49×10^{-5} compared with a minimum value of

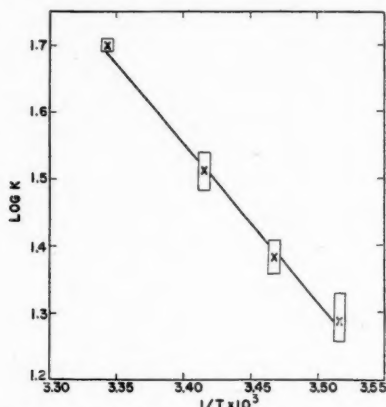


FIG. 2. Plot of $\log k$ against $1/T \times 10^3$ for the reaction between isopropyl cumene hydroperoxide and iron(II).

$b - a$ of 3.42×10^{-5} as calculated from analytical results. Both these facts indicate incomplete suppression of radical induced oxidation of the ferrous iron at the acrylonitrile concentrations used. This conclusion was further confirmed when the absolute value of b was lowered to values less than those shown by a and $a - b$ values were determined from analytical results. This would make radical induced oxidation reactions easier to suppress. When this was done the scatter in the experimental results decreased along with the apparent rate constant. Results for this varying between 10.8 and 17.0 were obtained when the initial acrylonitrile was $10^{-1} M$. However, in view of the general difficulty of measurement and more especially of the necessity to rely on calculations which

TABLE IV
RATE CONSTANTS OF TERTIARY BUTYL CUMENE
HYDROPEROXIDE - Fe^{++} REACTION

Temp., °C.	$(b - a),$ $M \times 10^5$	$k,$ $\text{l.mole}^{-1}\text{sec.}^{-1}$	$k_{av.},$ $\text{l.mole}^{-1}\text{sec.}^{-1}$	σ	ρ
15	5.45	60.4	54.9	± 4.0	2.7
15	4.23	52.9			
15	1.56	58.7			
15	2.55	48.4			
15	4.42	52.5			
15	3.70	56.0	36.8	± 2.9	2.0
9	3.45	37.5			
9	6.12	35.3			
9	4.80	34.2			
9	3.72	41.6			
9	5.46	35.8	21.3	± 2.0	1.3
0	5.52	19.5			
0	3.85	19.8			
0	3.28	23.8			
0	4.52	19.6			
0	4.80	21.4			
0	4.87	24.5			

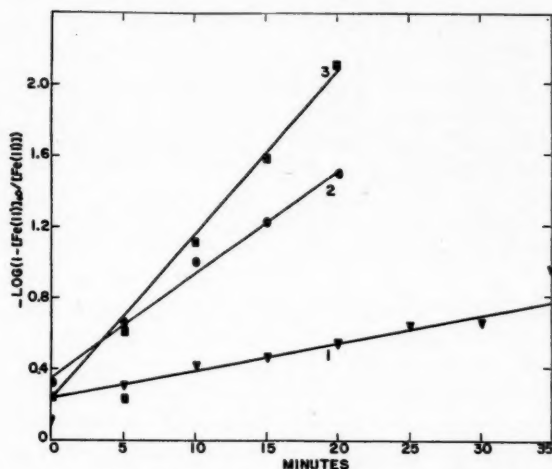


FIG. 3. Reaction between tertiary butyl cumene hydroperoxide and iron(II) at 15°C. Final iron(II): Curve 1, $1.56 \times 10^{-5} M$; Curve 2, $4.23 \times 10^{-5} M$; and Curve 3, $5.45 \times 10^{-5} M$.

neglected any effect due to oxygen, it was felt that pursuit of studies at this temperature would add little to the accuracy of the constants in the Arrhenius equation, and the attempt was abandoned.

So that the data might be expressed in the convenient form of the Arrhenius equation $k = Ae^{-E/RT}$, $\log k$ was plotted vs. $1/T$ (Fig. 2). The average of all rate constants measured at each temperature except 0°C. regardless of the methanol concentration was chosen as the correct one.

When the calculations are based on this graph in which an equal experimental error can be assigned to each point, the equation

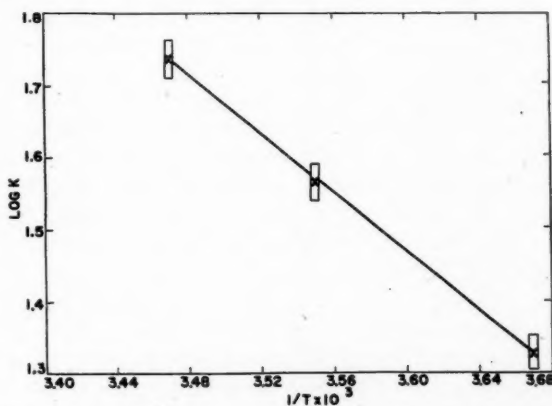


FIG. 4. Plot of $\log k$ against $1/T \times 10^3$ for the reaction between tertiary butyl cumene hydroperoxide and iron(II).

$$k = 4.0 \times 10^9 e^{-10,800/RT} \text{ l.mole}^{-1} \text{ sec.}^{-1}$$

is obtained.

The reaction between iron(II) and tertiary butyl cumene hydroperoxide was studied at three different temperatures 15°, 9°, and 0°C. The results of this work are shown in Table IV. Some typical data are plotted in Fig. 3. The sample was described as mostly para isomer (5).

From a plot of $\log k$ vs. $1/T$ (Fig. 4) the Arrhenius equation $k = Ae^{-E/RT}$ was calculated to be $k = 1.9 \times 10^9 e^{-9,900/RT}$.

DISCUSSION

The rate constant for the reaction of tertiary butyl cumene hydroperoxide and iron(II) was greater than the rate constant for the isopropyl cumene hydroperoxide - iron(II) reaction which was greater in turn than that for the cumene hydroperoxide - iron(II) reaction at the same temperature indicating that the reactivity of the hydroperoxide continually increases with the size of the substituent group on the benzene nucleus. The Arrhenius equations for each of the three hydroperoxides now investigated are:

Cumene hydroperoxide (3, 4)	$k = 1.0 \times 10^{10} e^{-12,000/RT}$
Isopropyl cumene hydroperoxide	$k = 4.0 \times 10^9 e^{-10,800/RT}$
Tertiary butyl cumene hydroperoxide	$k = 1.8 \times 10^9 e^{-9,900/RT}$

Thus the increased reactivity is due to a decrease in the activation energy. This decrease is partially compensated by a corresponding decrease in A . Experience (2) has shown differences in cold temperature emulsion polymerization recipes using these hydroperoxides. At a chosen iron(II) content, optimal conversion at any given time cycle is achieved by a lower tertiary butyl cumene hydroperoxide concentration than isopropyl cumene hydroperoxide concentration which in turn is lower than that required when cumene hydroperoxide is used. At optimal conditions for a given time cycle, tertiary butyl cumene hydroperoxide causes greater conversion than does isopropyl cumene hydroperoxide and each yields higher conversions than does cumene hydroperoxide.

The first difference may be related to the fact that the rate of the reaction with iron(II) changes in the same order. It is evident that with a constant Fe^{++} content much less tertiary butyl or isopropyl cumene hydroperoxide than cumene hydroperoxide is necessary to secure a given rate of formation of free radicals. If the partition coefficient between oil and water phases and if the efficiency of utilization of the free radicals in promoting polymerization are the same for the hydroperoxides, these differences in rate constants could explain the difference in optimal hydroperoxide contents.

However, the fact that greater conversions are obtained with tertiary butyl or isopropyl cumene hydroperoxide recipes than with cumene hydroperoxide recipes indicates that the $\text{RO}\cdot$ radicals generated in the former recipes are used more efficiently than those in the latter. This latter fact is outside the scope of this investigation and will eventually be made the subject of a separate study.

Since to bring about the same change in the rate of free radical production requires a greater change of temperature for the tertiary butyl or isopropyl

There seems to be at present no manner in which rate constants can be determined reliably at 0° C. for the isopropyl cumene hydroperoxide - iron(II) reaction owing to the fact that, at high $[\text{Fe}^{++}]_0/[\text{ROOH}]_0$ ratios, acrylonitrile does not completely suppress the radical induced oxidation of iron(II). It is under conditions of $[\text{Fe}^{++}]_0 > [\text{ROOH}]_0$ that it is most desirable to measure the rate constant.

complex of the type $\text{ROO}:\text{Fe}^{++}$. This immediately dissociates to $\text{RO}\cdot + \cdot\text{O}:\text{Fe}^{++}$. Now an electron excess at the O-O linkage would cause a more rapid rate of dissociation and hence a more rapid over-all rate, assuming this dissociation as the rate controlling step.

The variation in the A factor is more difficult to explain. The addition of the extra alkyl groups increases the number of the internal degrees of freedom in the system. It has been stated (1) that the greater the number of internal degrees of freedom, the lower will be the entropy of activation or the lower will be the A factor. Thus Amis states (1) "there is a factor of flux in this problem, i.e. the rate at which those molecules with sufficient energy can flow up to the energy barrier. It is conceivable that reactant molecules with numerous flailing appendages would have a longer time of approach to and of crossing over the energy barrier than a rigid molecule".

The authors thank Polymer Corporation Limited for permission to publish these results. The assistance of S. Butler and G. Vincent is acknowledged.

1. AMIS, E. S. Kinetics of chemical change in solution. MacMillan Co., New York. 1949. p. 123.
2. DAVIDSON, M. J. G., EMBREE, W. H., and WILLIAMS, H. L. To be published.
3. FORDHAM, J. W. L. and WILLIAMS, H. L. J. Am. Chem. Soc. 72: 4465. 1950.
4. FORDHAM, J. W. L. and WILLIAMS, H. L. J. Am. Chem. Soc. 73: 1634. 1951.
5. Hercules Powder Co., Wilmington, Delaware. Personal communications.
6. JACKSON, L. H. Ind. Eng. Chem. Anal. Ed. 10: 302. 1938.

CYANOACETIC ESTERS, AMINO ACIDS, AND PYRAZOLONES¹

BY PAUL A. BOIVIN,² PAUL E. GAGNON,³ ERNEST RENAUD,⁴
AND WILLIAM A. BRIDGE⁵

ABSTRACT

Ethyl α -substituted cyanoacetates were used to prepare hydrazides, azides, urethanes, and *dl*- α -amino- β -phenylbutyric acid, *dl*- α -amino- δ -*o*-bromophenoxyvaleric acid, and *dl*- α -amino- δ -*o*,*p*-dichlorophenoxyvaleric acid. Ethyl mono- and disubstituted cyanoacetates with hydrazine gave hydrazides which were transformed by treatment with sodium hydroxide into 4- α -phenylethyl-, 4-*m*-ethylphenoxyethyl-, 4-*o*-bromophenoxypropyl-, 4-*o*,*p*-dichlorophenoxypropyl-, 4,4-*m*-ethylphenoxyethyl-, and 4,4-*m*-methylphenoxypropyl-3-amino-5-pyrazolones. The ultraviolet absorption spectra of the pyrazolones were determined in neutral, acid, and alkaline solutions and their structures established.

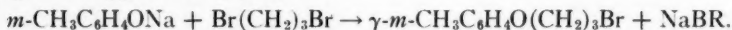
INTRODUCTION

The Curtius reaction, whereby acid azides break down on heating into isocyanates and nitrogen, was applied in 1915 to the preparation of an amino acid from cyanoacetic ester by Darapsky and Hillers (3), who obtained glycine. Since that time a considerable number of amino acids (2, 4, 5, 7, 11, 12, 13, 15) have been synthesized by the same method from substituted cyanoacetic esters.

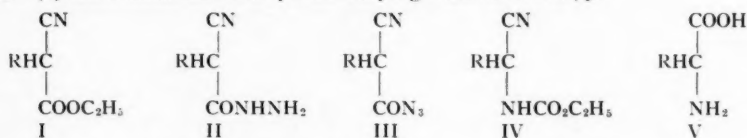
Most of the substituted cyanoacetic esters used for the preparation of amino acids gave hydrazides which were transformed by treatment with sodium hydroxide into 5-pyrazolones which were extensively studied to determine their structures (6, 8, 9, 10, 14, 15).

The object of the present work was to synthesize other amino acids and pyrazolones by the same methods and study their properties.

Substituted phenoxyalkyl bromides were prepared by a method which seems of general application (1, 16).



By refluxing the bromides with ethyl cyanoacetate and sodium ethylate, esters (I) were obtained with yields varying from 35 to 55%.



R = aryl group. RH is replaced by R₂ in the formulae I and II for disubstituted compounds.

Hydrazine hydrate mixed with the esters (I) at room temperature gave rise

¹ Manuscript received August 14, 1952.

Contribution from the Department of Chemistry, University of Ottawa, Ottawa. This paper constitutes a part of a thesis submitted to the Graduate School, University of Ottawa, in partial fulfillment of the requirements for the degree of Doctor of Philosophy.

² Professor of Chemistry, University of Ottawa, Ottawa.

³ Head of the Department of Chemistry, Laval University, Quebec, Que.

⁴ Head of the Department of Chemistry, University of Ottawa, Ottawa.

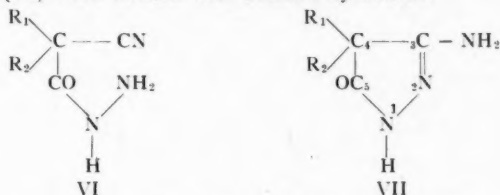
⁵ Holder of a Bursary under the National Research Council of Canada, in 1950-1951.

to the hydrazides (II). These were identified by their condensation products with acetone or anisaldehyde.

The conversion of the hydrazides into the corresponding azides (III) took place by treatment with nitrous acid, the azides being extracted with ether. On boiling the alcoholic solutions of the azides under reflux, the ethyl urethanes (IV) were formed.

The hydrolysis of the urethanes to the amino acids (V) namely, *dl*- α -amino- β -phenylbutyric acid, *dl*- α -amino- δ -*o*-bromophenoxyvaleric acid, and *dl*- α -amino- δ -*o*,*p*-dichlorophenoxyvaleric acid was effected by refluxing in hydrochloric acid (20%).

To obtain 3-amino-5-pyrazolones (VII), mono- and disubstituted ethyl cyanoacethydrazides (VI) were treated with sodium hydroxide.



R_1 = aryl group; R_2 = H or aryl group.

Four monosubstituted-3-amino-5-pyrazolones (VII, R_1 = α -phenylethyl, *m*-ethylphenoxyethyl, *o*-bromophenoxypropyl, and *o*,*p*-dichlorophenoxypropyl, R_2 = H) and two disubstituted-3-amino-5-pyrazolones (VII, both R_1 and R_2 = *m*-ethylphenoxyethyl or *m*-methylphenoxypropyl) were synthesized and their ultraviolet absorption spectra were determined.

EXPERIMENTAL*

Substituted Phenoxypropyl Bromides

In a 3 liter round-bottomed flask, fitted with a stopper carrying a long reflux condenser, a mechanical stirrer, and a separatory funnel, were placed water (1 liter), trimethylene bromide (2.47 moles), and the substituted phenol (1.95 moles). The stirrer was started and to the boiling solution was added a solution of sodium hydroxide (1.87 moles) in water (250 ml.) at such a rate that complete addition took about one hour. The mixture was refluxed for 10 to 15 hr., then cooled, and the upper water layer separated and discarded. The lower layer was washed with 5% sodium hydroxide to eliminate unreacted phenol and finally the mixture was washed with water. The solution was then distilled under reduced pressure.

The physical properties and yields of the bromides are summarized in Table I.

Substituted Cyanoacetic Esters (I)

Ethyl cyanoacetate (113 gm., 1.0 mole) was added to a clear solution of sodium ethoxide (11.5 gm. of sodium, 250 ml. of absolute ethanol) and the mixture was heated to the boiling point. After the mixture had cooled, the substituted halides (0.5 mole) were slowly added, and the reaction mixtures refluxed until

*All melting points are uncorrected.

TABLE I
 PHENOXYALKYL BROMIDES

Compound	B.p., °C.	Yield	n_D^{20} , °C.	Formula	Analysis, %hal.	
					Calc.	Found
γ - <i>m</i> -Methylphenoxy-propyl bromide	125-126 (6 mm.)	54	1.5389	C ₁₀ H ₁₃ OBr	34.9	34.7
β - <i>m</i> -Ethylphenoxyethyl bromide	143-144 (17 mm.)	50	1.5406	C ₁₀ H ₁₃ OBr	34.9	34.6
γ - <i>o</i> -Bromophenoxy-propyl bromide	166-172 (15 mm.)	70	1.5762	C ₉ H ₁₀ OBr ₂	54.4	53.9
γ - <i>o,p</i> -Dichlorophenoxy-propyl bromide	158-159 (6 mm.)	79	1.5676	C ₉ H ₉ OBrCl ₂	53.2	52.7

neutral to wet litmus paper. The alcohol was distilled off under reduced pressure and the residues poured into cold water (500 ml.). The aqueous solutions acidified with hydrochloric acid were extracted three times with ether and the combined extracts dried over anhydrous sodium sulphate. The ether was evaporated and the esters, mono- and disubstituted, were isolated by fractional distillation under reduced pressure.

The properties and yields are listed in Table II.

 TABLE II
 ETHYL α -SUBSTITUTED CYANOACETATES

Compound	B.p., °C.	Yield, %	n_D^{20} , °C.	Formula	Nitrogen, %	
					Calc.	Found
RCH(CN)COOC ₂ H ₅ R = <i>o</i> -Bromophenoxy-propyl	224-232 (12 mm.), m.p. 58° to 59°C.	45		C ₁₄ H ₁₆ O ₃ NBr	4.3	4.3
<i>o,p</i> -Dichlorophenoxypropyl	197-198 (6 mm.)	38	1.5208	C ₁₄ H ₁₅ O ₃ NCl ₂	4.4	4.7
RRC(CN)COOC ₂ H ₅ R = <i>m</i> -Methylphenoxy-propyl	184-185 (5 mm.)	57	1.4960	C ₂₆ H ₃₁ O ₄ N	3.4	3.2
<i>m</i> -Ethylphenoxy-ethyl	178-180 (6 mm.)	40	1.4978	C ₂₅ H ₃₁ O ₄ N	3.4	3.6

Substituted Cyanoacethydrazides (II)

The monosubstituted cyanoacetic esters (0.1 mole) were stirred vigorously for a few minutes with hydrazine hydrate (100%, 0.1 mole). There was evolution of heat and most of the hydrazides solidified readily. They were recrystallized from ethanol. The properties are summarized in Table III.

Derivatives of Substituted Cyanoacethydrazides

The hydrazides were dissolved in ethanol, and acetone or anisaldehyde was added to the hot solutions. If precipitation did not take place immediately,

TABLE III
 α -SUBSTITUTED CYANOACETHYDRAZIDES AND DERIVATIVES

Compound	M.p., °C.	Formula	Nitrogen, %		Derivative with	M.p., °C.	Formula	Nitrogen, %	
			Calc.	Found				Calc.	Found
RCH(CN)CONHNH ₂ R = α -Phenylethyl	—	C ₁₁ H ₁₂ ON ₂	13.5	13.3	Acetone	171–172	C ₁₁ H ₁₂ ON ₂	17.3	16.8
<i>o</i> -Bromophenoxypropyl	99–100	C ₁₂ H ₁₁ O ₂ N ₂ Br	13.9	13.8	Anisaldehyde	153–154	C ₂₀ H ₁₉ O ₂ N ₂ Br	9.7	9.6
<i>o</i> , <i>p</i> -Dichlorophenoxypropyl	110–111	C ₁₂ H ₁₀ O ₂ N ₂ Cl ₂			Anisaldehyde	183–184	C ₂₀ H ₁₈ O ₂ N ₂ Cl ₂	10.0	9.9
RRC(CN)CONHNH ₂									
R = <i>m</i> -Methylphenoxypropyl	95–96	C ₂₃ H ₂₂ O ₂ N ₂	10.6	10.3	Anisaldehyde	149–150	C ₃₁ H ₂₈ O ₄ N ₂	8.1	8.1
<i>m</i> -Ethylphenoxyethyl	140–141	C ₂₃ H ₂₂ O ₂ N ₂	10.6	10.4	Anisaldehyde	183–184	C ₃₁ H ₂₈ O ₄ N ₂	8.1	8.3

one drop of concentrated hydrochloric acid was added and the solutions were left standing until precipitation occurred. The products were purified by recrystallization from ethanol.

The properties are listed in Table III.

Amino Acids (V)

The hydrazides (0.05 mole) were dissolved in aqueous hydrochloric acid (15%, 100 ml.), cooled to 0°C., and covered with a layer of ether (75 ml.). Sodium nitrite (10 gm.) dissolved in water (30 ml.) was added dropwise to the mechanically stirred mixtures. The azides, on formation, passed into the ether layer. On completion of the reaction, the ether was decanted and the aqueous layers rapidly extracted with two fresh portions of ether. The extracts were combined, dried over anhydrous sodium sulphate, and filtered into absolute ethanol (75 ml.). The ether was evaporated and the azides (III) refluxed on a water bath for one hour to complete the transformation to the urethanes (IV). The alcohol was removed by distillation at reduced pressure. The urethanes were hydrolyzed to the amino acids by refluxing in aqueous hydrochloric acid (20%, 200 ml.) for 48 hr. at 140°C. The mixtures were evaporated to dryness, the residues dissolved in water, boiled with charcoal, and filtered several times. The filtrates were neutralized, concentrated to a small volume, and cooled. On the addition of acetone (2.5 liters) the amino acids precipitated. They were purified by reprecipitation in the same manner and dried in the oven at 100°C.

The following amino acids were prepared:

dl- α -amino- β -phenylbutyric acid which was identified by its hydantoin: m.p. 125–126°C. Calc. for $C_{11}H_{12}O_2N_2$: N, 13.7%. Found: N, 13.4%.

dl- α -amino- δ -*o*-bromophenoxyvaleric acid also identified by its hydantoin: m.p. 160–161°C. Calc. for $C_{12}H_{13}O_3N_2Br$: N, 8.5%. Found: 8.6%.

dl- α -amino- δ -*o*,*p*-dichlorophenoxyvaleric acid directly analyzed. Calc. for $C_{11}H_{13}O_3NCl_2$: N, 5.0%. Found: N, 4.9%.

4-Substituted-3-amino-5-pyrazolones (VII)

The hydrazides (0.1 mole) of the ethyl substituted cyanoacetates were treated with two equivalents of sodium hydroxide (40%) and stirred for a few minutes. The mixtures were allowed to stand for three hours and diluted with water (250 ml.). The solutions were then acidified with acetic acid (50%) and allowed to cool slowly. The crystalline compounds formed were separated by filtration, washed with water, and recrystallized several times from ethanol.

Pyrazolones of both types were soluble in water, acids, and alkalies, and insoluble in ether and sodium bicarbonate solution. The 4-monosubstituted compounds, however, were more soluble in water than the 4,4-disubstituted ones. The individual properties are given in Table IV.

ULTRAVIOLET ABSORPTION SPECTRA

The ultraviolet absorption spectra were taken on a Beckman spectrophotometer Model DU in the same way as previously described (9). Results are listed in Table IV and some of the data are plotted in Figs. 1–3.

TABLE IV
4-SUBSTITUTED-3-AMINO-5-PYRAZOLONES

Compound	Formula	M.p., °C.	Analysis, %		Ultraviolet absorption maxima					
			Nitrogen		Neutral		Acid		Alkaline	
			Calc.	Found	log E_m	λ	log E_m	λ	log E_m	λ
4-(α -Phenylethyl)-	$C_{11}H_{13}ON_2$	80-81	20.7	20.5	3.46 3.66	2840 2480	2.80 3.96	2820 2380		
4-(<i>m</i> -Ethylphenoxyethyl)-	$C_{13}H_{17}O_2N_2$	135-136	17.0	16.7	3.42 3.45 3.93	2780 2720 2440	3.13 3.15 4.12	2780 2720 2260	3.21 3.26	2800 2720
4-(<i>o</i> -Bromophenoxypropyl)-	$C_{12}H_{14}O_2BrN_2$	152-153	13.5	13.2	3.62 3.62 3.96	2820 2760 2460	2.73 3.46 3.50	3000 2820 2760	3.43 3.46	2840 2760
4-(<i>o,p</i> -Dichlorophenoxypropyl)-	$C_{12}H_{13}O_2Cl_2N_2$	183-184	13.9	13.6	3.44 4.18	2880 2300	3.48 4.54	2860 2300	3.32 3.38	2940 2860
4,4-(<i>m</i> -Ethylphenoxyethyl)-	$C_{23}H_{29}O_3N_2$	215-217	10.6	10.4	3.89 3.87	2790 2710	3.94 3.95	2780 2720		
4,4-(<i>m</i> -Methylphenoxypropyl)-	$C_{22}H_{25}O_3N_2$	215-216	10.6	10.5	3.96 3.94	2800 2740	3.91 3.92	2800 2740		

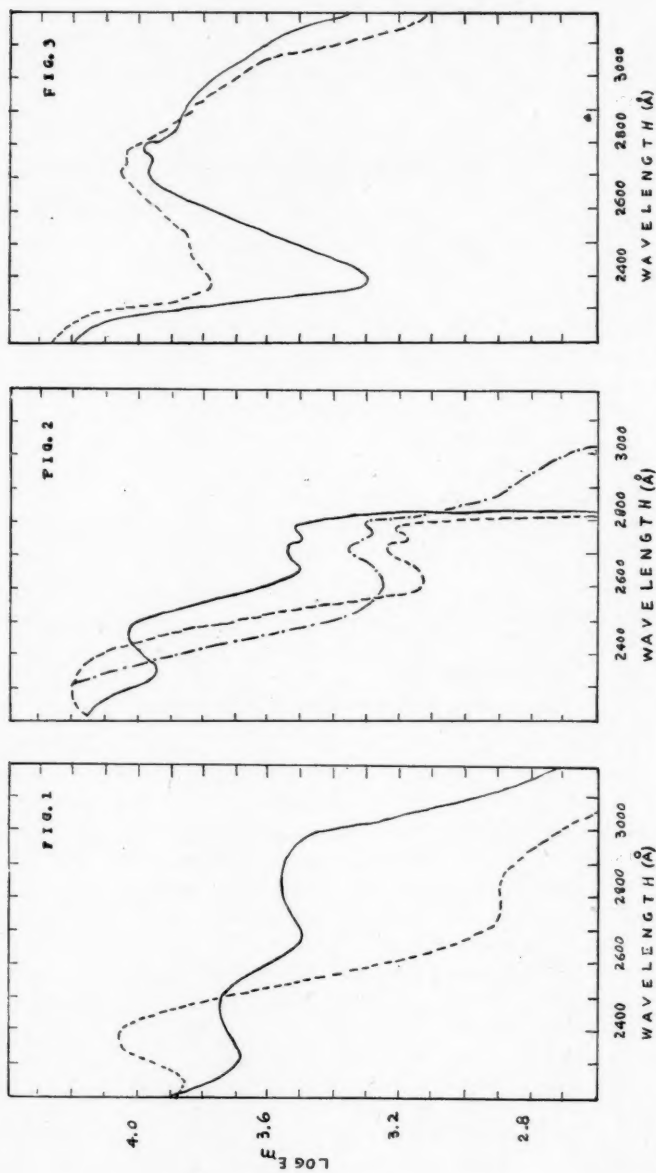


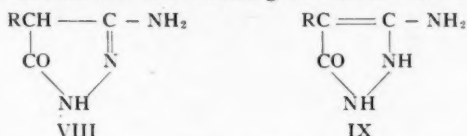
FIG. 1. Ultraviolet absorption spectrum of 4- α -phenylethyl-3-amino-5-pyrazolone: — in neutral solution; ----- in acid solution.

FIG. 2. Ultraviolet absorption spectrum of 4-*m*-ethylphenoxylethyl-3-amino-5-pyrazolone: — in neutral solution; ----- in acid solution; in alkaline solution.

FIG. 3. Ultraviolet absorption spectrum of 4,4-di-*m*-ethylphenoxylethyl-3-amino-5-pyrazolone: — in neutral solution; ----- in acid solution.

4-Monosubstituted-3-amino-5-pyrazolones

The spectrum of 4- α -phenylethyl-3-amino-5-pyrazolone (Fig. 1) shows a case of tautomerism as was encountered with 4-benzyl-3-amino-5-pyrazolone (9). Tautomerism occurs between the two following structures VIII and IX.



It has been demonstrated that pyrazolones of structure IX like 4-alkyl-3-amino-2-phenyl-5-pyrazolones (9) have their maximum absorption in the range from 2350 to 2450 Å, whereas pyrazolones of structure VIII like 4-alkyl-3-amino-5-pyrazolones absorb in the range from 2750 to 2850 Å (9).

In the case of 4- α -phenylethyl-3-amino-5-pyrazolone (Fig. 1), there are two absorption bands in neutral solution indicating tautomers. In acid solution, one maximum disappears leaving an inflection point at 2800 Å. There is evidence that acids catalyze the transformation of one tautomeric form (VIII) into the other (IX). This was observed with 4-benzyl-3-amino-5-pyrazolone (9).

The other 4-monosubstituted-3-amino-5-pyrazolones (Fig. 2) all have a phenoxyalkyl group in position 4, which might contribute to the absorption in addition to the pyrazolone ring. The spectra, in neutral solution, of 4-*m*-ethylphenoxyethyl-3-amino-5-pyrazolone (Fig. 2), 4-*o*-bromophenoxypropyl-3-amino-5-pyrazolone, and 4-*o,p*-dichlorophenoxypropyl-3-amino-5-pyrazolone are similar in shape, the pyrazolone ring is responsible for the absorption at shorter wave length, whereas the 4-substituents of the pyrazolone absorb in the range from 2750 to 2950 Å.

These spectra exclude the possibility of tautomers because in acid solution the spectra resemble very closely those in neutral media. It is believed that these compounds all have the same configuration (IX). Except at short wave lengths, the spectra in alkaline solution are all similar to those in neutral solution.

4,4-Disubstituted-3-amino-5-pyrazolones

The 4,4-disubstituted derivatives (Fig. 3) show also great similarity, a wide absorption band is observed in the range from 2600 to 3000 Å, having a maximum at about 2800 Å, which is similar to the spectrum of 4,4-dibenzyl-3-amino-5-pyrazolone (9).

The fine structure observed in the neighborhood of 2800 Å is due to the phenoxyalkyl substituent. The higher intensity of absorption observed with these disubstituted pyrazolones in comparison with the mono derivatives is due to the additive absorption of the pyrazolone chromophore and the phenoxy substituents.

These compounds have the ring structure shown above (VII).

REFERENCES

1. CLARKE, H. I. and MALM, C. J. *Org. Syntheses*, 9: 72. 1929.
2. DARAPSKY, A. *J. prakt. Chem.* 146: 250. 1936.

3. DARAPSKY, A. and HILLERS, B. *J. prakt. Chem.* 92: 297. 1915.
4. GAGNON, P. E. and BOIVIN, J. L. *Can. J. Research, B*, 26: 503. 1948.
5. GAGNON, P. E., BOIVIN, J. L., and BOIVIN, P. A. *Can. J. Research, B*, 28: 207. 1950.
6. GAGNON, P. E., BOIVIN, J. L., BOIVIN, P. A., and JONES, R. N. *Can. J. Chem.* 29: 182. 1951.
7. GAGNON, P. E., BOIVIN, J. L., and GIGUÈRE, J. *Can. J. Research, B*, 28: 352. 1950.
8. GAGNON, P. E., BOIVIN, J. L., and GIGUÈRE, J. *Can. J. Chem.* 29: 328. 1951.
9. GAGNON, P. E., BOIVIN, J. L., and JONES, R. N. *Can. J. Research, B*, 27: 190. 1949.
10. GAGNON, P. E., BOIVIN, J. L., and JONES, R. N. *Can. J. Research, B*, 28: 34. 1950.
11. GAGNON, P. E., BOIVIN, P. A., and CRAIG, H. M. *Can. J. Chem.* 29: 70. 1951.
12. GAGNON, P. E., GAUDRY, R., and KING, F. E. *J. Chem. Soc.* 13. 1944.
13. GAGNON, P. E. and NOLIN, B. *Can. J. Research, B*, 27: 742. 1949.
14. GAGNON, P. E., NOLIN, B., and JONES, R. N. *Can. J. Chem.* 29: 843. 1951.
15. GAGNON, P. E., SAVARD, K., GAUDRY, R., and RICHARDSON, E. M. *Can. J. Research, B*, 25: 28. 1947.
16. MARVEL, S. A. and TANENBAUM, A. L. *J. Am. Chem. Soc.* 44: 2645. 1922.

COAGULATION AND DEPOSITION IN STILL AEROSOLS OF VARIOUS SOLIDS¹

BY T. GILLESPIE AND G. O. LANGSTROTH

ABSTRACT

Studies have been made of the aging of magnesium oxide, zinc oxide, carbon, copal resin, and silica powder aerosols, under essentially uniform experimental conditions. The changes with time in the particulate number and in the number of particles lost from the system by deposition on chamber surfaces are well described in terms of the coagulation constant k and the deposition constant β with the aid of equations known to be applicable to ammonium chloride aerosols over a wide range of conditions. Marked differences were found in the values of k for different aerosols and lesser differences in the values of β . An electron microscope study of the shape and structure of the particles led to the conclusion that differences in these characteristics are not predominantly responsible for the observed differences in behavior, although they may be a contributing factor. A few preliminary experiments in which silica powder was dispersed through an electrically charged screen indicated that the coagulation and deposition processes are influenced by changes in the electrical charge distribution.

The particulate number of 'still' and stirred ammonium chloride aerosols and the deposition on chamber surfaces have been shown previously (2,4) to be described by simple equations containing as parameters the coagulation constant k and a deposition constant β . Furthermore, Corner and Pendlebury (1) have shown on theoretical grounds that the observed variation in these constants with the rate of stirring is consistent with expectation. Experiments with 'still' aerosols of five other solids have been performed to provide a more comprehensive test of the equations referred to above and to permit a comparison of the values of k and β for different systems. Although comparisons of k for various aerosols have been made in the past (6), it has become apparent (2) that data for deposition as well as particulate number are generally required for a critical evaluation of k and β . The aerosol particles were examined with an electron microscope in an attempt to find some influence of their shape and structure on the values of the constants. A few preliminary experiments were performed with silica powder dispersed through an electrically charged screen in order to ascertain whether or not the coagulation and loss processes are affected by the electrical charges carried by the particles.

1. APPARATUS AND PROCEDURE

All experiments were performed in a 60 cm. cube chamber with 'still' air at about 20°C. and 15% to 40% relative humidity. The method of production of each aerosol is indicated in Table VI. An attempt was made to control production to yield an initial particle size distribution similar to that obtained by heating 108 mgm. of ammonium chloride in the generator used previously (2,4).

Aerosols were fanned during dispersal and for three minutes afterward, and all recorded times were reckoned from the point at which the fan was stopped. Measurements of the particulate number and of the number of particles deposited

¹ Manuscript received August 5, 1952.

Contribution from the Defence Research Board, Suffield Experimental Station, Ralston, Alberta, Canada.

on chamber surfaces were made at frequent intervals for about an hour. The former were made on thermal precipitator samples, the latter on samples caught by microscope slides placed at the centers of the top, bottom, and one side of the chamber (a clean slide was substituted for each slide removed). A Patterson-Cawood graticule in the microscope eyepiece was used in determinations of particle size distribution. The details of the sampling and assessment procedures have been described previously (2,4). Samples for examination in the electron microscope were obtained by leaving specimen screens carrying a collodion film at the bottom of the chamber for the first 10 min. of an experiment.

An attempt to change the electrostatic charge distribution in silica powder* aerosols was made in three experiments. Normally the powder was blown from a small flask directly into the chamber with an air stream; in these experiments it was blown into the chamber through a wire screen maintained either at 2000 volts or at ground potential. In order to obtain a rough indication of a change in the charge distribution, two microscope slides backed by metal electrodes kept at 2000 volts potential difference were placed in the bottom of the chamber with their planes vertical, forming a condenser of 1 cm. plate separation. The total number of silica particles collected on the slides in three five-minute intervals at the beginning of an experiment was determined microscopically using a sampling procedure similar to that employed in measurement of deposition on chamber surfaces.

All data were analyzed with the aid of equations known to be applicable to ammonium chloride aerosols (2,4), i.e.

$$(1) \quad \ln\left(\frac{1}{n} + \frac{k}{\beta}\right) = \beta t + \ln\left(\frac{1}{n_0} + \frac{k}{\beta}\right),$$

$$(2) \quad (\Delta n)_t = \beta \int_0^t n \, dt,$$

$$(3) \quad \ln(n) + \beta t = -\frac{k}{\beta}(\Delta n)_t + \ln(n_0).$$

In these equations t denotes time, n the particulate number having a value n_0 at $t = 0$, k the coagulation constant, and β the deposition constant; $(\Delta n)_t$ represents the total number of particles deposited on chamber surfaces in the interval $t = 0$ to $t = \tau$ divided by the volume of the chamber. The use of these equations to determine values for k and β has been described in detail (2). According to equation (2), β may be found from the slope of the curve obtained by plotting $(\Delta n)_t$ values observed at various times τ against the area under the observed n vs. t curve up to $t = \tau$. According to equation (3), k may then be found from the slope of the $[\ln(n) + \beta t]$ vs. $(\Delta n)_t$ curve since β has been determined. The values may be checked by plotting $\ln\left(\frac{1}{n} + \frac{k}{\beta}\right)$ against t as suggested by equation (1). This procedure was found to be applicable to all the data with one exception, viz. for the two experiments in which silica powder

*Powdered Vycor (5) having a median particle diameter of about 1μ .

was dispersed through an electrically charged screen, values of $(\Delta n)_t$ in the first 10 min. of the experiments lay definitely below the linear relation required by equation (2) for the $(\Delta n)_t$ vs. $\int_0^t n dt$ plot. Since the relation was linear for times greater than 10 min., analysis of the data of these experiments was made by setting the arbitrary time origin at 10 min. after the fan had been stopped.

2. RESULTS

The observed values of $1/n$ and $(\Delta n)_t$ at various times are given in Tables I to V for the various aerosols studied. Corresponding values calculated from

TABLE I
A COMPARISON OF OBSERVED DATA FOR MAGNESIUM OXIDE WITH CALCULATED* VALUES

Time (min.)	$10^6/n$ (cc. ⁻¹)				Time (min.)	$(\Delta n)_t \times 10^{-3}$ (cc. ⁻¹)			
	Exp. 2		Exp. 3			Exp. 2		Exp. 3	
	Obs.	Calc.	Obs.	Calc.		Obs.	Calc.	Obs.	Calc.
2	14.6	14.5	2.8	2.8	5	1.7	1.9	4.5	4.4
9	15.7	15.7	3.4	3.4	10	2.7	2.9	8.7	9.4
16	17.3	16.8	4.6	4.0	15	3.6	3.8	12.2	13.5
23	17.8	17.9	5.2	4.6	20	4.5	4.6	16.2	17.2
30	18.8	19.0	5.1	5.4	25	5.2	5.5	19.5	20.6
37	19.6	20.1	5.3	6.1	30	6.3	6.6	22.5	23.9
44	24.1	21.3	7.5	6.7	35	7.1	7.1	25.3	26.6
51	21.4	22.1	7.8	7.5	40	7.8	7.7	28.0	29.0
58	24.1	23.7	7.9	8.4	45	8.6	8.5	30.7	32.1
65	25.4	25.0	8.3	9.0	50	9.2	9.5	33.6	33.6
					55	9.9	10.1	36.1	36.2
					60	10.4	10.4	38.6	37.3

* Using the values of Table VI for n_0 , k , and β .

TABLE II
A COMPARISON OF OBSERVED DATA FOR COPAL RESIN AND CARBON WITH CALCULATED* VALUES

Time (min.)	10 ⁶ /n (cc. ⁻¹)				Time (min.)	(Δn) _I × 10 ⁻³ (cc. ⁻¹)			
	Resin		Carbon			Resin		Carbon	
	Obs.	Calc.	Obs.	Calc.		Obs.	Calc.	Obs.	Calc.
2	2.9	2.9	4.1	4.0	5	4.5	4.6	7.5	6.8
9	3.6	3.5	5.8	5.0	10	8.3	8.5	13.1	11.5
16	4.9	4.4	5.7	6.0	15	11.1	11.6	17.1	15.6
23	5.8	5.1	7.1	7.0	20	13.9	14.1	20.5	19.3
30	6.2	5.9	7.6	8.0	25	16.4	16.6	23.4	22.5
37	6.5	6.5	8.3	8.5	30	18.6	18.7	26.0	25.5
44	6.4	7.4	9.6	9.2	35	20.8	20.5	28.4	28.5
51	9.4	8.3	10.8	10.0	40	22.8	23.2	30.2	30.5
58	9.0	9.0	10.0	11.0	45	24.4	24.0	32.0	33.0
65	8.8	9.8	15.0	13.0	50	25.9	25.0	33.6	35.5
					55	27.3	26.0	35.4	37.0
					60	28.5	28.0	36.8	39.0

* Using the values of Table VI for n_0 , k , and β .

TABLE III
A COMPARISON OF OBSERVED DATA FOR ZINC OXIDE WITH CALCULATED* VALUES

Time (min.)	10 ⁶ /n (cc. ⁻¹)				Time (min.)	(Δn) _t × 10 ⁻³ (cc. ⁻¹)			
	Exp. 6		Exp. 7			Exp. 6		Exp. 7	
	Obs.	Calc.	Obs.	Calc.		Obs.	Calc.	Obs.	Calc.
2	2.5	2.2	7.9	6.6	5	9.5	8.6	3.8	3.2
9	4.0	3.6	9.9	8.4	10	16.5	15.8	6.8	5.4
16	4.8	5.1	11.1	10.0	15	21.7	21.5	9.0	7.8
23	6.3	6.7	10.9	11.6	20	25.1	26.0	10.7	9.6
30	7.6	8.3	18.0	13.4	25	29.6	30.0	12.1	11.5
37	9.4	10.0	15.8	15.3	30	32.7	33.4	13.3	13.0
44	9.8	11.8	15.3	16.9	35	36.0	36.0	14.2	14.5
51	15.1	13.7	18.8	18.9	40	38.6	38.6	15.1	15.9
58	15.9	15.6	17.3	20.9	45	41.0	41.0	15.8	17.1
65	17.5	17.4	20.8	22.9	50	43.5	42.7	16.6	18.4
					55	44.5	44.4	17.3	19.5
					60	46.5	45.8	17.9	20.2

*Using the values of Table VI for n_0 , k , and β .

TABLE IV
A COMPARISON OF OBSERVED DATA FOR SILICA POWDER WITH CALCULATED* VALUES
(SILICA POWDER, LOT NO. 1)

Time (min.)	$10^6/n$ (cc. ⁻¹)				Time (min.)	$(\Delta n)_I \times 10^{-3}$ (cc. ⁻¹)			
	Exp. 8		Exp. 9			Exp. 8		Exp. 9	
	Obs.	Calc.	Obs.	Calc.		Obs.	Calc.	Obs.	Calc.
2	11.1	12.0	11.7	10.8	5	2.5	2.3	3.1	2.9
9	12.1	13.1	11.1	12.5	10	4.3	4.2	5.4	5.1
16	15.2	15.0	16.0	14.5	15	5.9	5.8	7.3	7.1
23	16.0	16.9	17.1	17.0	20	7.4	7.4	9.0	8.9
30	20.5	18.9	21.8	19.0	25	8.6	8.4	10.5	10.4
37	18.0	20.8	22.2	21.1	30	9.7	9.6	11.9	11.7
44	(32.9)	22.9	25.1	23.7	35	10.6	10.6	13.1	13.0
51	22.2	25.0	(32.3)	26.0	40	11.5	11.7	14.1	14.1
58	29.1	27.0	30.0	28.8	45	12.3	12.4	15.2	15.2
65	(22.9)	29.0	(24.7)	30.8	50	13.0	12.8	16.2	16.1
					55	13.6	14.0	17.2	17.1
					60	14.3	14.9	18.1	17.9

*Using the values of Table VI for n_0 , k , and β .

equations (1) to (3) with the aid of the determined constants n_0 , k , and β , listed in Table VI, have been included in these tables to show the nature of the agreement between theory and experiment. Some n_0 , k , and β values obtained previously for ammonium chloride aerosols have been included in Table VI, and their ability to describe observed data may be seen from reference to earlier papers (2,3); they are restricted to results obtained with a 60 cm. cube chamber, since it is known (2) that the β value depends on chamber dimensions. The data for particle size distribution have been omitted from this paper since all the aerosols had initially a median particle diameter of about 1μ and a distribution very similar to that given in Fig. 1 of Reference 2 (relative humidity =

TABLE V

A COMPARISON OF DATA FOR SILICA POWDER DISPERSED THROUGH A CHARGED OR GROUNDED SCREEN WITH CALCULATED* VALUES

Time (min.)	$10^6/n$ (cc. ⁻¹)						Time (min.)	$(\Delta n)_I \times 10^{-3}$ (cc. ⁻¹)					
	Exp. 12**		Exp. 11**		Exp. 10**			Exp. 12**		Exp. 11**		Exp. 10**	
	Obs.	Calc.	Obs.	Calc.	Obs.	Calc.		Obs.	Calc.	Obs.	Calc.	Obs.	Calc.
2	8.2	—	—	—	19.2	23.3	5	—	—	—	—	4.3	4.2
9†	10.2	(9.4)	19.9	(23.5)	27.	25.5	10†	—	—	—	—	7.1	6.7
16	11.6	10.5	31.5	27.0	25.	27.9	15	2.	1.8	1.5	1.4	9.4	8.6
23	12.8	11.6	29.2	31.0	33.3	30.0	20	3.8	3.5	2.5	2.5	10.5	10.7
30	12.8	12.8	35.3	35.0	34.5	32.0	25	5.4	5.2	3.3	3.6	13.3	12.4
37	13.5	14.0	39.5	39.0	38.8	34.5	30	6.9	6.5	4.2	4.6	14.9	14.1
44	18.2	15.2	42.6	43.0	40.	37.0	35	8.3	8.1	5.2	5.3	16.2	15.7
51	15.6	16.5	54.0	47.0	43.5	40.0	40	9.6	9.3	6.0	6.3	17.3	16.9
58	17.6	18.0	50.5	53.0	(54.2)	43.0	45	10.8	10.5	6.8	7.0	18.3	18.2
65	17.2	19.5	56.1	57.0	54.	46.0	50	11.9	11.8	7.6	7.8	19.1	19.4
							55	12.9	13.0	8.5	8.6	19.9	20.6
							60	14.0	14.2	9.3	9.1	20.5	21.7

*Using the values of Table VI for n_0 , k , and β .

**See tabulation below.

†Time origin.

Experiment	Screen	Silica powder	Time origin
12	2000 volts	Lot No. 1	Normal + 10 min.
11	2000 volts	Lot No. 2	Normal + 10 min.
10	Grounded	Lot No. 2	Normal

46%, $t = 5$ min.). Photomicrographs of typical particles of each of the aerosols are shown in Fig. 1. The data for silica powder dispersed through an electrically charged screen are given in Table V.

3. DISCUSSION

Examination of Tables I to V shows that both the particulate number and the deposition data for all aerosols studied are quite well represented by equations (1) to (3) in terms of the two experimentally determined parameters k and β . The average deviation of calculated from observed values was 4.6% for magnesium oxide, 4.4% for copal resin, 5.9% for carbon, 7.8% for zinc oxide, 6.6% for silica powder, and 5.0% for silica powder dispersed through a charged screen. These are comparable to the deviations in earlier data (2,4) for ammonium chloride aerosols (6% to 8%). The deviations in $1/n$ were somewhat greater than those in $(\Delta n)_t$ (7.7% as against 4.1% on the average), perhaps because the latter was favored by prior treatment in the analysis of data. The deviations are probably attributable for the most part to inaccuracies inherent in presently available sampling and assessment techniques since the experimental points are well distributed about the calculated curves.

The conditions of the experiments were sufficiently uniform to justify some

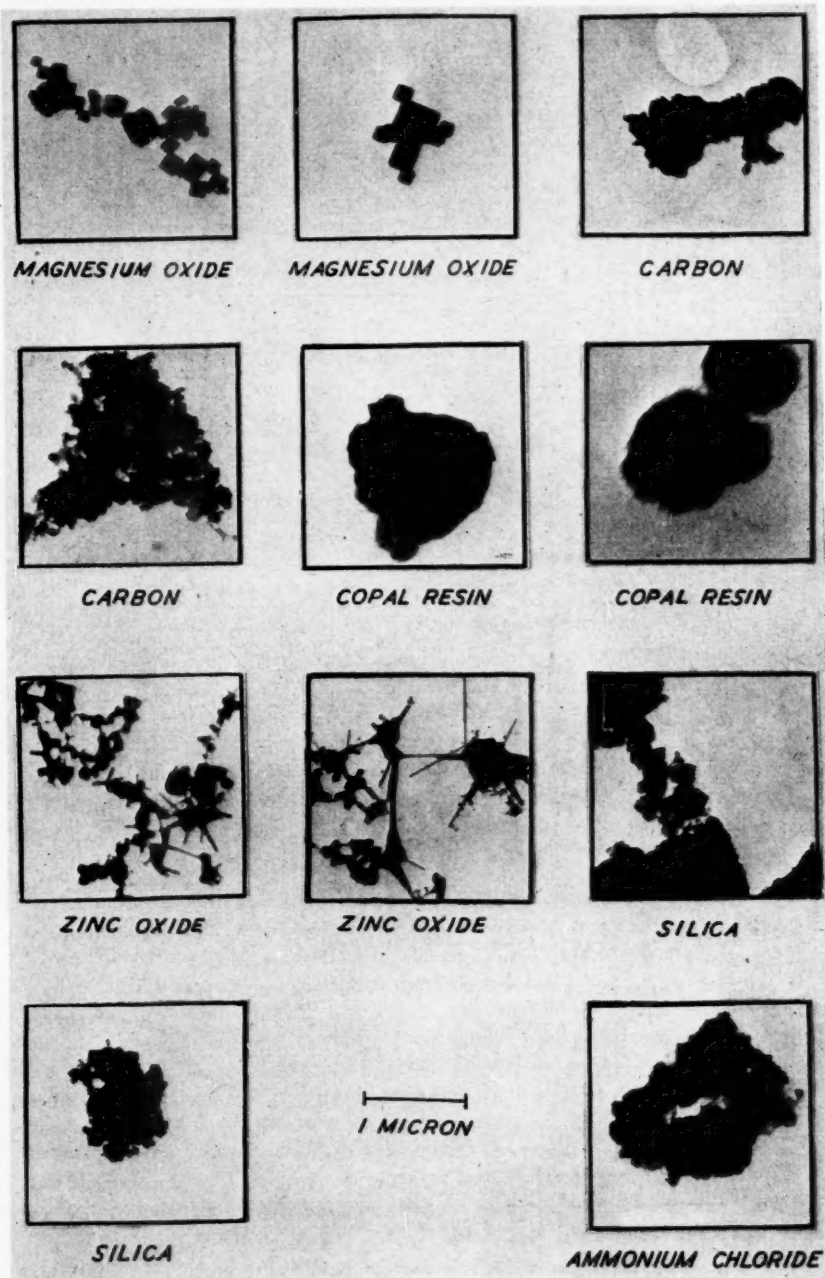


FIG. 1. Electron microscope photographs of aerosol particles.

consideration of the relative k and β values for different aerosols. While great differences in the amount of material dispersed can cause some variation in k and β through changes in initial particle size (see the examples for ammonium chloride given in Table VI and the more extensive data of Reference 2), conditions in these experiments were controlled to give similar initial particle size distributions for all aerosols. Furthermore, although the experiments were performed at relative humidities of from 15% to 40%, there is no reason to expect this feature to give rise to large differences in k and β ; with the slightly hygroscopic ammonium chloride for example, k and β are not seriously affected by an increase in relative humidity until a value of about 60% is reached when β begins to increase rapidly (3).

The results given for k and β in Table VI are summarized in the following tabulation which includes notes on the geometrical structure of particles at early times, as illustrated by the electron microscope pictures of Fig. 1. Experiments under varied conditions have been excluded, i.e. those characterized by dispersal of very large or very small amounts of ammonium chloride (R_1 , R_2 , and R_3) and by dispersal of silica powder through a screen (10, 11, and 12).

Aerosol	$k \times 10^8$ (cc./min.)		$\beta \times 10^8$ (min. ⁻¹)		Usual structure of particles (aggregates)
	Range	Mean	Range	Mean	
Ammonium chloride	3.3-4.7	4.1	1.8-2.9	2.2	Fairly compact
Magnesium oxide	8.5-10.9	9.7	3.0-3.4	3.2	Compact or stringlike
Copal resin	9.3	9.3	2.6	2.6	Fairly compact (spherical units)
Carbon	14.1	14.1	4.8	4.8	Fairly compact
Zinc oxide	18.9-19.6	19.3	4.5-4.6	4.6	Very open
Silica powder No. 1	26.0-28.0	27.0	4.5-5.0	5.0	Compact or stringlike

It is evident that there was considerable difference in k and some difference in β for the different aerosols. Purely on the basis of particle structure, one might expect the coagulation constant for zinc oxide to be large compared to that for the other substances, since zinc oxide particles have a large collision radius associated with small mass; it is, however, smaller than that for silica powder. Similarly one might expect the coagulation constant for magnesium oxide to be greater than that for copal resin, but it is not significantly so. It is concluded that while particle shape and structure may be a contributing factor as has been suggested (6), it is not predominantly responsible for the observed differences in the coagulation constant. The values observed for the different substances do not increase in the order of the bulk densities, which is not surprising in view of the fact that these differ considerably from the apparent densities of the particles (6). It is somewhat surprising that zinc oxide, whose particles must have a relatively small apparent density (cf. Fig. 1), has a larger β than magnesium oxide, copal resin, or ammonium chloride. An understanding of the differences in k and β values from aerosol to aerosol must await the investigation of other factors involved.

The few preliminary experiments in which silica powder was dispersed through an electrically charged screen are of interest in connection with the possible

TABLE VI
VALUES OF THE COAGULATION AND LOSS CONSTANTS FOR VARIOUS AEROSOLS AT ROOM TEMPERATURE AS DETERMINED FROM EXPERIMENTAL DATA
(60 CM. CUBE CHAMBER)

Aerosol	Method of production	Relative humidity	Exp. No. (Reference)	$n_0 \times 10^{-6}$ (cc. ⁻¹)	$k \times 10^8$ (cc./min.)	$\beta \times 10^3$ (min. ⁻¹)
Ammonium chloride	1020 mgm. of NH_4Cl heated in external generator	Room value	R2 (2)	12.5	5.1	3.4
	1020 " " " " " " " "	" "	R1 (2)	5.6	5.1	3.8
	108 " " " " " " " "	15%	17 (3)	12.4	4.7	1.8
	108 " " " " " " " "	46%	15 (3)	12.5	4.3	2.9
Magnesium oxide	108 " " " " " " " "	53%	14 (3)	14.3	3.3	1.9
	18 " " " " " " " "	Room value	R3 (2)	4.1	3.9	1.1
	90 mgm. of magnesium ribbon burned	" "	2	0.7	10.9	3.0
	48 " " " " " " " "	" "	3	3.8	8.5	3.4
Copal resin	Evaporation of solvent from sprayed solution	" "	4	3.8	9.3	2.6
	0.17 cc. of benzene burned in external generator	" "	5	3.3	14.1	4.8
	Carbon	" "	6	5.0	18.9	4.6
	Zinc oxide	" "	7	1.6	19.6	4.5
Silica powder No. 1	Electric arc between zinc electrodes	" "	8	0.9	26.0	4.5
	Blown directly into chamber	" "	9	1.0	28.0	5.5
Silica powder No. 2	Blown into chamber through charged screen	" "	12	0.9	9.0	4.1
	" " " " " " " "	" "	10	0.44	23.0	10.9
	" " " " " " " "	" "	11	0.43	37.0	6.8

Experiment 4: the sprayed solution consisted of 108 mgm. of gum copal resin in 10 cc. of chloroform plus 5 cc. of methanol. Experiments 11 and 12: the arbitrary time origin was chosen 10 min. later than for the other experiments.

effect of electrostatic charging on the coagulation and deposition mechanisms. In these experiments an altered deposition of particles in the condenser arrangement described in Section 1 indicated that passage through the screen had changed appreciably the electrical charge distribution of the aerosol. As may be seen from Table VI, this change led to a marked reduction of the coagulation constant for powder lot No. 1, but had little effect on the loss constant β . On the other hand with powder lot No. 2, dispersal through a charged screen led to a larger coagulation constant and a smaller loss constant than dispersal through a grounded screen. These results are not understood, beyond the indication that the electric charges on particles play a part in the coagulation and loss processes.

The authors are grateful to Mr. J. Maybank and Mr. F. L. McCallum for assistance in the experimental work and to Dr. R. B. Harvey for taking the electron microscope photographs.

REFERENCES

1. CORNER, J. and PENDLEBURY, E. D. *Proc. Phys. Soc. (London)*, B, 64: 645, 1951.
2. GILLESPIE, T. and LANGSTROTH, G. O. *Can. J. Chem.* 29: 201, 1951.
3. GILLESPIE, T. and LANGSTROTH, G. O. *Can. J. Chem.* 29: 133, 1951.
4. LANGSTROTH, G. O. and GILLESPIE, T. *Can. J. Research*, B, 25: 455, 1947.
5. NORDBERG, M. E. *J. Am. Ceram. Soc.* 27: 299, 1944.
6. WHYTLAW-GRAY, R. and PATTERSON, H. S. *Smoke*. E. Arnold and Co., London, 1932.

A STUDY OF ADSORPTION HYSTERESIS BY MEANS OF LENGTH CHANGES OF A ROD OF POROUS GLASS¹

By C. H. AMBERG² AND R. MCINTOSH³

ABSTRACT

From adsorption data and measurements of length changes of a porous glass rod, a qualitative description of the processes involved in the adsorption of water vapor is developed. Particular attention is devoted to the causes of the hysteresis loop. The qualitative theory appears to be useful in understanding the adsorption of water on charcoal, and may therefore be of value in interpreting the phenomenon of limited hysteresis on any porous adsorbent.

Three attempts to test the theory quantitatively are presented. These involve the computation of surface areas, of Young's moduli, and of isosteric heats of adsorption. The quantitative treatment also leads to an estimate of the total number of pores and the mean length of the pores, in addition to the pore radius. Such an assessment of a porous structure has apparently not been possible earlier.

INTRODUCTION

The occurrence of a hysteresis loop, closed at both ends, has been established for several adsorbate-adsorbent systems such as water and activated carbon, water and silica gel, water and porous glass. The existence of a hysteresis loop seems to be associated with the porous nature of the adsorbents which exhibit such loops, and a mechanism of adsorption by means of capillary condensation is generally postulated to account for the finding. The postulate that adsorption occurs by the formation of concave menisci in the capillaries, which therefore fill at a relative pressure given by the Kelvin equation, is not sufficient to account for the hysteresis. The theory must include some additional factor, such as a different value of the wetting angle along the two branches of the isotherm, or the assumption that the structure of the pore spaces is such as to permit condensation into the pores at a particular value of the relative pressure and emptying of the pores at another value of the relative pressure. Those theories which attribute the phenomenon to the structure of the pores are based on what is usually referred to as the "ink-bottle theory", due originally to Kraemer (14). By this is meant that the wide parts of the pores may govern the relative pressure at which the filling process begins, while the narrow parts of the pores will determine the relative pressure at which the emptying process occurs. The advantages of this view are that qualitatively the form of the hysteresis loop may be accounted for, and a successful rationalization of the results found on "scanning" the hysteresis loop may be presented. The disadvantage is that the theory has not yet been put on a quantitative basis, and indeed, it would appear impossible to do so in any general form.

A theory which is amenable to quantitative tests was proposed independently by Cohan (5) and Mrs. Coelingh (4). This theory, sometimes called the "delayed

¹ Manuscript received July 7, 1952.

Contribution from the Chemistry Department, University of Toronto, Toronto, Ont.

Based on a thesis submitted to the School of Graduate Studies, University of Toronto, in partial fulfillment of the requirements for the Ph.D. degree.

² Present address: Chemistry Department, University College, St. Andrew's University, Dundee, Scotland.

³ Associate Professor of Chemistry.

meniscus theory", was originally suggested in qualitative form by Foster (9), and is based on the concept that the capillaries begin to fill when a relative pressure is generated just in excess of the critical equilibrium pressure over a cylindrical annulus of adsorbate with the surface free energy of the liquid. For this mechanism to be applicable one must postulate open-ended pores. The hysteresis is then accounted for by desorption occurring from concave menisci which form when the pores fill. The filling of the pores is not a reversible process, since, as the annuli thicken, the pressure at which they would be stable is continuously lowered, and a spontaneous filling of the pores occurs. Many points in favor of this theory have been found experimentally, but inexplicable facts are also known, such as the different pore size distribution which would be obtained from the adsorption and desorption branches. Thus some additional phenomenon, such as the formation of an adsorbed film of varying thickness in the unfilled open-ended pores, is a requirement to surmount the difficulty (9). The more complex behavior is again more difficult to describe mathematically.

In the past few years a good deal of evidence has accumulated which appears to require that the view be maintained that concave menisci are established at some stage of the adsorption. Thus Haines and McIntosh (10) established that rods of activated charcoal contract below the dry length along the desorption branch, owing presumably to the formation of concave menisci with the creation of a negative pressure within the pores. This finding has been confirmed and extended by Wiig and Juhola (20), who also found a contraction along the adsorption branch, albeit a lesser one than the marked contraction which they observed along the desorption branch. These authors made very careful estimates of the pore size distribution by means of measurements of the quantity of nitrogen adsorbed on samples of chars which also contained adsorbed water, as well as by means of the isotherms for water and the use of the Kelvin equation. The hysteresis was again accounted for by the difference in the dimensions of the pore constrictions and those of the main pore bodies. Values of the wetting angle were given, but were regarded more reasonably as correction factors arising from the sizes of the constrictions and main parts of the pores. The length changes of the samples were accounted for by the variation of the negative pressure in the pore with relative pressure and by a swelling force attributed to hydrogen bonding among adsorbate molecules. The semi-empirical equation given by Wiig and Juhola does not fit the experimental data presented below, nor would one expect it to be valid generally on theoretical grounds unless the pore size range is quite narrow. Their work, however, is an extremely valuable contribution, and illustrates further the advantage of following the dimensional changes of the adsorbent.

In the present investigation, the adsorption of water on a porous glass rod has been studied, as well as the concomitant length changes of the rod. The length measurements led to the conclusion that certain mechanisms of adsorption and desorption were operative for this system, sometimes more than a single mechanism being operative over a given relative pressure range. Over certain parts of the relative pressure range it was found possible to make quite a clear-cut separation of mechanisms, and to test the conclusions quantitatively by means of

estimates of surface area, the evaluation of Young's moduli, and heats of adsorption. It was also possible to estimate the total number of pores and their mean length, as well as their diameters. The paper has therefore been divided into two parts. Part I contains the experimental results and a qualitative explanation of them; Part II consists of several quantitative tests of the postulates concerning the mechanisms of adsorption. Although the views put forward have been subjected to quantitative tests in the case of this one system only, they appear to have a bearing on the behavior of charcoal-water systems, as is indicated in Part I, and may be useful, therefore, in explaining observations wherever hysteresis is found with porous adsorbents.

PART I

EXPERIMENTAL

Adsorption-desorption isotherms at 25.80, 18.75, and 11.79°C. (all $\pm .02^\circ\text{C}.$) were determined, along with the length changes of the adsorbent. Scanning experiments were also performed to test certain postulates. Although the techniques employed were variations of well known procedures, a brief account of them is desirable.

After the glass rod had been cleansed and evacuated at $130^\circ\text{C}.$ as described below, a measured quantity of water was allowed to adsorb on it and the equilibrium pressure over the system was determined. The quantity of water admitted to the adsorbent was obtained from the change of height of liquid water in a capillary, which formed the principal part of a water doser so designed that the capillary could be recharged at will (18). The equilibrium pressures were measured for the range 5×10^{-2} to 5 mm. of Hg on a slanting McLeod gauge (15). Over the pressure range 5 to 25 mm. a spoon gauge was employed as a null instrument. The desorption branch of the curve was established by condensing adsorbate into small glass tubes, which were then sealed off, weighed, broken, and dried, and then re-weighed. This procedure was used also to check the performance of the capillary doser. Corrections to the weight taken up by the adsorbent were necessary owing to the dead space of the adsorption system and slanting McLeod gauge. A correction for the volume of air displaced by the tubes in the weighing procedure used for desorption points was also necessary.

The length changes of the adsorbent were followed by use of a parallel-plate extensometer described by Haines and McIntosh (10). The extensometer was improved by replacing the quartz rods of the original assembly by carefully insulated rods of Invar. In lieu of the Schering bridge system employed by Haines and McIntosh, a resonance circuit was used for obtaining capacitance values. The signal employed in the resonance circuit had a frequency of 317 kc. per sec.

The over-all performance of the assembly may be summarized by the following statements. Quantities of water were measured to 0.2 mgm. for each addition, a precision apparently obtained in all runs after the first, where greater error, due to lack of experience in handling the doser, was encountered. Pressure readings appear reliable to 1% over the whole range. Length changes of $\pm 0.3 \mu$ were detectable at the greater plate separations and of $\pm 0.2 \mu$ when the plates were

closer together. The absolute length of the adsorbent could be in error by $\pm 2 \mu$, but the maximum error in recorded length changes is considered to be much less than 4% of the particular length increment. The correction necessary to the length measurement because of water vapor between the condenser plates of the extensometer has been shown to be negligible.

The porous glass rod used as the adsorbent was supplied by Corning Glass, Corning, N.Y. It was a Vycor glass, No. 7930, containing 96% silicon dioxide, 3% boron trioxide, which was prepared by leaching a borosilicate glass with hot dilute acid (16). The rod was 11.1 cm. long and 0.73 cm. in diameter. The rods as received were slightly opalescent. The one employed had been kept in a desiccator for several months and had turned yellow in color. It was therefore soaked in acetone until the color had cleared, next immersed in methanol, washed in distilled water, and slowly pumped dry. After the extensometer assembly had been calibrated and placed in its housing, the assembly was evacuated at 130°C. until the pressure was 5×10^{-6} mm. of Hg at that temperature, and an appreciable "sticky" vacuum observed at room temperature. That a "reproducible" surface was thus established was confirmed by the adsorption and length data. Desorption to the dry state was carried out after the first isotherm by pumping at 50°C. until no further change of length could be detected and a sticky vacuum was obtained at room temperature.

RESULTS

The results obtained at the three temperatures are given in Tables I, II, and III. The data are recorded along with a number which designates the order in

TABLE I
EXPERIMENTAL RESULTS
Temperature, 25.80°C.; $P_0 = 24.91$ mm.

Point No.	% Linear expansion	Weight adsorbed, gm. H ₂ O/gm. glass	Equilibrium pressure, P/P_0
1	0.0089	0.00477	0.0032
2	0.0281	0.0136	0.0231
3	0.0608	0.0291	0.138
4	0.1172	0.0628	0.539
5	0.1372	0.0984	0.711
6	0.1436	0.1352	0.768
7	0.1486	0.1918	0.814
8	0.1552	0.2264	0.840
9	0.1890	0.2442	0.924
10	0.2134	0.2548	0.980
11D	0.1840	0.2326	0.840
12D	0.1414	0.2208	0.730
13D	0.1315	0.0858	0.660
14D	0.1222	0.0623	0.563
15D	0.0951	0.0414	0.335
16	0.0408	0.0188	0.0405
17	0.1185	0.0642	0.545
18	0.1385	0.0990	0.710
19	0.1432	0.1169	0.752
20D	0.1344	0.0960	0.676
21D	0.1262	0.0800	0.620
22D	0.1122	0.0614	0.487

TABLE II
EXPERIMENTAL RESULTS
Temperature, 18.75°C.; $P_0 = 16.22$ mm.

Point No.	% Linear expansion	Weight adsorbed, gm. H ₂ O/gm. glass	Equilibrium pressure, P/P_0
1	0.0173	0.00930	0.0075
2	0.0407	0.02049	0.0532
3	0.0712	0.0355	0.216
4	0.1052	0.0548	0.467
5	0.1215	0.0748	0.619
6	0.1378	0.1133	0.724
7	0.1419	0.1591	0.774
8	0.1431	0.1928	0.771
9	—	0.2302	0.828
10	0.0853	0.0417	0.234
11	0.1419	0.1886	0.776
12	0.1449	0.2093	0.810
13	0.1515	0.2313	0.829
14	0.1765	0.2450	0.914
15	0.1858	0.2510	0.926
16	0.1946	0.2564	0.938
17	0.2021	0.2618	0.945
18 <i>D</i>	0.1073	0.1599	0.681
19 <i>D</i>	0.1108	0.1400	0.673
20 <i>D</i>	0.1152	0.1233	0.663
21 <i>D</i>	0.1186	0.0992	0.659
22 <i>D</i>	0.1100	0.0631	0.531
23 <i>D</i>	0.0981	0.0510	0.429
24	0.1412	0.2011	0.782
25	0.1456	0.2236	0.818
26	0.1817	0.2470	0.905
27	0.1952	0.2562	0.930
28 <i>D, R</i>	0.1491	0.2340	0.824
29 <i>D, R</i>	0.1012	0.2212	0.706
30 <i>R</i>	0.1321	0.2269	0.767
31 <i>R</i>	0.1530	0.2334	0.841
32 <i>D, R</i>	0.1024	0.2203	0.714
33 <i>D</i>	0.0954	0.2131	0.681
34 <i>D</i>	0.0990	0.1903	0.686
35	0.1125	0.1949	0.727
36	0.1225	0.1996	0.753
37	0.1325	0.2102	0.781
38	0.1379	0.2200	0.800
39	0.1476	0.2297	0.826
40	0.1653	0.2394	0.872
41	0.1127	0.0615	0.524
42	0.1445	0.1699	0.786
43	0.1929	0.2545	0.924
44 <i>D, R</i>	0.1197	0.2241	0.743
45 <i>R</i>	0.1447	0.2300	0.810
46 <i>D, R</i>	0.1063	0.2212	0.719
47 <i>D</i>	0.1076	0.1806	0.688
48	0.1170	0.1837	0.714
49	0.1315	0.1941	0.762
50	0.1378	0.2043	0.786
51	0.1406	0.2200	0.800

which the data were obtained. Desorption points are marked *D*. An isotherm at 18.75°C. and a plot of the length variations corresponding with this isotherm are given in Figs. 1 and 2. In order to make the necessary comparisons of adsorption data and length changes, the adsorption isotherm is lettered *OABCDBAO* and a

TABLE III
EXPERIMENTAL RESULTS
Temperature, 11.79°C.; $P_0 = 10.37$ mm.

Point No.	ζ , Linear expansion	Weight adsorbed, gm. H ₂ O/gm. glass	Equilibrium pressure, P/P_0
1	0.0129	0.00680	0.00612
2	0.0377	0.01924	0.0463
3	0.0756	0.03651	0.256
4	0.1012	0.0517	0.432
5	0.1213	0.0737	0.607
6	0.1303	0.0945	0.685
7	0.1358	0.1301	0.754
8	0.1393	0.1724	0.786
9	0.1403	0.2138	0.812
10	0.1768	0.2367	0.879
11	0.2314	0.2550	0.989
12D	0.1610	0.2357	0.849
13D	0.1365	0.2290	0.793
14D	0.1221	0.2233	0.730
15D	0.0996	0.2199	0.700
16D	0.1046	0.1726	0.693
17D	0.1157	0.1217	0.667
18D	0.1208	0.0858	0.629
19D	0.1117	0.0623	0.529

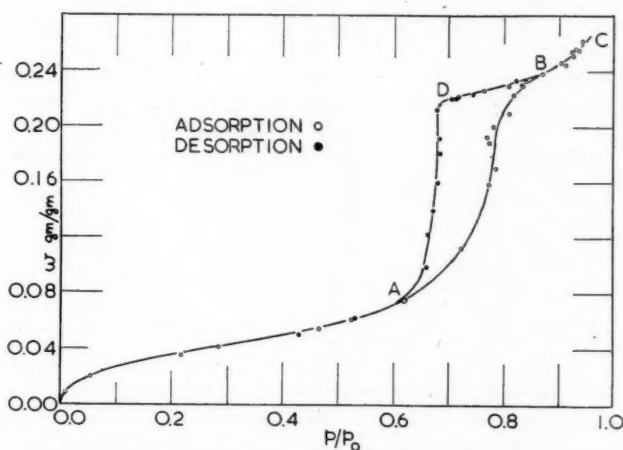


FIG. 1. Adsorption isotherm for water on porous glass at 18.75°C.

similar lettering indicates the length variations along a complete adsorption-desorption isotherm. In Figs. 3 and 4 scanning experiments are represented.

To clarify the quantitative discussions which are given later, a summary of the results and a qualitative interpretation of them are now necessary. Along OA adsorption occurs with the equilibrium pressure of the adsorbate increasing markedly. Accompanying this adsorption is a large extension of the rod, presumably arising from the reduction of the surface free energy occurring on ad-

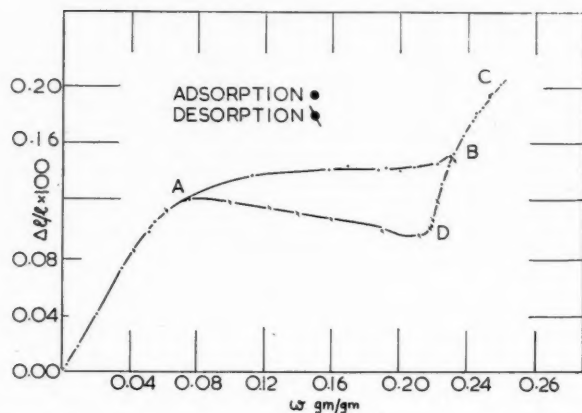


FIG. 2. Length changes arising from adsorption of water at 18.75°C.

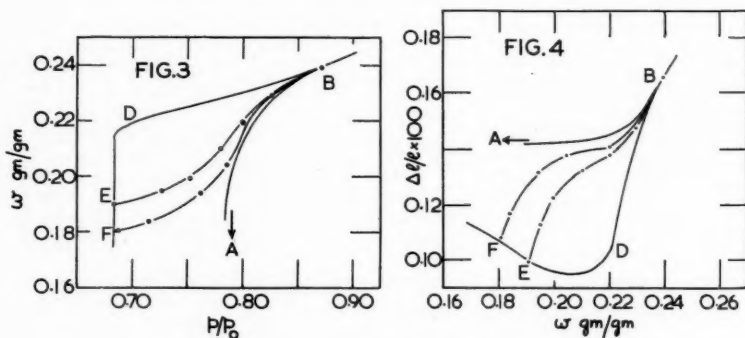


FIG. 3. Scanning curves of isotherm at 18.75°C.

FIG. 4. Length changes observed during scanning experiments.

sorption. Between points *A* and *B* about two-thirds of the total quantity adsorbed is taken up over the relative pressure range 0.60 to 0.87. As this material is adsorbed there is virtually no increase in the length of the adsorbent. We believe this to be due to a compensation of forces in the following way. At point *A* a layer of adsorbed water 6 Å thick (see method of estimation given in Part II) is considered to cover the walls of all the open-ended cylindrical pores* which we postulate to exist in the rod and which are assumed to be orientated in all directions. Moreover, as will be deduced later, almost the entire adsorbing surface of the rod is formed by the wall area of these open-ended pores. As the relative pressure is raised above 0.6, the smallest pores, the radii of which will be that of the glass

*The concept of open-ended pores implies voids between capillaries. This implication is not inconsistent with the treatment given, as the total void volume is not known, but is obviously greater than the volume of the capillaries, since adsorption occurs above the closure of the loop. In any event, the porous structure which is postulated is an equivalent structure, which permits a comparatively simple explanation of the experimental observations.

structure less the thickness of the adsorbed film, will fill spontaneously according to the Cohan mechanism, and concave menisci of a radius of curvature compatible with the final equilibrium pressure will be created. At the same time further reversible adsorption will occur in all pores with radii greater than the critical value which permits capillary condensation by the Cohan mechanism. Thus a further decrease in surface free energy is brought about, which, as before, would cause an extension of the rod if not opposed by some contractive force. The opposing force arises from the negative pressure created under the concave menisci, and thus no net increment of length is registered. This type of occurrence is repeated as larger pores are filled, and, indeed, a third factor must also be taken into account. The concave menisci with radius of curvature such that equilibrium conditions exist under a relative pressure of 0.6, for example, would not be in equilibrium with respect to transfer from and into the vapor phase at any higher relative pressure. Therefore a flattening of these menisci must occur until the curvature is such that equilibrium with respect to this transfer again obtains. The change in negative pressure brought about by this alteration of curvature would also act as a force tending to increase the length of the adsorbent. The nearly complete compensation of forces observed experimentally must arise from the combination of all these factors. Just below point *B* extension of the adsorbent again is noted. Between *B* and *C* marked extension is observed, so that along this region presumably no new concave menisci are being formed. The dimensional changes arise from the flattening of the menisci, the increasing spreading force of the adsorbed film in filled pores, and further adsorption in wide channels. It should be emphasized that adsorption and length changes are reversible along this section *BC*.

When water is desorbed from the rod along *BD*, although very little is removed from the adsorbent, a marked contraction of the rod is found. Along this section adsorption is again reversible as are the dimensional changes. This fact has not been emphasized previously to our knowledge, although adsorption may have been assumed to be reversible by other investigators. This observation was carefully checked by adsorbing and desorbing repeatedly along *BD*, since on the basis of this observation rests a great deal of the confirmatory quantitative treatment which has been developed (See Table II, points marked *R*). The interpretation of the finding is that, between *B* and *D* along the desorption branch, only a reversible adsorption or desorption on the concave menisci is occurring, and no capillaries are believed to be emptying. The contraction of the adsorbent is thus due to the increased value of the negative pressure as the equilibrium pressure is reduced, and to the reduced spreading force of the film which adsorbs on the pore walls before the filling of the pores takes place. Thus one may identify the position *D* of the length plot, at the point of inflection of the length plot, and the corresponding position of the adsorption isotherm, *D*, as representing a condition of all pores filled under concave menisci of the appropriate curvature. Along *DA* pores empty by evaporation from concave menisci, and the Kelvin equation may be employed along this section. The pores which are emptied in this manner still retain an adsorbed film along the walls, and some desorption from this film un-

doubtedly occurs. It must be remembered, however, that the relative pressure range over which the pores lose their concave menisci is narrow (0.7 to 0.6) and if the relation between quantity adsorbed as film and relative pressure is given by an extrapolation of *OA* through this relative pressure region, comparatively little desorption will occur and there will be little change of the spreading force of the film. Therefore the result of desorption along *DA* is a destruction of concave menisci, which will act as a force tending to cause expansion, and the rod is found to increase in length until *A* is reached. From *A* to *O* the sequence of events is the reverse of that along *OA*.

Scanning Experiments

The term "scanning the hysteresis loop" means following the path on desorption from the adsorption branch, or adsorption from the desorption branch. Perhaps the most exhaustive tests of this nature have been carried out by Rao (17), who concluded that certain of the results on scanning could only be accounted for by a "bottle neck" theory. We have been unable to carry out as complete tests as Rao performed, because of the difficulty experienced in repeating a desorption point exactly with our experimental procedure for removing adsorbate. However, some tests were performed in which length changes were followed, and these are again consistent with the views expressed above. Moreover, they point up a factor which is not usually considered for "rigid" gel systems, namely that such systems are undergoing shrinking and swelling to some extent. Because the porous adsorbent is in a contracted state along the desorption branch, the pore dimensions are not the same as along the adsorption branch. This means that adsorption from a state represented on the desorption branch can occur at a relative pressure lower than for the main adsorption branch. This additional consideration is sufficient to permit a prediction of the results which are reported and discussed below. The data obtained from the scanning experiments are recorded in Table II and represented in Figs. 3 and 4. In these plots two scanning curves crossing the hysteresis loop from the main desorption branch to the main adsorption branch are represented for the isotherm at 18.75°C. It is seen that the scanning curves join the main adsorption branch only at the closure of the loop, i.e. point *B*. This confirms the data for the upper part of the loop reported by Emmett and Cines (7), who expressed uncertainty in this regard because of the difficulty in distinguishing the point of junction within the limits of experimental accuracy. Here the definition of the expansion plots appears sufficient to show that the scanning curves join the adsorption branch at *B*.

Point *E* was approached from *D*, and a certain number of the pores would have emptied, leaving a reversibly adsorbed film on the walls in equilibrium with vapor at the particular P/P_0 value. If the value of P/P_0 above the adsorbent were raised, and if no increase of the thickness of the reversibly adsorbed film occurred, as well as no filling in of existing menisci, the amount adsorbed would increase by condensation into the pores at a Cohan pressure determined by the smallest empty pores at *E*. This pressure actually lies to the right of the main adsorption branch, as one may readily verify. Actually, on increasing P/P_0 from the value at *E*, adsorption will occur on existing menisci, and into the layers of adsorbed

vapor in the pores where no menisci exist. The effect of this will be to increase the quantity of adsorbate above the value at E , and to cause a reduction in the value of the Cohan equilibrium pressure which is necessary for spontaneous pore filling. (This is the reason that the adsorption branch lies to the left of the adsorption curve which could be constructed by means of the known desorption branch and the Cohan equation.) On this simple basis there should, however, be a joining of the scanning curve and the main adsorption branch, since the pores are now in the same condition, according to our postulates, as if adsorption from A had been brought about until the same number of pores had been filled. The experimental fact is that the curves do not join below B , and the explanation appears to be that at E the rod is in a contracted state relative to any system along the main adsorption branch. The contraction has an effect on the values of the pore radii. Therefore it is possible for the spontaneous process of pore filling to occur at relative pressures lower than would be necessary in the more extended state of the adsorbent along the adsorption branch. As this is true at all stages of the adsorption being followed from the main desorption branch, the curve will always lie above the adsorption branch. In the case of the system represented by F , the rod is less contracted than at E . This being so, the adsorption path from F will approach more closely to AB than does the path from E ; the junction will occur, however, at B , as in the former case.

These contentions are supported by the expansion results. Initially, paths EB and FB resemble path DB , which is indicative of meniscus flattening and reversible adsorption. Then, as pores begin to fill, there is a section similar to AB where there is compensation between forces of contraction and expansion. This section is closer to AB in the case of FB , since F is a less contracted state than E . For points nearer to A than F , the similarity to AB should be more marked. Some support of this statement may be derived from the data of Emmett and Cines (7). Those of their scanning results starting near A cross the loop and appear to join the main adsorption branch below B .

Unfortunately, our data for the desorption scanning branch (see Table I) are not well enough defined to locate the junction with the main branch. Emmett and Cines (7) were also not able to establish this point. A discussion along the lines set forth previously for adsorption scanning curves would predict the emptying of capillaries at pressures displaced towards the adsorption branch if the initial condition is one corresponding to an extended state of the adsorbent. This effect would be observable with difficulty at conditions far removed from B .

Discussion of Charcoal-Water Isotherms

No detailed attempt will be made to apply the views outlined above to charcoal-water systems. It should be recalled, however, that the (chemical) condition of the charcoal surface would appear in some cases to permit appreciable adsorption before the hysteresis loop, while in other cases, virtually no adsorption is found over the low relative pressure range. If reversible adsorption occurs before meniscus formation, an extension of the adsorbent should be noted. Depending upon the relative amounts of reversible adsorption and meniscus formation along the main adsorption branch, any length change from negative to positive may be

obtained. Thus is found a positive change for porous glass and for the charcoal studied by Haines and McIntosh (10), and first a negative, and ultimately a positive change, for the charcoal studied by Wiig and Juhola (20). Furthermore, the relative pressure range over which the emptying of capillaries from concave menisci occurs can then vary, from charcoal to charcoal, even if of the same pore radii, depending upon the thickness of the reversibly adsorbed film which remains along the walls. Indications that such observations may be made are apparent in work reviewed by Emmett (6) where a change in the form of the isotherm for a char is produced after treatment which would be expected to increase the amount of "oxygen complex" on the surface. Until data of the requisite type are available, further discussion is unwarranted. It may be emphasized, however, that the existence or nonexistence of reversibly adsorbed films, along with meniscus formation, can account for the extension data so far published.

PART II

Area of the Pore Walls

Along *OA*, since adsorption is reversible, the surface area was computed by the use of the BET (3) equation, and a cross-sectional area of 10.5 \AA^2 for the water molecule. The value obtained was 117 m^2 per gm. From what has been said in the qualitative discussion of results, the section *DA* of the adsorption branch is to be accounted for on the view that desorption occurs from concave menisci. There is left a film of reversibly adsorbed water along the walls. It was further stressed that little desorption from this film will occur in larger pores which have lost their menisci, because of the narrow range of relative pressure (0.6 to 0.7). Thus application of the Kelvin equation along *DA* as suggested by Kistler, Fischer, and Freeman (13) will yield the area of the film in the pores. This area must then be corrected to a larger value, which is dependent upon the film thickness, to yield the area of the pore walls which was found from the section *OA* to be 117 m^2 per gm. The surface area of the film adsorbed at *A* on the pore walls is then

$$\text{Area} = - \frac{RT}{M\rho\sigma} \int_A^D \ln P/P_0 dw = 107 \text{ m}^2 \text{ per gm.}$$

Here and throughout, $\cos \theta$ is taken as 1.0 in any applications of capillary condensation theory. The correction to the value of 107 m^2 per gm. to yield the wall area is carried out as follows.

For an assembly of cylindrical pores $dV_i = \pi r_i^2 d(n_i h_i)$ for any radius r_i . Thus

$$\left. \frac{1}{\pi r_i^2} \frac{dV}{dr} \right|_{r=r_i} = \left. \frac{d(n_i h_i)}{dr} \right|_{r=r_i}$$

where n_i is the number of pores and h_i the average length of pores of radius r_i . From this the variation with r of $d(n_i h_i)/dr$ is obtained, which is shown in Fig. 5, as is dV/dr vs. r . The curve of $d(n_i h_i)/dr$ vs. r was then divided into small segments of mean radius \bar{r}_i . If the volume adsorbed at *A* is distributed over all the pores at a constant thickness a , then the true pore radius is given by

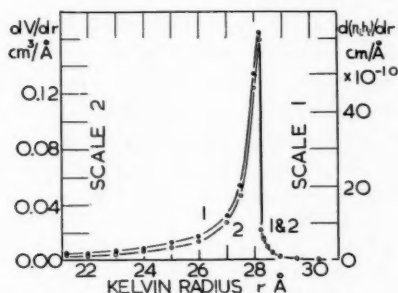


FIG. 5. Pore structure curves for porous glass: left-hand ordinate dV/dr , right-hand ordinate $d(n_i h_i)/dr$.

adding a to the value obtained using the Kelvin equation along DA . For each segment of the distribution curve

$$\Delta V_i = \pi n_i h_i [(\bar{r}_i + a)^2 - \bar{r}_i^2]$$

where ΔV_i is the volume of the reversibly adsorbed film for capillaries of mean radius \bar{r}_i . Summing over all pores, one obtains

$$\sum \Delta V_i = 2\pi a \sum n_i h_i \bar{r}_i + \pi a^2 \sum n_i h_i$$

where $\sum \Delta V_i$ is the volume adsorbed at A , and $\sum n_i h_i$ and $\sum n_i h_i \bar{r}_i$ may be obtained by graphical integration of $d(n_i h_i)/dr$ vs. r , and by summing the product of $n_i h_i \bar{r}_i$ for each segment of mean radius \bar{r}_i of the curve. Since $\sum \Delta V_i$ was 0.710 cm^3 per gm. the thickness a of the adsorbed film was found to be 6.1 \AA .

The thickness of the reversibly adsorbed film being known, the area of the pore walls was obtained through the relation

$$\Delta A_i = \frac{2\Delta V_i}{\bar{r}_i'}$$

where ΔA_i and ΔV_i are the area and volume per gram, respectively, for each group of capillaries taken to have \bar{r}_i' as its corrected mean pore radius. The area of the pore walls is $\sum \Delta A_i$, which is 129 m^2 per gm. To confirm the values, $\sum \Delta V_i = \sum \pi \bar{r}_i'^2 n_i h_i$ was evaluated and was 0.2118 cm^3 per gm. The experimental value was 3.5% higher, namely 0.2195 cm^3 per gm. The magnitude of the discrepancy appears quite reasonable in view of the graphical procedures of differentiation and integration which were utilized.

The values of the wall area are then 117 m^2 per gm. by the BET procedure, and 129 m^2 per gm. on the assumption of capillary condensation along DA . Since the mechanisms governing adsorption, the relative pressure ranges, and the quantity of material adsorbed are so different in the two cases, the agreement found appears to be highly significant. It follows, also, that the area on which reversible adsorption occurs is essentially also the area associated with the pores involved in the capillary condensation process, although since adsorption and length changes along BC appear to be greater than can be explained by

the process of filling concave menisci alone, some large pores or channels which contribute little to the area appear to exist.

Estimate of the Absolute Number of Pores and the Mean Length of Pores

The estimate of the total number and mean length of pores which is now to be made does not constitute confirming evidence of the theory, but is inserted here since the requisite curves and summations have been presented. It is made on the basis of the postulate concerning the process occurring along *DB*. Each pore, being open at both ends, has two menisci. Any change of pore dimensions due to swelling of the rod is neglected. At *D*, the smallest pores will possess menisci which are not hemispherical, because the relative pressure at *D* is greater than the equilibrium pressure at which such pores possess menisci of this shape. The largest pores will have menisci which are hemispherical. At *B* all pores will have menisci which are of the appropriate curvature for the relative pressure at that point. The volume adsorbed into the menisci will thus depend on the relative pressures at *D* and *B*, and the size of the capillary, and, of course, the number of capillaries of each size. It is thus necessary to have a knowledge of the distribution function for the number of capillaries in any size range. This information is not obtainable, and the difficulty is circumvented by assuming that all capillaries have the same mean length *h*. The plot of $d(n_i h_i)/dr$ vs. *r* may then be employed, which on the present assumption is $h d(n_i)/dr$ vs. *r*. In other words an n_i distribution having the same form as the $n_i h_i$ distribution is assumed. With this number distribution and the appropriate geometric formula giving the volume filled in each capillary between the two equilibrium values of the curvature of the menisci, the product of *h* and the total volume filled between *D* and *B* is obtained in arbitrary units. The value of *h* is then obtained by equating this arbitrary number to the value of the volume adsorbed between *D* and *B*. Once the value of *h* has been derived, the value of n_i in each section of the data is obtained. The data for this calculation are given in Table IV. (A less rigorous

TABLE IV
CALCULATION OF NUMBER AND LENGTH OF PORES

\bar{r}_i , Å	$2(V_1 - V_2)/r - \bar{r}_i \times 10^{20}$, cm. ³	$n_i h \times 10^{-10}$, cm.	$2n_i h(V_1 - V_2) \times 10^{10}$, cm. ³	$n_i \times 10^{-16}$
21.5	0.95	2.00	1.90	1.9
22.5	1.17	2.50	2.93	2.4
23.5	1.47	3.20	4.70	3.1
24.5	1.85	4.40	8.15	4.3
25.5	2.31	5.65	18.7	4.5
26.5	2.86	9.00	25.7	8.8
27.3	3.60	9.95	35.9	9.6
27.8	4.00	12.65	50.6	12.3
28.1	4.31	10.75	46.4	10.4
28.6	5.25	2.40	12.6	2.3
29.5	6.61	0.50	3.31	0.5

* $V = \frac{1}{2}\pi d(3\bar{r}_i^2 + d^2)$ where $d = R - (R^2 - \bar{r}_i^2)^{1/2}$. *R* is the radius of curvature of the meniscus. The values of *R* for the computation of *V*₁ and *V*₂ were *R*₁ = 30.0 Å and *R*₂ = 78.5 Å. \bar{r}_i is the mean radius of the pores covered with reversibly adsorbed film.

The sum of the fourth column is 2.11×10^{-8} cm.³; since the volume adsorbed between *D* and *B* is 2.05×10^{-2} cm.³, *h* has the value 103 Å.

procedure, assuming that all menisci are originally hemispherical and are filled completely at B , suffices to give order of magnitude agreement with the preceding method. In this case it was assumed that the contribution to the total volume taken up between D and B could be taken for each range of capillaries as proportional to the volume distribution dV/dr vs. r . If this is done both h_i and n_i in each size range may be estimated.) As can be seen in Table IV, the pores are about twice as long as they are wide. The number of pores per gram is of the order of 10^{16} in each size range, and the total number of pores is of the order of 10^{17} per gram. Even if one were to object to the model of cylindrical pores, n_i could be considered as the number of pairs of menisci of mean curvature \bar{r}_i , and h as the distance between them, for any segment of the distribution curve.

Constants of Elasticity

The spreading pressure of the film along OA may be computed by means of the Gibbs adsorption equation. The calculations were made on the assumption of an ideal gaseous phase. Γ/P was plotted against P and a graphical integration performed. As emphasized by Hill (11), absolute values of ϕ are uncertain owing to error in the total surface area, and to the difficulty of obtaining the area under the curve Γ/P vs. P at the low pressure end.

In Fig. 6 the fractional expansion of the rod, $\Delta l/l$, is plotted against calculated

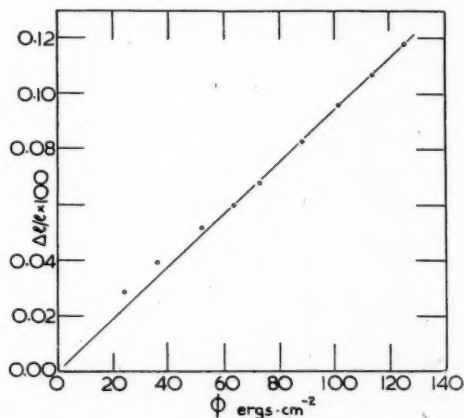


FIG. 6. Fractional expansion of rod as a function of calculated spreading force.

spreading force for the data at 11.79°C. Such data for all three temperatures are given in Table V. It is seen that $\Delta l/l$ vs. ϕ is a straight line, in agreement with the work of Bangham (1, 2) and Haines and McIntosh (10). The line should pass through the origin, and this was actually the case for all other runs. The discrepancy has been attributed to the difficulty in performing the integration, and a correction has been applied to these data, so that the elastic constant could be evaluated at the same temperature at which the other calculations

TABLE V
SPREADING PRESSURES AND CORRESPONDING
LENGTH CHANGES

Temp., °C.	$\Delta l/l \times 10^3$	ϕ , erg/cm. ²
25.80	0.359	26.1
	0.495	40.0
	0.641	59.9
	0.757	74.8
	0.864	87.0
	0.971	97.8
	1.087	107.9
	1.204	117.7
18.75	0.317	28.8*
	0.432	42.7
	0.517	52.8
	0.584	55.9
	0.694	68.8
	0.779	79.7
	0.854	89.0
	0.925	97.6
	0.996	105.3
	1.070	112.9
11.79	1.147	120.5
	1.183	124.3
	0.277	24.3
	0.391	36.2
	0.516	52.5
	0.600	64.0
	0.680	73.3
	0.826	88.6
	0.959	101.8
	1.071	114.0
	1.176	125.8

*0.7 has been added to all the values of ϕ at this temperature. See text.

have been made. The value of the surface area used is 129 m.² per gm. Writing the Bangham relation $\Delta l/l = k_1 \phi$, k_1 has the value 9.1×10^{-6} cm. per dyne. Bangham (1, 2) has used such data to obtain E , the Young's modulus, on the basis of equivalent structures, for example, a thread of dimensions to account for the measured surface area and the volume of the adsorbent structure. In the case of the porous glass, taking a density of 2.7 gm. per cm.³, E has the value 3.8×10^{11} dynes per cm.² This is in good agreement with the range of values for E given in International Critical Tables (12) for various types of glasses, namely 5.9 to 7.8×10^{11} dynes per cm.² Nothing is known about the exact manner in which the expansion of the pore walls is transmitted through the rod and any change in thickness of the pore wall is neglected here. Since the pores are presumably randomly orientated, only one-third of their expansion along the pore axis will register as linear expansion of the rod. Hence the E computed from the measured $\Delta l/l$ is too great by a factor of 3, but order of magnitude agreement is still obtained with the values of moduli quoted above. To recapitulate, a value of E of 3.8×10^{11} dynes per cm.² is deduced from the

adsorption data along *OA*. We next examine the section *DB*, where a different mechanism of adsorption has been postulated.

Along *DB* it is assumed that the movement of the rod arises from the change of negative pressure under the menisci and from the increased spreading force of the reversibly adsorbed annular film, the quantity of which is presumed to remain constant. Although these two effects are treated separately, it is not implied that any clear demarcation between annular film and capillary liquid exists. The annular film must always have the same chemical potential as the capillary liquid and as vapor in equilibrium with adsorbed matter. If the effects are assumed to be additive, there results

$$\left. \frac{\Delta l}{l} \right|_D^B = k_1 \Delta \phi + k_2 \Delta(-P) \frac{r_m}{2}$$

when an equivalent cylinder is considered, the radius of which is the mean radius of the system of capillaries. To relate a negative pressure with a tension acting along the walls, one requires a factor arising from the relation $T = Pr_m/2$, which has been employed in the equation above. A value of 28.3×10^{-8} cm. was taken for r_m . Since both $-P$ and ϕ may be related to the equilibrium pressure over the adsorbent, one obtains

$$\left. \frac{\Delta l}{l} \right|_D^B = k_1 RT \Gamma \ln P/P_0 \Big|_D^B + k_2 \frac{r_m}{2} \frac{RT}{V} \ln P/P_0 \Big|_D^B.$$

Dropping limits this becomes

$$\frac{\Delta l}{l} = 2.30 RT \left[k_1 \Gamma + \frac{k_2 r_m}{2V} \right] \log P/P_0$$

which, since Γ is constant over the range of P/P_0 where the equation is valid, is of the form, $\Delta l/l = K \log P/P_0$. To test this equation, $\Delta l/l$ was plotted against $\log P/P_0$, and as seen in Fig. 7 an excellent line is obtained. From the slope of

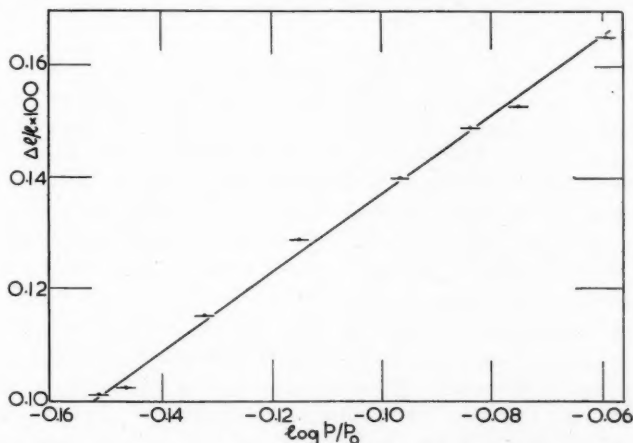


FIG. 7. Fractional expansion of rod as a function of $\log P/P_0$ for adsorption along *DB*.

this line, the value of k_1 obtained along OA , and the value of Γ at A , k_2 may be evaluated. Alternatively, one could subtract from $\Delta l/l$, between D and B , the fractional expansion to be expected due to $\Delta\phi$, and plot the residual $\Delta l/l$ vs. $\log P/P_0$. The value of k_2 was found to be 12.7×10^{-6} cm. per dyne, whereas k_1 was found to be 9.1×10^{-6} cm. per dyne along OA . These two values are not strictly comparable, however, since k_1 arises from a spreading force along the pore walls, whereas k_2 arises from a hydrostatic pressure which must have an effect on the radius as well as the length of a pore. To make the comparison a value of Young's modulus may be deduced from the length change occasioned by a hydrostatic pressure within a cylinder. Southwell (19) treats the elastic behavior of a hollow cylinder of which the radius is very much greater than the wall thickness, and which is long enough for end effects to be neglected. To apply this treatment to a pore of radius r_m , for which it can be readily shown that the wall thickness is about 85% of r_m , is admittedly a gross oversimplification. However, in view of the lack of knowledge regarding the transmission of dimensional changes throughout the rod, the use of more refined theories for thick-walled cylinders does not appear warranted.

If Poisson's ratio for glass is taken to be 0.25, Southwell gives for the fractional expansions of the cylinder

$$\epsilon_1 = 0.25 P/E$$

$$\epsilon_2 = 0.88 P/E$$

$$\epsilon_3 = -0.38 P/E$$

where ϵ_1 , ϵ_2 , ϵ_3 are the fractional expansions along the axis, the radius, and across the wall of the cylinder, respectively. P is the hydrostatic pressure acting on an imaginary "cap" of area πr_m^2 , in the case of a pore of radius r_m , and E is Young's modulus. Southwell's expressions are given here in simplified form, assuming that the wall thickness and pore radius are approximately equal. Again, the factor of $1/3$ which arises from random orientation of pores is neglected. Treating the dimensional change observed as being an additive effect,

$$\Delta l/l = \epsilon_1 + \epsilon_2 + \epsilon_3 \quad \text{or} \quad \Delta l/l = 0.75 P/E.$$

Further, the ratio $\Delta l/lP = k_2$, when k_2 has been converted to appropriate units by multiplication by $r_m/2$. It then has the value 1.80×10^{-12} cm.² per dyne. In this manner E is found to be 4.2×10^{11} dyne per cm.², a value in excellent agreement with that of 3.8×10^{11} dyne per cm.² found by Bangham's method and adsorption data along OA . Again, the assumptions of two distinct mechanisms of adsorption along the two sections OA and DB result in essentially the same value of the quantity it was desired to determine.

Differential Heat of Adsorption Along DB

A third possibility of checking the validity of the mechanism of adsorption along DB arises from a knowledge of the heat of adsorption. Heats of adsorption may be determined along DB by utilizing the experimental values of the equilibrium pressure at the three temperatures. The heats of adsorption thus found may be compared with those which should obtain for condensation into a meniscus of the same dimensions, formed by a liquid which thus differs from

bulk liquid in that it is under a negative pressure. In making the comparison two considerations must be recognized. First, the experimental values of the equilibrium pressure are known, at the various temperatures, for constant amounts adsorbed. It may be assumed that for any given quantity adsorbed, the area of the interface involved in the condensation remains the same at different temperatures. It is clear, however, that P , the hydrostatic pressure, is not identical at different temperatures. Second, in using the model of a liquid meniscus, the differential heat of adsorption must be computed for conditions which are consistent with the heats obtained from the experimental data. Thus if the experimental data are readily put into the form $(\partial \ln p / \partial T)_{P, A_s, n_s}$, it follows that the differential heat of adsorption to be computed for the liquid meniscus will be for T , P , and A_s constant.

On the assumption that the area of the interface has a single value at each of the three temperatures, the equilibrium pressures yield $(\partial \ln p / \partial T)_{A_s, n_s}$. It may be shown that

$$\left(\frac{\partial \ln p}{\partial T} \right)_{A_s, n_s} = \frac{q_{\text{isosteric}}}{RT^2} - \frac{2\bar{V}_s}{rRT} \left(\frac{\partial \sigma}{\partial T} \right)_{A_s, n_s}$$

Thus $q_{\text{isosteric}}$ may be evaluated since \bar{V}_s is taken to be the molar volume of the liquid, σ as the surface tension of liquid at the same temperature, and r the radius of curvature of the meniscus. For the system consisting of a liquid meniscus of the same radius of curvature, the latent heat of condensation is

$$\lambda_{\text{meniscus}} = \lambda_{\text{bulk}} + \int_0^P \left(\frac{\partial \lambda}{\partial P} \right)_{T, A_s} dP,$$

where λ_{bulk} is the latent heat of condensation into a bulk liquid phase at the required temperature. On substituting the requisite relations into this equation and assuming that \bar{V}_s has the value appropriate to bulk liquid and is not a function of pressure, one obtains

$$\lambda_{\text{meniscus}} = \lambda_{\text{bulk}} - \bar{V}_s P$$

where P is the hydrostatic pressure obtained by use of the Kelvin equation. A comparison of $\lambda_{\text{meniscus}}$ and $q_{\text{isosteric}}$ is made in Table VI.

It may be seen that the experimental values of $q_{\text{isosteric}}$ decrease with increasing quantity of adsorbed matter, and that the value of $\lambda_{\text{meniscus}}$ also decreases, but to a smaller extent. The experimental error in $q_{\text{isosteric}}$ is believed to be about 5%, and the discrepancy cannot definitely be said to be significant. It seems sufficient, therefore, to point out that, in principle, a test of the theory can be made by such a comparison but that our results are not sufficiently accurate to permit a decision.

Equilibrium Heat of Adsorption and Entropy of Adsorption

Hill (11) and Everett (8) have shown that the equilibrium heat of adsorption $H_a - H_s$ may be evaluated from equilibrium pressure measurements at various temperatures, provided that the values of equilibrium pressure are selected at constant values of area, hydrostatic pressure, and spreading force of the film. The utility of this particular heat of adsorption is that the entropy of adsorption

TABLE VI
COMPARISON OF HEAT OF ADSORPTION INTO CONCAVE MENISCI
AND THE ISOSTERIC HEAT OF ADSORPTION

$\frac{w, \text{H}_2\text{O}}{\text{gm. glass}}$	$\log p$			$RT^2 \left(\frac{\partial \ln p}{\partial T} \right)_{A_s, n_s}$, kcal./mole	$r_{\text{Kelvin}} \times 10^7$, cm.
	11.79°C.	18.75°C.	25.80°C.		
0.2200	0.861	1.060	1.275	10.9	3.11
0.2250	0.889	1.086	1.295	10.8	3.76
0.2300	0.917	1.111	1.314	10.6	4.85
0.2340	0.937	1.130	1.326	10.5	5.92
0.2380	0.954	1.146	1.339	10.3	7.46

$\frac{w, \text{H}_2\text{O}}{\text{gm. glass}}$	$\frac{2\bar{V}_s T \left(\frac{\partial \sigma}{\partial T} \right)_{A_s, n_s}}{r}$, kcal./mole	$\frac{2\sigma \bar{V}_s}{r}$, kcal./mole	$\lambda_{\text{meniscus}}$, kcal./mole	$q_{\text{isosteric}}$, kcal./mole
0.2200	-0.12	0.20	10.70	10.8
0.2250	-0.10	0.16	10.66	10.7
0.2300	-0.08	0.13	10.63	10.5
0.2340	-0.06	0.10	10.60	10.4
0.2380	-0.05	0.08	10.58	10.2

A value of 10.50 kcal./mole was chosen for λ_{bulk} .

may be obtained from it through the relation $\bar{H}_g - \bar{\mathcal{H}}_g = T(\bar{S}_g - \bar{S}_s)$ defined by equation (44) of Hill.

Hill (11) has also clearly shown that for systems which exhibit the phenomenon of hysteresis, the equilibrium heat of adsorption can only be obtained for adsorption up to the inception of the hysteresis loop, even though reversible adsorption may be found for ranges of relative pressure above the loop, such as *BC* of Fig. 1. This is because values of ϕ , the spreading force of the film, are indeterminate above the beginning of the hysteresis loop. Values of the equilibrium heat of adsorption are given, therefore, for adsorption along *OA* only. Owing to errors inherent in determining ϕ by graphical integration of the Gibbs equation and in obtaining the values of $(\partial\phi/\partial T)_{A_s, n_s}$, the values recorded in Table VII are not considered to be accurate to better than 10%. The short

TABLE VII
EQUILIBRIUM HEATS AND ENTROPIES OF ADSORPTION AT 18.75°C.

$\frac{w, \text{H}_2\text{O}}{\text{gm. glass}}$	$\Gamma \times 10^{10}$, moles/cm. ²	$\log p$			$q_{\text{isost.}}$, kcal./mole	$\frac{T}{\Gamma} \frac{\partial \phi}{\partial T}$, kcal./mole	$\bar{H}_g - \bar{\mathcal{H}}_g$, kcal./mole	$\bar{S}_g - \bar{S}_s$, cal./mole. deg.
		11.79°	18.75°	25.80°				
0.0100	4.31	-0.886	-0.854	-0.553	10.0	-8.1	18.1	62
0.0200	8.62	-0.284	-0.131	-0.899	10.1	-5.6	15.7	54
0.0300	12.93	-0.190	-0.378	-0.567	10.0	-3.3	13.3	46
0.0400	17.24	-0.470	-0.648	-0.869	10.3	-2.0	12.3	42
0.0500	21.55	-0.629	-0.813	-1.019	10.1	-1.1	11.2	38
0.0600	25.86	-0.726	-0.924	-1.108	10.3	-1.1	11.4	39
0.0700	30.17	-0.785	-0.983	-1.161	10.1	-1.1	11.2	38

temperature range and the lack of precision also result in making computations of the variation of entropy of adsorption with temperature useless. The data are therefore given for the temperature 18.75°C. only. Within the stated margin of error, it is seen in Fig. 8 that the equilibrium heat of adsorption is approaching

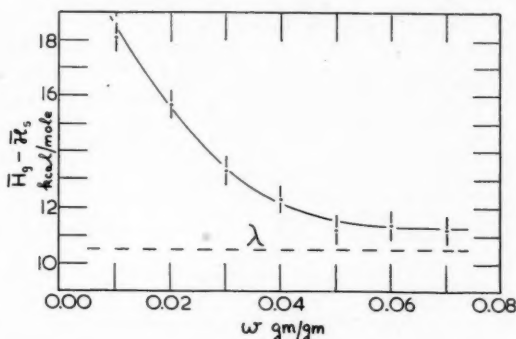


FIG. 8. Equilibrium heat of adsorption for region *OA* of isotherm at 18.75°C.

the latent heat of condensation of water vapor to liquid water. This finding suggests, therefore, that the postulates concerning the mechanisms of adsorption above *A* which have been put forward are not inconsistent with the thermodynamic data, that is, mechanisms based on the assumption of bulk liquid properties for the adsorbed phase appear warranted. This was the case, as already indicated, along *DB*, where the isosteric heat of adsorption may be calculated, although the equilibrium heat of adsorption may not.

That a changing value of the heat content per mole of the adsorbed phase is found may also be checked by the values of the spreading force. Bangham and more recently Everett (8) have shown that if ϕ may be expressed as

$$\phi = Tf\left(\frac{n_s}{A_s}\right)$$

where the function does not contain temperature implicitly, then the heat content per mole of the adsorbed phase is independent of the amount adsorbed. In the present case it has been shown that the function is not independent of temperature, and a variation of heat content per mole of the adsorbate is to be expected.

ACKNOWLEDGMENT

We should like to acknowledge the award of a Studentship to C. H. Amberg, and a grant in aid of this research, from the National Research Council. Financial support was also obtained from the Advisory Committee on Research, University of Toronto.

REFERENCES

1. BANGHAM, D. H. Proceedings of a conference on the ultrafine structure of coals and cokes. Brit. Coal Utilisation Research Assoc. 18, 1944.
2. BANGHAM, D. H. and MAGGS, F. A. Proceedings of a conference on the ultrafine structure of coals and cokes. Brit. Coal Utilisation Research Assoc. 118, 1944.
3. BRUNAUER, S., EMMETT, P. H., and TELLER, E. J. Am. Chem. Soc. 60: 309, 1938.
4. COELINGH, M. B. Kolloid-Z. 87: 251, 1939.
5. COHAN, L. H. J. Am. Chem. Soc. 60: 433, 1938.
6. EMMETT, P. H. Chem. Revs. 43: 69, 1948. (cf. Fig. 10.)
7. EMMETT, P. H. and CINES, M. J. Phys. & Colloid Chem. 51: 1248, 1947.
8. EVERETT, D. H. Trans. Faraday Soc. 46: 453, 942, 957, 1950.
9. FOSTER, A. G. Trans. Faraday Soc. 28: 645, 1932.
10. HAINES, R. S. and McINTOSH, R. J. Chem. Phys. 15: 28, 1947.
11. HILL, T. L. J. Chem. Phys. 17: 520, 1949.
12. International Critical Tables. Vol. 2. McGraw-Hill Book Company, Inc., New York and London, 1927, p. 93.
13. KISTLER, S. S., FISCHER, E. A., and FREEMAN, I. R. J. Am. Chem. Soc. 65: 1909, 1943.
14. KRAEMER, E. O. A treatise on physical chemistry, *edited by* H. S. TAYLOR. D. Van Nostrand Company, Inc., New York, 1931, p. 1661.
15. McINTOSH, R., RIDEAL, E. K., and SNELGROVE, J. A. Proc. Roy. Soc. (London), A, 208: 292, 1951.
16. NORDBERG, M. E. J. Am. Ceram. Soc. 27: 299, 1944.
17. RAO, K. S. J. Phys. Chem. 45: 506, 513, 1941.
18. SNELGROVE, J. A. and McINTOSH, R. Can. J. Chem. In press.
19. SOUTHWELL, R. V. Theory of elasticity. Oxford University Press, London, 1941, p. 146.
20. WHIG, E. O. and JUHOLA, A. J. J. Am. Chem. Soc. 71: 561, 2069, 1949.

THE VISCOMETRIC DETECTION OF BRANCHING IN POLYMERS

I. BRANCHING IN GR-S AS A FUNCTION OF CONVERSION¹

BY L. H. CRAGG AND A. T. BROWN²

ABSTRACT

Samples of GR-S—the familiar copolymer of butadiene and styrene—were taken from a continuous emulsion-polymerization system at conversions 32.0, 45.1, 61.2, and 73.4% respectively, and each, after careful drying, was carefully fractionated to give five or six "top" fractions. For each of these fractions values of intrinsic viscosity $[\eta]$ and of the viscosity slope "constants" β and k' were determined. As with normal and cross-linked polystyrene, β and k' appear to be constant for all linear species, but to have higher values for branched species, the increase being a measure of the extent or degree of branching. From the data obtained it is concluded that in GR-S there is little or no branching at low conversions, that the degree of branching increases markedly with increasing conversion, and that branching occurs to the greatest degree in the species of highest molecular weight.

There seemed to be, for this polymer at least, a molecular weight below which branching could not be detected, regardless of conversion, but above which branching increased with increasing molecular weight.

INTRODUCTION

It is common practice to classify fractions of diene polymers as "sol" or "gel", the sol fractions being those that will dissolve in a variety of suitable solvents and the gel fractions those that will not dissolve, but only swell to a greater or lesser degree, in these solvents. It is usually assumed that gel owes its insolubility to its three-dimensional netted structure and that, in contrast, the molecules in the sol fractions are linear. Indeed the term "linear polymers" as commonly used includes not only the unbranched-chain polymers but all polymers that are soluble in this sense (7, 11). It is now recognized, however, that the formation of branched molecules is possible in any addition polymerization. With simple vinyl monomers, like styrene, it can occur by chain transfer (a free-radical dehydrogenation of a growing or "dead" polymer molecule), and with dienes like butadiene it can occur both by this branching reaction and by the cross-linking reaction (a free-radical attack on a double bond either in the polymer chain or in a side vinyl group (6)). Although the branching reaction should yield soluble species (even when the molecular weight and extent of branching are high) the cross-linking reaction must lead eventually to an "infinite", and therefore insoluble, polymer network—the "gel" fraction. The formation of insoluble gel at high conversions is of course all too familiar in diene polymerizations. Often, for example in the preparation of synthetic rubber, it is considered desirable to stop such a reaction before the gel point is reached. The polymer so formed will be soluble but its molecules will not necessarily all be linear. Indeed, it is to be expected from theory (6) that branched species will be formed at all stages of the reaction and

¹ Manuscript received August 1, 1952.

Contribution from the Department of Chemistry, Hamilton College, McMaster University, Hamilton, Ontario, with financial assistance from the National Research Council of Canada through its Associate Committee on Synthetic Rubber Research.

This work was presented at the Canadian High Polymer Forum in Ottawa, June 1950.

² Present address: Irvington Varnish and Insulation Co. of Canada, Ltd., Hamilton, Ontario.

that the extent of branching will increase with increasing conversion.* It is to be expected also that the presence of branched species would affect the physical properties of the polymer. Unfortunately, for lack of a suitable method of detecting branching and estimating its extent, it has not been possible to test these predictions directly or to determine to what extent an improvement in the physical properties of a polymer was due to increased branching and to what extent to other factors (9).

The Huggins constant k' (10) has recently been shown to be a fairly sensitive indicator of branching in chain polymers (17, 13, 2). It seemed logical, therefore, to use it to study the factors that affect branching in a polymer. In the work reported in this paper branching was studied as a function of conversion. A second paper (1) will be concerned with the effect of the temperature of polymerization.

In these experiments samples of GR-S, prepared to four different conversions below the gel point, were carefully fractionated and the value of k' for each fraction determined by suitable viscosity measurements. Details of the experiments, and the conclusions drawn from them, follow.

EXPERIMENTAL

Materials

Polymer

The polymer was prepared by emulsion polymerization at 119°F., using the mutual recipe, in the continuous reactor system at the plant of Polymer Corporation Ltd., Sarnia, Ont. Four samples were removed at different points, the conversions being 32.0%, 45.1%, 61.2%, and 73.4%, respectively. Each sample was stabilized with 1.25 parts of antioxidant, "B.L.E."; then the unreacted monomers were removed by passing low pressure steam through the latex for about 30 min., and the rubber was coagulated by the addition of sodium chloride solution and sulphuric acid. The rubber was dried under vacuum at room temperature, these very gentle conditions being found necessary to avoid changes in the polymer samples during drying, especially in those prepared to the two lowest conversions.

Solvents

Benzene.—Steel Company of Canada, ASTM industrial grade. Redistilled and dried and stored over sodium. $n_D^{25} = 1.4971$.

Methanol.—Carbide and Carbon Chemical Company, dried over calcium oxide. (Redistillation effected no change in refractive index.) $n_D^{25} = 1.3269$.

Phenyl beta naphthylamine (PBNA), obtained from Polymer Corporation, was added to fractions as a solution in benzene (10 gm. per 100 ml. solution).

Precipitant.—A solution of equal volumes of the benzene and methanol

*The branching reaction and the cross-linking reaction both yield branched molecules. When polymerization proceeds beyond the gel point one gives a product easily distinguishable from the other. At lower conversions, however, the branched species formed by the two different mechanisms will be indistinguishable in their viscosity behavior (17). In this paper, therefore, such terms as "branched species" and "degree of branching" are used in their wider sense.

described above. One large batch was prepared and used for all fractionations.
 $n_D^{25} = 1.4102$.

Procedures

Fractionation

Each of the polymer samples was fractionated by successive precipitation from solution in benzene (1% by weight) using a 1:1 (by volume) solution of methanol and benzene as precipitant. The details of apparatus and technique are described elsewhere (4). The only variations were that the original volume was 500 ml., the precipitation mixture was always allowed to stand 48 hr. after cooling to 25.0°C., and the volume of PBNA solution added to the coacervate was 0.2 ml. Care was taken to keep the fractions small and fairly uniform in weight (most of them about 5–9% of the whole). They were obtained as liquid coacervates and were used without drying for the viscosity determinations. (Earlier experience had shown that with GR-S a careful primary fractionation such as this gave better results than could be obtained by refractionation of the primary fractions; with prolonged treatment changes in the fractions—particularly in those of highest molecular weight—were almost inevitable (4).)

Viscometry

The viscometer was of the Ubbelohde type, modified to permit dilution in the bulb. It had been calibrated, and the very small kinetic-energy corrections were applied to all the data. Measurements were made at $25.0 \pm 0.02^\circ\text{C}$., with the usual precautions (3), using four or five solutions of concentrations in the range 0.05 to 0.4% (see Fig. 1). Values of inherent viscosity $(\ln \eta_r)/c$ were computed and plotted against c , the concentration. The intrinsic viscosity $[\eta]$ was obtained by linear extrapolation to $c = 0$. (Since concentrations were calculated in the units gm. solute per 100 ml. solution, the units of intrinsic viscosity are dl. per gm.) Because good straight lines were obtained, the equation of Mead and Fuoss (14)

$$(\ln \eta_r)/c = [\eta] - \beta [\eta]^2 c$$

could be applied and the slope constant, β , calculated as $-\text{slope}/[\eta]^2$. From this constant β , the Huggins constant k' was calculated from the equation $k' = 0.50 - \beta$ (5).*

The concentration of the solution obtained by diluting the coacervate to 100 ml. was determined, in the manner described elsewhere (4), by careful evaporation of aliquot samples. The concentrations of the solutions used for viscometry measurements were calculated from the volume of this solution and of solvent used in preparing them, assuming no volume shrinkage on dilution.

RESULTS

In Tables I, II, III, and IV are recorded the experimental data:—for each fractionation: W , the weight of whole polymer fractionated, W' , the weight

*The constant β was determined instead of k' for reasons already cited (13). Nevertheless, k' is calculated and used in the discussions because it is the more familiar constant. It should be clearly understood, however, that the values of k' are calculated, not measured; the true value of k' will not be precisely the same as our calculated value because the equation used is probably not strictly valid at finite concentrations. The error will, however, be small and constant, and, particularly since we are interested in differences in k' , will not affect the conclusions.

TABLE I

DATA FOR THE FRACTIONS OBTAINED FROM GR-S
POLYMERIZED TO 32.0% CONVERSION
($W = 5.32$ gm., $W' = 4.47$ gm., $C = 1.07$ gm. per 100 ml.)

Fraction	w (gm.)	$w_x \times 10^2$	$[\eta]$	β	k'
1	0.128	2.8 ₆	2.00	0.15 ₈	0.34 ₂
2	0.431	9.6 ₄	1.70	0.16 ₃	0.33 ₇
3	0.603	13.4 ₅	1.30	0.16 ₆	0.33 ₄
4	0.521	11.6 ₆	0.99	0.15 ₉	0.34 ₁
5	0.449	10.0 ₄	0.85	0.17 ₃	0.32 ₇

TABLE II

DATA FOR THE FRACTIONS OBTAINED FROM GR-S
POLYMERIZED TO 45.1% CONVERSION
($W = 5.30$ gm., $W' = 4.74$ gm., $C = 1.06$ gm. per 100 ml.)

Fraction	w (gm.)	$w_x \times 10^2$	$[\eta]$	β	k'
1	0.159	3.3 ₅	3.30	0.09 ₈	0.40 ₂
2	0.278	5.8 ₆	2.70	0.14 ₁	0.35 ₉
3	0.442	9.3 ₂	2.17	0.16 ₉	0.33 ₁
4	0.449	9.4 ₇	1.74	0.16 ₆	0.33 ₄
5	0.394	8.3 ₁	1.43	0.16 ₆	0.33 ₄

TABLE III

DATA FOR THE FRACTIONS OBTAINED FROM GR-S
POLYMERIZED TO 61.2% CONVERSION
($W = 5.15$ gm., $W' = 4.71$ gm., $C = 1.04$ gm. per 100 ml.)

Fraction	w (gm.)	$w_x \times 10^2$	$[\eta]$	β	k'
1	0.168	3.5 ₇	4.69	- 0.00 ₅	0.50 ₅
2	0.233	4.9 ₅	4.12	+ 0.04 ₃	0.45 ₇
3	0.218	4.6 ₃	3.78	0.10 ₉	0.39 ₁
4	0.259	5.5 ₀	3.27	0.15 ₉	0.34 ₁
5	0.262	5.5 ₆	2.82	0.16 ₃	0.33 ₇

TABLE IV

DATA FOR THE FRACTIONS OBTAINED FROM GR-S
POLYMERIZED TO 73.4% CONVERSION
($W = 5.08$ gm., $W' = 4.71$ gm., $C = 1.01$ gm. per 100 ml.)

Fraction	w (gm.)	$w_x \times 10^2$	$[\eta]$	β	k'
1	0.188	3.9 ₉	5.09	- 0.04 ₃	0.54 ₃
2	0.321	6.8 ₂	5.09	- 0.04 ₃	0.54 ₃
3	0.200	4.2 ₅	4.75	- 0.01 ₃	0.51 ₃
4	0.203	4.3 ₁	4.08	+ 0.01 ₈	0.48 ₂
5	0.207	4.3 ₉	4.01	0.04 ₇	0.45 ₃
6	0.181	3.8 ₄	3.68	0.09 ₉	0.40 ₁

of rubber in W (i.e., the weight of material not extractable by the ethanol-toluene azeotrope (8)), and C the concentration, in gm. per 100 ml. of solution, of the solution before addition of precipitant; and for each fraction: w , the calculated weight of the dry fraction (this includes a negligible weight of antioxidant), w_z , the weight fraction ($= w/W'$), and the viscosity functions $[\eta]$, β , and k' . In Table V are the values of $[\eta]$, β , and k' for the whole samples.

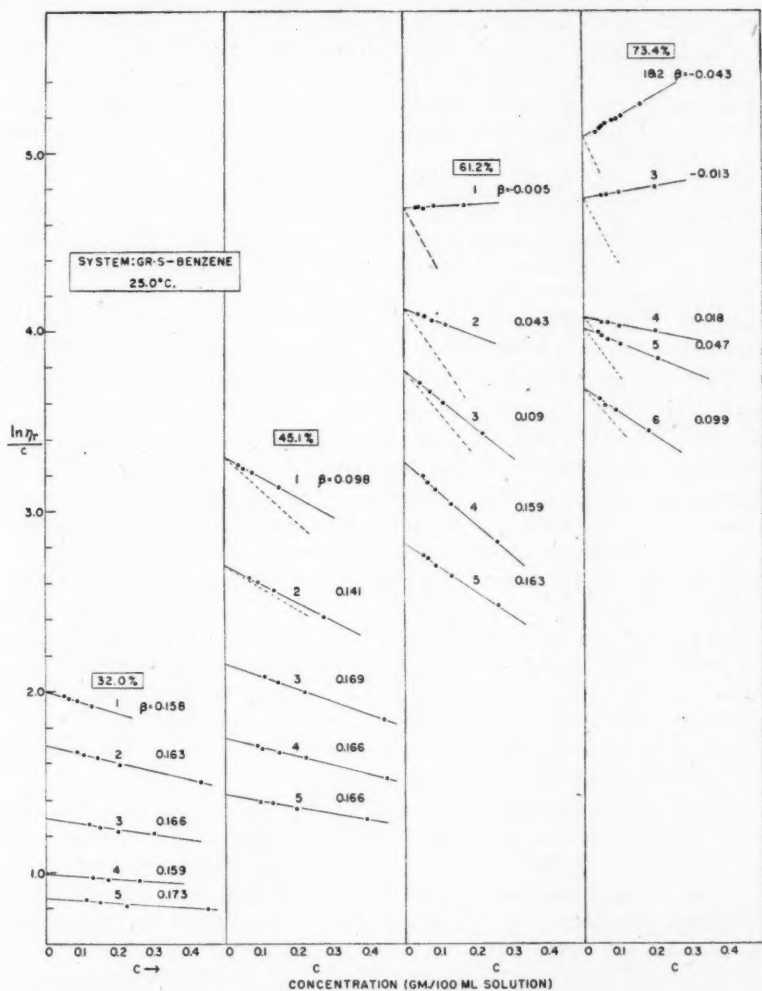


FIG. 1. Inherent viscosity vs. concentration curves for the top fractions at four conversions.

In Fig. 1 are drawn, for purposes of comparison, the $(\ln \eta_r)/c$ vs. c curves for all the fractions obtained. (Only the first five or six fractions were separated from

TABLE V
INTRINSIC VISCOSITIES AND SLOPE CONSTANTS
OF UNFRACTIONATED SAMPLES

Conversion	$[\eta]$	$[\eta]_{\text{corr.}}$	β	k'
32.0	0.75	0.89	0.16	0.34
45.1	1.13	1.26	0.16	0.34
61.2	1.68	1.84	0.14	0.36
73.4	2.17	2.34	0.08	0.42

each sample, as experience (4) had shown that branching, as indicated by high values of k' , occurred principally in these fractions.)

DISCUSSION

Two effects of increasing conversion are clearly indicated by these results: as conversion is increased, both the molecular weight and the extent of branching are increased. As would be expected, these effects can be discerned most readily from the properties of the top fractions. Comparisons involving corresponding fractions of the four different samples should be meaningful because the fractionations were done in the same manner from solutions of the same initial concentration and the fractions were small (most of them 4–9% of the whole sample).

Branching

In earlier papers (13, 2) it was shown that for all of the fractions obtained from polystyrene (formed by emulsion polymerization at 55°C.) the value of k' was the same, namely 0.38 ± 0.02 . When, however, a small proportion of divinylbenzene was copolymerized with the styrene the fractions were not all alike in this respect; for the lower molecular weight ones the value of k' was the same as for the normal polystyrene but for the higher ones the value of k' increased with increasing molecular weight. This increase in k' was attributed to branching, and it was concluded that when the degree of branching in a polymer was insufficient to cause gel the branching occurred chiefly in the higher fractions. Indeed, if the increase in k' above the base value (the normal value for linear polymer) was used as a measure, the degree of branching was too low to be detected in the lower fractions, but increased approximately linearly with molecular weight (intrinsic viscosity) in the higher fractions.

From the data of Tables I, II, III, and IV and Fig. 1, it is clear that GR-S behaves in these respects much like lightly cross-linked polystyrene. From this and other evidence (1) the "base value" of k' —for which we shall use the symbol k'_0 —for poly(butadiene-co-styrene) of this composition is 0.33 ± 0.01 , corresponding to a value of β of 0.17 ± 0.01 . At 32.0% conversion the first five fractions all have this value of β (and k'_0) and hence are presumably branched very little or not at all. At 74.3% conversion, on the other hand, none of the fractions has this value, and the discrepancy becomes more marked the higher the intrinsic viscosity. In Fig. 1 this discrepancy is emphasized, when it occurs, by drawing a dotted line to indicate what the slope of the line would have been if the fraction had had the normal value of β (i.e. — 0.17).

We conclude, therefore, that with GR-S (a) the degree of branching increases markedly with conversion, (b) there is little or no branching in the polymer formed at low conversion (30%), and (c) when branching does occur the species most affected are those of highest molecular weight.

This connection between molecular weight and branching deserves a little more attention. From our data it follows that polymer species formed in a polymerization of this type will not exhibit branching—at least not to a degree detectable by this method—unless the molecular weight exceeds a certain value. This is made clearer in Fig. 2(a) in which k' for each fraction is plotted against intrinsic

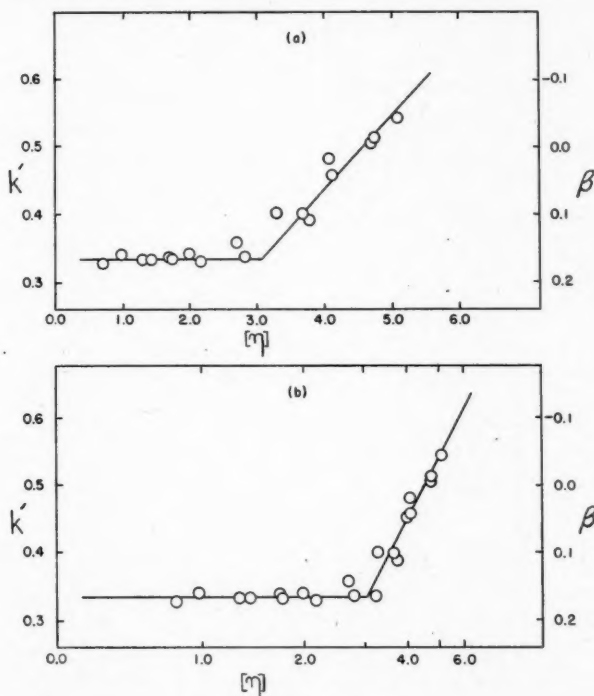


FIG. 2. Relation between slope constants and intrinsic viscosity for all fractions studied (a) k' (and β) vs. $[\eta]$, (b) k' (and β) vs. $\log [\eta]$.

viscosity. Below $[\eta] \approx 3$ the values of k' are normal; above $[\eta] \approx 3$, k' starts to increase. (In Fig. 2(b) k' is plotted against $\log [\eta]$ to emphasize the abruptness with which k' begins to increase.) One would expect on theoretical grounds that branching would take place all through the polymerization and that short molecules as well as long ones would be affected, though not as many of them nor to as high a degree. However, during the early stages of the reaction, when the mercaptan concentration is high, neither the polymer molecules nor any branches formed on them can grow long. The relatively few branched molecules would

have only one or two short branches and hence would differ little in their viscosity behavior from unbranched molecules. Later in the polymerization, when the mercaptan concentration is lower, a branch started on one of these shorter molecules can grow longer, but then the resulting molecule will now be a longer molecule more prone to further branching. (It must be remembered that the intrinsic viscosity of a fraction is an indication of the effective length of the finished molecules, not of the length of the molecules *before* any branching occurs.) The molecules that would differ appreciably in viscosity behavior (especially in respect to polymer-polymer and polymer-solvent interaction, which is what affects β and k') would be the "bushier" ones and these would be the ones of greater effective length. An increase in k' would not, therefore, be apparent at low molecular weights. If, for example, the degree of branching* were to increase with intrinsic viscosity as indicated by the curved line *OBD* in Fig. 3, and if the

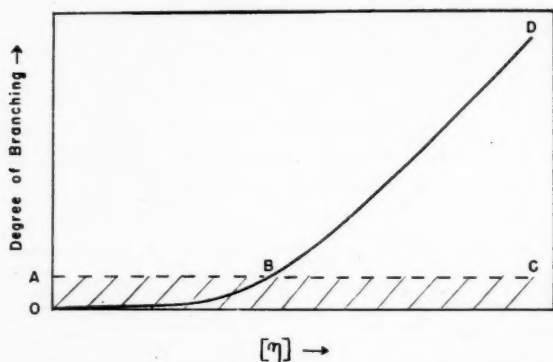


FIG. 3. Hypothetical variation of "degree of branching" with intrinsic viscosity.

degree of branching had to be greater than *OA* to be detectable as an increase in k' (greater than the experimental error), then, assuming that thereafter the increase in k' was roughly proportional to the degree of branching, k' would be constant up to an intrinsic viscosity corresponding to *B* and then increase rapidly (cf. Fig. 2). This would explain, too, why the points for the fraction from all four conversions fall approximately on the same curve. (The polymer molecules formed at all stages of the reaction up to 74% conversion have approximately the same butadiene content (10) and therefore the same number of potential sites for attack per unit length. By contrast, increasing the content of divinylbenzene in poly(styrene-co-divinylbenzene) should increase the likelihood of

*It is, and probably will continue to be, impossible to define "degree of branching" precisely in terms of structure, for branched molecules can differ in the length of the primary chain and in the length, complexity, and density (number per unit length of primary chain) of branches. Very short branches on a long primary chain will have little effect on viscosity behavior, but considerable effect on crystallizability. Hence "degree of branching" has quantitative meaning only in respect to a measurable effect on some specified physical property. As we use the term, the degree of branching increases when the changes in branching are such as to cause an increase in the effect on viscosity behavior (specifically, an increase in $k' - k''$).

attack on a given length of molecule, and hence cause detectable branching at lower molecular weights. This is indeed what is indicated by the data obtained with cross-linked polystyrene (2). And if, as seems likely (15), branching in butadiene-styrene copolymers is due mainly to the cross-linking reaction, one would expect that, other things being equal, the degree of branching in such copolymers would decrease with increasing proportion of combined styrene.)

Branching and Molecular Weight

The familiar increase in average molecular weight as emulsion polymerization proceeds is evidenced both by the increase in intrinsic viscosity of the whole rubber (Table V) and by the similar increase for the corresponding fractions. There are two principal reasons for this effect. Firstly, as the reaction proceeds the concentration of mercaptan decreases and hence a polymer molecule formed later has a better chance of growing large before its growth is terminated by an encounter with a mercaptan molecule; and secondly, the longer the period of reaction the greater is the chance that a given molecule will be attacked by a radical and start growing a branch and the greater is the chance, therefore, that it will become larger. The effects of these two factors on the molecular-weight distribution would not be the same. The first should affect all molecular species in the same proportion; the second should affect most those that already have the highest molecular weight. In other words, one might expect the increase in molecular weight to be relatively the same for the comparable low fractions but relatively higher for the top fraction or fractions in which branching is detectable.

Unfortunately a direct test of this prediction is not possible with these measurements because the corresponding fractions at different conversions are not strictly equal in weight. There is, however, sufficient similarity between the fractionations of the two low-conversion samples (32.0% and 45.1%) to make possible an indirect test. In Fig. 4(a) are plotted the integral molecular-weight distribution curves (as much of them as the data permit) for these two samples, s is a function (closely related to the cumulative weight fraction, q) whose value for the n^{th} fraction is obtained by adding one-half the weight fraction of the n^{th} fraction to the cumulative weight fraction for the $(n-1)^{\text{th}}$ fraction. From such a curve one can obtain the intrinsic viscosity for the molecular species precipitating at any given cumulative weight fraction, q .*

The ratio $[\eta]_{45}/[\eta]_{32}$ (where $[\eta]_{45}$ refers to species from the 45.1% conversion sample and $[\eta]_{32}$ to species taken, at the same cumulative weight fraction, from the 32.0% conversion sample) is thus a measure of the *relative* molecular weights of the species. Assuming the relation $[\eta] = K M^{2/3}$, which is sufficiently accurate for present purposes,

$$(1) \quad \begin{aligned} [\eta]_{45}/[\eta]_{32} &= (M_{45}/M_{32})^{2/3} \\ \text{or } M_{45}/M_{32} &= ([\eta]_{45}/[\eta]_{32})^{3/2}. \end{aligned}$$

In Fig. 4(b), values of $[\eta]_{45}/[\eta]_{32}$ are plotted against the values of s at which the

* For infinitesimal fractions the cumulative weight fraction $q (= \sum_{i=1}^n (w_x)_i)$ has for all practical purposes the same value as $s (= \sum_{i=1}^{n-1} (w_x)_i + \frac{1}{2}(w_x)_n)$.

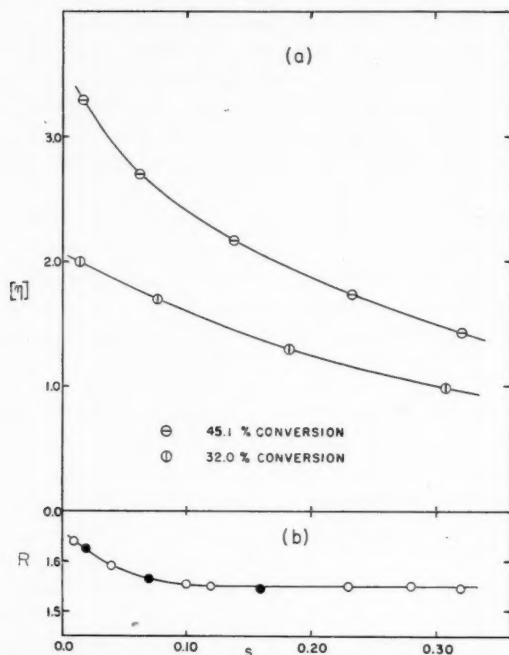


FIG. 4 (a) Distribution curves for the two low-conversion samples: intrinsic viscosity vs. (corrected) cumulative weight fraction, s .

(b) Intrinsic viscosity ratio, $R (= [\eta]_{45}/[\eta]_{32})$, vs. cumulative weight fraction, s .

intrinsic viscosities $[\eta]_{45}$ and $[\eta]_{32}$ are read from Fig. 4(a). This ratio apparently has a constant value, 1.50, except in the region of highest molecular weight (below $s = 0.10$) where it increases with increasing molecular weight. Since detectable branching appears only in this region, and only in the 45%-conversion fractions, this evidence is consistent with the suggestion that increase in molecular weight due to branching should be most apparent in the high molecular weight species, whereas the increase due to decrease in mercaptan concentration should be relatively the same for all species. (It might be objected that because the intrinsic viscosity - molecular weight relationship for branched species is different from that for linear species (12, 16), a change in the ratio $[\eta]_{45}/[\eta]_{32}$ does not necessarily mean a corresponding change in the ratio M_{45}/M_{32} . Since, however, the branching leads to a *lower* intrinsic viscosity for a given molecular weight, an unusually high value of the ratio $[\eta]_{45}/[\eta]_{32}$ is indicative of an even higher molecular-weight ratio than would be predicted from equation (1). The argument, then, is strengthened rather than weakened.)

The curves of Fig. 4(a) can also be used to estimate what would be the intrinsic viscosity of successive fractions of any specified size. Thus values at $s = 0.020$, 0.070, and 0.150 would be those of successive fractions of weight fractions 0.040, 0.060, and 0.120 respectively. (These points are chosen so that the hypothetical fractions at the two conversions will correspond as closely as possible to the

actual fractions obtained from the two samples.) Thus, if the fractionations had been done in such a way that the two first fractions had been exactly the same proportion of the whole (both 0.040), $[\eta]_{45}/[\eta]_{32}$ would have had the value 1.6₅. (The value for the two first fractions actually obtained—the only ones that were very close to being the same size proportionately—is in fact 1.6₅.) Similarly, for the second fractions—both 0.060—this ratio would have been 1.5₃, and for the third fractions 1.4₉. These three values are plotted, as filled circles, in Fig. 4(b). (The open circles represent values of $[\eta]_{45}/[\eta]_{32}$ calculated in a similar way for other values of s .) Assuming that a value of $[\eta]_{45}/[\eta]_{32}$ greater than 1.5₀ is due to branching, and that branching is negligible in all fractions at 32% conversion (see above), this means that at 45% conversion there is appreciable branching in the first fraction, a slight suggestion of it in the second, and none (detectable) in the third and subsequent fractions. It is significant, or else a remarkable coincidence, that these are precisely the conclusions reached from the slope-constant measurements.

Too much should not be made of this evidence, of course, but it is at least promising enough to suggest that further evidence of a similar nature might be worth seeking. And it certainly is consistent with the conclusion, based on the sounder evidence from slope constants, that the effects of branching are noticeable only in the high molecular weight species.

Recently, after this work was completed and the paper presented, Johnson and Wolfangel (12) reported that the exponent a in the relationship $[\eta] = K M^a$ decreased as the conversion of emulsion polybutadiene increased from 20.5 to 81%, and presented evidence to prove that this drop in the exponent was predominantly due to increasing degree of cross-linking (branching). Since polybutadiene and the copolymer of butadiene and styrene that we studied should behave similarly with respect to branching and cross-linking, their conclusions and ours are mutually supporting.

ACKNOWLEDGMENTS

We are grateful to Polymer Corporation, Ltd., and to Drs. H. L. Williams, J. S. Tapp, and N. R. Legge for assistance of various kinds, and to the National Research Council of Canada for financial aid.

REFERENCES

1. Cragg, L. H. and Fern, G. R. H. *J. Polymer Sci.* In press.
2. Cragg, L. H. and Manson, J. A. *J. Polymer Sci.* 9: 265. 1952.
3. Cragg, L. H., Rogers, T. M., and Henderson, D. A. *Can. J. Research, B*, 25: 333. 1947.
4. Cragg, L. H. and Switzer, D. F. Paper presented at Canadian High Polymer Forum, Hamilton, Ont. June, 1949.
5. Ewart, R. H. *In Advances in colloid science. Vol. 2 edited by H. Mark and G. S. Whitby.* Interscience Publishers, Inc., New York. 1946.
6. Flory, P. J. *J. Am. Chem. Soc.* 69: 2893. 1947.
7. Frith, E. M. and Tuckett, R. F. *Linear polymers.* Longmans, Green and Co., London. 1951.
8. Fuller, C. S. *Bell System Tech. J.* 25: 351. 1946.
9. Gehman, S. D. *Ind. Eng. Chem.* 44: 730. 1952.
10. Huggins, M. L. *J. Am. Chem. Soc.* 64: 2716. 1942.
11. Huggins, M. L. *et al.* *J. Polymer Sci.* 8: 257. 1952.
12. Johnson, B. L. and Wolfangel, R. D. *Ind. Eng. Chem.* 44: 752. 1952.
13. Manson, J. A. and Cragg, L. H. *Can. J. Chem.* 30: 482. 1952.
14. Mead, D. and Fuoss, R. M. *J. Am. Chem. Soc.* 64: 277. 1942.
15. Sivertz, C. S. Unpublished results, University of Western Ontario, London, Ont. 1951.
16. Thurmond, C. D. and Zimm, B. H. *J. Polymer Sci.* 8: 477. 1952.
17. Walker, O. J. Jr. and Winkler, C. A. *Can. J. Research, B*, 28: 298. 1950.

THE MOBILITY OF OIL DROPLETS, INTERFACIAL TENSION MEASUREMENTS, AND GEGEN ION ADSORPTION IN SOAP SOLUTIONS¹

BY B. D. POWELL² AND A. E. ALEXANDER

ABSTRACT

The electrophoretic mobility of oil droplets, in oil in water emulsions stabilized with paraffin chain salts, have been determined, together with interfacial tension measurements on the same systems, and the observations are explained. Electrokinetic theory is discussed and an estimate made of the fraction of the gegen ions which are bound to the droplet; the value of this fraction is similar to that found by others for the spherical soap micelle.

In this paper measurements which have been made of the electrophoretic mobility of Nujol droplets in water and the interfacial tension of water against Nujol, in the presence of a series of detergents, the anion-active sodium salts of sulphosuccinic esters, are described. Such studies are fundamental to the understanding of the mode of action of detergents, still not clear, though it is certain that both zeta potential and interfacial tension are of prime importance.

The charge density (E , electronic charges per cm^2) at an interface may be calculated from the zeta potential, obtained from electrophoretic mobility experiments. If the system in question is a soap adsorbed at the Nujol-water interface and the interfacial tension is determined, then application of the Gibbs Equation, or the assumption of an equation of state, will enable the surface excess—the number of long chain ions (L , per cm^2)—to be found.

Now, if no gegen ion adsorption took place, L , the number of long chain ions per square centimeter, would equal numerically the charge density E in electronic charges per square centimeter since each has a charge of one electronic unit. Actually L and E are quite dissimilar in magnitude, usually L/E is about 100/5 or more, a figure showing that for every 100 long chain ions 95 gegen ions are adsorbed too.

THE MEASUREMENT OF ELECTROPHORETIC MOBILITY

The method of electrophoresis is the most generally useful of the four available (the others being streaming potential, electroosmosis, and the Dorn effect) for measuring electrokinetic potentials, and the microelectrophoretic technique has many advantages, especially for the work described here.

The mobility of small particles can be determined fairly quickly and accurately, and from it information deduced about the nature of the surface. With a high power ultramicroscope sensitivity is great and with no other method can the changes in surface properties of small particles, brought about by the addition of salts and surface active substances, be followed so readily.

There are several designs (1) of cell but the type with a circular cross section

¹ Manuscript received August 28, 1952.

Contribution from the Department of Colloid Science, Cambridge, and Department of Chemistry, N.S.W. University of Technology, Sydney, Australia.

² Fellow, National Research Council of Canada, Ottawa.

was employed: the single tube cylindrical cell is constructed in the shape of a letter H from one piece of Pyrex glass and rests on the stage of an ultramicroscope; four taps, one at the extremity of each limb, enable it to be cleaned (with hot alcohol, water, chromic acid, and water again) and filled. The horizontal tube is of capillary section and the top and one face are ground flat and polished for a length of 2 cm. near the mid-point. Platinum electrodes made of foil in the form of a loose open roll, to give a large area, do not "gas" provided the current density is small, i.e. the current through the cell with these electrodes of large area does not exceed ca. 5 ma.

A potential divider permits a d-c. voltage to be applied, which can be reversed in direction and altered in magnitude, throughout the range 0-200 volts.

The microscope eyepiece contains a calibrated grating and by timing the particles as they migrate across it in the field of view with an accurate stop watch, the velocity can be calculated. Twenty or more readings are taken on different particles, reversing the direction of the current between each. An air thermostat surrounds the apparatus ($25 \pm 0.1^\circ$).

In principle, the field strength is obtainable directly by dividing the voltage applied across the cell electrodes by their separation. There is, however, an uncertainty in measuring this length and also there are "end effects" at the electrodes. For these reasons it is better to measure the current (I amp.) flowing through the cell, the area of cross section (A cm.²) at the plane of focus, and the specific conductivity (S) of the suspension. The field strength X (volts per cm.) is given by:

$$X = \frac{I}{A.S}.$$

Electroosmotic flow in the cell takes place because the walls assume a charge, usually negative, relative to the water. The observed velocity of the particle at any point is the sum of that of the particle, relative to the water, and that of the water itself caused by electroosmosis. At two levels, the stationary levels, distant $a/\sqrt{2}$ from the axis, the observed velocity will be the true velocity of electrophoresis (2) (a is the tube radius).

Account was taken of the refraction error of Henry (10) to ensure accurate focusing on the stationary level.

A suspension of Nujol, a highly refined petroleum fraction, free from aromatic impurities and vacuum distilled, was employed and prepared by the method of Powney and Wood (17). Mixing the stock Nujol suspension (which would remain stable for many days and had droplets of a size of about 10^{-4} cm.), a solution of the soap in water, and water (and also buffer or salt solution when included) gave the suspension for electrophoretic measurement, which always consisted of 15% of stock suspension by volume.

THE MEASUREMENT OF INTERFACIAL TENSION

The well-known drop volume method is simple and rapid and was used here—the stainless steel tip makes a tight push-on fit with the micrometer syringe

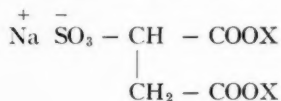
and the whole is rigidly held in a clamp attached to a water thermostat ($25 \pm 0.05^\circ$). Positioning of the syringe is such that the tip is 1 cm. below the surface of the Nujol (less dense than water), which fills to overflowing a small glass cell ($4 \times 4 \times 1$ cm.), which is almost immersed in the thermostat water and whose two largest faces are plane parallel in order that the optical system can throw a slightly magnified image of tip and falling drop onto a screen. Before being lowered into place the syringe is filled with the aqueous solution at 25° and the tip wiped dry with clean filter paper. With systems which have a low interfacial tension, trouble is sometimes experienced with "wetting". The aqueous phase, upon expulsion from the syringe, tends to creep up the outside surface of the tip, spreading over it; under these conditions the volume of the drop is greater than it should be making it necessary to watch carefully for this phenomenon. Rubbing the exterior of the tip with ferric stearate and polishing off the excess renders it hydrophobic and helps prevent "wetting". Although this substance is almost insoluble it is better to avoid all danger of introducing trivalent ferric ions, particularly when the surface active ion is negative.

The formation of the drop must be done sufficiently slowly, for, if too fast, too large a volume will fall. Usually about 10 min. are necessary, but by performing the initial stages rapidly and the final slowly, the period may be reduced to two or three minutes. At least four readings were taken and averaged to arrive at the volume which was used in the calculation (7) of γ .

When the aqueous solutions were very dilute "time-effects" were sometimes observed—i.e. the tension depended on time. There, the drop was formed to a stage just short of the approximate detachment volume and the time noted before it fell. The procedure was followed for successively smaller volumes until the drop did not fall after about 20 min. This was then the equilibrium volume.

SYSTEMS STUDIED

Attention was confined to the anion-active Aerosols of the general formula



where X is as follows:

A.O.T. dioctyl ester - 2-ethyl-1-hexyl alcohol,

A.M.A. dihexyl ester - methylamyl alcohol,

A.A.Y. diamyl ester - 2- and 3-methyl-1-butyl alcohol.

The Aerosols, the trade name of the products of the Cyanamid Company which kindly supplied them, are hydrolyzed to a negligible extent, but, owing to traces of the alcohol used in their manufacture, bad samples will be cloudy in solution, and must be discarded.

Nujol droplets are negatively charged in water, as are most chemically neutral substances such as air and other hydrocarbon oils. The inference is that the charge is a property of the water itself and may arise from a preferential adsorption of OH^- ions, an orientation of molecules at the interface, or a tendency on

the part of the water to expel electrons into a neutral substance. Neale and Peters (16) favor the last hypothesis on the basis of the pH sensitivity of such a negative charge, for the expulsion would be reduced in a strongly acid solution containing an excess of protons. The mobility of Nujol droplets in water is

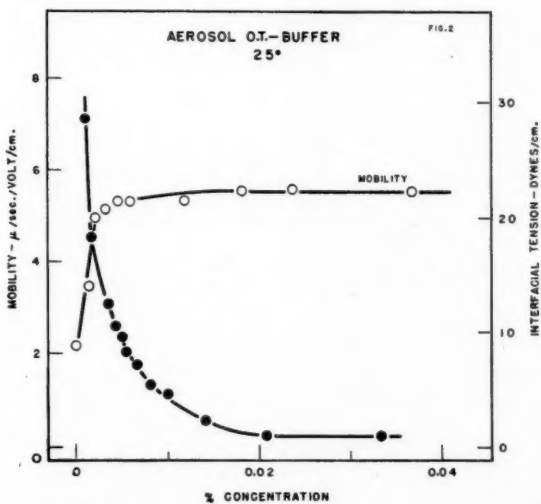
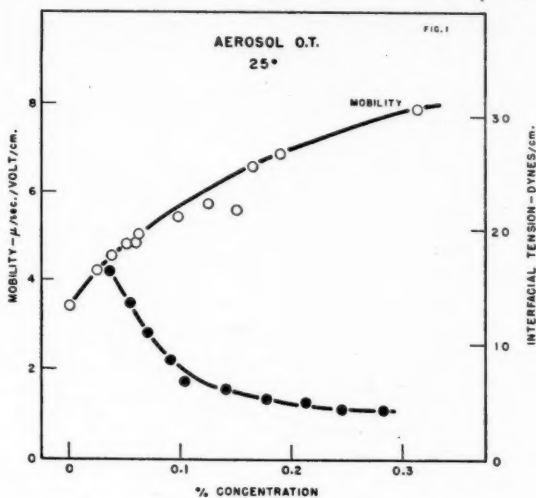


FIG. 1. Mobility of Nujol droplets in solutions of Aerosol O.T. Interfacial tension of aqueous solutions of Aerosol O.T. against Nujol.

FIG. 2. Mobility of Nujol droplets in solutions of Aerosol O.T. Interfacial tension of aqueous solutions of Aerosol O.T. against Nujol.

Solutions made up in 0.05 M acetate buffer, pH 6.

sensitive to traces of impurity and it is not possible to state a value more accurate than $4.0 \pm 0.5 \mu$ per sec. per volt per cm., though this is not serious from our point of view. Powney and Wood (17) give 4.35 and report those of other investigators as 6.65 (Urbain and Jensen (23)) and 3.65 (Limburg (12)).

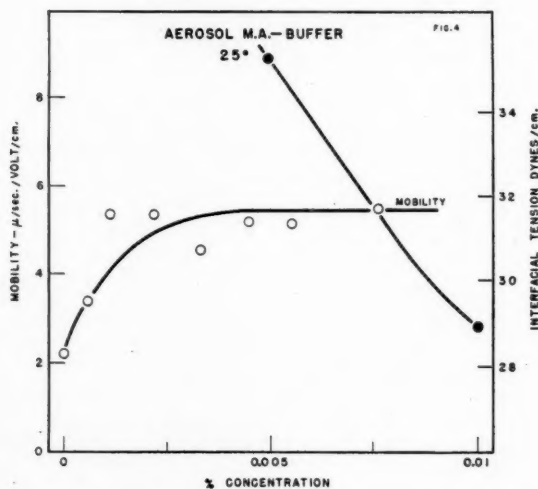
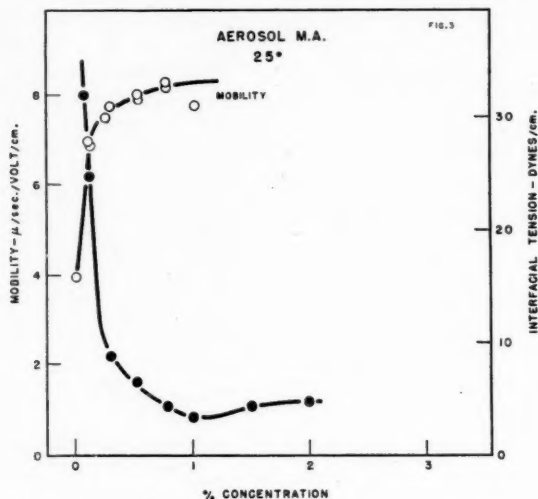


FIG. 3. Mobility of Nujol droplets in solutions of Aerosol M.A. Interfacial tension of aqueous solutions of Aerosol M.A. against Nujol.

FIG. 4. Mobility of Nujol droplets in solutions of Aerosol M.A. Interfacial tension of aqueous solutions of Aerosol M.A. against Nujol.
Solutions made up in 0.05 M acetate buffer, pH 6.

RESULTS

The curves of mobility in μ per sec. per volt per cm. and of interfacial tension in dynes per cm. against concentration are in Figs. 1, 3, 5, for Nujol droplets in solutions of A.O.T., A.M.A., and A.A.Y. respectively, and in Figs. 2, 4, 6 for

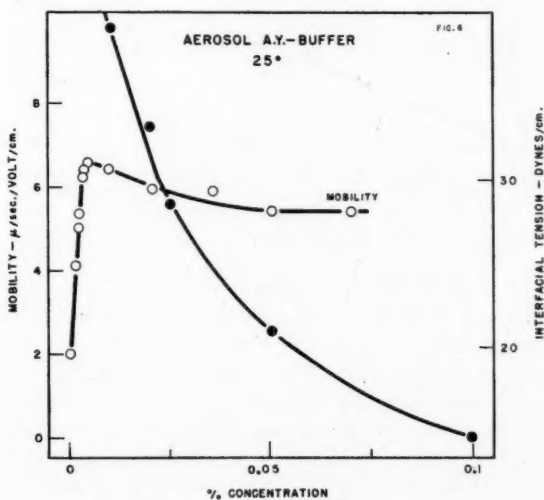
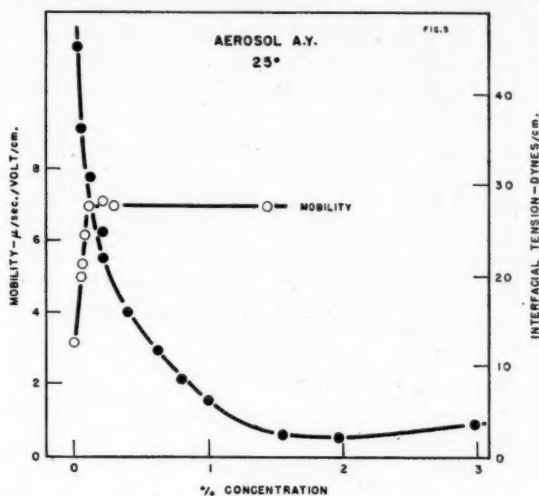


FIG. 5. Mobility of Nujol droplets in solutions of Aerosol A.Y. Interfacial tension of aqueous solutions of Aerosol A.Y. against Nujol.

FIG. 6. Mobility of Nujol droplets in solutions of Aerosol A.Y. Interfacial tension of aqueous solutions of Aerosol A.Y. against Nujol.

Solutions made up in 0.05 M acetate buffer, pH 6.

the same soaps when the solutions were made up in 0.05 *M* buffer of pH 6. In these latter experiments the soap concentration was relatively so small that the ionic strength remained constant.

A parallel behavior is seen in all the mobility concentration curves—a sharp initial rise followed by a flattening out to a more or less steady value of mobility. In the presence of buffer solution the initial slope is steeper and a lower constant mobility is attained; this is most evident in Fig. 7 where all the mobility-concentration curves are together for the region of low concentration. They are all set at the same zero, from which they differ by but little, to avoid confusion in the diagram, 2 μ per sec. per volt per cm. in buffer and 4 μ per sec. per volt per cm. in water. At high concentration all the droplets in buffer approach the same mobility, $2 + 3.5 = 5.5 \mu$ per sec. per volt per cm., whatever the soap adsorbed, and likewise in water, $4 + 4 = 8 \mu$ per sec. per volt per cm.

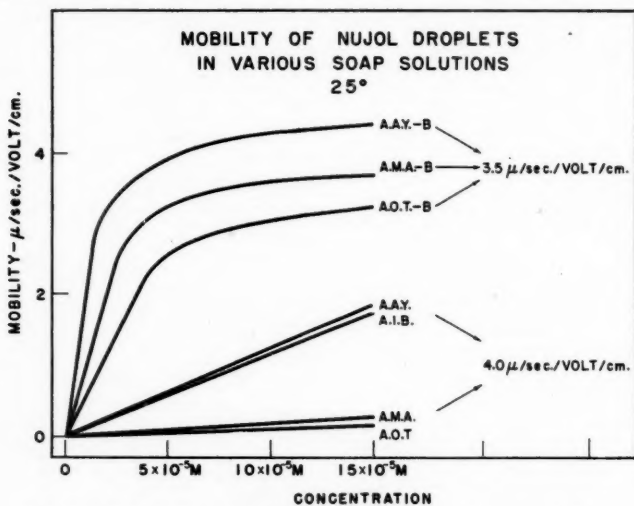


FIG. 7. Collected mobility curves, Nujol droplets in soap solutions.

DISCUSSION: ELECTROPHORESIS

The shape of the mobility concentration curve can be due to two factors for the mobility is known to be a function of two variables—the charge density of the interface and the thickness, $1/\kappa$, of the electrical double layer, both of which depend on the concentration, the former directly and the latter inversely. At small concentrations the increase of the charge is more important than the decrease of $1/\kappa$, the diminution of the electrical double layer thickness, so the mobility rises, but at higher concentrations the surface becomes more saturated and the influence of the double layer thickness predominates.

When the concentration of the soap is small the main effect of the ions from the added buffer will be to reduce the repulsive forces between the long chain ions, increasing their tendency to be adsorbed and raise the charge density.

Hence at these concentrations, for a given soap, the initial mobility slope will be greater for buffer than for water.

At high concentrations the Nujol particles will be saturated with long chain ions which have a very similar cross-sectional area whether A.O.T., A.M.A., or A.A.Y. Thus the charge density at the interface will not change from one case to another and the maximum mobility will be independent of the particular soap and a function of the double layer thickness only. Since $1/\kappa$ is less in buffer solution, the mobility will be less, 5.5μ per sec. per volt per cm. instead of 8.0μ per sec. per volt per cm.

It will be noticed that the slope (buffer or water) is greater (Fig. 7) for soaps of lower surface activity (Fig. 8).

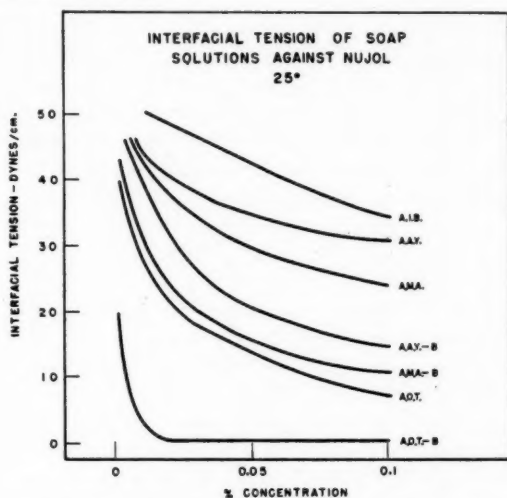


FIG. 8. Collected interfacial tension curves, soap solutions against Nujol.

Mobility and Zeta Potential

The relationship between electrophoretic mobility and zeta potential is given, for a nonconducting droplet, by Henry's (9) equation:—

$$v = \frac{D\xi}{6\pi\eta} f(\kappa r)$$

where η denotes the coefficient of viscosity, D the dielectric constant, r the droplet radius, κ the Debye-Huckel function, and $f(\kappa r)$ the Henry function, the value of which approaches 1.5 when $\kappa r \gg 1$, and 1 when $\kappa r \ll 1$. Since the radius of the droplets is about 1μ , and the concentrations low, about $10^{-4}M$, the use of the limiting value of 1.5 is justified.

Strictly, the equation is applicable only to solid particles, but it can be extended to liquid droplets provided that:—

1. The diffuse electrical double layer is entirely in the aqueous phase. This is

an assumption proved by Powell and Alexander (20).

- Bond's (3) correction is introduced, i.e. the right-hand side of Henry's equation is multiplied by a factor

$$\frac{3\eta + 3\eta'}{2\eta + 3\eta'}$$

where η and η' are the coefficients of viscosity of the dispersion medium and disperse phase respectively. For highly viscous Nujol droplets in very dilute soap solutions this differs from unity by less than the experimental error.

There would seem to be no correction necessary for surface conductance. Zeta potentials in systems of this type calculated from the Henry equation and by another method agree well (20).

Zeta Potential and Charge Density

The relation between potential and charge, and electrokinetic theory have been studied by several workers,* usually from a different point of view, though the underlying principles are the same, being those of Debye and Huckel (6). Combining the equation for the volume charge density and Poisson's equation gives the so-called "fundamental equation" which can be only solved accurately for a plane surface to yield:—

$$\sigma = \sqrt{\frac{NDkT}{2000\pi}} \sqrt{\sum c_i(e^{-z_i\epsilon\zeta/kT} - 1) + \sum c_j(e^{z_j\epsilon\zeta/kT} - 1)}$$

where N is Avogadro's number, D the dielectric constant, σ the charge density, ζ the zeta potential which has the same sign as σ , c_i and c_j the concentrations in moles per liter of the cations and anions with valencies z_i and z_j respectively, ϵ the charge on the electron, k the Boltzmann constant, and T the absolute temperature.

When $c_i = c_j = c$ and $z_i = z_j = 1$ the equation reduces to

$$\sigma = 2\sqrt{\frac{NDkT}{2000\pi}} \sqrt{c} \sinh \frac{\epsilon\zeta}{kT}$$

which is accurate for a plane surface and does not involve the Debye-Huckel approximation that the ratio of the electrical to the thermal energy of the ions be less than unity.

To solve the fundamental equation for a sphere the Debye-Huckel approximation must be made and then it can be shown that

$$\sigma = \frac{D(1 + \kappa r)}{4\pi r} \zeta$$

where the symbols have the same significance as before, r is the radius of the sphere, and κ the Debye-Huckel function. LaMer (11) and others have pro-

*For example:

- | | |
|------------------------|---|
| Abramson (2) | —electrophoresis of proteins. |
| Cassie and Palmer (5) | —effect of salts on ionized monolayers. |
| Neale (15) | —electrokinetic measurements with textile fibers. |
| Breyer and Gutmann (4) | —electrode potentials. |

duced approximate solutions of the fundamental equation for the spherical case and Muller (14) has attempted a graphical evaluation. His results do not differ greatly from those of Debye and Huckel but he did proceed to higher values of the electrical to thermal energy ratio.

The Nujol droplets have a radius of about 1μ so it is better to apply the equation for a sphere, remembering that $\kappa r \gg 1$.

DISCUSSION: INTERFACIAL TENSION

As the soap concentration increases, the tension at the Nujol-soap solution interface falls fairly rapidly until the micelle point is reached, whereat there is a transition, after which it remains approximately constant (Figs. 1 and 2) or passes through a shallow minimum (Figs. 3 and 5).^{*} Micelle formation, the aggregation of the long chain ions to form particles of high molecular weight with the ionic groups outwards and the long chains inwards, enables the system to reduce its free energy, for the nonpolar portion will move from an aqueous environment to one where it is surrounded by its fellows, in the interior of the micelle. Opposing this tendency will be the electrostatic repulsive forces between the like charges on the ions and their kinetic energy, but the net reduction in the potential energy is sufficient to stabilize the micelle, fairly certain to be spherical, with a radius of 25 or 30 Å and a content of some 40 to 50 long chain (plus gegen) ions in solutions less concentrated than about 1%. Aggregation is assisted, i.e. the critical micellar concentration is reduced, and capillary activity is increased, by lengthening the hydrocarbon chain (compare Figs. 1 and 3 where A.O.T. with a greater chain length has a lower C.M.C.^{**} than A.M.A.), by the addition of salts which reduce the magnitude of the electrostatic repulsive forces (compare Figs. 1 and 2), and by other factors which it would not be relevant to discuss. The minimum in the tension-concentration curve is probably due to the presence of an organic impurity, such as a higher alcohol (13) in the soap sample or heavy metal cations (21) in the distilled water used in making up the soap solutions.

THE FRACTION OF THE GEGEN IONS BOUND

The number of long chain ions adsorbed on to the Nujol droplets can be calculated from an equation of state (19):—

$$\pi(A - 40) = 210$$

where π is the surface pressure in dynes per cm. and A the area per molecule in Å², the reciprocal of which (with attention to units) gives the number L per cm.² It has been demonstrated above how, from mobility measurements, the number of electronic charges E , per cm.², can be determined. If the ions opposite in sign to the long chain ions adsorbed on a droplet were fully dissociated as gegen ions in the surrounding ionic atmosphere, E would equal L , for each long chain ion has a charge of one electronic unit. E is very much less than L showing that the fraction of gegen ions adhering to the droplet is near to unity, see Table

^{*}Figs. 4 and 6 would be similar if observations were extended to higher concentrations.

^{**}Critical micellar concentration.

TABLE I

Soap	Percentage concentration of aqueous solution	Number of gegen ions adhering per 1000 long chain ions on droplet
Aerosol O.T.	.01	994
	.02	991
	.04	984
Aerosol A.Y.	.01	986
	.02	980
	.04	968
Aerosol O.T. (in buffer solution)	.001	933
	.002	892
	.005	874
Sodium dodecyl sulphate	.01	970
	.07	931
	.19	900

I, which includes, also, figures calculated from the data of Powney and Wood (18) on sodium dodecyl sulphate and using the equation of state:—

$$\pi(A - 15) = 615$$

It is interesting to compare this fraction, of the order of 0.9, with that found by others for gegen ion adherence to the soap micelle:— for example, from measurements of the e.m.f. and freezing point depression of dodecyl benzyl-dimethyl ammonium chloride, Walton, Hiebert, and Sholtes (24) concluded that the fraction of the chloride ions combined in the micelle was 0.6 at concentrations above the critical micellar and Hartley (8), from work (studying transport numbers) on cetyl trimethyl ammonium bromide, estimated that the fraction of bromide ions adhering was about 0.74.

This parallel behavior is not unexpected. At concentrations where the mobility curve becomes horizontal, the surface of a Nujol droplet will be saturated with adsorbed long chain ions, oriented with their (hydrophilic) head groups outwards and (hydrophobic) hydrocarbon chains in the interior, together with undissociated gegen ions. A soap micelle will resemble the emulsified Nujol droplet, but on a much reduced scale, being a sphere of some 50 liquid close-packed long chain ions, aggregated with their chains together and away from the water and the end group outwards, plus bound gegen ions.

Salley *et al.* (22) measured the adsorption of water soluble surface active agents at interfaces by a radioactive tracer method and their results show that the head groups of the long chain ions and the bound gegen ions do not occupy the same plane, i.e. the latter are more remote from the interface.

It is seen from Table I that the fraction bound decreases slightly with increased concentration but it is not possible to put forward an explanation of this at present.

REFERENCES

1. ABRAMSON, H. A. Electrokinetic phenomena. Reinhold Publishing Corporation, New York. 1934.
2. ABRAMSON, H. A., MOYER, L. S., and GORIN, M. Electrophoresis of proteins. Reinhold Publishing Corporation, New York. 1942.
3. BOND, W. N. Phil. Mag. 4: 889. 1927.
4. BREYER, B. and GUTMANN, F. Australian J. Sci. 11: 96. 1948.
5. CASSIE, A. B. D. and PALMER, R. C. Trans. Faraday Soc. 37: 156. 1941.
6. DEBYE, P. and HUCKEL, E. Physik. Z. 24: 185. 1923.
7. HARKINS, W. D. and BROWN, F. E. J. Am. Chem. Soc. 41: 499. 1919.
8. HARTLEY, G. S., COLLIE, B., and SAMIS, C. S. Trans. Faraday Soc. 32: 795. 1936.
9. HENRY, D. C. Proc. Roy. Soc. (London), A, 133: 106. 1931.
10. HENRY, D. C. J. Chem. Soc. 997. 1938.
11. LAMER, V. K., GRONWALL, T. H., and GRIEFF, L. J. J. Phys. Chem. 35: 2245. 1931.
12. LIMBURG, H. Rec. trav. chim. 45: 854. 1926.
13. MILES, G. D. and SHEDLOVSKY, L. J. J. Phys. Chem. 48: 57. 1944.
14. MULLER, H. Physik. Z. 28: 324. 1927.
15. NEALE, S. M. Trans. Faraday Soc. 42: 473. 1946.
16. NEALE, S. M. and PETERS, R. H. Trans. Faraday Soc. 42: 478. 1946.
17. POWNEY, J. and WOOD, L. J. Trans. Faraday Soc. 36: 57. 1940.
18. POWNEY, J. and WOOD, L. J. Trans. Faraday Soc. 37: 152. 1941.
19. POWELL, B. D. Ph.D. Thesis, University of Cambridge. 1951.
20. POWELL, B. D. and ALEXANDER, A. E. J. Colloid Sci. In press. 1952.
21. REICHENBURG, D. Trans. Faraday Soc. 43: 467. 1947.
22. SALLEY, D. J., WEITH, A. J., ARGYLE, ANN A., and DIXON, J. K. Proc. Roy. Soc. (London) A, 203: 42. 1950.
23. URBAIN, W. M. and JENSEN, L. B. J. Phys. Chem. 40: 821. 1936.
24. WALTON, H. F., HIEBERT, E. N., and SHOLTES, E. H. J. Colloid Sci. 1: 385. 1946.

AN INSTRUMENT FOR DETERMINING THE ELECTRIC CHARGE DISTRIBUTION IN AEROSOLS¹

BY T. GILLESPIE AND G. O. LANGSTROTH

ABSTRACT

An instrument has been developed to permit measurement of the electric charges on a relatively large number of particles during a comparatively short period in the history of an aerosol. These novel characteristics have been obtained by depositing a sample on microscope slides in such a way that the charge on any particle at deposition can be determined in a subsequent examination from the size of the particle and its position on the slide. There is evidence to show that the act of sampling with this instrument does not cause spurious charging of particles. The construction and theory of the instrument are described in some detail and results of tests are given to show that the theory is applicable. The use of the instrument is illustrated by an account of a preliminary study of the charge distribution in a silica dust aerosol at various times after generation.

There is a need in aerosol research for a method of determining the electric charges on a sufficiently large number of particles to give a good statistical representation of the distribution with a sampling time sufficiently short to avoid serious changes in aerosol characteristics. Such a method must necessarily be free from spurious effects such as charging or deposition of particles by the act of sampling. No method hitherto described in the literature meets these requirements. A method involving the use of a novel instrument described in this article is considered to do so.

In principle the instrument provides for a thin ribbon of aerosol surrounded by a sheath of clean air to be drawn through a transverse electric field between two microscope slides. Since the charge and size of a particle determine the distance that it travels in the direction of air-flow before deposition on a slide, microscopic assessment of the numbers and sizes of particles at each point along the deposits permits calculation of the charge distribution. A thermal precipitator (4) at the exit end of the instrument provides for deposition of uncharged particles which are taken into account in arriving at the complete distribution.

In the present instrument a flow rate of 2.7 cc. per min. for the combined air-sheath and aerosol corresponded to a rate of 0.076 cc. per min. for the latter. Consequently the total deposit for a five minute sample of a cloud of 8×10^4 cc.⁻¹ particulate number contained about 30,000 particles, all of which could be assessed if desired. The instrument was suitable for Vycor particles up to about 7μ diameter with this flow rate, and to about 13μ diameter with half the rate. Modifications of operating conditions were possible over a wide range, but the combined flow rate was limited to that suitable for the thermal precipitator, or in the absence of this device, by the condition that singly charged large particles should not be carried beyond the end of the microscope slides.

Section 1 of this article is concerned with a description of the instrument,

¹ Manuscript received August 5, 1952.

Contribution from the Defence Research Board, Suffield Experimental Station, Ralston, Alberta, Canada.

Section 2 with the theory of operation, Section 3 with tests to show that the theory is applicable, and Section 4 with an example of its use.

1. THE DESIGN AND OPERATION OF THE INSTRUMENT

The instrument is represented approximately to scale in Fig. 1. The flushing

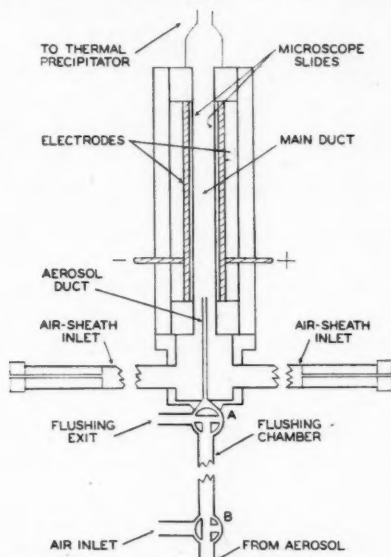


FIG. 1. Diagram of the instrument, approximately to scale.

chamber, required to bring aerosol as close as possible to the instrument proper for sampling, was a 12.6 cm. long copper tube with three-way metal valves *A* and *B* at either end. The aerosol duct was constructed of a No. 16 hypodermic needle (internal diameter, 1.1 mm.) with a squared end, and was carefully centered in the main duct by adjustment screws not shown in the diagram. The two air inlets for the air-sheath about the aerosol ribbon were 12 cm. long tubes fitted with 3.5 cm. long plugs drilled lengthwise to provide a 1.1 mm. diameter passage. This arrangement was found to be the most satisfactory of several tried. The dimensions of the plug passages are quite critical since it is necessary to balance their resistance to flow against that of the aerosol duct in order to obtain undistorted laminar flow in the main duct when suction is applied at the exit end.

The two plane parallel field electrodes were removable to provide for easy changing of the 7.6 cm. \times 2.5 cm. \times 0.8 mm. microscope slides held against their inner surfaces. These slides formed the side walls of the main duct which had a rectangular cross section 1.20 cm. wide in the direction of the electric field and 0.50 cm. in the other. The main body of the instrument was made of ebonite and plastic. The whole was enclosed in a wooden box to prevent convection and other air currents from affecting its operation.

The flushing chamber, valves, and aerosol duct were connected electrically to

earth in order to minimize spurious charging and deposition of particles. The d-c. voltage for the electric field was supplied by the circuit represented in Fig. 2.

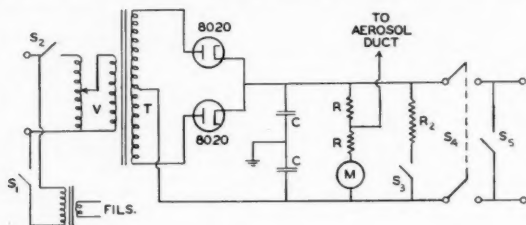


FIG. 2. The voltage supply for the instrument.

It was designed to maintain one electrode as much above ground potential as the other was below, in order to minimize distortion of the field by the end of the aerosol duct. In the figure, V denotes a Variac voltage control and T a 15 kv. transformer. C , R , and R_2 respectively had values of $1\ \mu\text{f.}$ (15 kv.), 150 megohms, and 200 megohms. Switches S_4 and S_5 were coupled mechanically so that only one could be in closed position at any time. The voltage applied to the electrodes was usually about 6.6 kv.

In taking a sample, the flushing chamber was first filled with the aerosol under test by lowering the level of water in a bottle connected to the flushing exit tube (valves A and B in the position shown in Fig. 1). Valve A was then turned counterclockwise through 90° , the voltage was applied to the electrodes, and the aerosol was drawn into the main duct by lowering the water level in a 500 cc. cylindrical separating funnel connected to the outlet of the thermal precipitator. An 8 ft. head of water and a special glass needle valve were used for careful control of the flow rate (2.0 to 6.5 cc. per min.). After the desired time, suction and voltage were turned off simultaneously and the slides were removed for microscopic assessment.

The nature of the deposits on the microscope slides was found to be a good indication of the performance of the instrument. For satisfactory performance, a deposit should be a rectangular strip with a width about equal to the internal diameter of the aerosol duct and a length shorter than the microscope slide. An unsuitable flow rate or applied voltage may permit some charged particles to pass beyond the end of the slide, and is evident from the length of the deposit. An improper balance between the resistances of air-sheath inlets and the aerosol duct distorts the flow pattern and produces deposits wider or narrower than they should be. Leaks in the instrument may distort the flow pattern and are normally evident from the shape and width of deposits. It has been found desirable to check for leaks after each insertion of microscope slides.

2. THEORY OF THE INSTRUMENT

The theory has been developed for spherical particles, but is expected to hold well for other shapes provided the departures from sphericity are not too great (see Reference 5). Consider the instrument placed vertically with an upward air

flow through the main duct. Let the y axis be coincident with the axis of the aerosol duct, and the x and z axes be respectively parallel and perpendicular to the field direction. Let the origin of coordinates lie at the exit end of the aerosol duct. The equations of motion of a particle of radius r and charge q , which enters the field at $x = x_0$, $y = 0$, $z = 0$, are

$$(1) \quad \begin{aligned} dy/dt &= V(x) - v_g, \\ dx/dt &= Eq/6\pi\eta r \end{aligned}$$

where t denotes time, $V(x)$ the air velocity at coordinate x in the x - y plane, v_g the terminal velocity of fall under gravity, E the field strength, and η the viscosity of air. If the main duct width in the x direction is $2b$, it follows that the particle will be deposited on the slide after going a distance y_0 along it, where

$$(2) \quad y_0 = \frac{6\pi\eta r}{Eq} \int_{x_0}^b (V(x) - v_g) dx.$$

For laminar flow, the air velocity at any point (x, z) in the main duct is given by solution of

$$\begin{aligned} \frac{\partial^2 V}{\partial x^2} + \frac{\partial^2 V}{\partial z^2} &= \alpha \\ x &= \pm b, V = 0 \\ z &= \pm a, V = 0 \end{aligned}$$

where α is a constant and $2a$ denotes the width of the main duct in the z direction. This equation appears to have been solved by Boussinesq (2) but the reference was not available to us. The solution is

$$(3) \quad \begin{cases} V(x, z) = \frac{\bar{V}}{\theta} \left[1 - \frac{x^2}{b^2} - \frac{16}{\pi^3} \sum_1^\infty \frac{1 - (-1)^n}{n^3} \psi \cdot \sin \frac{n\pi}{2} \left(1 + \frac{x}{b} \right) \right] \\ \psi = \left[\sinh \frac{n\pi a}{2b} \left(1 - \frac{z}{a} \right) + \sinh \frac{n\pi a}{2b} \left(1 + \frac{z}{a} \right) \right] / \sinh \frac{n\pi a}{b} \end{cases}$$

where \bar{V} denotes the velocity of flow averaged over the cross section of the main duct, and θ is a constant for the instrument, i.e.

$$(4) \quad \theta = \frac{2}{3} - \frac{64b}{\pi^5 a} \sum_1^\infty \frac{1 - (-1)^n}{n^5} \left[\frac{\cosh \frac{n\pi a}{b} - 1}{\sinh \frac{n\pi a}{b}} \right].$$

On inserting $2a = 0.50$ cm., $2b = 1.20$ cm. as for our instruments, and letting $z = 0$, equations (3) and (4) lead to

$$(5) \quad V(x) = 11.5 \bar{V} \left[1 - \frac{x^2}{b^2} - 0.52 \sum_1^\infty \frac{1 - (-1)^n}{n^3} \operatorname{sech} 0.66n \cdot \sin \frac{n\pi}{2} \left(1 + \frac{x}{b} \right) \right].$$

According to equation (3), equation (5) should be valid to better than 1% anywhere between the planes $z = \pm 0.028$ cm. (tangent to the sides of the aerosol duct). In order to test equation (5), the instrument was operated horizontally with the electric field absent and with smoke drawn through the air-sheath inlets as well as the aerosol duct; the transit times between graticule marks were

measured for particles at various points between the axis and the wall, and from these the velocities in the y direction were calculated. The results agreed with the predictions of equation (5) within the limits of experimental error.

It follows from combining equations (2) and (3) that for $z = 0$,

$$(6) \quad y_0 = \frac{6\pi\eta r}{Eq} \frac{\bar{V}}{\theta} \left[\frac{2}{3}b - x_0 + \frac{x_0^3}{3b^2} + \frac{32b}{\pi^4} \sum_{n=1}^{\infty} \frac{1 - (-1)^n}{n^4} \operatorname{sech} \frac{n\pi a}{2b} \cdot \left\{ \cos n\pi - \cos \frac{n\pi}{2} \left(1 - \frac{x_0}{b} \right) \right\} \right] - \frac{6\pi\eta r}{Eq} v_0(b - x_0).$$

According to this, all particles of the same size and charge would be deposited at the same distance y_0 along the slide if all entered the field at the same point. In practice such particles enter at different points because of the finite diameter of the aerosol duct and so are deposited over a range of y_0 values. The limits of the range are found from equation (6) by setting x_0 equal to the positive and negative values of the internal radius of the aerosol duct. Thus for our instrument ($2a = 0.50$ cm., $2b = 1.20$ cm., $x_0 = \pm 0.055$ cm.) particles of radius r and charge q should be deposited within the y_0 range given by

$$(7) \quad \frac{5.4\pi\eta r}{Eq} (\bar{V} - 0.8 v_0) \geq y_0 \geq \frac{4.2\pi\eta r}{Eq} (\bar{V} - 0.7 v_0).$$

3. TESTING OF THE INSTRUMENT

Lacking aerosols of known charge distribution for direct tests, experiments were performed to determine whether changes in the field strength and flow rate altered the positions of particles deposited on the slides in accordance with the predictions of equation (7). It appeared undesirable to compare results for successive samples taken with one instrument because of possible changes in aerosol characteristics with time. Accordingly, two instruments were constructed to be as nearly identical as possible, and comparisons were made between samples taken simultaneously from the same aerosol under different operating conditions. The test aerosol in all instances was silica powder* having 80% of the particles with diameter less than 3μ ; the median diameter was less than 1μ .

Counts of particles on the slides were made microscopically with dark field illumination using a $40\times$ objective and a $12\times$ eyepiece containing a Patterson-Cawood graticule. Distances along a deposit were measured from a reference point coinciding with the foot of the perpendicular dropped to the slide from the end of the aerosol duct. The numbers of particles in 0.075 mm. wide strips across the deposit were counted at intervals of 0.5 mm. in the first centimeter of deposit, of 1 mm. in the second centimeter, and of 2 mm. in the remainder. Application of the appropriate areal factors to these data provided a quantitative description of the distribution of particles along the deposit. In general about 2000 particles were counted on each slide.

The two instruments were found to give practically the same distribution of

*Powdered Vycor (7).

particles along the deposits when sampling the same aerosol under identical conditions of operation. This is illustrated by the data of Fig. 3. Furthermore, no

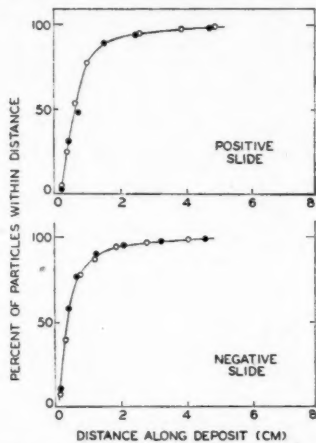


FIG. 3. The distribution of particles along the deposits of two instruments operated under the same conditions and simultaneously sampling the same aerosol. Points designated by \circ refer to one instrument and those designated by \bullet refer to the other; both were operated with $E = 12.6$ e.s.u. and $\bar{V} = 0.56$ mm. per sec. The ordinates give the percentage of the total number of particles which lay between the reference point and the distance indicated by the abscissa.

significant differences in distribution were found in similar experiments in which the flow was upward in one instrument and downward in the other. This indicated that for the particular test aerosol used, the v_0 term in equation (7) could be disregarded without introducing serious error.

When the two instruments were operated at the same field strength but at different flow rates, that with the higher rate produced a more elongated deposit as illustrated by the plot at the top of Fig. 4. It was possible to compare the magnitude of this difference with theoretical expectation by considering the distribution over a new variable equal to the product of the distance from the reference point and the ratio of field strength to flow velocity. According to equation (7) the percentage of the particles deposited from a given aerosol within any given range of the new variable ought to be independent of field strength and flow velocity. The data replotted on this basis in the lower part of Fig. 4 show that the distributions over the new variable were practically coincident, in satisfactory agreement with theory.

When the two instruments were operated at the same flow rate but at different field strengths, that with the smaller field strength produced a more elongated deposit as illustrated by the plot at the top of Fig. 5. On replotting the data in terms of the new variable defined above, the two distributions were essentially coincident in agreement with theory (lower part of Fig. 5).

From the results of these tests it is believed that the instrument operates according to the theory and may be used with some confidence for the determi-

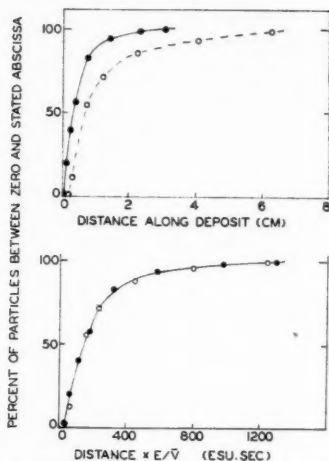


FIG. 4. The distribution of particles along the deposits of two instruments operated with the same field strength ($E = 21.4$ e.s.u.) but with different flow rates (\bullet refers to $\bar{V} = 0.52$ mm. per sec. and \circ to $\bar{V} = 1.12$ mm. per sec.). The data for the upper part of the figure are replotted in the lower using another variable as abscissa. The results shown are for the positive slide; those for the negative slide were similar.

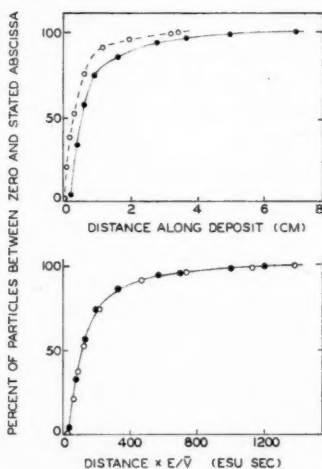


FIG. 5. The distribution of particles along the deposits of two instruments operated with the same flow rate ($\bar{V} = 0.54$ mm. per sec.) but with different field strengths (\bullet refers to $E = 10.7$ e.s.u. and \circ to $E = 21.4$ e.s.u.). The data in the upper part of the figure are replotted in the lower using another variable as abscissa. The results shown are for the negative slide; those for the positive slide were similar.

nation of charge distribution in aerosols. Furthermore, the agreement of theory and experiment over a range of flow rates and field strengths indicates that spurious charging or deposition of particles is not produced by the act of sampling,

since the dependence of such effects on the varied quantities would have led to discrepancies in the tests described.

4. THE DETERMINATION OF CHARGE DISTRIBUTION

Since determination of the charge distribution involved some considerations not discussed above, the procedure is illustrated by the following account of a preliminary study of the charge distribution in a silica powder aerosol at various times after generation. The powder was similar to that used in testing the instrument. The aerosol was produced by blowing up 200 mgm. in a 60 cm. cube chamber and fanning it for three minutes. Samples were taken with the instrument backed by a thermal precipitator at 6, 28, 60, 115, and 200 min. after shutting off the fan.

Microscopic assessment of the slides was made with a 40 \times objective and a 12 \times eyepiece containing a Patterson-Cawood graticule for sizing the particles. Examination of a pair of analyzer slides required about two hours, and proved to be less tedious with blue light at grazing incidence to the slide than with substage illumination. The assessments were consistent and reproducible, and close agreement was found with checks made on some of the deposits using substage illumination. About 2000 particles were examined on each slide.

In assessing analyzer slides, the number and sizes of particles in 0.075 mm. wide strips extending across the deposit were determined at intervals of 0.5 mm. in the first centimeter of the deposit, of 1 mm. in the second centimeter, and of 2 mm. in the remainder. Sizing involved classification of particles into 11 groups having ranges of apparent radius as given at the top of Table I. Table I illustrates the nature of the assessment data. Thermal precipitator deposits were assessed in the usual way.

The complete data for a sample permitted calculation for each size group of (a) the number of particles lying between any two points of an analyzer deposit, and (b) the number of neutral particles. The theory of Section 2 was applied to these data to find the charge distribution. The value of \bar{V} was calculated from the known rate at which air was drawn through the instrument and the cross-section area of the main duct. The value of E was calculated from the known applied voltage and the distance between the electrodes, taking into account the dielectric effect of the microscope slides and assuming a uniform field.

The following procedure was applied in turn to each size group. Equation (7) was used to calculate the minimum distance of deposition for the smallest, and the maximum distance for the largest particle in the group, on the assumption of a charge of one electron unit, two electron units, and so on. The results of these calculations were drawn up in tabular or graphical form to show the charge associated with each distance from the reference point. The method is illustrated by Fig. 6 which represents an 'exploded view' calculated for a deposit of particles of size group 2. The scale shows the distance in millimeters along the deposit and each shaded strip above it gives the region occupied by particles carrying a charge of N electron units ($q = 4.8 \times 10^{-10} N$ e.s.u.). The possible values of N for particles lying in various regions of the deposit are given at the bottom of the figure.

TABLE I

TYPICAL ASSESSMENT FOR AN ANALYZER SLIDE GIVING THE COUNTED NUMBER OF PARTICLES OF EACH SIZE GROUP IN 0.075 MM. WIDE STRIPS AT VARIOUS DISTANCES FROM THE REFERENCE POINT (POSITIVE POTENTIAL SLIDE FOR SAMPLE AT 60 MIN.)

Radius (μ) Dist. (mm.)	<0.33	0.33 - 0.66	0.66 - 1.00	1.00 - 1.35	1.35 - 1.65	1.65 - 2.0	2.0 - 2.7	2.7 - 3.3	3.3 - 4.2	4.2 - 5.0	5.0 - 6.5
2.0	18	33	48	54	30	30	12	0	3	0	0
2.5	21	78	120	150	39	24	12	6	3	3	3
3.0	21	63	105	129	24	12	0	3	3	0	6
3.5	9	45	75	78	15	9	3	3	0	0	0
4.0	0	18	27	63	18	12	3	0	0	0	0
4.5	0	18	15	18	12	18	3	3	0	0	0
5.0	0	6	12	45	12	9	6	0	0	0	0
5.5	9	15	15	27	9	3	0	0	0	0	0
6.0	3	24	15	12	0	0	0	0	0	3	0
6.5	15	9	9	27	3	0	3	0	0	0	0
7.0	6	9	6	9	3	0	0	0	0	0	0
7.5	4	3	8	8	3	1	1	1	0	0	0
8.0	1	5	10	13	2	2	4	0	0	0	0
8.5	7	9	6	4	3	1	2	0	0	0	0
9.0	4	5	4	7	4	3	1	0	0	0	0
9.5	0	1	8	4	1	1	0	0	0	0	0
10.0	2	2	3	6	3	1	0	0	0	0	0
11.0	2	3	5	2	0	1	0	0	0	0	0
12.0	1	5	2	5	1	0	0	0	0	0	0
13.0	1	3	3	4	0	0	0	0	0	0	0
14.0	2	4	0	2	0	0	0	0	0	0	0
15.0	0	3	1	1	0	1	0	0	0	0	0
16.0	0	1	1	2	0	0	0	0	0	0	0
17.0	0	0	2	2	1	0	0	0	0	0	0
18.0	0	0	3	1	0	0	0	0	0	0	0
19.0	0	0	1	1	0	1	0	0	0	1	0
20.0	0	2	1	1	1	0	0	0	0	0	0
22.0	0	1	1	0	0	0	0	0	0	0	0
24.0	0	0	2	1	0	0	0	0	0	0	0
26.0	0	0	1	1	0	0	0	0	0	0	0
28.0	0	0	0	0	0	0	0	0	0	0	0
30.0	0	0	0	0	0	0	0	0	0	0	0
32.0	0	0	0	0	0	0	0	0	0	0	0
34.0	0	0	0	1	0	0	0	0	0	0	0
36.0	0	0	0	0	1	0	0	0	0	0	0
38.0	0	0	0	0	0	0	0	0	0	0	0
40.0	0	0	0	0	1	0	0	0	0	0	0
42.0	0	0	0	1	0	0	0	0	0	0	0
44.0	0	0	0	0	0	0	0	0	0	0	0

NOTE: The sums of the above figures for the 1st, 2nd, and 3rd centimeters of the deposit are respectively 2000, 73, and 11; the total number of particles on the slide was estimated to be 14,600.

It is evident, for example, that all particles of this group lying between 7.4 and 14.9 mm. should be assigned a single charge, those lying between 5.8 and 7.4 mm. a single or double charge, those lying between 5.0 and 5.8 mm. a double charge, and so on. In applying such calculations, the assessed number of particles in a region characterized by several possible charge values was divided equally between the different possibilities. This may have introduced some error in the distribution as between neighboring charge values, but could hardly have caused serious distortion in the distribution as a whole. Having found the distribution for each size group, the results were summed together with the thermal precipitator

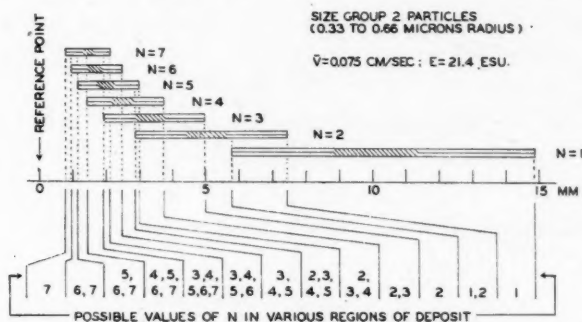


FIG. 6. 'Exploded view' of a hypothetical deposit of 0.33 to 0.66 μ radius particles carrying charges from 1 to 7 electron units, showing the calculated distribution along the slide. The diagonally shaded section near the center of each component indicates the region of deposit of 0.5 μ radius particles.

data to give the charge distribution for the whole aerosol. Application of corrections was sometimes necessary before summation; these are discussed below.

The great length and marked overlapping of the strips in Fig. 6 result mainly from the fact that a size group as assessed with a Patterson-Cawood graticule contained a wide range of particle sizes. The situation would be improved considerably if accurate determinations of particle size were made. This is evident from the diagonally shaded portions near the center of each strip, which represent the regions of deposit for particles of 0.50 μ radius. The lengths of these portions are a result of the finite diameter of the aerosol duct as pointed out in Section 2.

Corrections to the data were sometimes necessary to take into account particles which had left the aerosol duct but had not been deposited by the time the electric field and suction were cut off at the end of the sampling period. The need for correction is most obvious with thermal precipitator data. The precipitator wire was 15 cm. from the end of the aerosol duct in our arrangement, and the flow velocity on the main duct axis was 1.86 \bar{V} (equation 5), or 0.14 cm. per sec. at a flow rate of 2.7 cc. per min. Consequently, uncharged particles required 15/0.14 = 108 sec. to reach the precipitator, and no deposit could have been obtained there in a shorter sampling time. It is easily shown that if n particles were deposited in the precipitator in a sampling time of T sec., the corrected number n_c is given by

$$(8) \quad n_c = n \cdot 1.86 \bar{V} T / (1.86 \bar{V} T - 15)$$

for our arrangement. The size of the correction for a flow rate of 2.7 cc. per min. in the main duct is illustrated by the following values

T (min.)	5	10	20	40
n_c/n	1.54	1.21	1.10	1.05

Similarly, a small correction was sometimes necessary in the data for charged particles. According to equation (1), the time τ taken for a particle of radius r to reach the slide is given by $\tau = 6\pi\eta r b / Eq$. On expressing r in microns and setting

$q = 4.8 \times 10^{-10}$ N e.s.u., $b = 0.60$ cm., $E = 21.4$ e.s.u., and $\eta = 1.82 \times 10^{-4}$ c.g.s. units, this becomes

$$(9) \quad \tau = 20.1 r/N \text{ sec.}$$

If n denotes the number of particles of radius r and charge N found in a deposit obtained with a sampling time T , the corrected number n_c is given by

$$(10) \quad n_c = n T/(T - \tau).$$

The size of the correction is illustrated by the following values.

r (μ)	N (e.u.)	n_c/n for T values (min.) of			
		5	10	20	40
0.33	1	1.02	1.01	1.00	1.00
	5	1.00	1.00	1.00	1.00
1.0	1	1.07	1.04	1.02	1.01
	5	1.02	1.01	1.00	1.00
3.0	1	1.25	1.07	1.05	1.02
	5	1.04	1.02	1.01	1.00

TABLE II

THE DETERMINED CHARGE DISTRIBUTION FOR FIVE SAMPLES TAKEN AT DIFFERENT TIMES. THE RESULTS FOR THE MORE HIGHLY CHARGED PARTICLES HAVE BEEN CONDENSED FROM MORE DETAILED DATA

Time (min.)		6	28	60	115	200
No. of particles in sample		34,560	28,530	24,760	16,460	10,560
% with no charge		36.5	14.1	6.1	8.5	14.2
% with neg. charge		28.1	49.1	59.3	47.8	48.1
% with pos. charge		35.3	36.6	34.4	43.6	37.9
Max. neg. N (electron units)		100	70	40	40	22
Max. pos. N (electron units)		70	70	60	40	24

N	% of total particles having charge N electron units									
	6 min.		28 min.		60 min.		115 min.		200 min.	
	Neg.	Pos.	Neg.	Pos.	Neg.	Pos.	Neg.	Pos.	Neg.	Pos.
1	5.2	3.5	6.4	7.9	6.4	5.4	5.5	6.4	10.6	10.5
2	3.9	3.7	4.5	3.7	6.9	4.1	5.1	7.1	10.5	6.0
3	3.2	4.0	4.8	2.1	5.2	3.1	5.9	5.3	8.8	4.5
4	2.5	3.5	3.9	2.4	5.4	2.7	4.2	4.6	5.1	3.6
5	1.9	2.7	3.8	1.9	5.0	2.3	3.7	3.5	3.2	3.0
6 to 7	3.2	5.2	8.1	3.8	9.6	4.3	6.4	4.3	5.1	3.7
8 to 10	2.9	5.7	7.6	4.7	10.0	4.3	6.1	3.7	3.0	2.9
11 to 15	2.4	3.9	5.2	4.9	6.5	3.6	6.7	3.8	1.5	2.3
16 to 20	1.5	1.3	2.4	2.5	2.4	2.2	3.0	2.5	0.23	1.1
21 to 30	1.0	1.1	1.6	2.2	1.4	2.1	0.87	2.0	0.06	0.34
31 to 40	0.22	0.51	0.60	0.38	0.48	0.22	0.26	0.35	0.00	0.00
41 to 100	0.16	0.14	0.16	0.12	0.00	0.06	0.00	0.00	0.00	0.00
Sum	28.1	35.3	49.1	36.6	59.3	34.4	47.8	43.6	48.1	37.9

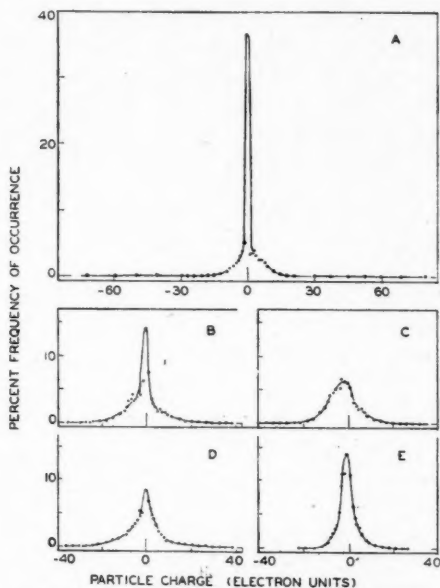


FIG. 7. The determined charge distribution for a silica powder aerosol at 6 min.(A), 28 min.(B), 60 min.(C), 115 min.(D), and 200 min.(E) after generation.

The final results are given in somewhat condensed form in Table II, and the charge distributions plotted from more detailed data are shown in Fig. 7. Extended discussion appears unjustified since the data refer to only one cloud. The

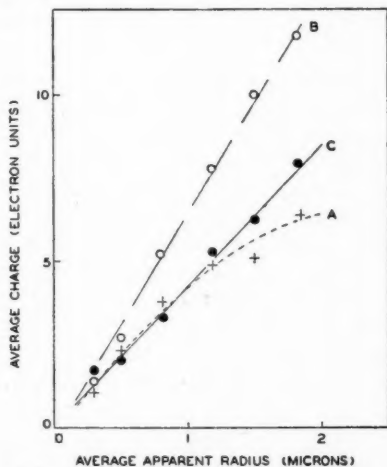


FIG. 8. The relation between particle size and average charge carried for a silica powder aerosol at 6 min.(A), 60 min.(B), and 200 min.(C) after generation.

relation between the charge carried and the size of a particle has been studied by several investigators however, and it is interesting to compare the present data with their findings. Sachsse (9) was unable to find clear evidence of a definite relationship for dust or mist particles. Proportionality between the average charge and the square of the radius was reported by Rosenblum (8) for dust or mist, and inferred by Daniel and Brackett (3) for fine silica dust. Kunkel (6) found the charge on dust particles to increase somewhat less rapidly than the square of the radius. Arendt and Kallmann (1) found the limiting charge carried by small fog particles in regions of high ion density to be approximately proportional to the radius. Typical plots of the average radius for each size group against the average charge per particle (calculated with disregard to sign) are shown in Fig. 8. For the aerosol studied the average charge carried was proportional to the particle radius, except for small times after generation.

REFERENCES

1. ARENDT, P. and KALLMANN, H. *Z. Physik*, 35: 421. 1926.
2. BOUSSINESQ, J. *J. Math. pures appl.* p. 377. 1868.
3. DANIEL, J. H. and BRACKETT, F. S. *J. Applied Phys.* 22: 542. 1951.
4. GREEN, H. L. and WATSON, H. H. Physical methods for the estimation of the dust hazard in industry. Medical Research Council Special Report 199. His Majesty's Stationery Office, London, 1944.
5. KUNKEL, W. B. *J. Applied Phys.* 19: 1056. 1948.
6. KUNKEL, W. B. *J. Applied Phys.* 21: 820. 1950.
7. NORDBERT, M. E. *J. Am. Ceram. Soc.* 27: 299. 1944.
8. ROSENBLUM, N. *Tech. Phys. U.S.S.R.* 4: 564. 1937.
9. SACHSSE, H. *Ann. Physik*, 14: 396. 1932.

NOTE

Note on the Polarographic Determination of Zirconium*

We have found that a useful polarographic method for the determination of zirconium can be based on the findings that *m*-nitrobenzoic acid is polarographically reducible (1, 4) and that this compound is a highly selective precipitant for zirconium (3, 5). In principle, the method consists of precipitating zirconium with *m*-nitrobenzoic acid, dissolving the filtered and washed precipitate in hydrochloric acid, and measuring the height of the polarographic wave corresponding to the reduction of the *m*-nitrobenzoic acid (to the hydroxylamine stage) in a suitable supporting electrolyte. The method is accordingly an indirect one for zirconium, and depends on the specificity of *m*-nitrobenzoic acid as a precipitant. We have applied the method successfully to the determination of zirconium in magnesium-base alloys.

PROCEDURE

To a 5-gm. sample of the alloy, about 25 ml. of water is added followed by sufficient 16 *M* nitric acid (about 35 ml., in small portions) to cause ready dissolution, except for the relatively small residue which contains the so-called "insoluble" zirconium. The mixture is filtered through paper (Whatman No. 42) and the residue washed with 2.0 *M* nitric acid. The filtrate and washings are caught in a 250 ml. volumetric flask, from which, after making up to the mark with 2.0 *M* nitric acid, one or more 25 ml. aliquot samples are taken. To each of these is added aqueous ammonia (1:1) to the Congo red end point, with care being taken to avoid precipitation of zirconium. There are then added 20 ml. of 2.0 *M* hydrochloric acid, 10 gm. of ammonium nitrate, water to give a volume of about 100 ml., and then, at the boiling point with stirring, about 100 ml. of a hot 1% aqueous solution of *m*-nitrobenzoic acid (5). The mixture is boiled gently for five minutes and then filtered hot through a Gooch crucible. The precipitate is washed with hot water and then dissolved in 25 ml. of 6.0 *M* hydrochloric acid by placing the crucible and acid in the original beaker and warming the mixture. The crucible, after it is washed down with water, is removed from the beaker and the contents of the beaker are neutralized to the Congo red end point with aqueous ammonia (1:1) and washed with water into a 250 ml. volumetric flask. One or more 25 ml. aliquot samples are then pipetted into 100 ml. volumetric flasks, and, to each, 50 ml. of a 0.20 *M* solution of potassium chloride, 10 ml. of 0.20 *M* hydrochloric acid (by pipette), and 1 ml. of 0.75% gelatin solution (as a maximum suppressor) are added. The solution is made up to volume with water, a portion is decanted into the polarographic cell, bubbled with purified nitrogen for 15 min., and then polarographed.

The polarographic wave for the first reduction step of *m*-nitrobenzoic acid

*This work was supported by a grant from the Defence Research Board.

is measured and the corresponding concentration of zirconium is assessed by reference to a calibration curve prepared from measurements made in the same way with solutions of known zirconium content. Such solutions were prepared by dissolving zirconium nitrate (Titanium Alloy Manufacturing Co.) in hydrochloric acid; the zirconium content was determined by the gravimetric method using *m*-nitrobenzoic acid (5). The calibration curve was a straight line, at least for the range of concentrations investigated (0 to $1.1 \times 10^{-4} M$).

All solutions were made up to volume at $25.0^\circ C$. and the polarographic determinations were carried out at this temperature. The asbestos (from the Gooch crucible) that remained in the solutions had a negligible volume and such as was transferred to the polarographic cell caused no difficulty there.

The polarograph was a Tinsley pen-recording instrument (Type V722/13) with the setting of the galvanometer sensitivity at $1/50$ th of the maximum; the waves were of form suitable for easy measurement, particularly when use was made of the counter current device of the polarograph.

The *m*-nitrobenzoic acid was a B. D. H. Certified Chemical, and all other reagents were of a grade appropriate to analytical work.

RESULTS

The results given by this method when it was applied to the analysis of different commercial magnesium-base alloys (supplied with routine analyses through the courtesy of Mr. S. Abbey and Dominion Magnesium Ltd., Haley, Ontario) are shown in the accompanying table. The analyses furnished were obtained by a colorimetric method using alizarin red S. The values given in the table refer in all cases only to the zirconium soluble in dilute acid. The "insoluble" zirconium (0.01 – 0.1%) may be put into solution by an appropriate fusion of the black residue which remains after dissolution of the bulk of the alloy.

ANALYSES OF MAGNESIUM ALLOYS

Sample	"Soluble" zirconium (%)		Other elements present*
	Colorimetric	Polarographic	
K-1(83)	0.59	0.58 ± 0.01	Zinc: 3.15% Rare earths: 2.9%
K-1(91)	0.59	0.63 ± 0.02	
EZK 331(30)	0.67	0.64**	

* Apart from magnesium and very low concentrations of manganese (0.005%), iron (0.001%), nickel (0.0005%), and copper (0.0005%).

** Sample of alloy treated with hydrochloric rather than nitric acid.

Each of the polarographic values is an average obtained from eight polarograms. The sample taken, 5 gm., was much larger than necessary from the point of view of the sensitivity of the method but large samples are desirable because segregation effects are pronounced in these alloys.

DISCUSSION

The data given in the table do not permit positive statements about the accuracy of the method to be made because the values with which comparison is made were obtained by routine rather than by umpire methods. An effort is being made to obtain additional samples in which the zirconium concentration is known with a high degree of certainty, in order that the procedure may be tested further, and other experiments designed to shorten the method and improve its precision are under way. The procedure appears, however, to be a useful one; it is easy to carry out and is faster than the gravimetric methods which are now commonly used. An approach that holds promise of leading to an even shorter polarographic method is to add a carefully-measured amount of *m*-nitrobenzoic acid to the zirconium solution, and then, after the precipitation of the zirconium, to determine polarographically the amount of the organic reagent remaining in solution. This would eliminate the filtering and the dissolving of the zirconium *m*-nitrobenzoate.

Experiments with prepared solutions showed that magnesium, even at the high concentration present in these alloys, gave no precipitate with *m*-nitrobenzoic acid. The same is true for the zinc which occurs in some of the alloys at a concentration of a few per cent. Cerium (IV) can be quantitatively precipitated by *m*-nitrobenzoic acid but cerium (III) is not affected by the reagent (3). The chloride ion present at the time of dissolution of the EZK alloy (which contains cerium to the extent of about 1.5%) apparently served to prevent the oxidation of any cerium to the quadrivalent state. In any case it would be easy to reduce cerium (IV) to cerium (III) before adding the precipitant. It is reasonable to suppose that a polarographic method for cerium could be developed along the lines of the one presented here for zirconium.

The selectivity of *m*-nitrobenzoic acid as a precipitating agent for zirconium is such that this method, which we believe to be the first polarographic method for zirconium that has appeared, should be applicable to the determination of this element in the presence of a variety of others. It should be mentioned, however, that there are interferences (3): mercury (I) and (II) can give trouble, as can tin (II) and (IV) (owing to hydrolysis effects); hafnium, in part or all, is precipitated with the zirconium.

The acidity for the precipitation is not highly critical, although if it is too low (e.g., 0.02 *N* after the addition of the *m*-nitrobenzoic acid) thorium will yield a precipitate, and if it is too high (e.g., 0.4 *N*) zirconium may be lost (3). In our work, the acidity was about 0.25 *N* after the addition of the precipitant. When the zirconium *m*-nitrobenzoate is to be ignited to zirconium dioxide in a gravimetric determination, a double precipitation may be necessary to eliminate coprecipitated ions of thorium and of certain other elements (5). The reagent will precipitate plutonium as plutonium (IV) but not as plutonium (III) (2).

The polarographic diffusion current for a given concentration of *m*-nitrobenzoic acid (and also the half-wave potential) depends on the pH of the solution (1, 4), which accordingly must be controlled. Our procedure yields a pH of 1.8 at which value the half-wave potential for the first reduction step was found to be

about -0.2 volts vs. the saturated calomel electrode, which is in accord with the data of Page *et al.* (4) rather than with that of Dennis *et al.* (1).

1. DENNIS, S. F., POWELL, A. S., and ASTLE, M. J. J. Am. Chem. Soc. 71: 1484. 1949.
2. HARVEY, B. G., HEAL, H. G., MADDOCK, A. G., and ROWLEY, E. L. J. Chem. Soc. 1010. 1947.
3. OSBORN, G. H. Analyst, 73: 381. 1948.
4. PAGE, J. E., SMITH, J. W., and WALLER, J. G. J. Phys. & Colloid Chem. 53: 545. 1949.
5. VENKATARAMANIAN, M. and RAGHAVA RAO, Bh. S. V. Z. anal. Chem. 133: 248. 1951.

RECEIVED AUGUST 25, 1952.
DEPARTMENT OF CHEMISTRY,
HAMILTON COLLEGE, MCMASTER UNIVERSITY,
HAMILTON, ONTARIO.

R. P. GRAHAM
E. VAN DALEN
A. M. C. UPTON

CONTENTS OF VOLUME 30

- ADAMS, G. A.—The constitution of a polyuronide hemicellulose from wheat straw, 698.
See Colvin, J. R.
- ADAMS, G. A. and CASTAGNE, A. E.—Purification and composition of a polyuronide hemicellulose isolated from wheat straw, 515.
- ALEXANDER, A. E.—See Powell, B. D.
- AMBERG, C. H. and MCINTOSH, R.—A study of adsorption hysteresis by means of length changes of a rod of porous glass, 1012.
- ARMSTRONG, R.—See Wiesner, K.
- ARNELL, J. C.—See McDermot, H. L.
- AZIZ, P. M. and WETMORE, F. E. W.—Molten salts. Electrical transport in the system silver nitrate-sodium nitrate, 779.
- BARCLAY, L. R. C.—See Thorn, G. D.
- BARRÉ, R.—See Perron, Y.
- BARTLETT, M. F.—See Wiesner, K.
- BARTLETT, M. F., FIGDOR, S. K., and WIESNER, K.—Synthesis of para-bridged benzene compounds. III, 291.
- BAUER, T. W. and DORLAND, R. M.—A note on the thermodynamic properties of the hydrates of sodium carbonate, 76.
- BERMAN, L., HALL, R. H., PYKE, R. G., and WRIGHT, G. F.—The methoxymercuration of 2-methyl-1-phenylpropene-1, 541.
- BERNSTEIN, H. J. and PULLIN, A. D. E.—Vibration spectra of *cis* and *trans* dichloroethylene-*d*₁, 963.
- BETTS, R. H. and MACKENZIE, A. N.—Radiochemical measurements of activity coefficients in mixed electrolytes, 146.
- BIGEISEN, J.—A theoretical evaluation of the nitrogen isotope effect in the thermal deamination of phthalamide, 443.
- BISHOP, C. T.—The action of liquid ammonia on wheat straw holocellulose, 229.
- BOIVIN, J. L.—See Gagnon, P. E.
- BOIVIN, P. A.—See Gagnon, P. E.
- BOIVIN, P. A., GAGNON, P. E., RENAUD, E., and BRIDGEO, W. A.—Cyanoacetic esters, amino acids, and pyrazolones, 994.
- BOLKER, H. I.—See Vavasour, G. R.
- BOURNS, A. N.—See Lindsay, J. G.; Stacey, F. W.
- BOURNS, A. N., EMBLETON, H. W., and HANSULD, M. K.—The reaction of tetrahydropyran with primary aromatic amines over activated alumina, 1.
- BOURNS, A. N. and TUDGE, A. P.—A new synthesis of piperidine, 71.
- BRECKENRIDGE, J. G.—See Stone, A. L.
- BRICE, C.—See Lemieux, R. U.
- BRIDGEO, W. A.—See Boivin, P. A.
- BROWN, A. T.—See Cragg, L. H.
- BROWN, F. and HOLLAND, D. A.—Isotope effects: Reaction at the carbonyl group, 438.
- BURKELL, J. E. and SPINKS, J. W. T.—Measurements of self-diffusion in aqueous solutions of sodium dihydrogen phosphate, 311.
- BYRNE, J., FLEMING, H., and WETMORE, F. E. W.—Molten salts. Electrical conductivity in the system silver nitrate-sodium nitrate, 922.
- BYWATER, S. and ROBERTS, R.—Temperature independent factors of hydrogen abstraction reactions in the gas phase, 773.
- CAMPBELL, A. N. and KARTZMARK, E. M.—The conductances of strong solutions of strong electrolytes at 95°, 128.
- CASTAGNE, A. E.—See Adams, G. A.
- CHISHOLM, A.—See Gagnon, P. E.
- COCKBURN, W. F. and MARION, L.—The papilionaceous alkaloids. XV. The structure and the partial synthesis of rhombifoline, 92.
- COLVIN, J. R.—The binding of anions by lysozyme, calf thymus histone sulphate, and protamine sulphate, 320. The size and shape of lysozyme, 831. Binding of anions by denatured proteins, 973.
- COLVIN, J. R., COOK, W. H., and ADAMS, G. A.—Electrophoretic homogeneity of polysaccharides in molar alkali, 603.
- COOK, W. H.—See Colvin, J. R.
- CÔTÉ, R.—See Gagnon, P. E.
- CRAGG, L. H.—See Manson, J. A.
- CRAGG, L. H. and BROWN, A. T.—The viscometric detection of branching in polymers. I. Branching in GR-S as a function of conversion, 1033.

- CRAIG, A. and MCINTOSH, R.—The preparation of sodium chloride of large specific surface, 448.
- CRAIG, H. M.—See Gagnon, P. E.
- CRAWFORD, V. A.—A theoretical study of 2,3-dinaphthylene, 47.
- DARWENT, B. DEB.—See Meadows, G. W.
- DELONG, W. A.—See Fiskell, J. G. A.
- DORLAND, R. M.—See Bauer, T. W.
- DOWNING, D. C.—2,2,5,5-Tetramethylolcyclopentanol pentanitrate, 124. The nitrosation of hexamine, 165.
- DRAIN, L. E.—See Morrison, J. A.
- DUGDALE, J. S.—See Morrison, J. A.
- EASTHAM, A. M. and LATREMOUILLE, G. A.—The chemistry of ethylene oxide. V. The reaction of ethylene oxide with halide ions in neutral and acid solution, 169.
- EDWARDS, O. E. and MARION, L.—Lycotoxine and its oxidation products, 627.
- EISENHAEUER, H. R., PEPPER, J. M., JAQUES, L. B., and SPINKS, J. W. T.—Dicumarol-2-C¹⁴: Synthesis and metabolism studies, 245.
- EMBLETON, H. W.—See Bourns, A. N.
- ENGLISH, W. D., TAURINS, A., and NICHOLLS, R. V. V.—Disilyl alkanes, 646.
- EPSTEIN, S. and WINKLER, C. A.—Studies of RDX and related compounds. VII. Relation between RDX and HMX production in the Bachmann reaction, 734.
- FAINER, P., MYERS, J. L., and KEIRSTEAD, K. F.—The reduction of some chlorinated azobenzenes with titanous sulphate, 498.
- FARMILO, C. G.—See Levi, L.
- FIGDOR, S. K.—See Bartlett, M. F.; Wiesner, K.
- FISKELL, J. G. A., DELONG, W. A., and OLIVER, W. F.—Investigation of the forms of phosphorus in neutron-bombarded phosphates. Nature of the phosphorus-32, 9. Investigation of the forms of phosphorus in neutron-bombarded phosphates. III. Superphosphate and calcium sulphate hemihydrate, 185.
- FLEMING, H.—See Byrne, J.
- FLEMING, W.—See Macnamara, J.
- FLOOD, E. A., TOMLINSON, R. H., and LEGER, A. E.—The flow of fluids through activated carbon rods. I, 348. II. The pore structure of activated carbon, 372. III. The flow of adsorbed fluids, 389.
- FUNT, B. L.—Dielectric dispersion in solid polyvinyl butyral, 84.
- FUNT, B. L. and SUTHERLAND, T. H.—Dielectric properties of polyvinyl acetals, 940.
- GAGNON, P. E.—See Boivin, P. A.
- GAGNON, P. E., BOIVIN, J. L., BOIVIN, P. A., and CRAIG, H. M.—Study of 4-mono- and 4,4-disubstituted-3-imino-2-benzoyl-5-pyrazolones, 52.
- GAGNON, P. E., BOIVIN, J. L., and CHISHOLM, A.—Synthesis of pyrazolones from α -keto and α -cyano esters, 904.
- GAGNON, P. E., NADEAU, G., and CÔTÉ, R.—Synthesis of α -amino acids from ethyl cyanoacetate, 592.
- GEORGIEFF, K. K.—Preparation of ketene from glacial acetic acid, methyl acetate, and ethyl acetate, 332.
- GIGUÈRE, P. A. and LIU, I. D.—Infrared spectrum, molecular structure, and thermodynamic functions of hydroxylamine, 948.
- GIGUÈRE, P. A. and WEINGARTSHOFER OLMOS, A.—A spectroscopic study of hydrogen bonding in performic and peracetic acids, 821.
- GILLESPIE, T. and LANGSTROTH, G. O.—Coagulation and deposition in still aerosols of various solids, 1003. An instrument for determining the electric charge distribution in aerosols, 1056.
- GILPIN, V. and WINKLER, C. A.—Studies of RDX and related compounds. VIII. Thermochemistry of RDX reactions, 743.
- GRAHAM, R. P., HITCHEN, A., and MAXWELL, J. A.—The polarographic determination of titanium in steels and nickel-base alloys, 661.
- GRAHAM, R. P., VANDALEN, E., and UPTON, A. M. C.—Note on the polarographic determination of zirconium, 1069.
- HABGOOD, H. W.—See Weinberger, M. A.
- HAINES, R. L.—See Hodgins, J. W.
- HALL, R. H.—See Berman, L.
- HANSULD, M. K.—See Bourns, A. N.
- HARDWICK, T. J.—The oxidation of ferrous sulphate solutions by γ -rays—The absolute yield, 17. The reduction of ceric sulphate solutions by ionizing radiation, 23. Radiation chemistry investigation of aqueous solutions using P³² and S³⁵ as internal sources, 39.
- HATTON, W. G.—See McKay, A. F.
- HENDERSON, D. R.—See Wiesner, K.
- HERBST, J. H. E.—The preparation of chlorite holocellulose, 668.
- HITCHEN, A.—See Graham, R. P.

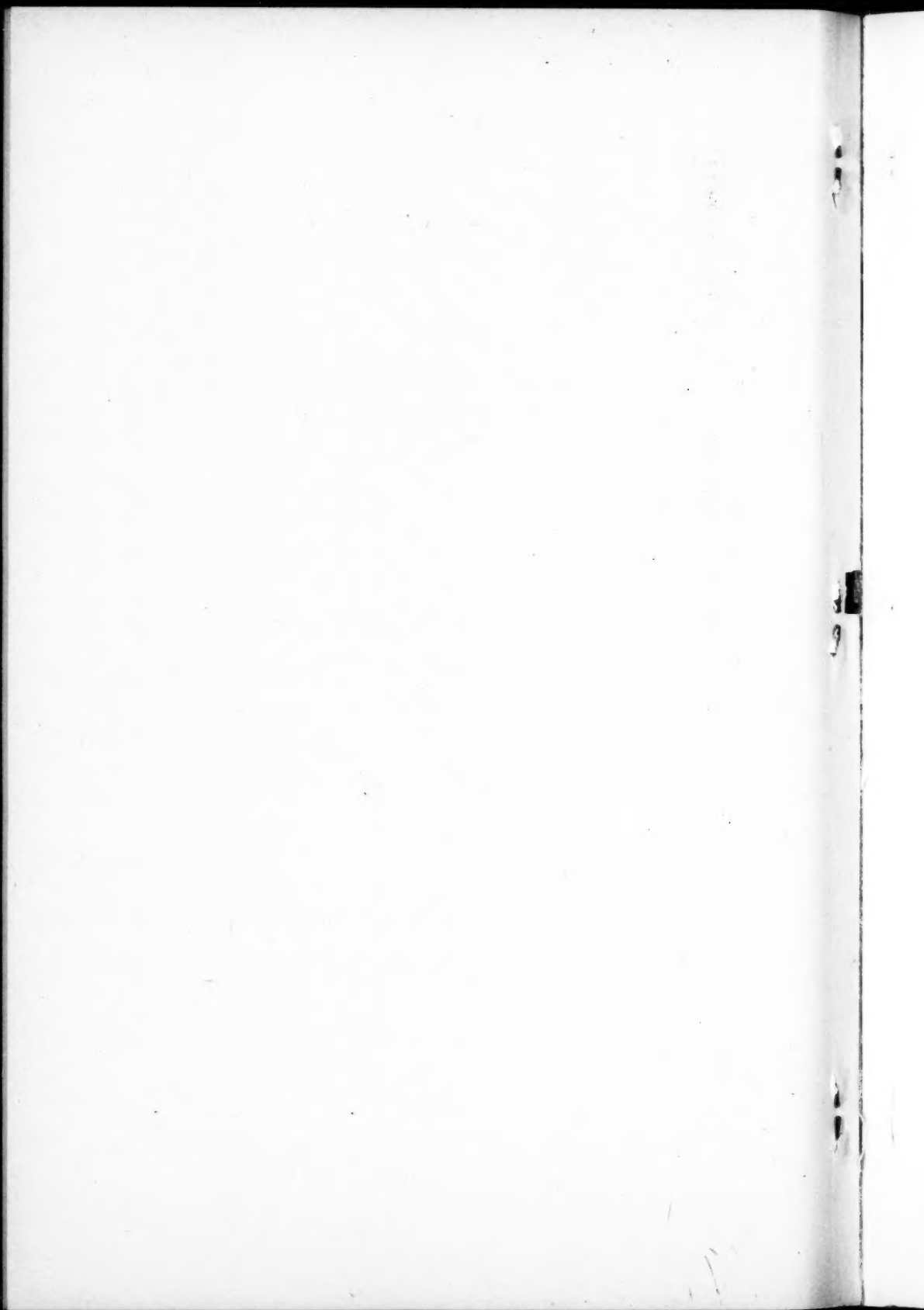
- HODGINS, J. W. and HAINES, R. L.—The formation of trifluoromethyl radicals in the gas phase, 473.
- HOLLAND, D. A.—See Brown, F.
- HYDE, J. C.—See Sheffer, H.
- INGRAHAM, T. R.—Note on the preparation of hydrazine by arc electrolysis in liquid ammonia, 168.
- INGRAHAM, T. R. and PIDGEON, L. M.—The reactions of titanium tetraiodide on heated titanium and tungsten surfaces, 694.
- INGRAHAM, T. R. and WINKLER, C. A.—Studies on the formation of hexamine, 687.
- JAQUES, L. B.—See Eisenhauer, H. R.; Phillips, R. V.
- JONES, R. N.—See Nolin, B.
- KARTZMARK, E. M.—See Campbell, A. N.
- KEIRSTEAD, K. F.—See Fainer, P.
- KIRKWOOD, S.—See Leete, E.
- KNOP, O. and MACLEAN, D. B.—*Lycopodium* alkaloids. I. Physical properties and X-ray crystallographic data of some *Lycopodium* alkaloids, 598.
- KULKA, M. and MANSKE, R. H. F.—The synthesis of pyridocarbazoles, 711. The nitration of some quinoline derivatives, 720.
- LANGSTROTH, G. O.—See Gillespie, T.
- LATREMOUILLE, G. A.—See Eastham, A. M.
- LEETE, E., KIRKWOOD, S., and MARION, L.—The biogenesis of alkaloids. VI. The formation of hordenine and N-methyltyramine from tyramine in barley, 749.
- LEETE, E. and MARION, L.—The papilionaceous alkaloids. XVII. The synthesis of structural isomers of sparteine, 563.
- LEGER, A. E.—See Flood, E. A.
- LEITCH, L. C. and MORSE, A. T.—Synthesis of organic deuterium compounds. III. 1,2-Dibromoethane- d_4 and its derivatives, 924.
- LEITCH, L. C. and RENAUD, R.—Synthesis of organic deuterium compounds. II. Propyne-3- d_3 and propyne- d_4 , 79.
- LEMIEUX, R. U.—See Neish, A. C.
- LEMIEUX, R. U. and BRICE, C.—The mechanisms of glucose pentaacetate anomerization and levoglucosan formation, 295.
- LEVI, L. and FARMILLO, C. G.—The characterization of narcotics as reineckates, 783. The quantitative determination of narcotics by ion exchange, 793.
- LINDSAY, J. G.—See Stacey, F. W.
- LINDSAY, J. G., BOURNS, A. N., and THODE, H. G.—Influence of temperature on the intermolecular C^{13} isotope effect in the decarboxylation of normal malonic acid, 163.
- LISTER, M. W.—The decomposition of hypochlorous acid, 879.
- LIU, I. D.—See Giguère, P. A.
- LOUNSBURY, M.—See Stevens, W. H.
- LUCIEN, H. W. and TAURINS, A.—The synthesis of dibenz [*a,c*] [1,3] cycloheptadiene-5,7-dione, 208.
- LUNER, P. and WINKLER, C. A.—Solvent effects in *cis-trans* isomerization, 679.
- MCCONNELL, W. B.—The estimation of free amino acids using a microdiffusion technique, 522.
- MCDERMOT, H. L. and ARNELL, J. C.—Charcoal sorption studies. I. The pore distribution in activated charcoals, 177.
- MACDONALD, D. M.—See Wiesner, K.
- MCGILVER, J. D. and WINKLER, C. A.—The mercury photosensitized reactions of nitric oxide, 194.
- MCINTOSH, R.—See Amberg, C. H.; Craig, A.
- MCKAY, A. F.—See Vavasour, G. R.
- MCKAY, A. F. and HATTON, W. G.—Urea derivatives, 225.
- MACKENZIE, A. N.—See Betts, R. H.
- MACLEAN, D. B.—See Knop, O.
- MACNAMARA, J., FLEMING, W., SZABO, A., and THODE, H. G.—The isotopic constitution of igneous sulphur and the primordial abundance of the terrestrial sulphur isotopes, 73.
- MAJURY, T. G. and STEACIE, E. W. R.—The reactions of CH_3 and CD_3 radicals with hydrogen and deuterium, 800.
- MANSKE, R. H. F.—See Kulka, M.
- MANSON, J. A. and CRAGG, L. H.—Normal and cross-linked polystyrene. I. Huggins' k' as a measure of nonlinearity, 482.
- MARION, L.—The papilionaceous alkaloids. XVI. Trilupine and dilupine, 386. See Cockburn, W. F.; Edwards, O. E.; Leete, E.
- MASON, S. G.—See Murray, F. E.
- MAXWELL, J. A.—See Graham, R. P.
- MEADOWS, G. W. and DARWENT, B. DEB.—The reactions of acetaldehyde with methanol, 501.
- MEEN, R. H.—See Picard, J. P.
- METRO, S. J. and TAURINS, A.—The reaction of pyridine and picolines with 2-bromo-2-nitro-1,3-indandione, 466.

- MOIR, R. Y.—See Smith, W. S.
- MORRISON, J. A., DRAIN, L. E., and DUGDALE, J. S.—Phase transitions in multimolecular layers of adsorbed nitrogen, 890.
- MORSE, A. T.—See Leitch, L. C.
- MORTIMER, D. C.—Paper chromatographic separation of some biologically important phosphate esters, 653.
- MURPHY, D.—Structure of a levan produced by *Bacillus polymyxa*, 872.
- MURRAY, D. H. and SPINKS, J. W. T.—Synthesis of P^{32} labeled parathion, 497.
- MURRAY, F. E. and MASON, S. G.—Coexistence phenomena in the critical region. I. The gravity effect in ethane from light scattering, 550.
- MYERS, J. L.—See Fainer, P.
- NADEAU, G.—See Gagnon, P. E.
- NEISH, A. C.—See Spyker, J. W.
- NEISH, A. C. and LEMIEUX, R. U.—The preparation of *p*-bromophenacyl esters and the characterization of *p*-bromophenacyl formate, 454.
- NICHOLLS, R. V. V.—See English, W. D.
- NOLIN, B. and JONES, R. N.—The preparation of some steroids containing deuterium, 727.
- OLIVER, W. F.—See Fiskell, J. G. A.
- ORR, R. J. and WILLIAMS, H. L.—The polymerization of isoprene and 2,3-dimethylbutadiene and copolymerization with styrene at -18°C . in emulsion, 108. Kinetics of the reactions between isopropyl cumene and tertiary butyl cumene hydroperoxides and iron (II) in dilute aqueous solutions in the absence of oxygen, 985.
- PEPPER, J. M.—See Eisenhauer, H. R.; Stevens, W. H.
- PERLIN, A. S.—Thermal decarboxylation of uronic acids, 278.
- PERRON, Y. and BARRÉ, R.—Synthesis of 1,1,1-trichloro-2,2-bis-(*p*-cyanophenyl)-ethane, 203.
- PERRY, E. J. and WINKLER, C. A.—The reaction between silver and triphenylmethyl chloride, 235.
- PHILLIPS, R. V., TREVOY, L. W., JAKES, L. B., and SPINKS, J. W. T.—Synthesis of 2-methyl- C^{14} -1,4-naphthoquinone, 844.
- PICARD, J. P. and MEEN, R. H.—The preparation of polynitroethyleneamines, 102.
- PIDGEON, L. M.—See Ingraham, T. R.
- POWELL, B. D. and ALEXANDER, A. E.—The mobility of oil droplets, interfacial tension measurements, and gegen ion adsorption in soap solutions, 1044.
- PULLIN, A. D. E.—See Bernstein, H. J.
- PURVES, C. B.—See Segall, G. H.
- PYKE, R. G.—See Berman, L.
- RENAUD, E.—See Boivin, P. A.
- RENAUD, R.—See Leitch, L. C.
- RICE, H. M. and SOWDEN, F. J.—X-ray diffraction patterns of dinitrophenyl derivatives of amino compounds, 575.
- ROBERTS, R.—See Bywater, S.
- SCHNEIDER, W. G.—See Weinberger, M. A.
- SEGALL, G. H. and PURVES, C. B.—The action of hydroxylamine, its *o*-methyl ether, and their hydrochlorides on cellulose trinitrate in pyridine, 860.
- SCHEFFER, H. and HYDE, J. C.—An important reflectance correction in light-scattering studies, 817.
- SMITH, W. S. and MOIR, R. Y.—1-Indoleacetic acid, 411.
- SOWDEN, F. J.—See Rice, H. M.
- SPINKS, J. W. T.—See Burkell, J. E.; Eisenhauer, H. R.; Murray, D. H.; Phillips, R. V.
- SPYKER, J. W. and NEISH, A. C.—A new synthesis of C^{14} labeled cyanide, 461.
- STACEY, F. W., LINDSAY, J. G., and BOURNS, A. N.—Isotope effects in the thermal deamination of phthalamide, 135.
- STEACIE, E. W. R.—See Majury, T. G.
- STEVENS, W. H., PEPPER, J. M., and LOUNSBURY, M.—The decarboxylation of anthranilic acid, 529.
- STONE, A. L. and BRECKENRIDGE, J. G.—Optical stability in bipyridyl compounds, 725.
- STONE, J. E. and TANNER, K. G.—Wheat straw native lignin, 166.
- SUTHERLAND, T. H.—See Funt, B. L.
- SWENSON, E. G. and THORVALDSON, T.—The quantitative determination of the free monoxides of calcium, strontium, and barium, and of calcium ethylate by the alcohol-glycerol method, 257.
- SZABO, A.—See Macnamara, J.
- TANNER, K. G.—See Stone, J. E.
- TAURINS, A.—See English, W. D.; Lucien, H. W.; Metro, S. J.
- THODE, H. G.—See Lindsay, J. G.; Macnamara, J.
- THORN, G. D.—6,8-Dimethoxy-4-chromanone, 224.
- THORN, G. D. and BARCLAY, L. R. C.—Some methyl ethers and acetates of purpurogallin, 251.
- THORVALDSON, T.—See Swenson, E. G.

- TOMLINSON, R. H.—See Flood, E. A.
TREVROY, L. W.—See Phillips, R. V.
TRICK, G. S. and WINKLER, C. A.—The reaction of active nitrogen with propylene, 915.
TROST, W. R.—Addition compounds of the group IV halides. I. Triethylamine and the tetrachlorides of silicon, germanium, tin, and titanium, 835. II. Ethylamine and the tetrachlorides of silicon, germanium, tin, and titanium, 842.
TUDGE, A. P.—See Bourns, A. N.
TURNER, R. C. and WINKLER, C. A.—Effect of addition agents on copper deposition in a convection-free system, 507.
UPTON, A. M. C.—See Graham, R. P.
VALENTA, Z.—See Wiesner, K.
VANDALEN, E.—See Graham, R. P.
VAVASOUR, G. R., BOLKER, H. I., and MCKAY, A. F.—Steroids. I. A case of Walden inversion with nucleophilic substitution at position 3 of Δ^5 -steroids, 933.
WEINBERGER, M. A., HABGOOD, H. W., and SCHNEIDER, W. G.—On the liquid-vapor coexistence curve of xenon in the region of the critical temperature. II, 815.
WEINBERGER, M. A. and SCHNEIDER, W. G.—On the liquid-vapor coexistence curve of xenon in the region of the critical temperature, 422. Density distributions in a vertical tube containing xenon near the critical temperature as measured by a radioactive tracer technique, 847.
WEINGARTSHOFER OLMOS, A.—See Giguère, P. A.
WELLINGTON, E. F.—An ultramicro method for quantitative determination of amino acids, 581.
WETMORE, F. E. W.—See Aziz, P. M.; Byrne, J.
WIESNER, K.—See Bartlett, M. F.
WIESNER, K., FIGDOR, S. K., BARTLETT, M. F. and HENDERSON, D. R.—*Garrrya* alkaloids. I. The structure of garryine and veatchine, 608.
WIESNER, K., MACDONALD, D. M., VALENTA, Z., and ARMSTRONG, R.—*Pithecolobine*, the alkaloid of *Pithecolobium saman* Benth. I, 761.
WILLIAMS, H. L.—See Orr, R. J.
WINKLER, C. A.—See Epstein, S.; Gilpin, V.; Ingraham, T. R.; Luner, P.; McGilvery, J. D.; Perry, E. J.; Trick, G. S.; Turner, R. C.
WRIGHT, G. F.—Mechanism of guanidine nitration. I. *Azo-bis-nitroformamidine*, 62. Reaction of oxymercureals with hydrazine, 268. See Berman, L.

CORRECTION

Page 371. In line 3, Equation 11 should read Equation 13.



CANADIAN JOURNAL OF CHEMISTRY

Notice to Contributors

GENERAL: Manuscripts should be typewritten, double spaced, and the **original and one extra copy** submitted. Style, arrangement, spelling, and abbreviations should conform to the usage of this Journal. Names of all simple compounds, rather than their formulas, should be used in the text. Greek letters or unusual signs should be written plainly or explained by marginal notes. Superscripts and subscripts must be legible and carefully placed. Manuscripts should be carefully checked before being submitted, to reduce the need for changes after the type has been set. If authors require changes to be made after the type is set, they will be charged for changes that are considered to be excessive. **All pages, whether text, figures, or tables, should be numbered.**

ABSTRACT: An abstract of not more than about 200 words, indicating the scope of the work and the principal findings, is required.

ILLUSTRATIONS:

(i) **Line Drawings:** All lines should be of sufficient thickness to reproduce well. Drawings should be carefully made with India ink on white drawing paper, blue tracing linen, or co-ordinate paper ruled in blue only; any co-ordinate lines that are to appear in the reproduction should be ruled in black ink. Paper ruled in green, yellow, or red should not be used unless it is desired to have all the co-ordinate lines show. Lettering and numerals should be neatly done in India ink preferably with a stencil (do not use typewriting) and be of such size that they will be legible and not less than one millimeter in height when reproduced in a cut three inches wide. All experimental points should be carefully drawn with instruments. Illustrations need not be more than two or three times the size of the desired reproduction, but the ratio of height to width should conform with that of the type page. **The original drawings and one set of small but clear photographic copies are to be submitted.**

(ii) **Photographs:** Prints should be made on glossy paper, with strong contrasts; they should be trimmed to remove all extraneous material so that essential features only are shown. Photographs should be submitted in duplicate; if they are to be reproduced in groups, one set should be so arranged and mounted on cardboard with rubber cement; the duplicate set should be unmounted.

(iii) **General:** The author's name, title of paper, and figure number should be written in the lower left hand corner (outside the illustration proper) of the sheets on which the illustrations appear. Captions should not be written on the illustrations, but typed together at the end of the manuscript. All figures (including each figure of the plates) should be numbered consecutively from 1 up (arabic numerals). **Each figure should be referred to in the text.** If authors desire to alter a cut, they will be charged for the new cut.

TABLES: Each table should be typed on a separate sheet. Titles should be given for all tables, which should be numbered in Roman numerals. Column heads should be brief and textual matter in tables confined to a minimum. **Each table should be referred to in the text.**

REFERENCES: These should be listed alphabetically by authors' names, numbered in that order, and placed at the end of the paper. The form of literature citation should be that used in this Journal. Titles of papers should not be given. The first page only of the references cited should be given. All citations should be checked with the original articles. Each citation should be referred to in the text by means of the key number.

REPRINTS: A total of 50 reprints of each paper without covers are supplied free to the authors. Additional reprints will be supplied according to a prescribed schedule of charges. On request, covers can be supplied at cost.

Approximate charges for reprints may be calculated from the number of printed pages, obtained by multiplying by 0.6 the number of manuscript pages (double-spaced typewritten sheets, 8½ in. by 11 in.) and making allowance for space occupied by line drawings and halftones (not inserts). The cost per page is tabulated at the back of the reprint request form sent with the galley.

Contents

	Page
The Reaction of Active Nitrogen with Propylene— <i>G. S. Trick and C. A. Winkler</i> - - - - -	915
Molten Salts. Electrical Conductivity in the System Silver Nitrate—Sodium Nitrate— <i>June Byrne, Helen Fleming, and F. E. W. Wetmore</i> - - - - -	922
Synthesis of Organic Deuterium Compounds. III. 1,2-Dibromoethane- <i>d</i> ₂ and its Derivatives— <i>L. C. Leitch and A. T. Morse</i> -	924
Steroids. I. A Case of Walden Inversion with Nucleophilic Substitution at Position 3 of Δ^5 -Steroids— <i>G. R. Vavasour, H. I. Bolker, and A. F. McKay</i> - - - - -	933
Dielectric Properties of Polyvinyl Acetals— <i>B. L. Funt and T. H. Sutherland</i> - - - - -	940
Infrared Spectrum, Molecular Structure, and Thermodynamic Functions of Hydroxylamine— <i>Paul A. Giguère and I. D. Liu</i> -	948
Vibration Spectra of <i>cis</i> and <i>trans</i> Dichloroethylene- <i>d</i> ₂ — <i>H. J. Bernstein and A. D. E. Pullin</i> - - - - -	963
Binding of Anions by Denatured Proteins— <i>J. Ross Colvin</i> - - -	973
Kinetics of the Reactions Between Isopropyl Cumene and Tertiary Butyl Cumene Hydroperoxides and Iron(II) in Dilute Aqueous Solutions in the Absence of Oxygen— <i>R. J. Orr and H. Leverne Williams</i> - - - - -	985
Cyanoacetic Esters, Amino Acids, and Pyrazolones— <i>Paul A. Boivin, Paul E. Gagnon, Ernest Renaud, and William A. Bridgeo</i> - -	994
Coagulation and Deposition in Still Aerosols of Various Solids— <i>T. Gillespie and G. O. Langstroth</i> - - - - -	1003
A Study of Adsorption Hysteresis by Means of Length Changes of a Rod of Porous Glass— <i>C. H. Amberg and R. McIntosh</i> - - -	1012
The Viscometric Detection of Branching in Polymers. I. Branching in GR-S as a Function of Conversion— <i>L. H. Cragg and A. T. Brown</i>	1033
The Mobility of Oil Droplets, Interfacial Tension Measurements, and Gegen Ion Adsorption in Soap Solutions— <i>B. D. Powell and A. E. Alexander</i> - - - - -	1044
An Instrument for Determining the Electric Charge Distribution in Aerosols— <i>T. Gillespie and G. O. Langstroth</i> - - - - -	1056
Note on the Polarographic Determination of Zirconium— <i>R. P. Graham, E. VanDalen, and A. M. C. Upton</i> - - - - -	1069
Contents of Volume 30 - - - - -	1073

